Low Carbon Biomass Fuel Combustion and Ash Recycling for Sustainable Cement Production

Yu Wang

Department of Natural Resource Sciences

McGill University

February 2015

A thesis submitted to McGill University in partial fulfillment of the

requirements for the degree of Doctor of Philosophy

ABSTRACT

Switching to low carbon fuel (LCF) can help the cement industry reduce carbon dioxide (CO_2) emissions effectively. This is because LCF generates energy that can lower the coal consumption in the kiln. Biomass fuel originating from perennial grass crops and woody materials is LCF that can be converted to clean energy (e.g. heat or steam) via combustion, which is an independent process from cement production. Meanwhile, the residual ash from the biomass combustion may be recycled by blending with cement if this ash possesses a high pozzolanic activity, which can reduce the demand for cement and accordingly lessen the CO_2 emissions associated with cement production. Hence, the overall objectives of this thesis were to 1) investigate the combustion characteristics of switchgrass (*Panicum vigratum L.*) compared to hardwood; 2) characterize the physiochemical properties of switchgrass combustion ash, and assess the strength in mortars made from blended cement containing up to 20% switchgrass combustion ash content; 3) and optimize the combustion conditions to achieve a high energy conversion and ash pozzolanic value simultaneously.

Switchgrass and hardwood contained 17.5 and 17.7 $MJ \cdot kg^{-1}$ of energy value, which was appropriate for energy generation. Using a laboratory-scale experimental platform that studied the air supply effect on combustion performance, the greatest energy conversion efficiency and combustion completeness rate were obtained with an excess air of 20% for switchgrass and 30% for hardwood (4 mm particle size). Kinetic analysis also confirmed that increasing the oxygen availability resulted in a superior energy conversion. Switchgrass ash had lower fouling and slagging tendencies than hardwood, and could be a better biomass fuel for a commercial-scale boiler.

Switchgrass combusted at 411 °C generated 5% ash by mass. After grinding for 30 s, ground ash had a porous structure with 65.0 μm of mean particle size and 41.2 $m^2 \cdot g^{-1}$ of BET surface area. Ground ash contained 67.2% of SiO_2 and its structure was 72.2% amorphous crystal. This ash was a good pozzolan in blended cement, and its pozzolanic activity was improved by adding chemical accelerators (5% Na_2SO_4 and 5% $CaCl_2 \cdot 2H_2O$ were equally effective). Blended cement with 10% ash and either 5% Na_2SO_4 or 5% $CaCl_2 \cdot 2H_2O$ had similar material strength and expansion resistance as conventional cement. Furthermore, considering the effect of switchgrass combustion temperature (350, 450, 550 or 650 °C) and retention time (1 or 4 h), the combustion conditions of 550 °C for 4 h were recommended for concurrently optimizing the ash pozzolanic activity (114%) and energy output (4.21 $kJ \cdot g^{-1}$) from switchgrass.

In conclusion, it was technically feasible to offset energy demands in cement production by relying on switchgrass or hardwood combustion in parallel to coal burning. Recycling 10% of the switchgrass ash generated under optimal combustion conditions (550 °C for 4 h) in blended cement not only offset the disturbance in the cementitious composition due to ash substitution, but also contributed to greater strength microstructural compound (C-S-H) formation, thus improving the concrete strength by 14.2%. If these findings can be extrapolated directly to an average-size cement production plant (3.06 GJ coal /1000 kg cement product), the life-cycle CO_2 emission would decrease by 1.77% when 5% of the coal burned is replaced by switchgrass energy with ash recycling.

RÉSUMÉ

Le passage au combustible à faible teneur en carbone (LCF) peut aider l'industrie cimentière à réduire efficacement les émissions du dioxyde de carbone (CO_2). Ceci grâce à l'énergie que génère ce combustible (LCF) et qui peut diminuer la consommation en charbon dans le four. La biomasse combustible provenant des graminées vivaces et des matières ligneuses constitue un LCF qui peut être converti par combustion, processus étant indépendant de la production du ciment, en énergie propre (comme chaleur ou vapeur). Si la cendre résiduelle issue de cette combustion possède une activité pouzzolanique élevée, elle peut être recyclée en la mélangeant avec du ciment et réduire donc la demande en celui-ci et par conséquence les émissions de CO_2 associées à la fabrication du ciment. Ainsi, les objectifs généraux de cette thèse étaient de: 1) étudier les caractéristiques de combustion du panic raide (Panicum vigratum L.) par rapport au bois de feuillus; 2) caractériser les propriétés physico-chimiques de la cendre issue de la combustion du panic raide et évaluer la rigidité des mortiers fabriqués à base du ciment mélangé avec 20% de cette cendre; 3) et optimiser les conditions de combustion pour parvenir simultanément à une conversion élevée d'énergie et à une cendre ayant une haute valeur pouzzolanique.

Le panic raide et le bois de feuillus contenaient respectivement 17.5 et 17.7 $MJ \cdot kg^{-1}$ de la valeur énergétique, ce qui a été approprié pour la production d'énergie. Une plate-forme expérimentale a été utilisée au laboratoire afin d'étudier l'effet de l'alimentation en air sur le rendement de combustion. Le rendement énergétique de conversion et le taux de complétude de combustion les plus élevés ont été obtenus avec un excès d'air de 20% pour le panic raide et 30% pour le bois du feuillus (taille des

particules de 4 mm). L'analyse cinétique a également confirmé que l'augmentation de la disponibilité de l'oxygène a entraîné une conversion d'énergie supérieure. La cendre du panic raide avait des tendances d'encrassement et de scorification inférieures par rapport au bois de feuillus et pourrait être un meilleur combustible pour une chaudière à l'échelle commerciale.

Le panic raide brûlé à 411 °C a généré 5% de cendres en poids. Après broyage pendant 30 s, la cendre avait une structure poreuse ayant une taille moyenne des particules de 65.0 μm et une surface spécifique, mesurée par la méthode BET, égale à 41.2 $m^2 \cdot g^{-1}$. La cendre broyée contenait 67.2% de SiO_2 et 72.2% de sa structure était cristalline amorphe. Elle a constitué une bonne pouzzolane dans le ciment mélangé et son activité pouzzolanique a été améliorée par l'addition de catalyseurs chimiques (5% Na_2SO_4 et 5% de $CaCl_2 \cdot 2H_2O$ ont été aussi efficaces). Le ciment mélangé avec 10% de cendres et 5% soit du Na_2SO_4 ou du $CaCl_2 \cdot 2H_2O$ s'est caractérisé par une rigidité du matériau et une résistance d'expansion identiques au ciment conventionnel. En outre, compte tenu de l'effet de la température de combustion du panic raide (350, 450, 550 ou 650 °C) et le temps de rétention (1 ou 4h), les conditions de combustion à 550 °C pendant 4h ont été recommandées pour optimiser aussi bien l'activité pouzzolanique de cendres (114%) que la production d'énergie (4.21 $kJ \cdot g^{-1}$) à partir du panic raide.

En conclusion, il était techniquement possible de compenser la demande énergétique dans la fabrication du ciment en s'appuyant sur la combustion du panic raide ou du bois de feuillus en parallèle avec la combustion du charbon. Le recyclage de 10% des cendres du panic raide, issues des conditions optimales de combustion (550 °C pendant 4 h), dans le ciment mélangé a compenser la perturbation dans la composition du

ciment due à la substitution des cendres, mais a également contribué à une plus grande rigidité de la formation du composé microstructural (C-S-H), améliorant ainsi la résistance du béton de 14.2%. Si ces résultats peuvent être extrapolés directement à une cimenterie de moyenne taille (3.06 GJ charbon /1000 de produit de ciment kg), le cycle biologique des émissions de CO_2 pourrait diminuer de 1.77% quand 5% du charbon est remplacé par l'énergie issue du panic raide avec recyclage des cendres.

PREFACE AND CONTRIBUTIONS OF AUTHORS

This thesis was composed of six chapters, preceded by a general introduction that provides the overall objectives of this thesis. Four chapters were written in the form of manuscripts, and the sixth chapter was the overall conclusions and future research recommendations. A statement of the contributions to knowledge was also provided, as per the guidelines of the Graduate and Postdoctoral Studies Office, McGill University. The first chapter was a comprehensive literature review that examined the up-to-date research on the recycling of solid wastes as cement additives. Original research results were presented in chapter two to five, which were written as scientific manuscripts, with connecting paragraphs between each chapter to show their connections. Chapter six consisted of overall conclusions and future recommendations, which synthesized all of the findings from previous chapters, and related them to the thesis objectives and hypotheses.

The candidate was the first author on all manuscripts. Co-authors included Dr. Yixin Shao, Dr. Miodrag Darko Matovic, and Dr. Joann K. Whalen. Thesis research was funded by Natural Science and Engineering Research Council (NSERC) of Canada, and the McGill Collaborative Research Development Fund. The candidate wrote the literature review in chapter one and undertook all of the original research in chapter two to five, including data collection, analysis and interpretation, and writing the manuscripts. Dr. Whalen provided financial support, advisory guidance on these research, and editorial supervision with the manuscripts. Dr. Yixin Shao and Dr. Miodrag Darko Matovic provided technical comments on experimental design and manuscript writings.

The manuscript-based chapters are presented in the following order:

Chapter 1. Yu Wang, Yixin Shao, Miodrag Darko Matovic, Joann K. Whalen. Recycling solid wastes as pozzolans in blended cement: a critical review. (In preparation for *Construction and Building Materials*)

Chapter 2. Yu Wang, Yixin Shao, Miodrag Darko Matovic, Joann K. Whalen. Exploring switchgrass and hardwood combustion on excess air and ash fouling/slagging potential: laboratory combustion test and thermogravimetric kinetic analysis. *Energy Conversion and Management* (revision request)

Chapter 3. Wang, Y., Shao, Y., Matovic, M.D., Whalen, J.K. 2014. Recycling of switchgrass combustion ash in cement: Characteristics and pozzolanic activity with chemical accelerators. *Construction and Building Materials*, 73, 472-478.

Chapter 4. Yu Wang, Yixin Shao, Miodrag Darko Matovic, Joann K. Whalen. Optimization of switchgrass combustion for simultaneous production of energy and pozzolan. *Journal of Materials in Civil Engineering*. DOI: 10.1061/(ASCE)MT.1943-5533.0001312.

Chapter 5. Yu Wang, Yixin Shao, Miodrag Darko Matovic, Joann K. Whalen. Predicting the pozzolanic activity of solid wastes using artificial neural network with time-series analytic model. (In preparation for *Construction and Building Materials).*

CONTRIBUTION TO KNOWLEDGE

This thesis research technically proved the concept of LCF combustion with ash recycling as a pozzolan. The significant original contributions to knowledge made by this thesis are as follows.

I critically reviewed the recent research progress in recycling solid wastes as pozzolans, including the mechanism of pozzolanic reaction, the sources of eligible materials, and the methods of pozzolanic activity (PA) improvement.

I creatively built a laboratory combustion system to provide air supply recommendations for biomass combustion in real boiler operations. Based on this platform, I suggested that 20% or 30% excess air (for switchgrass or hardwood) would optimize the combustion to produce the highest energy conversion and complete combustion, which is essential to generate ash that is suitable as a pozzolan.

This was the first research that assessed the physiochemical characteristics and pozzolanic activities of the ash from switchgrass combustion, and investigated the impact of chemical accelerators on its pozzolanic reaction. Blended cement with 10% ash and either 5% Na_2SO_4 or 5% $CaCl_2 \cdot 2H_2O$ had similar material strength and expansion resistance as conventional cement.

This was the first research that simultaneously optimized switchgrass combustion to achieve high energy conversion and ash recycling value. Combustion at 550 °C for 4 h was recommended for the highest energy output (4.21 $kJ \cdot g^{-1}$) and best ash pozzolanic activity (114%).

Furthermore, I created a data-mining artificial neural network (ANN) model for PA prediction, based on 707 groups of data reported in the scientific literature over the past 17 years. From this database, I was also able to forecast the effect of curing age on PA with a time-series model, which is another first in cement research.

ACKNOWLEDGEMENTS

First of all, I am truly thankful to my supervisor Dr. Joann K. Whalen for her world-class supervision and unbelievably great support at all times. As a top professor worldwide, she is the role model in my entire life, who champions me and makes a huge difference in my future. I am grateful for the supervision by Dr. Yixin Shao (McGill) and Dr. Miodrag Darko Matovic (Queen's). Their invaluable technical guidance makes me strong in this extremely interdisciplinary thesis research between civil and mechanical engineering. A special thank you to Dr. Miodrag Darko Matovic, who brings me to the PhD exchange program at Department of Mechanical Engineering of Queen's, and an engineering internship at Lafarge Cement North America. I would also like to thank my industrial director Mr. Rob Cummings at Lafarge. Working with him lets me obtain plenty of real-world engineering management talents.

I sincerely appreciate the fellowships from McGill University and research stipend from Natural Sciences and Engineering Research Council (NSERC) of Canada, and McGill collaborative research funding.

I am very fortunate to have worked with such wonderful lab groups across McGill and Queen's. Thank you to Hicham Benslim, Leonardo León Castro, Mohamed Laila, Zhor Abail, Habib Diop. Also thank you to Qiuchi Yang and Duo Zhang at McGill Civil, and Geoffrey Leslie and Dr. Graham Payne at Queen's Mechanical.

I would greatly like to thank my close friends in Canada, Cong Li, Yang Ji and Yi Li. Our friendships make my PhD program thoroughly inspired and enjoyed.

Lastly, I dedicated this thesis to my beloved parents and Mengtian Zhang, who encourages and supports me endlessly.

LIST OF CONTENTS

LIST OF FIGURES AND TABLES

FIGURES

Chapter 1

Chapter 2

Chapter 3

TABLES

Chapter 1

Chapter 2

Chapter 5

APPENDICES

Chapter 1: Supplemental table

Chapter 2: Supplemental figure

Chapter 2: Supplemental table

Chapter 3: Supplemental figure

Chapter 4: Supplemental figure

Chapter 4: Supplemental table

ABBREVIATION

LCF	Low carbon fuels
PA	Pozzolanic activity
ANN	Artificial neural network
GHG	Greenhouse gas
CH	$Ca(OH)_2$
C-S-H	$(CaO)_x \cdot (SiO_2)_y \cdot (H_2O)_z$
C_3S	Tricalcium silicate $(CaO)_3 \cdot SiO_2$
C_2S	Dicalcium silicate $(CaO)_2 \cdot SiO_2$
C_3A	Tricalcium aluminate $(CaO)_3 \cdot Al_2O_3$
C_4AF	Tetracalcium aluminoferrite $(CaO)_4 \cdot Al_2O_3 \cdot Fe_2O_3$
C-A-H	$(CaO)_x \cdot (Al_2O_3)_y \cdot (H_2O)_z$
C-A-F-H	$(CaO)_x \cdot (Al_2O_3)_y \cdot (Fe_2O_3)_z \cdot (H_2O)_w$
ASR	Alkali silica reaction
W/B	Water-binder ratio
LOI	Loss on ignition
EAR	Excess air ratio
HHV	Higher heating value
ICP	Inductively Coupled Plasma
BA	Basic-acid ratio
FI	Fouling index
SI	Slagging index
SVR	Slag viscosity ratio

SAFR	Stoichiometric air-fuel ratio
ECE	Energy conversion efficiency
CCR	Combustion completeness rate
XRF	X-ray fluorescence
TGA-DSC	Thermalgravimetric analysis-differential scanning calorimetry
D_2	Diffusion two-way transport
GB	Ginstling–Brounshtein equation
D_3	Diffusion three-way transport
DAQ	Data acquisition system
BET	Brunauer Emmett Teller
XRD	X-Ray diffraction
M[CaO]	Ca^{2+} concentration
LSD	Least significant difference
ANOVA	Analysis of variance
SEM	Scanning electron microscope
PE	Processing elements
RMS	Root-mean-squared error

GENERAL INTRODUCTION

Canadian cement manufacturers produce an estimated 2% of regional CO_2 emissions. Cement manufactured by the calcination process requires a temperature of about 1450 °C, which is maintained by coal combustion inside the kiln (Schneider et al., 2011b). According to the life cycle assessment (LCA) of cement production, an average-size cement plant consumes 3.06 GJ of coal per 1000 kg of final cement produced, which releases 549 kg of CO_2 from the calcination process and another 303 kg from coal combustion (Wang et al., 2014b). One effective way to lessen the CO_2 emissions is to replace a part of coal by LCF, e.g. biomass fuel (Baxter, 2005; Demirbaş, 2003). A cement plant can set up an independent biomass combustion unit to generate "green" energy from the LCF, which partially supplants fossil energy in the kiln. Compared to other biomass energy conversion systems (e.g. gasification or pyrolysis), direct combustion requires little extra infrastructure when biomass fuel is substituted for fossil fuel (Jenkins et al., 1998; Nussbaumer, 2003; Tillman, 2000). Thus, it is more technically feasible and has lower capital cost, particularly for commercial-scale plants that are already generating power at megawatt levels. For instance, Lafarge Cement accomplished full-scale cement production trials with biomass fuel in 2010, but still had several unanswered questions about the biomass fuel, such as its combustion characteristics and possibility for ash recycling.

Air-fuel ratio is an important controller of biomass combustion that should be examined thoroughly. The air intake at combustion determines the energy conversion and emissions from biomass. Insufficient air causes more CO emission and inferior energy efficiency due to unburnt carbon (Demirbaş, 2001). Heat and mass transfer delays are

among the many factors in boilers that decrease the air utilization efficiency and retard the combustion completeness (Demirbas, 2004). Hence, a biomass boiler typically incorporates 10-30% of excess air, above that required by stoichiometric condition (0% of excess air), to maximize the energy output (Nussbaumer, 2003). Yet, an overly high input of excess air in boilers will actually lower the combustion temperature due to heat convection and radiation, thereby degrading the theoretical energy efficiency according to the Carnot thermodynamic cycle.

Besides, burning 1 kg biomass fuel generates 0.05-0.2 kg of ash, and this ash would be a hazardous contaminant owing to its fine particle size and rich mineral content (Lim & Seow, 2012). Thus, another challenge of large-scale biomass combustion systems is how to dispose of the ash generated from the biomass fuel in an efficient, sustainable and economical way. It is technically possible to recycle the residual ash from biomass combustion in cement. Biomass ash can enhance the strength and durability of concrete because it contains SiO_2, which can cause supplementary formation of calcium silicate hydrate ($(CaO)_x \cdot (SiO_2)_y \cdot (H_2O)_z$, C-S-H) from calcium hydroxide ($Ca(OH)_2$, CH) by the pozzolanic reaction (Foo & Hameed, 2009). Pozzolans are siliceous or siliceous and aluminous materials with virtually no cementing value; however, in the presence of water, they react with CH to form C-S-H, which is the main contributor to concrete strength (Duan et al., 2013a). A satisfactory pozzolan should have small particle size (<0.45 μm of mean particle size) and contain more than 70% of $SiO_2 + Al_2O_3 + Fe_2O_3$ (ASTM, 2004). Yet, compared to conventional pozzolans like silica fume (containing ≥ 99% SiO_2), the pozzolanic activity of biomass ash is still inferior due to its lower SiO_2 content (≈ 50-80%). Hence, it is critical to evaluate the practicability of this recycling strategy and

consider how to enhance the pozzolanic reaction when biomass ash is blended with cement.

Switchgrass (*Panicum vigratum* L.) is a leading choice as biomass-based LCF that can be substituted for fossil fuels in eastern Canada. (Abbasi & Abbasi, 2010). Switchgrass is a perennial warm-season bunchgrass that yields up to 25 tonnes of dry matter per hectare under the climatic conditions of eastern Canada, and there is an estimated 3 million hectares of marginal agricultural land available for its cultivation (Mabee et al., 2006). It is rich in volatile content (70.1-85.2%) and has an excellent calorific value (18.0-26.2 $MJ \cdot kg^{-1}$) (Guretzky et al., 2011), which is comparable or superior to hardwood trees (Antizar-Ladislao & Turrion-Gomez, 2008; Cherubini & Jungmeier, 2010). Its ash is rich in silicon (4.0-6.3%), which implies that the ash might possess pozzolanic activity (Madani Hosseini et al., 2011; Monti et al., 2008). However, we are not aware of any published work that examines how excess air affects switchgrass combustion, and there is no research heretofore to evaluate the recycling of combusted switchgrass ash in blended cement, or to explore an optimizing solution to make this concept technically applicable.

Hence, the overall objectives of this thesis are to, 1) investigate the combustion characteristics of switchgrass compared to hardwood; 2) characterize the physiochemical properties of switchgrass combustion ash, and assess the strength and durability of mortar made from blended cement containing 10-20% switchgrass ash (by mass); and 3) optimize the combustion conditions to achieve a high energy conversion and ash with high pozzolanic value simultaneously.

FORWARD TO CHAPTER 1

Chapter 1 is a literature review that critically summarizes the recent research progress in using solid wastes (e.g. the ash from biomass combustion) as pozzolans, including the mechanism of pozzolanic reaction, the sources of eligible materials, and the methods to improve pozzolanic activity. This review provides a comprehensive synthesis of the opportunities for recycling of solid wastes as pozzolans in blended cement, and deeply discusses the complexity of the cement—pozzolan—water system in concrete-making.

CHAPTER 1. Literature Review

Recycling solid wastes as pozzolans in blended cement: a critical review

1.1. Abstract

Numerous solid wastes can be used as pozzolans in blended cement due to the similarity of their physiochemical properties to conventional pozzolans (e.g. silica fume). This strategy effectively recycles these pozzolanic-active "waste" resources and replaces a significant proportion of Portland cement, which potentially reduces the greenhouse gas (GHG) emissions from cement production. However, there are few papers that synthesize, critically analyze and discuss the findings to date. Hence, the objective of this paper is to critically review the recent research progress in using solid wastes as pozzolans, including the mechanism of pozzolanic reaction, the sources of eligible materials, and the methods of pozzolanic activity (PA) improvement. An acceptable pozzolan should be significantly rich in amorphous SiO_2, Al_2O_3 and Fe_2O_3, and its particle size should be fine enough to assure a highly reactive crystal surface. Solid wastes with the greatest potential as pozzolans, based on those currently used in the cement industry are widely available, thus having a lower cost compared to an ultrafine amorphous silica fume. Blending these materials with cement saves raw materials, fuel and energy due to less Portland cement use, but results in the same or even superior concrete properties.

1.2. Introduction

The current Portland cement industry usually depends on pozzolanic reaction to make the final cement products achieve the desired binding and structural strength, with

lower economic cost than using Portland cement alone. A pozzolan is a siliceous or siliceous-aluminous material with virtually no cementitious function. In the presence of water, it reacts with $Ca(OH)_2$, hereafter referred to as CH to generate $(CaO)_x \cdot (SiO_2)_y \cdot (H_2O)_z$, the C-S-H complex that is the key strength contributor in concrete (Chandrasekhar et al., 2003; Mehta, 1983). Supplemental C-S-H formation during cement hydration due to the pozzolanic reaction can modify the properties of concrete, such as strength and durability (Thomas, 2011). Yet, cement—pozzolan—water mixture is a complex system, consisting of many physicochemical processes that are easily influenced by temperature, mixing proportion, etc. The challenge is to choose a suitable pozzolan to assure the final quality of concrete, as the activity of a pozzolan is strongly determined by its physicochemical characteristics.

Up to 50% of the Portland cement can be replaced by a pozzolan in a blended cement without any adverse impact on concrete performance (Gastaldini et al., 2009; Johari et al., 2012). Blending cement with silica-rich pozzolans like volcanic ash, diatomaceous earth and silica fume is a practice dating back to antiquity, based on structures built more than 2000 years ago by Greek and Roman civilizations (Idorn, 1997). Many solid wastes (e.g. combustion ash, catalyst residue) can be used as a pozzolan if they possess physiochemical properties akin to conventional pozzolans (e.g. silica fume). An eligible pozzolan should be rich in siliceous or siliceous-aluminous compounds and have a fine particle size (< 45 μm) (Rukzon et al., 2009). This strategy effectively recycles these pozzolanic-active resources and reduces the amount of Portland cement needed to make strong and durable concrete, which potentially eases the greenhouse gas (GHG) emissions from cement production (Heede et al., 2012;

Huntzinger & Eatmon, 2009). In view of these ecological and sustainable benefits, many researchers have tested the pozzolanic activity (PA) of various solid wastes and reported their findings in the scientific literature, leading to more than 1612 publications on this topic in the past 10 years (Web of Science, from 2005 to 2014). On the other hand, there are few papers that synthesize, critically analyze and discuss the findings to date. If solid wastes could be recycled as pozzolans without adverse impact on cement properties, these abundant wastes that costs little or nothing can lessen the real demand of cement production, thus helping cement industry reduce its greenhouse gas (GHG) emissions. Therefore, a review study is indispensable to comprehensively understand the potential for recycling of solid wastes as a pozzolan.

Hence, the objectives of this paper is to systematically review the up-to-date research on using solid wastes as a pozzolan, including the mechanism of pozzolanic reaction, the source of eligible materials, and the method of PA improvement.

1.3. Mechanism of pozzolanic reaction

As the pozzolanic reaction is highly associated with cement hydration, the principle of cement hydration must be elaborated first. Primarily, there are four cementitious components in a typical Portland cement, including 45-75% tricalcium silicate ($(CaO)_3 \cdot SiO_2$, abbreviated as C_3S), 7-32% dicalcium silicate ($(CaO)_2 \cdot SiO_2$, C_2S), 0-13% tricalcium aluminate ($(CaO)_3 \cdot Al_2O_3$, C_3A), and 0-18% tetracalcium aluminoferrite ($(CaO)_4 \cdot Al_2O_3 \cdot Fe_2O_3$, C_4AF) (Bullard et al., 2011). When these compounds interact with water, cement hydration occurs by the following reactions (Eq. 1-1, 1-2, 1-3 and 1-4):

$$(CaO)_3 \cdot SiO_2 + H_2O \rightarrow (CaO)_x \cdot (SiO_2)_y \cdot (H_2O)_z + Ca(OH)_2 \qquad (1\text{-}1)$$

$$(CaO)_2 \cdot SiO_2 + H_2O \rightarrow (CaO)_x \cdot (SiO_2)_y \cdot (H_2O)_z + Ca(OH)_2 \quad (1\text{-}2)$$

$$(CaO)_3 \cdot Al_2O_3 + H_2O \rightarrow (CaO)_x \cdot (Al_2O_3)_y \cdot (H_2O)_z \quad (1\text{-}3)$$

$$(CaO)_4 \cdot Al_2O_3 \cdot Fe_2O_3 + H_2O \rightarrow (CaO)_x \cdot (Al_2O_3)_y \cdot (Fe_2O_3)_z \cdot (H_2O)_w \quad (1\text{-}4)$$

where the $(CaO)_x \cdot (SiO_2)_y \cdot (H_2O)_z$, C-S-H complex is the key hydration product and a main contributor to the strength of cementitious products, e.g. concrete (Richardson, 1999). C_2S is hydrated more gently than C_3S, so the early and late strengths measured during curing benefit from C_3S and C_2S hydration, respectively. Conversely, the roles of C_3A and C_4AF hydration are trivial, since their hydrated products $(CaO)_x \cdot (Al_2O_3)_y \cdot (H_2O)_z$, hereafter designated as C-A-H and $(CaO)_x \cdot (Al_2O_3)_y \cdot (Fe_2O_3)_z \cdot (H_2O)_w$. known as C-A-F-H, are microstructurally weaker than C-S-H (Jolicoeur & Simard, 1998). Hence, the hydration of C_3S and C_2S will release Ca^{2+} ions, dissolved rapidly from solid C_3S and C_2S after mixing the cement with water, leading to a supersaturated Ca^{2+} concentration in the cement-water slurry. With excess Ca^{2+}, the C-S-H gel forms swiftly along with the crystallization of CH. This process is controlled by ionic diffusion through the porous structure formed by C-S-H and tends to decrease with time owing to the diminution of capillary porosity, which slows down the hydration rate steadily (Yajun & Cahyadi, 2004). Compared to C-S-H, the byproduct CH is unfavourable to the growth of C-S-H crystal in a single direction, making the concrete susceptible to failure if a force is applied across the C-S-H crystal plane. Therefore, lowering the CH proportion might be an option to improve the properties of concrete.

The pozzolanic reaction is one way to reduce the CH proportion because it can transforms CH into other compounds that contribute to concrete strength (Fraay et al., 1989). When a pozzolan is added during the cement hydration phase, the surface of the

pozzolan is attacked by dissolved OH^-, thus forming a thin film around the pozzolan particle. As CH dissolution is reversible, the concentrations of Ca^{2+} and OH^- increase quickly, which stimulates the dissolution of SiO_2, Al_2O_3 and Fe_2O_3 from the pozzolan (Eq. 1-5, 1-6 and 1-7) (Shi & Day, 2000b).

$$Ca(OH)_2 + SiO_2 \rightarrow (CaO)_x \cdot (SiO_2)_y \cdot (H_2O)_z \quad (1\text{-}5)$$

$$Ca(OH)_2 + Al_2O_3 + H_2O \rightarrow (CaO)_x \cdot (Al_2O_3)_y \cdot (H_2O)_z \quad (1\text{-}6)$$

$$Ca(OH)_2 + Al_2O_3 + Fe_2O_3 + H_2O \rightarrow (CaO)_x \cdot (Al_2O_3)_y \cdot (Fe_2O_3)_z \cdot (H_2O)_w \quad (1\text{-}7)$$

Extra C-S-H, C-A-H and C-A-F-H are produced by the transformations described above, which promotes the strength and durability of concrete (Hossain & Lachemi, 2007). These reactions generally commence one or more weeks after the start of cement hydration. This delay is ascribed to the dependency of the pozzolanic reaction on the formation of crystallized CH, and the evolution of the pH to a level that permits dissolution of pozzolanic compounds. Despite these descriptions, this cement—pozzolan—water system is still not yet wholly understood, since numerous, interdependent physiochemical changes take place during this process.

To microscopically study the pozzolanic reaction, a few papers performed numeric simulations in cement—pozzolan—water system, using the pozzolan of silica fume (Bentz et al., 1992; Swaddiwudhipong et al., 2003; Ukrainczyk et al., 2013; Wang et al., 2010; Yajun & Cahyadi, 2004) or low-calcium fly ash (Wang et al., 2009a). Besides the additional C-S-H formation, the fine size of pozzolan has a filler effect as well, which reduces the pore size and blocks capillary pores of the C-S-H gel, thus making the concrete denser (Givi et al., 2010b). In practice, the cement-pozzolan-water mixture exhibited a delay (normally > 10 h) in the pozzolanic reaction that made concrete

more permeable at early curing age (owing to the reduction of cement proportion), and then the concrete would become more compact (Ukrainczyk et al., 2013). Once curing was complete, the lower permeability and denser structure generated from the cement-pozzolan-water mixture augmented the concrete durability in terms of a stronger resistance to the sulfate attack, efflorescence, shrinkage, thermal cracking, chlorine corrosion, and alkali silica reaction (ASR) expansion (Marsh & Day, 1988). In summary, these microscopic studies attest that the overall function of pozzolans is to make concrete stronger and more durable.

1.4. Sources of the eligible solid wastes as pozzolans

1.4.1. Eligibility of pozzolanic materials

In view of the requirements of the pozzolanic reaction, a qualified pozzolan should contain an adequate content of amorphous SiO_2, Al_2O_3 and Fe_2O_3 to assure its chemical reactivity. Its particle size should be fine enough to guarantee the a sufficiently large reactive surface area enough for pozzolanic reaction (Madani Hosseini et al., 2011). At present, there are two internationally recognized standards to define the eligibility of pozzolans, including ASTM C618 (ASTM, 2012a) and EN 196 (BS-EN, 2013). ASTM C618 is prevalent in the North America. An acceptable pozzolan is expected to have at least 70% SiO_2+Al_2O_3+Fe_2O_3, and no more than 34% of particles are retained on a 45 μm sieve (No. 325) (Table 1-1). However, the scope of ASTM C618 is restricted to coal fly ash. Accordingly, several authors studied the applicability of ASTM C618 to other pozzolans, such as biomass ash. For example, Wang et al. (2008b) argued that ASTM C618 should consider the feasibility of biomass fly ash as pozzolan, since the properties of concrete were not be affected by mixtures containing 25% of herbaceous and wood

ash with Portland cement. This argument was also supported by Wang and Baxter (2007), who completely investigated the impact of biomass fly ash on concrete strength, microscopic structure and durability. However, ASTM C618 did not regulate the water-binder ratio (W/B) during the concrete preparation. For this reason, Pourkhorshidi et al. (2010) questioned the rationality of ASTM C618 compared to EN 196, since the pozzolans (Trass, Tuff and Pumice) with a high PA determined by ASTM C618 did not consistently improve the strength and durability of concrete, but the pozzolanic classification made by EN 196 could always agree well with experimental results. Furthermore, a few studies attempted to develop another unbiased method to define the eligibility of pozzolans. For instance, based on the amorphous (glassy) content in ash crystal, Vassilev and Vassileva (2007) classified the ash as high PA (82-100% of glass), medium PA (65-82%) and low PA (30-65%). This method could simply and precisely estimate the PA of ash by testing its mineral-phase composition (quartz, mullite, sulphates, oxyhydroxides and glass). Regardless of the standard or alternative method of classifying pozzolans, a highly active pozzolan should feature a high amount of amorphous SiO_2+Al_2O_3+Fe_2O_3 with a fine particle size.

Many solid wastes meet these requirements, which indicates their possibility of being used as pozzolans. This literature review finds more than 158 reports of PA in solid wastes, and indicates that variation in their pozzolanic function is related to their different physiochemical characteristics (Table 1-2). Still, some general trends can be assessed based on the origin of these materials, which are categorized in this review as combustion ash, blast furnace slag, and other solid wastes.

1.4.2. Ash from combustion process

1.4.2.1. Coal ash

The fly ash from coal combustion is the most common solid waste used as a pozzolan. Fly ash is captured and removed by bag-houses or electrostatic precipitators from exhaust flue before it exits the chimney of a coal-fired power plant. It is normally light tan in color and consists mostly of silt-sized and clay-sized glassy spheres (Blissett & Rowson, 2012). Since this ash may be rich in SiO_2+Al_2O_3+Fe_2O_3, recycling it as a pozzolan is one way of disposing of it. Based on its chemical properties, fly ash is categorized as a Class F or Class C pozzolan by ASTM C618 (Table 1-1). Class F is the fly ash from anthracite or bituminous coal combustion, and is expected to have ≥ 70% SiO_2+Al_2O_3+Fe_2O_3. By contrast, Class C is the fly ash from lignite or subbituminous coal combustion, with 50-70% SiO_2+Al_2O_3+Fe_2O_3 content. It might contain ≥ 10% CaO, thus also possessing a cementitious property in addition to its pozzolanic function (ASTM, 2012a). Accordingly, Class F and C fly ashes have been studied extensively for their PA.

Class F fly ash is an acceptable pozzolan in blended cement. For instance, fly ash with 86.3% SiO_2+Al_2O_3+Fe_2O_3 content could be substituted for up to 50% cement without any negative impact on concrete strength (Siddique, 2004). Mixing this ash in cement before casting further improved the properties of concrete (strength and abrasive resistance) continuously after 91 d or 365 d curing. However, the concrete made from blended cement was weaker than that from Portland cement in the early stage of curing (≤ 28 d) due to the delay pozzolanic reaction than cement hydration. This implies that a longer curing period may be required for blended cement with fly ash. Still, another Class F fly ash (96.6% SiO_2+Al_2O_3+Fe_2O_3) lessened the micro-cracking width of concrete from

4.80 μm to 3.73 μm, since the Si proportion in concrete increased from 1.67 to 2.09 of Si/Ca ratio (Guru Jawahar et al., 2013). In addition to these regular strength and structure analyses, Lorenzo et al. (2003) assessed the performance of a Class F ash (82.3% SiO_2+Al_2O_3+Fe_2O_3) in a simulated marine environment (0.03 mol·L^{-1} $Na2SO_4$ + 0.45 mol·L^{-1} NaCl). Replacing 35% cement by fly ash raised the corrosion resistance of concretes by nearly two-fold. The diffusion of SO_4^{2+}, Na^+ and Cl^- activated the reactivity of ash, thus making the microstructure of concrete more compact and durable.

Despite having lower SiO_2+Al_2O_3+Fe_2O_3 content, Class C fly ash can be mixed with cement as a qualified pozzolan. Nassar et al. (2013) assessed the practicality of blending a Class C fly ash with cement during large-scale road construction. The concrete road base with 25% fly ash showed better strength (≈ 36 MPa) and abrasive resistance (≈ 0.31 mg mass loss) than concrete made from Portland cement alone (≈ 32 MPa and ≈ 0.35 mg). These advantages were attributed to the pozzolanic reaction of the fly ash, which made the microstructure of cement paste stronger and more compact. Accordingly, the use of fly ash can reduce the demand for cement, thus making the capital cost of construction more economical while guaranteeing the service life and quality of infrastructure.

Coal-fired power plants also generate another agglomerated ash that is not carried by exhaust gas, termed bottom ash (Canpolat et al., 2004; Kurama & Kaya, 2008). Its immobility is due to its larger particle size or its adherence to the hot side walls of boiler. Bottom ash is gray to black in color, and it is normally coarser (35.0 μm) than fly ash (13.9 μm) (Cheriaf et al., 1999; Papadakis, 1999). Yet, bottom ash has chemical properties akin to Class F fly ash, being rich in SiO_2+Al_2O_3+Fe_2O_3 (e.g. 85.0%) but

virtually free of CaO (e.g. 0.80%) (Cheriaf et al., 1999; Vasugi & Ramamurthy, 2014). Mortars with 25% bottom ash had nearly the same strength as plain mortars (97.0% at 90 d curing) (Cheriaf et al., 1999). In spite of its coarse particle size of 35 μm, a 6 h grinding could considerably enhance its PA, which made the blended mortar stronger by 27% than that with untreated bottom ash.

1.4.2.2. Biomass ash

The ash from biomass combustion might be used as a pozzolan, but its PA is not as consistent as that of coal ash pozzolans due to greater variability in the chemical composition of the starting material. Biomass is a biological organic matter from plants or plant-based lignocellulosic materials. It can be used as a fuel by the direct combustion in boilers to generate steam or heat. This energy is carbon-neutral in the short-term, which has the potential to partially replace fossil fuel for CO_2 reduction (Panwar et al., 2011). However, burning 1 kg biomass generates 0.05-0.20 kg ash, which is a solid waste with pollution potential due to its fine particle size and mineral content (Williams et al., 2012). Recycling biomass ash as a pozzolan might be an option, but its feasibility needs to be gauged more carefully than coal ash due to inconsistency in chemical composition of biomass, even when considering the same source. For example, switchgrass is a biomass fuel that can be harvested at several times during the year, depending on the producer's objectives. The SiO_2+Al_2O_3+Fe_2O_3 content of combusted switchgrass ash varied from 44.2% to 67.9% when harvested occurred from July to November (Ogden et al., 2010). Therefore, each biomass ash should be well characterized before its use as a pozzolan is considered.

Rice husk ash is frequently presented as an example of a qualified pozzolan, due to specific properties of the rice husk that make it suitable for this purpose. A typical rice husk ash (from 600 °C combustion) contained 91.7% SiO_2 with a large specific surface area of 77.4 $m^2 \cdot g^{-1}$. Mixing 10% of this ash with cement improved the strength of mortar by 16.8% (compared to a plain mortar) (Xu et al., 2012). In addition to its pozzolanic function, its fine particle size also provided a filler effect, which could significantly lessen the permeability of concrete. When mixing 10% rice husk ash (88.1% SiO_2+Al_2O_3+Fe_2O_3) with cement, the air permeability of concrete decreased from 1.08×10^{-16} m^2 to 0.08×10^{-16} m^2 after 28 d curing (Rodríguez de Sensale, 2006). Furthermore, an ultrafine fine rice husk ash could be used for high strength concrete preparation. By mixing 10% ash (88.0% amorphous SiO_2, 3.60 μm mean particle size) in cement and adjusting W/B to 0.18, the compressive strength of concrete reached 180 MPa and 210 MPa at 28 and 91 d curing (Van Tuan et al., 2011). In view of these verdicts, rice husk ash is a competitive substitute for the ultra-fine amorphous silica fume (conventional pozzolan), which is limited in its availability and is more costly than rice husk ash (Van Tuan et al., 2011).

Palm oil fuel ash also showed a competitive pozzolanic function owing to its high SiO_2+Al_2O_3+Fe_2O_3 content (45.8-79.1%) (Chandara et al., 2012; Chindaprasirt et al., 2008; Sata et al., 2010). An ultrafine ash was an efficient pozzolanic additive to produce high strength concrete. By substituting 40% or 50% cement by this ash (75.14% SiO_2+Al_2O_3+Fe_2O_3, 2.06 μm median particle size), the concrete sample achieved a compressive strength higher than 104 MPA or 158 MPa at 28 d (Aldahdooh et al., 2013; Johari et al., 2012). Due to the filler effect from the ultrafine particles, palm oil fuel ash

addition further decreased the porosity of concrete, thus lowering its chloride, air and water permeability (Johari et al., 2012). An even higher cement substitution (70%) was also appropriate with palm oil fuel ash (67.2% SiO_2+Al_2O_3+Fe_2O_3), which effectively minimized the thermal cracking risk by diminishing the hydration heat release from 57.3 °C to 41.5 °C (Awal & Shehu, 2013).

Sugarcane processing wastes might be a satisfactory pozzolan as well, such as bagasse ash and straw ash. Bagasse ash was rich in SiO_2+Al_2O_3+Fe_2O_3 (e.g. 71.1-73.9%), which enhanced the strength of concrete (20% ash) by 13% after 28 d (Chusilp et al., 2009; Somna et al., 2012). Mixing 10-30% ash could further lessen the thermal cracking risk by lowering the hydration heat release by 13 to 33%. Montakarntiwong et al. (2013) also reported the practicability of mixing 20-30% bagasse ash (89.2% SiO_2+Al_2O_3+Fe_2O_3) with cement without any reduction in concrete strength. Similar to other fine pozzolans, bagasse ash had a dual role in concrete formation, specifically, a chemical pozzolanic function and a physical filler effect (Cordeiro et al., 2008). Compared with bagasse ash, research on sugarcane straw ash concentrated mainly on its pozzolanic kinetic properties. Villar-Cociña et al. (2003) developed a simple conductivity test for kinetic analysis, which could distinguish whether the pozzolanic reaction was controlled by physical diffusion or by chemical equilibrium. This method was then validated by Frías et al. (2005). The method revealed that the sugarcane straw ash from 800 °C combustion had a higher pozzolanic reaction rate ((8.12±0.67) $\times 10^{-2}$ h^{-1}) than that from 1000 °C combustion ((6.34±0.42) $\times 10^{-2}$ h^{-1}) (Frías et al., 2007).

Aside from the biomass ash described above, there are also quite a few biomass ashes studied as pozzolans in a few papers, such as corn cob ash (Adesanya & Raheem,

2010), olive residue ash (Cuenca et al., 2013), switchgrass ash (Wang et al., 2014a), wheat straw ash (Biricik et al., 2000), bark ash (Chalee et al., 2013), bamboo ash (Villar-Cociña et al., 2011) and sawdust ash (Elinwa & Mahmood, 2002). Despite their different biomass sources and combustion regimes, they all possess a similar physiochemical trait, namely an amorphous and fine SiO_2-rich crystal structure. We conclude that such ash from biomass combustion has a comparable pozzolanic function as coal ash.

1.4.2.3. Other miscellaneous ash

There are many natural or artificial ashes that might be used as a pozzolan. For instance, ground volcanic ash is a good natural pozzolan due to its high SiO_2+Al_2O_3+Fe_2O_3 content of 83.9% (Hossain, 2005; Shi & Day, 2001). Mortars with 10% volcanic ash exhibited practically the same compressive strength as plain mortars (27 MPa at 7 d, and 36 MPa at 28 d). In the meantime, its pozzolanic contribution lessened the ASR expansion of mortar bars from 0.089 mm (plain mortars) to 0.088 mm (20% ash), 0.082 mm (30% ash) or 0.075 mm (40% ash).

The ash from municipal solid waste (MSW) incineration can be used as cement substitute. Incineration is a common treatment of MSW, since it can reduce the waste volume up to 90% while recovering the latent heat from MSW. Blending MSW ash in concrete immobilized the heavy metal elements of ash, thereby avoiding pollution from metal leaching (Shi & Kan, 2009). A fine MSW ash is also a good pozzolan. It reached a melting state after a 96 h grinding, due to the ultra-high reactive specific surface area of 79.7 m^2/g in the ash crystal (Chen et al., 2013). Mixing this ash increased the cement paste strength by ≈ 4.5% (5% ash) or ≈ 18.2% (10% ash) at 28 d. This improvement in

cement paste was exclusively attributed to the supplemental formation of C-S-H by pozzolanic reaction.

1.4.3. Blast furnace slag

Blast furnace slag is a non-metallic byproduct from iron production in blast furnace, and is also frequently used as a common pozzolan. Slag is a non-metallic byproduct from iron production that contains > 80% amorphous crystal when the molten slag is rapidly chilled by water immersion. It normally consists of 28-38% SiO_2, 30-50% CaO, 8-24% Al_2O_3 and 1-18% MgO, which indicates its pozzolanic function and cementitious property. Mixing 10-20% slag with cement kept the strength of mortar comparable to plain mortar (Tsai et al., 2014), and even boosted its chloride corrosion durability by 53.4% at 90 d (Chen et al., 2012). The high CaO content of slag increased the alkalinity of hydration solution, thus accelerating the dissolution of SiO_2 and boosting the pozzolanic reaction. Blast furnace slag also improved the durability when the concrete was exposed to extreme temperature conditions. Blending 20-30% slag in cement eased the high temperature impairment (900 °C) of concrete by up to 60% (Karakurt & Topçu, 2012). This observation was then confirmed by (Işıkdağ & Topçu, 2013),who ran a 30 cycle freeze-thaw test on the mortars with 40% slag. Moreover, curing conditions played an important role in its pozzolanic reaction. For instance, compared to a regular water curing, seawater curing was beneficial to the early strength (7 d) of the concrete with slag (from 37.6 MPa to 41.3 MPa), but harmful to the 360 d

ultimate strength (from 66.0 MPa to 56.3 MPa) (Chen et al., 2012). However, substituting cement partially with slag in a regular curing condition certainly improved the concrete performance, with lower operating cost owing to less cement usage (Gastaldini et al., 2009).

1.4.4. Other solid wastes

In addition to the ashes generated from high-temperature combustion, other solid wastes from industry possess pozzolanic function. For example, the fluid catalytic cracking catalyst residue (FC3R) from petroleum refineries was rich in reactive silica-alumina-based compounds (Zornoza et al., 2007). Payá et al. (1999) began to test this material as a "new" pozzolan. FC3R contained 48.2% SiO_2 and 46.0% Al_2O_3 with an amorphous predominately crystal structure. When mixing 30% FC3R in cement, it increased the strength of mortar by 31.8% at 28 d. FC3R also lessened the permeability of hydration products, thereby advancing the chloride resistance of the steel rebar in mortar specimens (Morozov et al., 2013). These improvements were attributed to the auxiliary formation of C-S-H, C-A-H and C-A-S-H by the SiO_2 and Al_2O_3 in FC3R (Payá et al., 2013a; Payá et al., 2003; Payá et al., 2013b).

Other solid waste materials can exhibit a good pozzolanic function, such as paper/sewage/alum sludge ash (Cyr et al., 2012; Goñi et al., 2014; Owaid et al., 2014), waste glass (Shao et al., 2000), river sand (Sinsiri et al., 2012), tincal ore waste (Kula et al., 2002), calcium carbide residue (Rattanashotinunt et al., 2013), ceramic waste (Medina et al., 2013), English red brick dust (Grist et al., 2013), and light-emitting diode

sludge (Lin et al., 2014a). The current research progress on these materials and their pozzolanic evaluation is summarized in Table S1-1. Although this review cannot cover all of them in detail, those that were identified as pozzolanic-active material possess the same physicochemical traits, namely a high SiO_2+Al_2O_3+Fe_2O_3 content with a fine particle size and amorphous structure.

1.5. Improvement of pozzolanic activity

There are several effective methods to advance the PA, such as optimizing the combustion that produces pozzolanic ash, adding chemicals during cement hydration, elevating the curing temperature, or pretreating the pozzolans (longer grinding time to reduce particle size, washing step to improve the purity of SiO_2 + Al_2O_3 + Fe_2O_3). The rationale behind these options is to increase the SiO_2 + Al_2O_3 + Fe_2O_3 content and amorphous crystal proportion of pozzolans.

1.5.1. Combustion optimization

Combustion conditions can alter the physiochemical properties of ash, thus potentially changing its PA. The factors that may be considered include the combustion temperature, retention time, cooling method, etc. These factors determine the carbon removal degree during combustion (thus affecting the SiO_2 + Al_2O_3 + Fe_2O_3 purity of ash) and influence the thermal-sensitive amorphous—crystalline transformation in ash. So far, the influence of these factors were primarily investigated with biomass combustion (Table 1-3), since the firing conditions for other combustion ashes are set by the energy generator or iron smelter. Feng et al. (2004) found that an 800 °C combustion for 4 h

produced a rice husk ash containing the highest amorphous SiO_2 of 95.7%. This ash increased the compressive strength of mortar (with 10% ash) by 42% at 91 d. However, Xu et al. (2012) supported a 600 °C combustion for 2 h for the best PA from rice husk ash. By adding 10% of this ash in mortars (W/B = 0.4), the samples had the highest compressive strength of 59.9 MPa (28 d), compared to the ash from combustion at 500 °C (49.8 MPa), 700 °C (47.4 MPa) or 800 °C (46.5 MPa). This contradiction may be attributed to other factors that differed between the experiments, such as the type of combustion furnace or cooling method. Accordingly, Nair et al. (2008) explored the impact of cooling on the microstructure of rice husk ash. They suggested a combustion at 500 °C for 12 h, with a quick cooling by immediately removing ash from oven. Compared to the slow cooling that allowed the ash to cool naturally inside the oven, quick cooling increased the amorphous ash structure, improving its PA by 1.9%. Furthermore, combustion retention (30-60 min), air supply duration (60-105 min) and cooling time (1-2 d) could jointly affect the PA of rice husk ash (Zain et al., 2011). Rice husk ash reached the highest SiO_2 content of 86.5% and lowest C content of 3.21% when the combustion, air supply and cooling lasted for 30 min, 60 min and 2 d, respectively.

Further evidence of the importance of combustion temperature in controlling PA was shown as wheat straw ash from 670 °C combustion made the cement pastes stronger by 11.5% than that from 570 °C (Biricik et al., 2000). Besides, a 700 °C and 2 h combustion could produce the paper sludge ash with the best PA (García et al., 2008). This paper sludge ash could deplete more CH at a concentration of 14.2 $mmol \cdot L^{-1}$, compared to 700 °C/5 h ash (≈ 12.4 $mmol \cdot L^{-1}$), 750 °C/2 h ash (≈ 12.6 $mmol \cdot L^{-1}$), or 750 °C/5 h ash (≈ 11.8 $mmol \cdot L^{-1}$). This illustrates the interactive effect of combustion

temperature and time on PA, which led other researchers to search for optimal combustion conditions for the best PA with corn stover bioethanol residue ash (Ataie & Riding, 2014b) and sugar cane straw ash (Frías et al., 2007), among others. Despite the evidence to date, there is no consensus in the recommended combustion parameters to maximize PA, even if the same biomass is used. The inconsistency in scientific reports is ascribed to the fact that researchers are not using uniform experimental conditions during combustion tests, since furnace type, ignition manner, airflow ventilation and other factors affecting combustion are also influencing the PA of the biomass ash generated.

1.5.2. Chemical addition during hydration

1.5.2.1. Hydration accelerator

Since pozzolanic reaction is strongly associated with cement hydration, some accelerators that are originally used for hydration may change the PA. Common hydration accelerators are Na_2SO_4, K_2SO_4, Na_2SO_3, $CaSO_4$, $CaCl_2$ (or $CaCl_2{\cdot}2H_2O$) and NaOH. Shi and Day (2001) blended 4% Na_2SO_4 or 4% $CaCl_2{\cdot}2H_2O$ to advance the PA of volcanic ash by 83.3% (Na_2SO_4) and 87.5% ($CaCl_2{\cdot}2H_2O$) at 270 d. Na_2SO_4 improved the PA at early curing age by quickening the CH consumption, but did not contribute any enhancement thereafter. Conversely, $CaCl_2{\cdot}2H_2O$ enhanced the PA throughout 270 d curing period. Shi and Day (2000b) looked into the mechanism of these accelerations in CH—volcanic ash—water mixtures. Adding 4% Na_2SO_4 could react with CH in the following manner (Eq. 1-8):

$$Na_2SO_4 + Ca(OH)_2 \rightarrow CaSO_4 \cdot 2H_2O + NaOH \qquad (1\text{-}8)$$

Consequently, the formation of NaOH promoted the alkali dissolution of SiO_2 from pozzolan, thereby accelerating the rate of pozzolanic reaction (Zhang et al., 2000). If mixing $CaCl_2 \cdot 2H_2O$ (or $CaCl_2$), a new crystal $(CaO)_3 \cdot Al_2O_3 \cdot CaCl_2 \cdot 10H_2O$—$(CaO)_3 \cdot Al_2O_3 \cdot Ca(OH)_2 \cdot 12H_2O$ formed rapidly around the C-S-H gel. This crystal was stronger and denser than C-S-H, which developed the strength and durability of concrete. However, the presence of dissolved $CaCl_2$ depressed the pH in mixtures, thus retarding the SiO_2 alkali dissolution. Consequently, a lower early strength of cement paste but a higher late strength were observed by Shi and Day (2000a) with $CaCl_2 \cdot 2H_2O$. K_2SO_4 had a similar function with Na_2SO_4 due to the same SO_4^{2-} ion (Poon et al., 2003) such that both 4% Na_2SO_4 and 4% K_2SO_4 deepened the hydration degree from 14.2% to between 21.0 and 22.3%. The enhanced hydration improved the PA by ≈ 55.5% (Na_2SO_4) or ≈ 47.8% (K_2SO_4) at 90 d of curing. The benefit of these chemical accelerators were also verified by Zhang et al. (2000) (3% Na_2SO_4), Wang et al. (2014a) (5% Na_2SO_4), and Gastaldini et al. (2007) (1% K_2SO_4). Moreover, several other chemicals also proved feasible, including 6-14% $CaSO_4$ (Poon et al., 2001b), 1% Na_2SiO_3 (Gastaldini et al., 2007), or NaOH-based synthesized compounds (Chi & Huang, 2013; Yusuf et al., 2014). Adding these chemicals would have an effect akin to Na_2SO_4, which created a stronger alkali environment either to form more crystalized CH, or to intensify the SiO_2 dissolution from pozzolans.

1.5.2.2. Other chemicals

In addition to the conventional hydration accelerators mentioned above, there are emerging materials that can improve the PA. For instance, 5-15% polypropylene fiber enhanced the PA of metakaolin and zeolite, which made blended concrete (5-10%

pozzolan) more resistant to $MgSO_4$ attack (Behfarnia & Farshadfar, 2013). Adding ≤ 10% of waste aluminosilicate catalyst improved the PA of fly ash due to a faster hydration rate in the early phases of curing (Wilińska & Pacewska, 2014). Amendment with 3% polyvinyl alcohol lessened the porosity of the cement paste with rice husk ash due to the formation of supplementary amorphous compounds (Singh & Rai, 2001). Addition of 2.25-5.00% colloidal nanosilica reinforced the early strength of cement—fly ash mortars, which was attributed to its nearly 100% amorphous SiO_2 content (Hou et al., 2013). Increasing the mixing ratio of this nanosilica was consistently beneficial to the mortar strength in early stages, but adversely affected the long-term strength after 3 month. The reason for loss of physical strength in concrete was not determined by Hou et al. (2013), and remains to be explained.

1.5.3. Elevation of curing temperature

As hydration is a temperature-sensitive and exothermic process, PA might be altered by different curing temperatures (Shi & Day, 1993). Most studies thus far stated that a higher curing temperature was advantageous, especially to the short-term PA. For example, Narmluk and Nawa (2014) found that a higher curing temperature (50 °C) improved the PA of coal fly ash in mortars by 6 times that measured at room temperature (20 °C), since it shortened the initiation of the pozzolanic reaction, from 28 d to 12 h. A similar observation was also made by Shi and Day (2000b). Moreover, the higher curing temperature (23-65 °C) merely increased the pozzolanic reaction rate, as verified with pozzolanic kinetic analysis (Shi and Day, 2000a), but did not alter any composition or microstructure of concrete. Conversely, Rojas and Sánchez de Rojas (2003) argued that the better PA of metakaolin at a 60 °C curing was attributed to greater amorphous content

of stratlingite ($Ca_2Al_2(SiO_2)(OH)_{10}\cdot 2.5(H_2O)$) in hydration products caused by the higher curing temperature.

The practicability of elevating the curing temperature for a better long-term PA was evaluated by several authors. Compared to curing at 20 °C, Hanehara et al. (2001) proved that a 40 °C curing could raise the PA of fly ash by 33.3% after 1 year. The blended mortars (20% or 30% fly ash) had a higher long-term strength with curing at 40 °C (55.0 or 55.2 MPa) than that at 20 °C (53.2 or 46.5 MPa). Yet, a 40 °C curing was rather harmful to plain mortars, and weakened the strength from 51.0 MPa to 44.7 MPa. This contrast was due to the more compact microstructure of blended mortars, which lessened the thermal expansion (Maltais & Marchand, 1997). Similar conclusions were reached by Escalante-Garcıa and Sharp (2001) and Ezziane et al. (2007) in 10-60 °C with volcanic ash, ground granulated blast furnace slag and natural pozzolan.

In spite of the studies above, no consistent correlation between curing temperature and PA emerges thus far, due to the complexity of cement—pozzolan—water system. In light of this need, Payá et al. (2000) developed a model that addressed several key factors, including curing temperature (T) (20-80 °C), cement replacement percentage by fly ash (R) (10-60%), and the compressive strength of blended mortar (S) (Eq. 1-9).

$$S = a + b \times R + c \times (T - d)^2 + e \times R \times T \qquad (1\text{-}9)$$

where a, b, c, d and e were the model coefficients, listed in Table 1-4. Consequently, this model mathematically advised a 50-60 °C curing for the strongest blended mortar. While elevated curing temperature is experimentally feasible to obtain a better PA, however, we do not recommend this method for large-scale construction, since increasing the water

temperature for curing demands much greater energy inputs than are currently feasible, particularly in cold climates where building continues through winter months and external temperatures drop to below 0 °C.

1.5.4. Pretreatment of alternative pozzolanic materials

1.5.4.1. Longer grinding

Prolonging the grinding time of a pozzolan is beneficial to its PA, since a sufficiently fine particle size increases the reactive surface area of pozzolan, and provides a strong filler effect in the microstructure of concrete. For example, a 60 min grinding could make ≥ 90% rice husk ash pass a 45 μm sieve (Zain et al., 2011). Cordeiro et al. (2008) systematically investigated the correlation among the grinding time, median particle size, Blaine fineness, PA and Ca^{2+} consumption capacity of sugar cane bagasse ash (Figure 1-1). A finer particle size (from 76.3 to 1.7 μm) consistently resulted in better PA (49-103%). The improvement of PA enhanced the strength of mortars via promoting CH consumption in the pozzolanic reaction (36-298 mg $CaO \cdot g^{-1}$). A longer grinding (10-120 min) enlarged the exterior surface area (496-979 $m^2 \cdot kg^{-1}$) of sewage sludge ash, however, it did not affect its crystalline constituent, specific gravity and internal surface area. Finer sewage sludge ash also acted as a lubricant in the microstructure of mortar, thus improving its workability by ≈ 20% (Pan et al., 2003). Conversely, Givi et al. (2010a) hold an opposite view towards the fineness of ash and the workability of concrete, based

on their study with rice husk ash. Mixing 5-20% of this fine ash (5 μm by 180 min grinding) improved the strength but reduced the workability of concrete. Their explanation was that a coarser ash particle was absorbed on the oppositely charged surface of cement particles, which restricted these particles from flocculation. Consequently, the cement particles were dispersed and could capture a larger amount of water, which reduced the water requirement to obtain a satisfactory consistency. This explanation was substantiated by Van et al. (2013). They found that a finer rice husk ash absorbed part of the aqueous phase from the C-S-H gel, thus decreasing the effective water content. Since the ash can retain water within its microstructure, longer grinding time that reduces the water-holding capacity of the ash pores would reduce PA, as demonstrated when comparing a ≥ 120 min grinding, which reduced the pore volume of ash to 116.4 $mm^3 \cdot g^{-1}$, with a 45 min grinding that yielded 135.1 $mm^3 \cdot g^{-1}$. This implies that selection of the best grinding pretreatment for a pozzolan must not simply consider the direct effect of particle size on PA and as a filler in concrete, but also how the mortar workability and water adsorption are affected by grinding.

1.5.4.2. Thermal and acid washing

Thermal and acid washing pretreatment aim to alter the chemical composition of pozzolans heating (to remove carbon) or washing (to remove alkali metal oxides and phosphate), leading to a higher purity of $SiO_2 + Al_2O_3 + Fe_2O_3$ that makes the pozzolans more reactive. For instance, after heated at 500±50 °C for 90 min in a gas furnace, palm oil fuel ash contained less carbon, based on Loss on Ignition (LOI) results of 2.62% in treated ash than untreated ash (21.6%) (Johari et al., 2012). Although treating the palm oil fuel ash at 500 °C for 1 h reduced the LOI content from 9.88% to 2.20%, this

pretreatment did not result in any amorphous-crystalline transformation or particle agglomeration (Chandara et al., 2012; Chandara et al., 2010), so the treatment simply improved the purity of the pozzolan. Acid washing of pozzolans is commonly achieved with dilute HCl or H_2SO_4 solution (1-4 $mol \cdot L^{-1}$). Acid washing can be implemented before or after the combustion that produces the pozzolanic ash, as both times are effective in removing soluble alkali metals such as Na and K, giving similar removal rates of Na_2O and K_2O (Donatello et al., 2010a; Feng et al., 2004; Rubio et al., 2011).

Despite the effectiveness of these pretreatments in controlled laboratory experiments, we do not recommend either to improve the PA of combustion ash at a commercial scale. The pretreatments imply extra energy requirements to heat or dry the pozzolans after washing. Besides, the liquid waste generated from acid washing becomes another unnecessary pollutant due to its high concentration of chloride and sulfate. These drawbacks are contradictory to the original purpose of reusing solid wastes, which is to minimize the waste volume and to diminish the GHG emissions from energy and cement consumption without increasing economic costs.

1.6. Concluding remarks

An acceptable pozzolan should be significantly rich in amorphous SiO_2, Al_2O_3 and Fe_2O_3, and its particle size should be fine enough to assure a highly reactive crystal surface. Numerous solid wastes possess these properties and have potential for use as pozzolans in blended cement. Solid wastes with the greatest potential as pozzolans, based on those currently used in the cement industry are widely available, thus having a lower cost compared to an ultrafine amorphous silica fume. Blending these materials with

cement saves raw materials, fuel and energy due to less Portland cement use, but results in the same or even superior concrete properties.

Before the industry will adopt a solid waste as pozzolan in blended cement, there are multiple considerations to be made. First, what is the appropriate criteria upon which to select an eligible pozzolan? Initial physicochemical properties give a good indication of the subsequent pozzolanic reaction, but PA changes with the pozzolan-cement ratio, the proportion of water added, use of accelerators and the curing age of the mortar. Second, is the solid waste pozzolan locally available at a competitive or lower cost than the conventional pozzolan? Third, does the concrete have equal or better strength and durability when made from a pozzolan-cement blend where the PA was conferred by solid waste? If these criteria are met, the follow-up question is whether there is a process that would enhance the PA of the solid waste ash, without generating more pollution and while producing at least as much, if not more, energy as the traditional combustion method. Some of these research avenues will be explored in the next chapters of this thesis.

1.7. Figures and tables

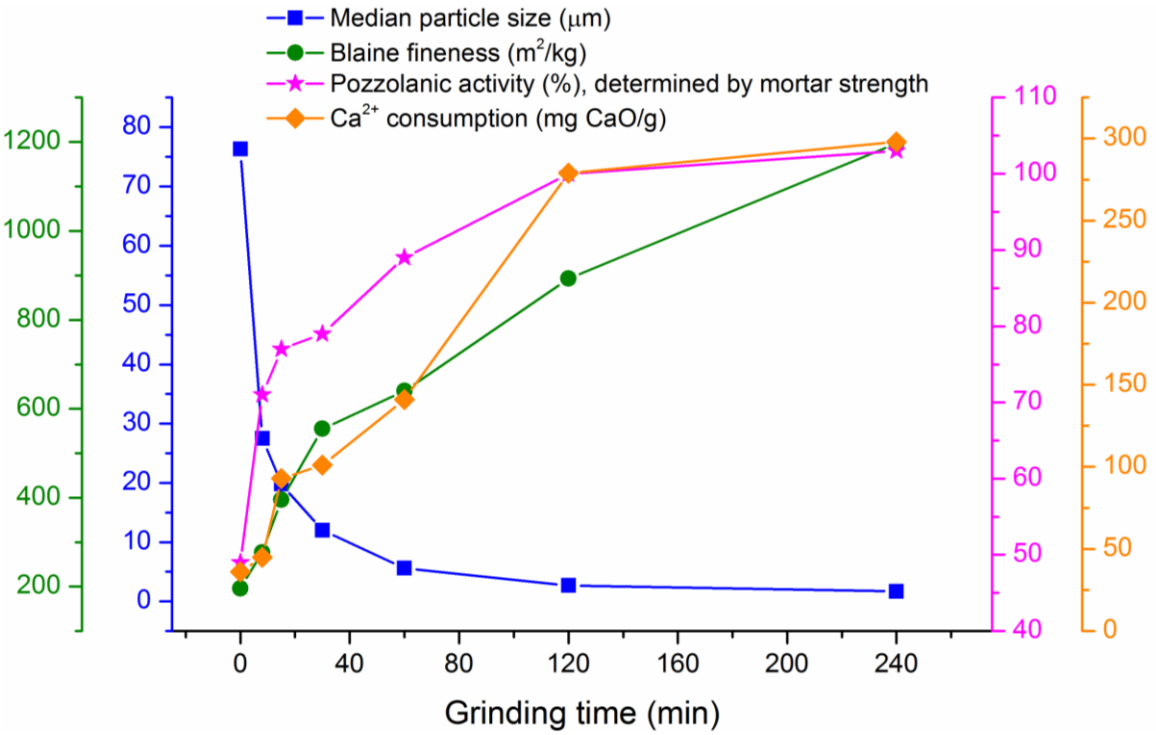

Figure 1- 1. Correlation among the grinding time, median particle size, Blaine fineness, pozzolanic activity, and Ca^{2+} consumption capacity of sugar cane bagasse ash.

It is modified from the work of Cordeiro et al. (2008).

Table 1- 1. Chemical and physical criteria that qualify coal fly ash as a pozzolan, regulated by ASTM C618 (ASTM, 2012a).

ASTM C618 criteria	Class N (Natural pozzolan)	Class F	Class C
Chemical requirement			
$SiO_2+Al_2O_3+Fe_2O_3$, min, %	70	70	50
SO_3, max, %	4	5	5
Moisture content, max, %	3	3	3
Loss on Ignition (LOI), max, %	10	6	6
Physical requirement			
Amount retained when wet-sieved on 45 um (No. 325) sieve, max, %	34	34	34
Strength with Portland cement, at 7 d, min, % of control	75	75	75
Strength with Portland cement, at 28 d, min, % of control	75	75	75
Water requirement, max, % of control	115	105	105
Autoclave expansion or contraction, max, %	0.8	0.8	0.8

Table 1- 2. Representative physiochemical characteristics of conventional pozzolans and solid wastes that were tested as pozzolans.

Class	Pozzolanic materials	Chemical composition (wt. %), determined by X-ray diffraction (XRD)									Mean particle size	Median particle size (d_{50})	Specific gravity	BET surface area	Ref.
		SiO_2	CaO	Al_2O_3	Fe_2O_3	MgO	K_2O	Na_2O	SO_3	LOI	μm	μm	1	m^2/g	
Conventional	Silica fume	94.00	0.40	0.10	0.10	0.40	0.90	0.10	1.50	2.70	0.10	—	2.16	—	(Nehdi et al., 2003)
Conventional	Metakaolin	52.10	0.07	41.00	4.32	0.19	0.63	0.26	0.00	0.60	—	—	2.50	—	(Payá et al., 2013a)
Coal ash	Coal fly ash	53.50	3.38	20.40	8.66	0.00	0.00	0.00	0.00	0.86	13.90	—	2.25	1.20	(Papadakis, 1999)
Coal ash	Coal bottom ash	56.00	0.80	26.70	5.80	0.60	2.60	0.20	0.10	4.60	35.00	—	2.00	—	(Cheriaf et al., 1999)
Biomass ash	Rice husk ash	84.75	2.78	0.16	0.00	2.32	2.57	0.37	0.60	3.72	—	10.00	2.16	—	(Sata et al., 2012)
Biomass ash	Palm oil fuel ash	65.30	6.40	2.60	2.00	3.10	5.70	0.30	0.50	10.10	—	10.10	2.33	—	(Sata et al., 2007)
Biomass ash	Sugar cane bagasse ash	55.00	11.00	5.10	4.10	0.90	1.20	0.20	2.20	19.60	—	5.60	2.27	—	(Somna et al., 2012)
Biomass ash	Wood ash	41.00	11.40	9.30	2.60	2.30	3.90	0.90	0.00	0.00	—	—	—	40.29	(Rajamma et al., 2009)
Biomass ash	Corn cob ash	66.38	11.57	7.48	4.44	2.06	4.92	0.41	1.07	0.00	—	—	—	—	(Adesanya & Raheem, 2009b)
Biomass ash	Switchgrass ash	67.18	12.28	0.68	0.31	2.05	1.24	0.11	0.00	14.77	65.00	—	1.79	41.25	(Wang et al., 2014a)
Biomass ash	Wheat straw ash	83.80	12.54	4.55	1.05	2.39	0.00	0.00	1.49	7.22	—	—	2.41	—	(Biricik et al., 2000)
Biomass ash	Olive residue ash	11.84	54.82	2.60	1.38	4.36	9.26	0.16	0.00	11.73	—	—	—	—	(Cuenca et al., 2013)
Biomass ash	Sawdust ash	67.20	9.98	4.09	2.26	5.80	0.11	0.08	0.45	0.00	—	—	2.29	—	(Elinwa & Mahmood, 2002)
Other ash	Sewage sludge ash	50.60	1.93	12.80	7.21	1.48	1.70	0.32	2.38	21.58	—	—	2.61	1.09	(Pan et al., 2003)
Other ash	Fluid bed combustion ash	35.40	23.50	12.90	3.30	1.60	1.60	0.60	10.60	8.30	—	—	—	—	(Havlica et al., 1998)

Other ash	Activated alum sludge ash	47.00	0.41	41.94	4.86	0.40	0.99	0.09	0.10	2.64	—	—	2.53	—	(Owaid et al., 2014)
Other ash	Cattle manure ash	52.00	15.40	7.79	3.20	2.94	4.91	0.66	1.54	2.50	—	—	0.81	0.56	(Zhou et al., 2012)
Blast furnace slag	Ground granulated blast furnace slag	35.11	37.56	17.63	0.35	5.52	0.00	0.32	0.00	0.75	—	—	—	—	(Karakurt & Topçu, 2012)
Other solid wastes	Fluid catalytic cracking catalyst residue	48.20	0.01	46.00	0.95	0.01	0.01	0.50	0.04	1.50	—	—	2.42	—	(Payá et al., 2013a)
Other solid wastes	Zeolite	67.79	1.68	13.66	1.44	1.20	1.42	2.04	0.50	0.00	—	—	2.20	—	(Behfarnia & Farshadfar, 2013)
Other solid wastes	Glass powder	72.80	4.90	1.40	0.00	3.40	0.30	16.30	0.00	0.00	150.00	—	2.40	—	(Shao et al., 2000)
Other solid wastes	River sand	91.20	0.70	1.80	0.20	0.10	2.30	0.10	0.00	1.80	—	2.20	2.61	—	(Sinsiri et al., 2012)
Other solid wastes	Milos earth	58.23	7.40	14.22	4.31	1.43	2.24	1.30	1.16	0.00	—	—	—	—	(Papadakis & Tsimas, 2002)
Other solid wastes	Diatomaceous earth	22.33	45.89	0.96	1.00	1.54	0.10	0.32	1.24	0.00	—	—	—	—	(Papadakis & Tsimas, 2002)
Other solid wastes	Silica breccia	82.10	0.83	8.78	0.82	0.04	3.10	2.33	0.00	0.70	75.00	—	2.70	—	(Hassan et al., 2014)
Other solid wastes	Tincal ore waste	17.11	16.94	2.61	0.41	15.40	1.05	0.21	0.00	28.90	—	—	2.41	—	(Kula et al., 2002)
Other solid wastes	Ceramic Waste	67.03	0.11	19.95	6.29	1.37	3.54	0.21	0.00	0.47	—	—	—	3.00	(Sánchez de Rojas et al., 2014)
Other solid wastes	Slate waste	62.74	1.13	18.55	6.80	2.30	4.26	1.18	0.21	0.00	—	63.00	—	—	(Frías et al., 2014)
Other solid wastes	Refinery waste catalyst	39.20	0.10	59.40	0.00	0.00	0.00	0.00	0.00	1.30	—	—	2.60	—	(Lin et al., 2014b)

Table 1- 3. Experimental details of pozzolan testing and final recommendations for improving the pozzolanic activity of biomass combustion ash

Materials	Initial load g	Temperature ℃	Heating rate ℃/min	Retention h	Combustion equipment	Grinding min	Condition recommended for the best pozzolanic activity	Ref.
Rice husk ash	—	500, 600, 700, 800	20	2	Electric oven	120	600 ℃ combustion	(Xu et al., 2012)
Rice husk ash	100	700	10	0.25, 1, 4, 8, 16	20×28×2 cm stainless steel tray	20	4 h combustion	(Vayghan et al., 2011)
Rice husk ash	—	550, 600, 700, 800, 900, 1000	—	4	—	60	800 ℃ combustion + 1 mol HCl washing	(Feng et al., 2004)
Rice husk ash	—	—	—	—	Designed oven	30, 60	60 min grinding + 30 min fire + 60 min air supply + 2 d cooling	(Zain et al., 2011)
Rice husk ash	—	600, 750, 900 (combustion & gasification)	—	0.5	—	—	750 ℃ gasification	(Wansom et al., 2010)
Rice husk ash	20,000	Max. 600 (open combustion)	—	—	—	—	—	(Chindaprasirt et al., 2007b)
Rice husk ash	20,000-25,000	—	—	—	Modified incinerator	0-540	45 min grinding	(Van et al., 2013)
Rice husk ash	—	500, 700, 900	—	0.25, 6, 12, 24	—	—	500 ℃ combustion + 12 h + quick cooling	(Nair et al., 2008)
Rice husk ash	—	850	—	0.17-0.25	Boiler	75	—	(Chatveera & Lertwattanaruk, 2011)
Rice husk ash	—	750, 830	—	—	—	—	750 ℃ combustion + extra air supply	(Nehdi et al., 2003)
Rice husk ash	20,000	Max. 650	—	—	Open burning in small heap	—	—	(Chindaprasirt et al., 2008)

Rice husk ash	—	650	3.3	1	Industrial furnace	—	—	(Ganesan et al., 2008)
Wheat straw ash	200	500, 650, 700, 800	—	1, 2, 3	Programmable electric muffle furnace	60	650 °C/1 h combustion + 80 °C/24 h 0.1 mol·L^{-1} HCl washing	(Ataie & Riding, 2012)
Wheat straw ash	—	670	—	5	Electric furnace	—	Quick cooling after combustion	(Biricik et al., 2000)
Wheat straw ash	—	570, 670	—	5	Steel trays	—	670 °C combustion	(Hasan et al., 1999)
Bagasse-rice husk-wood ash	—	700-900	—	—	—	—	Grinding until < 2% particle retained on sieve No. 325	(Horsakulthai et al., 2011)
Rice husk-bark ash & palm oil fuel ash	—	800-900	—	—	Fluidized bed combustion	—	Grinding until < 3% particle retained on sieve No. 325	(Sata et al., 2007)
Palm oil fuel ash	—	500±50	—	1.5	Gas furnace	—	Grinding to the median particle size of 2.06 µm	(Johari et al., 2012)
Palm oil fuel ash	—	800-1000	—	—	Steam power plant	—	Grinding until < 3% particle retained on sieve No. 325	(Tangchirapat et al., 2012)
Paper sludge	—	600, 650, 700, 750, 800	—	2, 5	Electric laboratory furnace	—	700 °C/2 h combustion	(García et al., 2008)
Paper sludge	—	700, 720-740	—	2	Lab furnace, fluidized bed combustion system	—	700 °C/2 h combustion in lab furnace	(Frías et al., 2013)
Paper sludge	—	700	—	2	Electric laboratory furnace	—	—	(Goñi et al., 2014)
Banana leaves ash	—	900	—	24	—	30	—	(Kanning et al., 2014)
Slate waste	—	1000	—	2	Electric furnace	—	—	(Frías et al., 2014)
Activated alum sludge ash	—	800	5	2	Electric laboratory furnace	—	Pretreatment of 105 °C/24 h thermal activation	(Owaid et al., 2014)
Bioethanol byproduct (corn	200	500, 650	—	1, 2	—	—	500 °C/2 h combustion + 80 °C/4 h 0.1 mol·L^{-1}	(Ataie & Riding, 2014b)

stover)							HCl washing	
Switchgrass ash	492-1323	≈ 411	—	0.083	Lab-designed furnace	0.5	Adding 5% Na_2SO_4 or 5% $CaCl_2 \cdot 2H_2O$	(Wang et al., 2014a)
Sugar cane straw ash	—	800, 1000	—	0.3	Electric furnace	—	800 °C combustion	(Frías et al., 2007)
Corn cob ash	—	650 (open air combustion)	—	8	Blacksmith furnace	—	—	(Adesanya & Raheem, 2009a)
Bamboo leaf ash	—	600	—	2	Electric furnace	—	Grinding to < 90 μm of particle	(Villar-Cociña et al., 2011)

Table 1- 4. Model coefficients (a, b, c, d and e) and standard deviation (δ) derived by Eq. 1-9 to address the correlations among curing temperature, cement replacement by fly ash (R), and the compressive strength of blended mortar, modified from the work of Payá et al. (2000).

R (%)	a	b	C	d	e	δ (MPa)
0	39.55	-0.403	-0.00567	68.41	0.00169	2.3
10	40.80	-0.419	-0.00727	62.87	0.00219	2.5
40	40.98	-0.396	-0.00768	62.46	0.00302	3.0
60	42.07	-0.383	-0.00866	61.85	0.00278	2.7

CONNECTING PARAGRAPH TO CHAPTER 2

As concluded in Chapter 1, numerous solid wastes have potential for use as pozzolans in blended cement. The ash from biomass fuel combustion is a major category of these solid wastes. When considering biomass combustion with ash recycling as a pozzolan, the energetic output needs to be quantified to ensure that capital expenses and operating costs can be recovered, given the low value of biomass combustion ash, even if it possesses PA. . Chapter 2 aims to optimize the energy produced from combustion by 1) investigating the effect of excess air on the combustion of switchgrass and hardwood, 2) assessing their ash fouling and slagging tendencies, and 3) performing an in-depth thermogravimetric kinetic analysis to understand their combustion performance.

CHAPTER 2. Characterizing the Combustion of Low Carbon Fuel

Exploring switchgrass and hardwood combustion on excess air and ash fouling/slagging potential: laboratory combustion test and thermogravimetric kinetic analysis

2.1. Abstract

Biomass combustion generates renewable energy, which is optimized by designing a biomass combustion system that controls excess air intake and evaluates the ash fouling/slagging potential. The objective of this study was to 1) investigate the effect of excess air ratio (EAR) on the combustion of switchgrass (*Panicum vigratum L.*) and hardwood, 2) assess their ash fouling and slagging tendencies, and 3) perform an in-depth thermogravimetric kinetic analysis to understand their combustion. Switchgrass and hardwood contained 17.5 and 17.7 $MJ \cdot kg^{-1}$ of energy value, which was appropriate for heat generation. The greatest energy conversion efficiency and combustion completeness rate were obtained with an EAR of 20% for switchgrass and 30% for hardwood based on our combustion system design with 4 mm particle of fuel form. Kinetic analysis confirmed that increasing the oxygen availability resulted in superior energy conversion. Switchgrass ash had lower fouling and slagging tendencies than hardwood, and could be a better biomass fuel for a commercial-scale boiler. Heat and mass transfer delays were still observed from this combustion system, thus making the combustion request more air to even achieve a stoichiometric condition. However, rather than an ideal test (e.g. single particle combustion), the conclusions made by this study were particularly valuable for

boiler operations, since the heat and mass transfer delays were a common phenomenon in real applications that should not be eliminated in our lab-scale studies.

2.2. Introduction

Switching to biomass fuel has the potential to lower the carbon footprint in many industries because biomass is carbon-neutral, compared to fossil fuels such as coal (Demirbas et al., 2009). Energy conversion from biomass fuel is readily achieved by direct combustion, an exothermic chemical reaction between carbohydrate material and oxygen. Compared to other common biomass energy conversions (e.g. gasification or pyrolysis), direct combustion requires little extra infrastructure when fossil fuel is switched to biomass fuel. Thus, it is more technically feasible and has lower capital cost particularly for large power levels (Demirbaş, 2001). The air intake at combustion determines the energy conversion and emissions from biomass (Demirbas, 2004). Insufficient air causes more CO emission and inferior energy efficiency due to unburnt carbon (Varol et al., 2014). However, there are many factors in boilers that decrease the air utilization efficiency and retard the combustion completeness, such as the heat and mass transfer delays. Hence, a biomass boiler typically incorporates 10-30% of excess air, above that required by stoichiometric condition (0% of excess air), to maximize the energy output (Nussbaumer, 2003). Yet, an overly high input of excess air in boilers will actually lower the combustion temperature due to heat convection and radiation, thereby degrading the theoretical energy efficiency according to the Carnot thermodynamic cycle.

Another crucial factor in biomass combustion is ash deposition. Alkali metals (Na_2O and K_2O) in biomass can react with SiO_2 to form alkali silicate that melts at $\leq$ 700 °C. When these sticky particles adhere to the cooler surface of the combustor, it

results in a fouling problem. Meanwhile, Na_2O and K_2O also react with sulfur if the temperature is ≥ 700 °C, which forms alkali sulphate that deposits on the heat transfer surface (slagging problem) (Fang & Jia, 2012). Fouling and slagging reduce the heat transfer and accelerate corrosion of the combustor walls (Teixeira et al., 2013). Thus, some empirical indices were developed to assess the fouling and slagging tendencies of biomass fuel, including basic-acid ratio (BA), fouling index (FI), slagging index (SI) and slag viscosity ratio (SVR) (Teixeira et al., 2012). These predictive indices have proved consistent with real observation of combustion systems that were fed with woody and agricultural waste (Tortosa Masiá et al., 2007), straw and wood pellet (Teixeira et al., 2012) and sewage sludge (Degereji et al., 2013). Hence, the fouling and slagging tendencies of biomass fuels need to be considered in designing biomass combustion systems.

Several biomass fuels are emerging as substitutes for fossil fuels in eastern Canada due to the suitable climate and acreage available for their growth, including switchgrass and hardwood residues. Switchgrass is a perennial warm-season bunchgrass that yields up to 25 tonnes of dry matter per hectare (Kumar & Sokhansanj, 2007). It is rich in volatile content (70.1-85.2%) and has an excellent calorific value (18.0-26.2 $MJ \cdot kg^{-1}$) (Vamvuka et al., 2010). Hardwood residues are forestry wastes from sawmills and other forestry operations that have a great gross energy value compared to conventional biomass, such as poplar (18.5 $MJ \cdot kg^{-1}$), cereal straw (17.3 $MJ \cdot kg^{-1}$) or bagasse (19.4 $MJ \cdot kg^{-1}$) (McKendry, 2002). Although combustion of these fuels was studied, including fuel characterization (Ogden et al., 2010), emissions (Amaral et al., 2014) and ash properties (Wang et al., 2014a), I am not aware of any published work that

examined how excess air affects their combustion, and the fouling and slagging risks of these fuels in biomass combustion systems.

Empirical data can be obtained from pilot-scale combustion systems where switchgrass or hardwood residues are the fuel sources, but such data is specific to the operating system and cannot be extrapolated to larger-scale biomass combustors. Kinetic analysis generates information that can be scaled up to optimize the function of commercial-scale biomass combustion systems in real-time (Kok, 2012). For instance, choosing the right temperature to optimize the energy conversion process requires kinetic analysis (White et al., 2011), through methods such as non-isothermal thermogravimetric analysis with the Coats-Redfern algorithm (Várhegyi, 2007; Vyazovkin & Wight, 1997). With this method, blends of coal and pine sawdust were studied from 25 to 700 °C with 15 °C·min^{-1} of heating rate. Coats-Redfern algorithm was applied to determine the kinetic parameters, assuming combustion was a two-state solid-state reaction (Gil et al., 2010). Furthermore, this method was also successfully used to investigate the combustion of corn straw (Fang et al., 2013), peanut-tamarind shells (Kuprianov & Arromdee, 2013), and sewage sludge (Xiao et al., 2010).

This paper aimed to build up a laboratory combustion system to provide some recommendations for real boiler operations. Based on this design, I investigated the effect of excess air (0, 10, 20 and 30%) on the combustion of switchgrass and hardwood (4 mm particle size). During these energy conversion processes, I examined the factors including fuel mass loss, temperature and gaseous emissions. Additionally, the ash from the 30% excess air test was characterized to assess its fouling and slagging tendencies. Furthermore, kinetic analysis of data collected from a non-isothermal thermogravimetric

analysis-differential scanning calorimetry (TGA-DSC) provided an in-depth understanding of the combustion properties of switchgrass and hardwood.

2.3. Material and methods

2.3.1. Materials preparation and characterization

Switchgrass was collected from Williamsburg and hardwood residues (made of sawdust, free of additives) was gathered from Groupe Savoie Inc., Canada. Subsamples of each residue were pulverized with a Pellet Pros Electric 1000E hammer mill to ≈ 4 mm of particle size (No. 5 mesh) and all analyses were performed in triplicate. About 10 mg of ground sample was tested by the sequential thermogravimetric method for proximate analysis. Ultimate analysis was performed on about 25 mg of ground sample by micro-combustion with a Carlo Erba EA 1108 elemental analyzer. Sulfur content was measured with a HELIOS analyzer at 1350 °C. Higher heating value (HHV) was measured with an oxygen bomb calorific meter. Major mineral oxides and trace metal elements were characterized by the Fusion Inductively Coupled Plasma (Fusion-ICP) with a Varian Vista 735 ICP analyzer. Molecular formula $CH_xO_yN_zS_w$ were determined from the ultimate analysis. Stoichiometric air-fuel ratio (SAFR) was calculated by assuming a stoichiometric combustion of switchgrass and hardwood (Eq. 2-1 and 2-2) (Yang et al., 2005).

$$CH_xO_yN_zS_w + (1 + \frac{x}{4} + z + w - \frac{y}{2})(O_2 + 3.76N_2) = CO_2 + \frac{x}{2}H_2O + 3.76 \times aN_2 + zNO_2 + wSO_2 \quad (2\text{-}1)$$

$$SAFR = \frac{\left(1 + \frac{x}{4} + z + w - \frac{y}{2}\right) \times 28.97}{12 + x + 16 \times y + 14 \times z + 32 \times w} \quad (2\text{-}2)$$

where I assumed an exact stoichiometric condition for switchgrass or hardwood combustion, and the molecular mass of air was 28.97 $g \cdot mol^{-1}$.

2.3.2. Combustion system design

A microscopic combustion system was designed for this study (Figure 2-1 and S2-1). The geometry of combustion chamber was 23.0 × 30.5 × 17.0 cm^3. A fine mesh-wire basket (400 μm, No. 40 mesh) as a fuel holder (9.2 × 9.2 × 9.2 cm^3) was installed inside the combustion chamber. The fine mesh ensured even distribution of air around the fuel. Fuel was ignited by an external torch at the vertical midpoint of fuel holder. To measure the fuel mass loss during combustion, the fuel holder was suspended from an Elane load cell with an Inter-technology P3 strain interpreter. Two thermocouple sensors were placed, one at the bottom and one at the top of the fuel holder. Airflow was expelled through a Bernoulli's ejector with an airflow volume speed sensor (Rahman et al., 2010). In addition to an initial ventilation unit that provided 9.93 $g \cdot min^{-1}$ of air, I set up an adaptable pump for extra air supply (Figure S2-2). A fine gas sampling pipe was set on the ejector. Emissions (O_2, CO and CO_2) were analyzed by a Gasboard-3100P gas analyzer. All *in situ* measurements were recorded by a data acquisition system.

2.3.3. Combustion test

Adjusting the pump voltage and initial fuel load permitted control of the EAR from 1.0 to 1.3 (0%-30% of excess air) to determine how this parameter affected combustion of switchgrass and hardwood (Table 2-1). The stoichiometric test with 0% of

excess air (1.0 EAR) was considered as the control group. In each test run, biomass was loaded in the fuel holder before combustion. Fuel mass loss and temperature change were monitored throughout a 90 min combustion. Based on the *in-situ* gaseous volume concentration V(t) (%) in exhaust measured by gas analyzer, the total CO and CO_2 emissions and O_2 consumption by 90 min combustion were calculated by Eq. 2-3 and 2-4.

$$CO\ or\ CO_2\ total\ emission = \frac{5400 \times N \times S \times \int_0^{90} V(t)\ dt}{100 \times 22.4 \times M_f} \quad (2\text{-}3)$$

$$O_2\ total\ consumption = \frac{5400 \times N \times S \times \int_0^{90} 21 - V(t)\ dt}{100 \times 22.4 \times M_f} \quad (2\text{-}4)$$

where N was the molecular mass of CO, CO_2 and O_2 ($g \cdot min^{-1}$), and S was the volume velocity of exhaust ($L \cdot s^{-1}$). M_f corresponded to the mass of fuel load in each batch of tests (g). After the tests, the residues were sampled, and char was separated from ash using a No. 35 sieve (500 μm). Each test was replicated three times.

2.3.4. Combustion performance evaluation

Energy conversion efficiency (ECE) and combustion completeness rate (CCR) were estimated to compare the combustion performance. By considering the combustion as a "black box" with various calorific inputs and outputs (Figure S2-3), ECE (%) referred to the ratio of heat release versus the total calorific inputs (Eq. 2-5). Meanwhile, the CCR ($\%\cdot min^{-1}$) was obtained by Eq. 2-6 to reveal the speed of fuel mass loss during the 90 min combustion.

$$ECE = \frac{M_f \times HHV_f - M_{CO} \times HHV_{CO} - M_{ch} \times HHV_{ch}}{M_f \times HHV_f} \times 100 \quad (2\text{-}5)$$

$$CCR = \frac{M_f - M_{ch} - M_a}{90\ min} \quad (2\text{-}6)$$

where M_f, M_{CO}, M_{ch} and M_a are the initial fuel mass, total CO emission and char product mass. HHV_f, HHV_{CO} and HHV_{ch} correspond to the HHV of fuel (17.5 $MJ \cdot kg^{-1}$ switchgrass, 17.7 $MJ \cdot kg^{-1}$ hardwood), CO (20.5 $MJ \cdot kg^{-1}$) and char (29.6 $MJ \cdot kg^{-1}$), respectively.

2.3.5. Ash characterization and fouling/slagging assessment

As 30% of excess air is commonly injected into commercial-scale boiler systems, I selected the ash from 1.3 EAR test for fouling and slagging assessment. The mineral composition of ash was analyzed by X-ray fluorescence (XRF) with a PW2400 wavelength dispersive XRF spectrometer. Several empirical indices of the fouling and slagging tendencies were estimated, including the base-acid ratio (BA), fouling index (FI), slagging index (SI) and slag viscosity ratio (SVR) (Barroso et al., 2007).

2.3.6. Combustion kinetic analysis

2.3.6.1. Experimental setup

Kinetic analysis requires experimental data on the thermal decomposition rate, which was collected from the TGA-DSC performed on a NETZSCH TG 449 F3 Jupiter Analyzer. About 18 mg of switchgrass or 36 mg of hardwood (owing to their density difference) was heated to 900 °C (10 $°C \cdot min^{-1}$) in air atmosphere (20 $mL \cdot min^{-1}$) during the TGA-DSC analysis. Each test was replicated three times.

2.3.6.2. Kinetic modelling

Kinetic analysis used the Coats-Redfern algorithm with a two-step solid-state reaction model (Figure S2-4) (Gil et al., 2010; Sahin et al., 2001; White et al., 2011). By assuming the combustion process was governed by the first-order Arrhenius law, the kinetic model was expressed by Eq. 2-7, 2-8 and 2-9,

$$\alpha = \frac{m_0 - m_t}{m_0 - m_f} \tag{2-7}$$

$$\frac{d\alpha}{dt} = kf(\alpha) \tag{2-8}$$

$$k = Aexp(\frac{-E_a}{RT}) \tag{2-9}$$

where α is the decomposition rate obtained from the TGA-DSC and m_0, m_t and m_f (mg) represented the initial mass, the mass at time t (min), and the final mass of sample. The function f(α) represents the mechanism functions usually employed for the kinetic study of solid-state reaction, which depends on the chemical reaction/diffusion control or the size and shape of the reacting particles. Additional details on the 14 groups of probable mechanisms of solid-state combustion model, including units associated with each mechanism function, are provided in Table S2-1. k is the reaction rate, and A (min^{-1}) is the pre-exponential factor. E_a ($kJ \cdot mol^{-1}$) corresponds to the activation energy of combustion. R is the gas constant (8.314 $J \cdot mol^{-1} \cdot K^{-1}$) and T (K) the absolute temperature. Thus, the kinetic modeling was performed according to Eq. 2-10 and 2-11,

$$g(\alpha) = \int_0^{\alpha} \frac{d\alpha}{f(\alpha)} = \frac{A}{\beta} \int_{T_0}^{T} \exp\left(\frac{-E_a}{RT}\right) dT \tag{2-10}$$

$$\ln\left[\frac{g(\alpha)}{T^2}\right] = \ln\left[\frac{AR}{\beta E_a}\left(1 - \frac{2RT}{E_a}\right)\right] - \frac{E_a}{RT} \quad (2\text{-}11)$$

where g(α) is the integral function of solid-state reaction mechanism and further described in Table S2-1. T_0 (K) stands for the initial temperature of TGA-DSC test. β corresponds to the heating rate during TGA-DSC test, at 10 °C·min^{-1} in this work. For most values of E_a and T generated during combustion, the term $\ln[AR/\beta E_a(1\text{-}2RT/E_a)]$ in Eq. 2-11 is considered to be a constant. A linear regression is attained after plotting $\ln[g(\alpha)/T^2]$ versus 1/T. Meanwhile, a high linear correlation coefficient ($-R^2$) should be obtained if the f(α) in Table S2-1 is optimized. Consequently, combustion mechanism and E_a could be acquired by choosing an $-R^2$ that is close to 1.

2.3.7 Statistical analysis

Comparison of switchgrass and hardwood combustion (effect of excess air) was analyzed statistically using a Fisher's Least Significant Difference (LSD) test (at a 0.05 significant level).

2.4. Results and discussion

2.4.1. Physiochemical properties

Initially, switchgrass and hardwood contained 80.6% and 80.0% of volatile content, and 8.21% and 12.7% of fixed carbon by mass, respectively (Table 2-2(a)). As shown in Table 2-2(b), the oxygenation of switchgrass (52.2% of oxygen) and hardwood

(51.0%) resulted in higher heating values of 17.7 $MJ \cdot kg^{-1}$ (switchgrass) and 17.5 $MJ \cdot kg^{-1}$ (hardwood) that are less than the 24.1 $MJ \cdot kg^{-1}$ reported for coal (Weiland et al., 2012). Nitrogen and sulfur contents of switchgrass (0.60% of N and 0.06% of S) and hardwood (0.01% of N and 0.02% of S) were much less than a representative coal (1.20% of N and 4.87% of S) (Weiland et al., 2012), suggesting that greater reliance on biomass fuel might reduce NO_x and SO_x emissions compared to the coal.

Molecular formula of switchgrass was $CH_{1.7027}O_{0.9476}N_{0.0125}S_{0.0005}$ (29.1 $kg \cdot kmol^{-1}$) and hardwood was $CH_{1.7299}O_{0.8937}N_{0.0002}S_{0.0002}$ (28.0 $kg \cdot kmol^{-1}$) (Table 2-2(c)). Stoichiometric air-fuel ratio (SAFR) was 0.96 for switchgrass and 1.02 for hardwood, which is much lower than fossil fuels such as coal (7.1), natural gas (17.2) and gasoline (14.7) (Nussbaumer, 2003). Their lower SAFR were attributed to the considerably less C but higher H and O contents than fossil fuels. Hardwood had 0.78% ash, which was approximately 5-fold less than switchgrass (4.69%); as well hardwood contained nearly 10-fold less SiO_2 and tended to have lower alkali metal (Na_2O and K_2O) content than switchgrass (Tables 2-2(a), Table 2-3). The appreciable ash content and presence of alkali metals, SiO_2 and sulfur in these biomass fuels is an indication that fouling and slagging could occur in biomass combustion systems using switchgrass and hardwood (Jenkins et al., 1998).

2.4.2. Effect of excess air on fuel combustion

The mean yield of ash and char were affected by different EAR (Figure 2-2 and Table S2-2). Hardwood combustion consistently generated less residues (1.01%-1.27% of ash and 1.61%-2.50% of char, by mass) than switchgrass (3.19%-4.94% ash and 3.82%-5.73% of char). Higher char yield of switchgrass can be explained by the ash coagulation,

whereby ash agglomerates with unburned carbon (Lind et al., 2000; McLennan et al., 2000). Because the char was separated by screening, some agglomerated ash was categorized as the char, which could be increasing the apparent char yield from switchgrass combustion. Compared to the control group, more excess air (10%-30%) boosted the combustion completeness and reduced the amount of unburned residues. As for the switchgrass, there was no significant difference in the ash yield from 1.0 EAR (4.93%) and 1.1 EAR (4.94%) tests (P = 0.90). Ash yield declined to 4.20% and 3.18% with more air supply (1.2 and 1.3 EAR) and the lowest char production (3.82%) occurred at 1.2 EAR compared to the other excess air levels, which was interpreted to mean that more complete switchgrass combustion was achieved at 1.2 EAR condition. Regarding the hardwood, there was no statistically significant difference in the ash yield from among the 1.0, 1.2 and 1.3 EAR treatments (Figure 2-2). Increasing the EAR from 1.0 to 1.1 reduced the char yield significantly (P = 5.84E-4), from 2.50% to 1.87%. Yet, continuing to increase the EAR to 1.3 resulted in no further reduction in char yield. This observation indicates that 10% of excess air was sufficient for a complete hardwood combustion.

Mass loss profiles follow a predictable pattern, where the first stages of combustion result in early moisture removal (minor mass loss), followed by fast volatile separation (dramatic mass loss) and slow char oxidation (gentle mass loss) (Nussbaumer, 2003). Increasing the EAR altered the mass loss profile of switchgrass, compared to stoichiometric conditions (1.0 EAR) during the fast volatile separation step (up to 65 min in the combustion), such that greater mass loss due to volatile combustion occurred when the EAR was set at 1.2 and 1.3 (Figure 2-3(a)). By contrast, the major variance in

hardwood mass loss profiles at various EAR occurred from 0-20 min (Figure 2-3(b)). This indicated that excess air injected in the combustion system accelerated the early steps of fast volatile separation of hardwood in the first 20 min following ignition. Thereafter, mass loss was slower with EAR > 1 than the stoichiometric condition, although all mass loss curves converged from 50-90 min indicating that the late char oxidation phase was unaffected by EAR during hardwood combustion.

Combustion temperature measured in the fuel holder was always lower at the top (e.g., from 523 to 662 ^{o}C with switchgrass; Table 2-4) than the bottom (882 to 1129 ^{o}C with switchgrass) because the top of the fuel holder encountered an intense convective heat transfer effect. The greatest combustion temperatures for switchgrass were achieved with 1.1 EAR. This disparity was also be observed in the hardwood combustion test, where temperatures at the top of the fuel holder were generally lower than those at the bottom (Table 2-4). The greatest combustion temperatures were reached at 1.3 EAR (821 ^{o}C at the bottom of the fuel holder) and 1.0 EAR (735 ^{o}C at the top of the fuel holder).

Since oxygen supply for combustion was determined by the excess air amount, the total CO and CO_2 emissions as well as O_2 consumption were related to the EAR (Figure 2-4). Consequently, CO_2 emission and O_2 consumption were greater with a higher EAR during the combustion of switchgrass. Simultaneously, the 1.3 EAR level gave a significantly higher CO emission (18.0%) than 1.0 EAR (16.9%, $P = 0.02$), 1.1 EAR (16.5%, $P = 0.01$) and 1.2 EAR tests (16.7%, $P = 0.01$). A probable explanation was that more CO was formed from char oxidization at 30% of excess air, but there was insufficient oxygen in the air supply to oxidize the extra CO. In contrast, the CO emission from hardwood combustion diminished significantly ($P = 0.01$) from 8.72% (kg gas/ kg

fuel) to 5.38% as the EAR increased from 1.0 to 1.3. Accordingly, more excess air augmented the CO_2 emission from 9.88% (1.0 EAR) to 36.8% (1.3 EAR), and the total O_2 consumption also increased from 16.9% at 1.0 EAR to 31.8% with 1.3 EAR. These results indicate that 1.3 EAR assured complete hardwood combustion in the experimental combustion system.

However, the incompleteness of combustion was evidently observed from the results above even when 10-30% excess air was supplied. For instance, theoretically there should not be any char products (Figure 2-2), or the O_2 consumption should be unchanged if the combustion is actually completed with 10-30% excess air (Figure 2-4). These contradictions were attributed to the physical limitations of our combustion system design, in contrast with an ideal manner that only used a single fine particle of fuel at a perfect air supply condition. Despite the fine size of fuel (4 mm), there were still many factors that resulted in heat and mass transfer delays, which made the fuel unable to react with air rapidly and completely in 90 min. Yet, compared to any ideal tests that mostly entirely eliminated these deficiencies, the findings by this research was particularly valuable for real boiler, since heat and mass transfer delays were an inevitable phenomenon in any large-scale operations. Therefore, aside from the research above, I should further assess the influence on energy conversion and combustion completeness to find the optimal EAR for this combustion system.

2.4.3. Energy conversion efficiency (ECE) and combustion completeness rate (CCR) as affected by excess air

Numerically, the highest ECE for switchgrass was 75.1% at 1.2 EAR, which was not statistically different from the ECE at other EAR levels (Figure 2-5). Switchgrass

consistently exhibited lower energy efficiency than hardwood due to the higher char yield of switchgrass than hardwood in the experimental combustion system. With a calorific output of 29.6 $MJ \cdot kg^{-1}$ (Figure S2-3), char formation reduced the heat release, thus reducing the energy conversion. Since the CCR of switchgrass reached a maximum between 1.1 EAR (0.421 $\%\cdot min^{-1}$) and 1.2 EAR (0.410 $\%\cdot min^{-1}$), I suggested that 20% of excess air would be optimal to achieve the highest ECE and CCR for switchgrass, while simultaneously lowering the mass of char and ash produced, relative to the 1.0 and 1.1 EAR levels, in the experimental combustion system.

Compared to the control group of hardwood, which had an ECE of 85.7% at 1.0 EAR, there was no significant difference in the ECE at 1.1 EAR (87.5%, $P = 0.14$) or 1.2 EAR test (88.0%, $P = 0.07$) (Figure 2-5). Yet, the 1.3 EAR remarkably enhanced the ECE to 91.0% ($P = 0.03$, compared to the 1.2 EAR test). This higher energy output produced the highest flame temperature (821 °C at the bottom of the fuel holder, Table 2-4), presumably because fast volatile separation and slow char oxidization processes were both exothermic. Moreover, excess air accelerated the CCR from 0.471 $\%\cdot min^{-1}$ (1.0 EAR) to a maximum of 0.537 $\%\cdot min^{-1}$ (1.2 EAR) and 0.535 $\%\cdot min^{-1}$ (1.3 EAR), the latter two measurements being similar ($P = 0.75$). The slowest CCR of 0.404 $\%\cdot min^{-1}$ measured at 1.1 EAR implies that 10% of excess air was insufficient for the complete combustion of hardwood while air intake causes heat transfer and a "cooling effect" that reduces the flame temperature at the top of the fuel holder, relative to the control group (Table 2-4). This is consistent with other reports that hardwood combustion at 1.1 EAR was controlled by limited oxygen availability and adversely affected by heat transfer, including conductive, convective and radiative effect (Ryu et al., 2006; Smart et al.,

2010). Consequently, 30% of excess air was recommended to obtain the greatest energy efficiency during hardwood combustion in our experimental system.

2.4.4 Fouling and slagging assessment

The fouling and slagging potential of biomass fuel is a function of the chemical composition of its ash, particularly the Na_2O, K_2O and SiO_2 contents. Ash from the 1.3 EAR combustion test was considered for this evaluation since 30% of excess air is commonly injected into commercial-scale boiler systems. Hardwood ash contained substantially less SiO_2 but more alkali metals than switchgrass ash (Table 2-5), meaning that switchgrass ash was more acidic, which lowers the risk of fouling and slagging in combustion systems (Vamvuka et al., 2009). Consequently, the basic-acid ratio (BA) of hardwood (3.0) was more than 10-fold higher than switchgrass (0.2). Hardwood ash had a medium fouling index (FI) of 19.7 and switchgrass ash had a minor FI of 0.3. The slagging index (SI) of hardwood (5.9) was 4 times higher than switchgrass (1.4), although the slag viscosity ratio (SVR) of switchgrass was much higher than hardwood due to the high SiO_2 content in its ash (67.6%). In summary, switchgrass had lower potential of fouling and slagging in a biomass combustion system than hardwood.

2.4.5 Combustion kinetics

2.4.5.1. TGA-DSC results

Switchgrass and hardwood combustion exhibited a similar mass loss (Figure 2-6), which consists of three steps: moisture removal (28-261 °C switchgrass, 26-262 °C hardwood), fast volatile separation (261-364 °C switchgrass, 262-366 °C hardwood) and slow char oxidization (364-861 °C switchgrass, 366-862 °C hardwood) (Table 2-6).

Maximal thermal decomposition rate (D_{max}) of hardwood (-2.40 %·°C^{-1}) was faster than switchgrass (-1.68 %·°C^{-1}). Fast volatile separation was the period of highest mass loss (54.0% switchgrass, 60.1% hardwood), but did not release much energy (1.11 kJ·g^{-1} switchgrass, 0.710 kJ·g^{-1} hardwood). Energy release was greatest during the slow char oxidization phase (7.09 kJ·g^{-1} for switchgrass, 4.09 kJ·g^{-1} for hardwood). Thus, complete combustion is necessary to achieve the greatest energy conversion from biomass fuel, as illustrated in Figure 2-5.

2.4.5.2. Kinetic analysis results

Kinetic analysis of the combustion process was performed with a two-step reaction model (Figure S2-4) that described the fast volatile separation and slow char oxidization steps according to the experimental temperatures achieved from the TGA-DSC analysis of switchgrass and hardwood. The reliability of kinetic results was confirmed by the high -R^2 values, from 0.9785 to 0.9997 (Table 2-7 and Table S2-3). The mechanisms describing the fast volatile separation phase of switchgrass and hardwood were diffusion two-way transport (D_2) and the Ginstling–Brounshtein equation (GB), respectively. Hardwood had a smaller E_a (94.1 kJ·mol^{-1}) than switchgrass (103 kJ·mol^{-1}), which means that the volatile separation of compounds contained in hardwood occurred at a lower activation energy than those contained in switchgrass. This different was probably due to the lower oxygen content in hardwood (51.0%) than switchgrass (52.2%). Both switchgrass and hardwood had lower E_a values in the slow char oxidization phase, which was described by the mechanisms of diffusion two-way transport (D_2) (2.29 kJ·mol^{-1}) and diffusion three-way transport (D_3) (3.77 kJ·mol^{-1}). This indicated that char oxidization was expected to progress easily after the volatile separation phase, and it should not be

limited by the rates at which chemical bonds were broken to release energy in an oxygen-rich environment (Sait et al., 2012). This is another reason why increasing oxygen availability during the combustion process should be advantageous to achieve complete energy conversion from biomass

2.5. Conclusions

Based on our laboratory combustion system design with 4 mm particle form of the fuels, I recommended that 20% or 30% excess air (for switchgrass or hardwood) would optimize the combustion to produce the highest energy conversion and combustion completeness rate. Excess air can be regulated by controlling the fuel feeding rate and air supply amount in commercialized boiler operations. Switchgrass is less likely to create fouling and slagging problems, making it a better biomass fuel in a commercial-scale boiler. Kinetic analysis pointed to the need to increase the oxygen availability to achieve better energy conversion efficiency from biomass.

However, there are still some physical limitations in our combustion system design that we still cannot utterly avoid, particularly the heat and mass transfer delays. These delays retarded the combustion even if an excess air was supplied, so that our design required more air to even achieve a stoichiometric condition. Yet, this phenomenon is fairly common when the combustion is conducted in a commercial-scale boiler, which should not be entirely eliminated in any laboratory-scale studies. Therefore, the recommendations made by this study is particularly valuable to boiler operations, but the further studies should be expanded to, 1) a single particle fuel test at an ideal condition without any heat and mass transfer delays, and 2) a boiler test to confirm the conclusions by this study.

2.6. Figures and tables

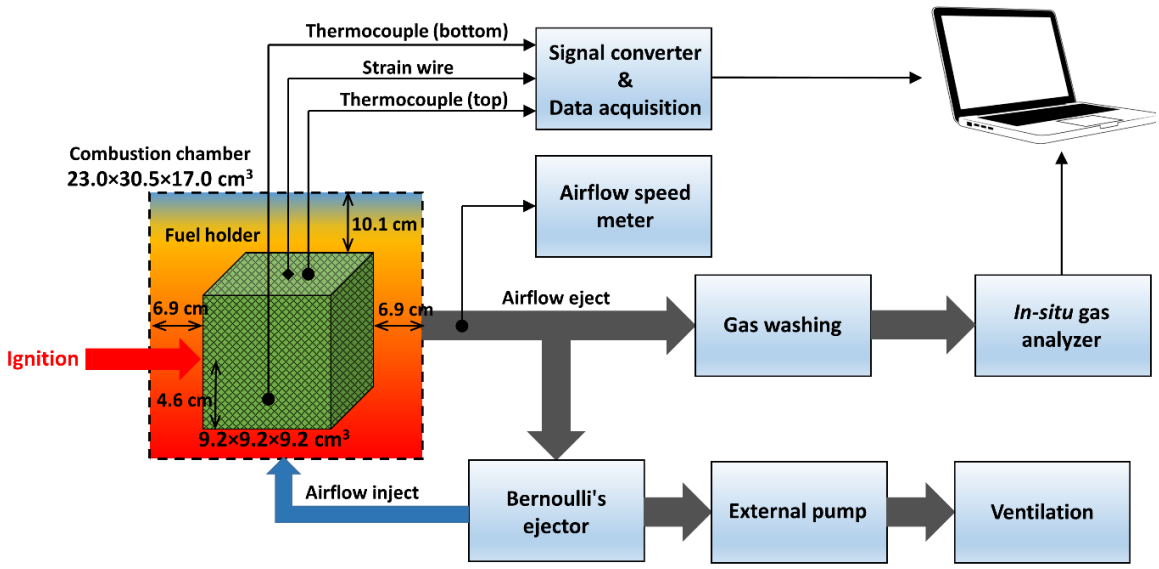

Figure 2- 1. Schematic diagram of the biomass fuel experimental combustion system designed for this study.

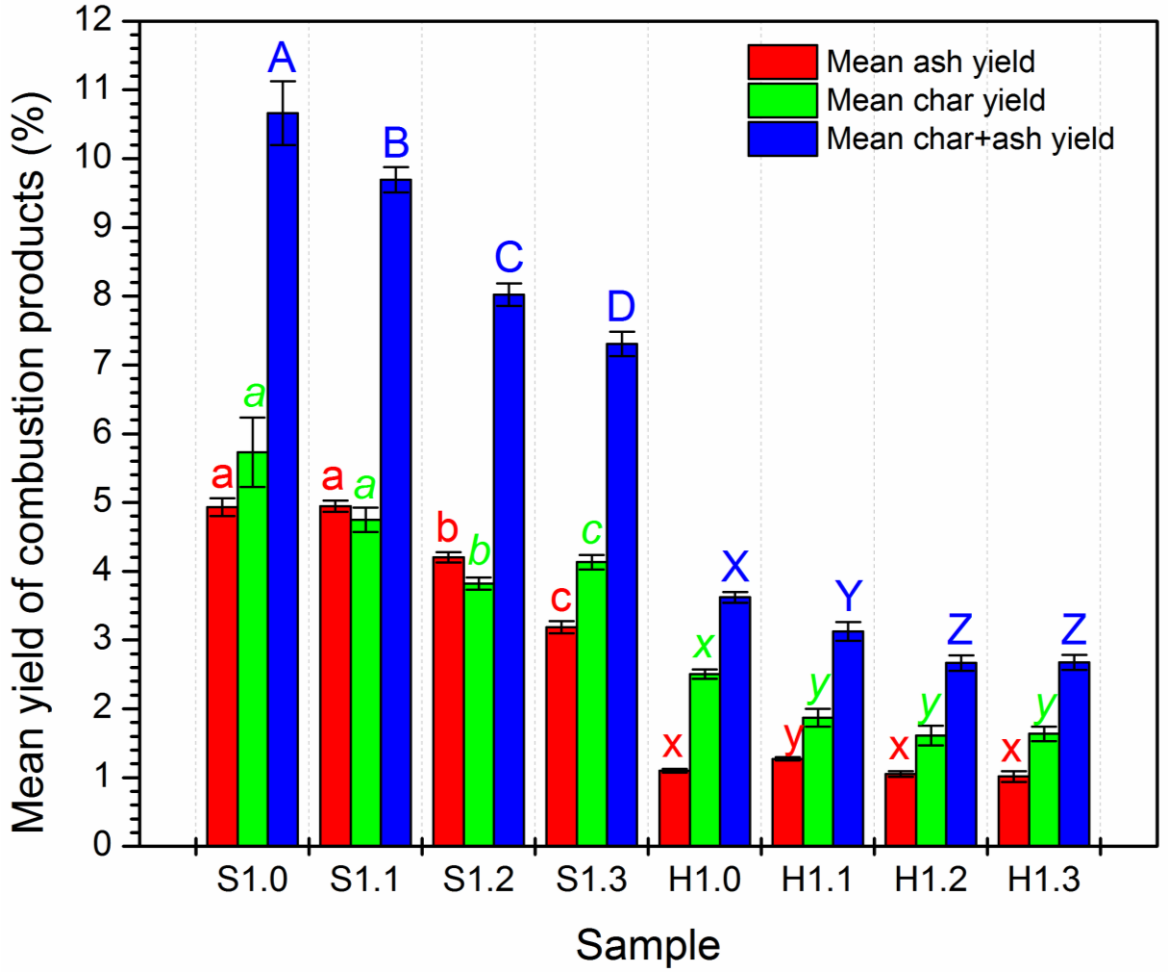

Figure 2- 2. Mean yield (w.t. %) of the ash and char combustion products from combustion tests, presented separately and as the sum of ash + char.

Samples are labeled as S = switchgrass or H = hardwood that were combusted with an excess air ratio of 1.0 (stoichiometric conditions), 1.1, 1.2 or 1.3. Columns with different letters were significantly different at $P < 0.05$ level, assessed by a Fisher's LSD test.

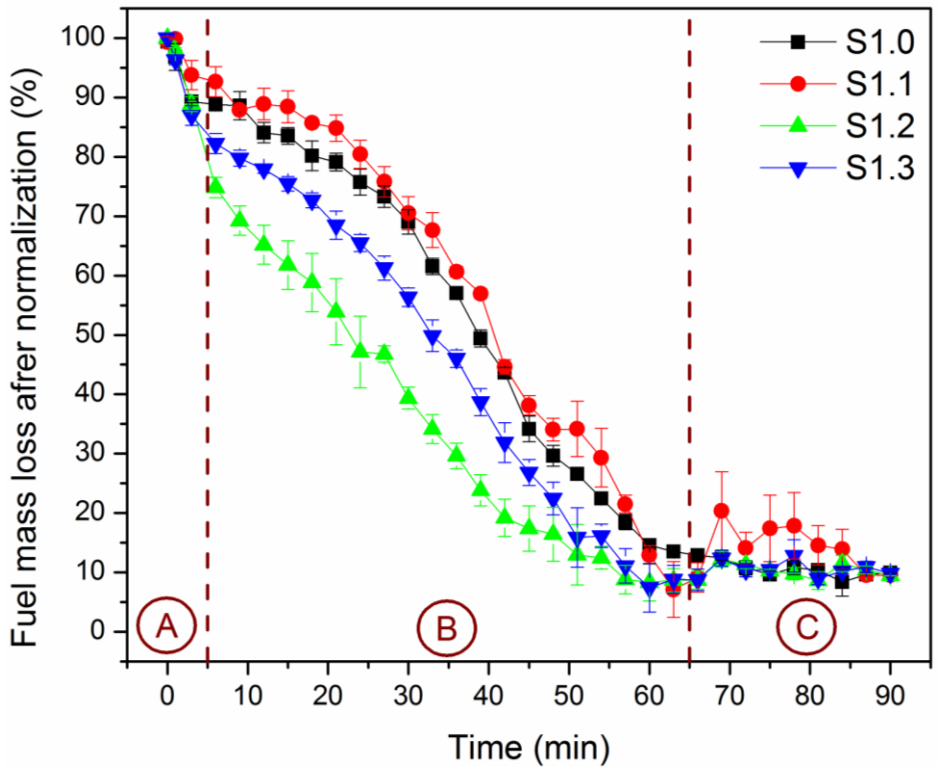
Fuel mass loss afrer normalization (%)
Time (min)
S1.0
S1.1
S1.2
S1.3
A
B
C

(a)

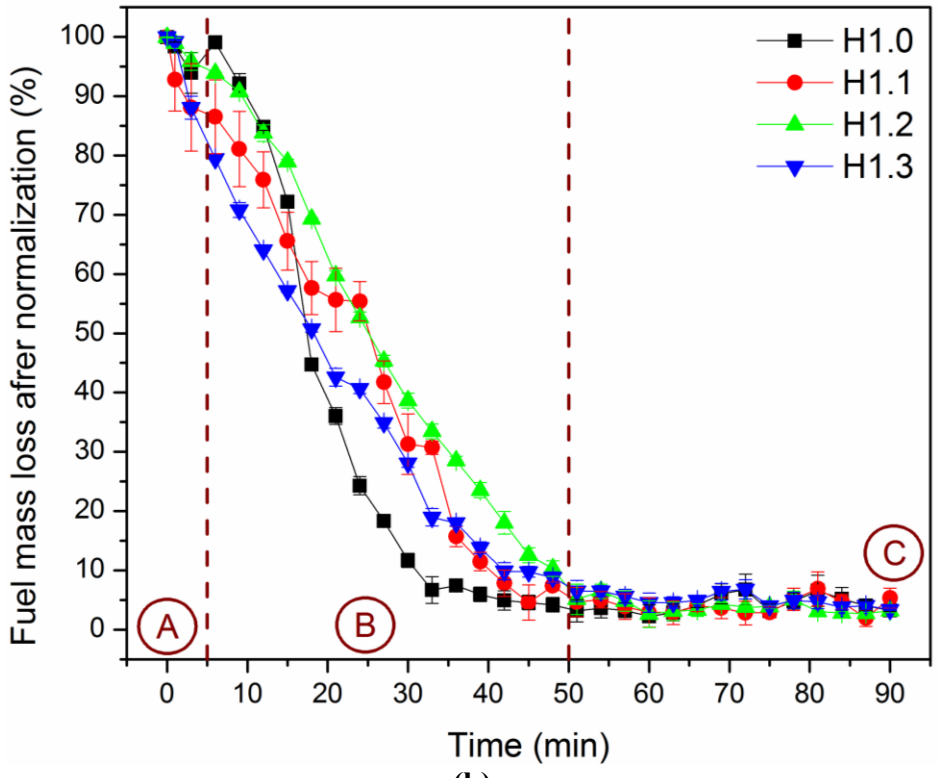
Fuel mass loss afrer normalization (%)
Time (min)
H1.0
H1.1
H1.2
H1.3
A
B
C

(b)

Figure 2- 3. Mass loss profile during a 90 min combustion of switchgrass (a) or hardwood (b) with excess air ratios of 1.0, 1.1, 1.2 and 1.3, which received 0, 10, 20 and 30% excess air intake, respectively.

Samples are labeled as S = switchgrass or H = hardwood that were combusted with an excess air ratio of 1.0 (stoichiometric conditions), 1.1, 1.2 or 1.3. The mass loss is divided into three phases, including A: early moisture removal, B: fast volatile separation, and C: slow char oxidization.

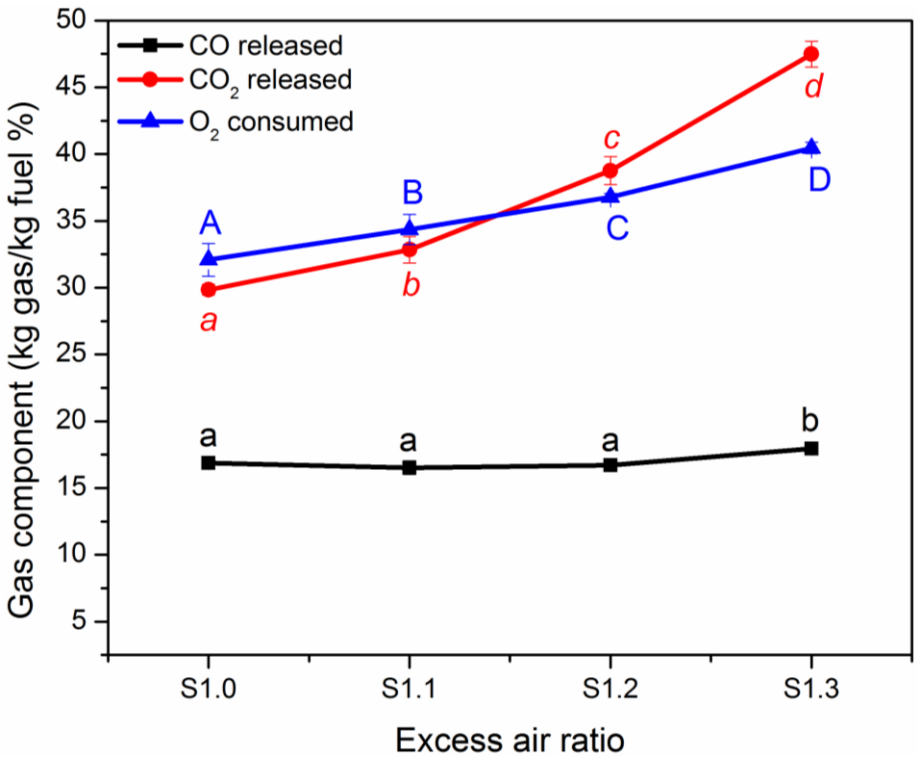
CO released
CO2 released
O2 consumed
Gas component (kg gas/kg fuel %)
Excess air ratio
S1.0
S1.1
S1.2
S1.3
A
B
C
D
a
b
c
d

(a)

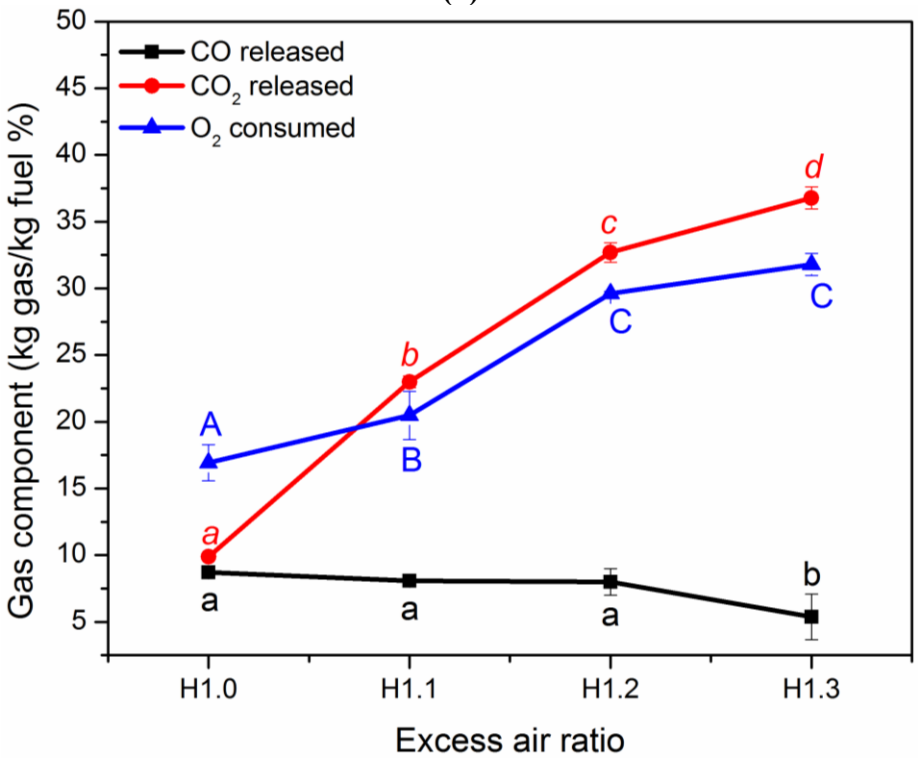
CO released
CO2 released
O2 consumed
Gas component (kg gas/kg fuel %)
Excess air ratio
H1.0
H1.1
H1.2
H1.3
A
B
C
a
b
c
d

(b)

Figure 2- 4. Total CO and CO_2 released, and O_2 consumed (kg gas/kg fuel, %) during the 90 min combustion of switchgrass (a) or hardwood (b) with excess air ratios of 1.0, 1.1, 1.2 and 1.3 respectively.

Samples are labeled as S = switchgrass or H = hardwood that were combusted with an excess air ratio of 1.0 (stoichiometric conditions), 1.1, 1.2 or 1.3. Points on each curve with different letters were significantly different at the $P < 0.05$ level, assessed by a Fisher's LSD test.

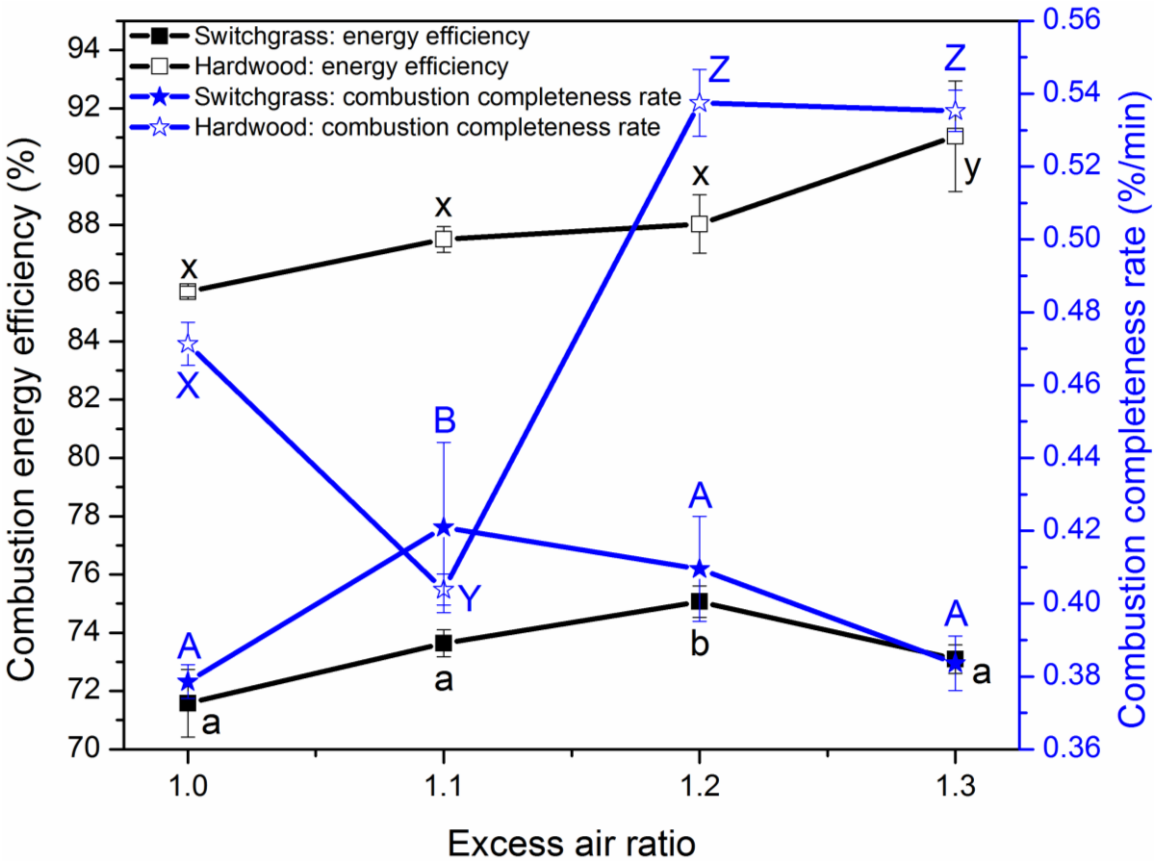

Figure 2- 5. Energy conversion efficiency (%) and combustion completeness rate (%/min) during the 90 min combustion of switchgrass (a) or hardwood (b) with different excess air ratio (1.0, 1.1, 1.2 and 1.3).

Points on each curve with different letters were significantly different at the $P < 0.05$ level, assessed by a Fisher's LSD test.

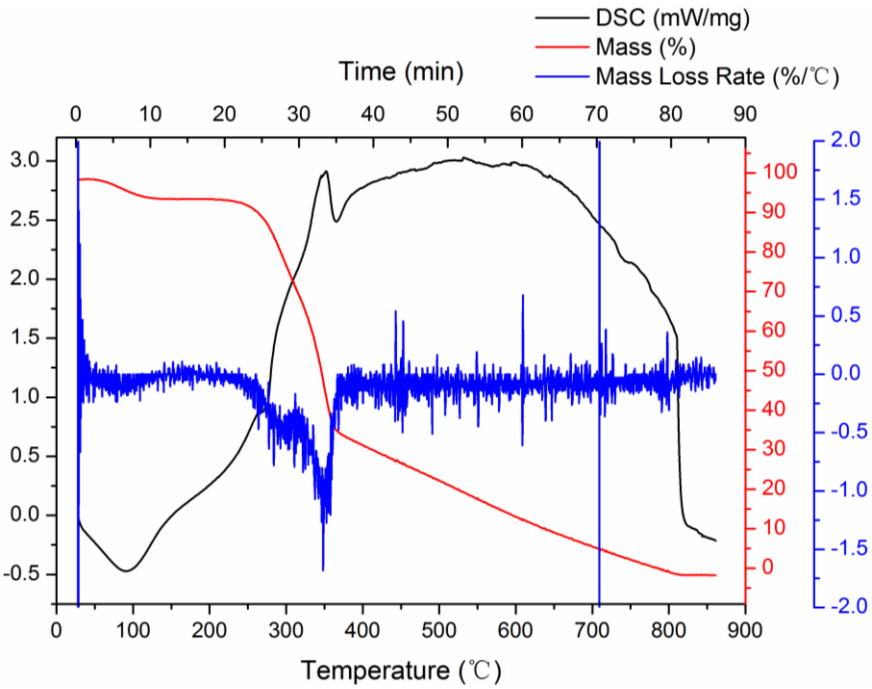

(a)

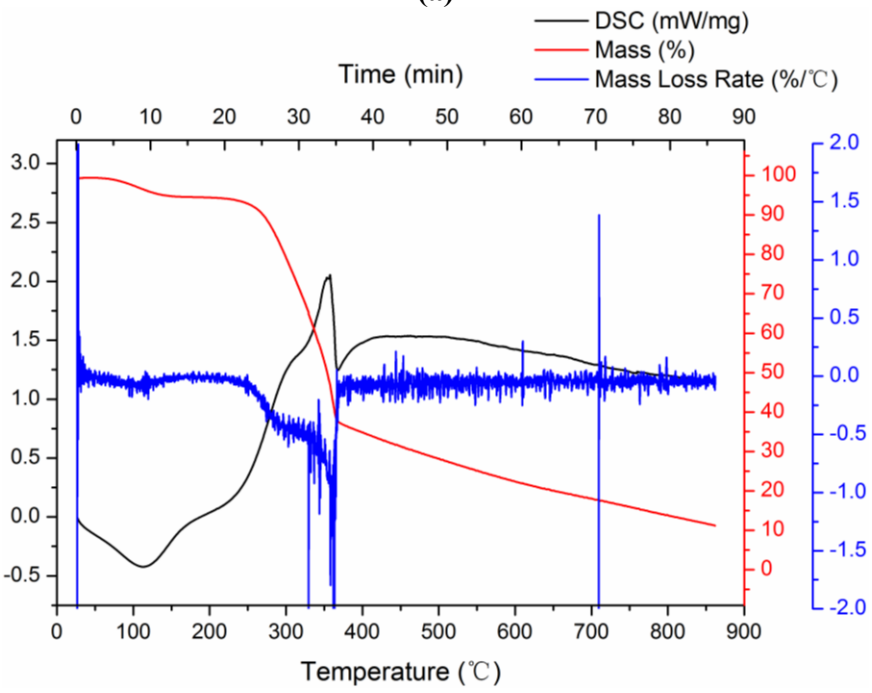

(b)

Figure 2- 6. Non-isothermal thermogravimetric analysis-differential scanning calorimetry (TGA-DSC) profile of switchgrass (a) or hardwood (b).

Table 2- 1. Experimental design for investigating the effect of different excess air ratio on the combustion of switchgrass and hardwood in the experimental system.

Designation	Fuel	Excess air ratio	External pump voltage %	Actual Air supply kg	Stoichiometric air demand kg	Initial fuel load kg	Replication
S1.0 (control)	Switchgrass	1.0	0	0.89	0.89	0.20	3
S1.1	Switchgrass	1.1	10	1.03	0.94	0.21	3
S1.2	Switchgrass	1.2	20	1.34	1.12	0.24	3
S1.3	Switchgrass	1.3	30	1.65	1.27	0.28	3
H1.0 (control)	Hardwood	1.0	0	0.89	0.89	0.19	3
H1.1	Hardwood	1.1	10	1.03	0.94	0.19	3
H1.2	Hardwood	1.2	20	1.34	1.12	0.23	3
H1.3	Hardwood	1.3	30	1.65	1.27	0.26	3

Table 2- 2. Properties of switchgrass and hardwood used in the experimental combustion system.

(a) Proximate analysis; (b) ultimate analysis and calorific value (higher heating value, $MJ \cdot kg^{-1}$); (c) molecular formula and mass ($kg \cdot kmol^{-1}$), and stoichiometric air-fuel ratio (SAFR) at stoichiometric combustion condition.

(a)

Fuel	Basis	Moisture w.t. %	Volatile matter w.t. %	Ash w.t. %	Fixed carbon w.t. %
Switchgrass	Air	6.55	80.6	4.69	8.21
	Dry	—	86.2	5.02	8.78
Hardwood	Air	6.51	80.0	0.78	12.7
	Dry	—	85.6	0.83	13.6

(b)

Fuel	C w.t. %	H w.t. %	N w.t. %	S w.t. %	O w.t. %	Higher heating value (HHV) $MJ \cdot kg^{-1}$
Switchgrass	41.3	5.86	0.60	0.06	52.2	17.5
Hardwood	42.8	6.17	0.01	0.02	51.0	17.7

(c)

Fuel	Molecular formula	Molecule mass $kg \cdot kmol^{-1}$	Stoichiometric air-fuel ratio (SAFR)
Switchgrass	$CH_{1.7027}O_{0.9476}N_{0.0125}S_{0.0005}$	29.1	0.96
Hardwood	$CH_{1.7299}O_{0.8937}N_{0.0002}S_{0.0002}$	28.0	1.02

Table 2- 3. Major mineral oxides and trace metal elements (w.t. %) in switchgrass and hardwood used in the experimental combustion system.

Major mineral oxides			
Elements	Unit	Switchgrass	Hardwood
SiO_2	w.t.%	2.23	0.23
Al_2O_3	w.t.%	0.25	0.03
Fe_2O_3	w.t.%	0.20	0.04
MnO	w.t.%	0.01	0.02
MgO	w.t.%	0.08	0.04
CaO	w.t.%	0.56	0.24
Na_2O	w.t.%	0.04	0.01
K_2O	w.t.%	0.14	0.11
TiO_2	w.t.%	0.01	0.00
P_2O_5	w.t.%	0.09	0.02
Loss on Ignition (LOI)	w.t.%	96.4	99.4
Trace metal elements			
Ba	ppm	39	23
Sr	ppm	21	10
Y	ppm	< 1	< 1
Sc	ppm	< 1	< 1
Zr	ppm	3	3
Be	ppm	< 1	< 1
V	ppm	< 5	< 5

Table 2- 4. Highest temperature (mean ± standard deviation) measured at the bottom and top of fuel holder in the 90 min combustion of switchgrass (a) or hardwood (b) with different excess air ratio (1.0, 1.1, 1.2 and 1.3).

Designation	Highest combustion temperature (°C)			
	Bottom		Top	
	Average	Standard deviation	Average	Standard deviation
S1.0 (control)	905	20.5	523	3.3
S1.1	1129	35.9	662	23.7
S1.2	938	18.8	576	11.4
S1.3	882	24.5	528	13.1
H1.0 (control)	386	9.8	735	22.2
H1.1	762	22.5	673	15.2
H1.2	801	19.3	709	19.6
H1.3	821	17.2	721	13.0

Table 2- 5. (a) Mineral oxide component (w.t. %) of the ash from the combustion of switchgrass and hardwood at an excess air ratio of 1.3, representing 30% excess air intake; (b) fouling and slagging indices estimated by empirical equations based on the mineral composition of combustion ash from the experimental combustion system.

(a)

Mineral oxides	Switchgrass ash	Hardwood ash
SiO_2	67.6	13.1
Al_2O_3	0.67	3.15
Fe_2O_3	0.31	2.44
MnO	0.06	2.37
MgO	2.00	5.24
CaO	11.8	34.4
Na_2O	0.11	1.30
K_2O	1.29	5.34
TiO_2	0.07	0.17
P_2O_5	1.12	2.97
Loss on Ignition (LOI)	14.7	26.8

(b)

Indices	Empirical equation	Switchgrass	Hardwood	Criteria		
				Low	Medium	High
Base-acid ratio (BA)	$(Fe_2O_3+CaO+MgO+K_2O+Na_2O)/(SiO_2+TiO_2+Al_2O_3)$	0.2	3.0	< 0.5	0.5-1.0	> 1.0
Fouling index (FI)	$BA\times(K_2O+Na_2O)$	0.3	19.7	< 0.6	0.6-40	> 40
Slagging index (SI)	$BA\times S^{d*}$	1.4	5.9	< 0.6	0.6-2.0	> 2.0

Slag viscosity ratio (SVR)	$100\times SiO_2/(SiO_2+Fe_2O_3+CaO+MgO)$	82.7	23.7	< 65	65-72	> 72

*: S^d corresponded to the sulfur content in dried initial fuel, and others referred to the mineral oxide content in ash.

Table 2- 6. Critical parameters of non-isothermal thermogravimetric analysis-differential scanning calorimetry (TGA-DSC) of switchgrass or hardwood.

Parameter		Unit	Switchgrass	Hardwood
Maximal decomposition rate (D_{max})		$\%\cdot°C^{-1}$	-1.68	-2.40
Maximal decomposition rate temperature (T_{max})		°C	348	362
Total enthalpy release		$kJ\cdot g^{-1}$	8.15	4.63
Temperature zone	Step 1: moisture removal	°C	26-262	28-261
Conversion rate		%	9.53	9.46
Heat release		$kJ\cdot g^{-1}$	-0.17	-0.05
Temperature zone	Step 2: fast volatile separation	°C	262-366	261-364
Conversion rate		%	60.1	54.0
Heat release		$kJ\cdot g^{-1}$	0.71	1.11
Temperature zone	Step 3: slow char oxidization	°C	366-862	364-861
Conversion rate		%	30.4	36.5
Heat release		$kJ\cdot g^{-1}$	4.09	7.09

Table 2- 7. Kinetic parameters, E_a (activation energy of combustion) and A (pre-exponential factor), and mechanisms describing switchgrass and hardwood combustion based on thermogravimetric kinetic analysis with the Coats-Redfern algorithm in a two-step solid-state reaction model.

Goodness of fit ($-R^2$) is provided for models of the fast volatile separation and late char oxidation phases for each biomass fuel.

Fuel	Switchgrass						Hardwood					
Stage	Fast volatile separation			Slow char oxidization			Fast volatile separation			Slow char oxidization		
	E_a	A	$-R^2$	E_a	A	$-R^2$	E_a	A	$-R^2$	E_a	A	$-R^2$
Kinetic parameters	$kJ \cdot mol^{-1}$	min^{-1}	1	$kJ \cdot mol^{-1}$	min^{-1}	1	$kJ \cdot mol^{-1}$	min^{-1}	1	$kJ \cdot mol^{-1}$	min^{-1}	1
	103	2.67E+07	0.9988	2.29	2.83E-03	0.9785	94.1	1.14 E+06	0.9993	3.77	2.44 E-03	0.9939
Mechanism/ Equation	Diffusion two-way transport			Diffusion two-way transport			Ginstling-Brounshtein equation			Diffusion three-way transport		

CONNECTING PARAGRAPH TO CHAPTER 3

Switchgrass contains 17.5 $MJ \cdot kg^{-1}$ of energy value, which is appropriate for heat generation. The ash from its combustion has low fouling and slagging tendencies, and can be an appropriate biomass fuel for a commercial-scale boiler. Still, there are questions about the suitability of switchgrass combustion ash as a pozzolan in blended cement. The purpose of Chapter 3 is to 1) characterize switchgrass combustion ash produced in a lab-designed furnace, and 2) evaluate the material properties of cement containing switchgrass combustion ash. Cement-ash blends tested in this chapter contained 10% or 20% of ground ash (by mass) and chemical accelerators (5% Na_2SO_4 or 5% $CaCl_2 \cdot 2H_2O$). I conclude by commenting on the feasibility of blending switchgrass ash in cement, with and without accelerators, to improve concrete strength and durability.

CHAPTER 3. Assessing the Recycling Value of Switchgrass Ash

Recycling of switchgrass combustion ash in cement: Characteristics and pozzolanic activity with chemical accelerators

3.1. Abstract

Biomass combustion produces renewable energy, but generates hazardous ash that must be disposed. High-volume of fine ash from the biomass combustion could be a harmful pollutant which causes lung cancer. Recycling the ash in cement is an environmentally-friendly solution especially for the cement industry. The objectives of this paper were to 1) characterize the ash from switchgrass combustion in a lab-designed furnace and 2) evaluate the material properties of cement containing switchgrass combustion ash. Cement-ash blends tested in this study contained 10% and 20% of ground ash (by mass) and chemical accelerators (5% Na_2SO_4 or 5% $CaCl_2 \cdot 2H_2O$). Switchgrass combusted at 411 °C generated 5% ash by mass. After grinding for 30 s, ground ash had a porous structure with 65.0 μm of mean particle size and 41.2 $m^2 \cdot g^{-1}$ of BET surface area. Ground ash consisted of 67.2% of SiO_2 and its structure contained 72.2% of amorphous crystal. This ash was a good pozzolan in blended cement, and its pozzolanic activity was improved by adding chemical accelerators (5% Na_2SO_4 and 5% $CaCl_2 \cdot 2H_2O$ were equally effective). Blended cement with 10% ash and either 5% Na_2SO_4 or 5% $CaCl_2 \cdot 2H_2O$ had similar material properties (strength and expansion resistance) as conventional Portland cement. Hence, recycling the switchgrass ash in the cement proved to be technically applicable.

3.2. Introduction

Biomass combustion generates renewable energy, which is appealing to energy-intensive industries such as cement producers. Since cement is produced at ≈ 1450 °C, an average-size cement plant uses 3-6 GJ of fossil fuel per tonne of cement fabricated (Huntzinger & Eatmon, 2009). Cement industry can use biomass fuel to supplement fossil fuel and partially reduce its carbon footprint. For instance, Lafarge Canada accomplished full-scale cement production trials with biomass fuel in 2010, but noted several obstacles for the biomass fuel. Burning 1 kg of the biomass fuel would generate 0.05-0.20 kg of fine ash, and the fine ash was a hazardous contaminant that could potentially cause lung cancer (Lim & Seow, 2012). Owing to large volume of the fine ash when it was present on-site, it was not appropriate to adopt conventional industrial waste treatments, such as land fill. Consequently, one challenge was how to dispose of the ash generated from the biomass fuel in an efficient, sustainable and economical way.

It is technically possible to recycle the ash produced during biomass combustion in cement. The most important constituent of ash that can enhance the strength and durability of concrete is SiO_2, owing to the supplementary formation of calcium silicate hydrate ($(CaO)_x \cdot (SiO_2)_y \cdot (H_2O)_z$, C-S-H) from calcium hydroxide ($Ca(OH)_2$, CH) by the pozzolanic reaction (Foo & Hameed, 2009). Pozzolans are siliceous or siliceous and aluminous materials with virtually no cementing value; however, in the presence of water, they react with CH to form C-S-H, which is the main contributor to concrete strength (Duan et al., 2013a). A satisfactory pozzolan should have small particle size and contain more than 70% of $SiO_2 + Al_2O_3 + Fe_2O_3$ (ASTM, 2004). Yet, compared to the conventional pozzolans like silica fume (containing ≈ 99% SiO_2), the pozzolanic activity

of biomass ash is still inferior due to its lower SiO_2 content (≈ 50-80%). Hence, it is critical to consider how to enhance the pozzolanic reaction when biomass ash is used in cement.

To stimulate the pozzolanic activity of ash, chemical acceleration is achieved by adding 3-5% Na_2SO_4 or $CaCl_2 \cdot 2H_2O$ in cement-ash mixtures. By adding Na_2SO_4, the reaction between Na_2SO_4 and $Ca(OH)_2$ produces NaOH, which accelerates the dissolution of SiO_2 in the cement-pozzolan-water system, thus enhancing the pozzolanic reaction rate. Blended cement pastes (with 10% or 30% of oil shale ash) possessed stronger mechanical properties after being accelerated by 2.25%, 4.5% or 6.25% Na_2SO_4 (Radwan et al., 2013). Adding 4% Na_2SO_4 efficiently accelerated the pozzolanic activity of low grade ash (reject fly ash) when cement was replaced by 10%, 25% and 40% ash (Poon et al., 2003). Moreover, when cement pastes contained a high volume of fly ash (≈ 80%), Na_2SO_4 effectively reduced the setting time and increased the compressive strength (Donatello et al., 2013), and improved both of the early and later strengths at 23-65 °C (Shi & Day, 2000a). In contrast, mixing $CaCl_2 \cdot 2H_2O$ with cement generates a new crystal $C_3A \cdot CaCl_2 \cdot 10H_2O$–$C_3A \cdot Ca(OH)_2 \cdot 12H_2O$, which was formed during the interaction between $CaCl_2$ and $Ca(OH)_2$. This new compound provides a more robust microstructure than C-S-H but also improves cementing characteristics (Shi & Qian, 2001). In cement pastes containing 80% of volcanic ash, mixing 4% $CaCl_2 \cdot 2H_2O$ decreased the early strength but increased the later strength at 23 °C, and advanced both of the early and later strengths at 35-65 °C (Shi & Day, 2000a). Meanwhile, $CaCl_2 \cdot 2H_2O$ was also effective in the cement mortar with 20% bagasse ash (Amin et al., 2011) and 20%

pozzolanic clay (Alam et al., 2013). Therefore, the chemical acceleration by Na_2SO_4 or $CaCl_2 \cdot 2H_2O$ has the potential to improve the pozzolanic activity of biomass ash.

Switchgrass (*Panicum vigratum L.*) is an emerging biomass fuel in North America and Europe (Kumar & Sokhansanj, 2007). Compared to other biomass sources, it has an excellent calorific value (17-20 $MJ \cdot kg^{-1}$) and is rich in silicon (4.0-6.3%) (Hoagland et al., 2013), which implies that its ash might have a positive pozzolanic activity. However, there is no research heretofore to evaluate the recycling of switchgrass ash in the cement, or to explore the solution to make this concept technically applicable.

This paper aimed to characterize the ash from switchgrass combustion in a lab-designed furnace, and evaluate the material properties of cement containing switchgrass combustion ash. The cement-ash blends tested in this study contained 10% and 20% of ground ash (by mass) and chemical accelerators (5% Na_2SO_4 or 5% $CaCl_2 \cdot 2H_2O$). To compare the results to other studies, the pozzolanic activities and cement properties were evaluated by standard methods, including Frattini test, lime-ash test, concrete compressive strength test, and expansion test.

3.3. Material and methods

3.3.1. Switchgrass preparation and characterization

Switchgrass was gathered from a farm in Williamsburg, Ontario, Canada, and characterized in lab with two replications. Before combustion, switchgrass was manually sheared to 2 cm long roughly. About 10 mg of ground switchgrass (≈ 500 μm) was used for the proximate analysis by the sequential thermogravimetric method (ASTM, 2012b). Ultimate analysis was performed by micro-combustion method, with ≈ 25 mg of dried ground switchgrass, using an elemental analyzer equipped with thermal conductivity

detectors. As defined in ASTM D4239-13e1 (ASTM, 2013b), the sulfur content was measured by combustion method on a sulfur analyzer at 1350 °C. The calorific value (higher heating value) of the dried switchgrass was tested in an oxygen bomb calorific meter following the ASTM D5865-13 method (ASTM, 2013a).

3.3.2. Switchgrass combustion

3.3.2.1. Design of combustion furnace

A multiple-purpose stove was connected into a combustion furnace in the lab (Figure 3-1). Dimension of combustion chamber was 84 × 38 × 51 cm. An exhaust expelling system was set up to provide sufficient air (≈ 2500 cm^3/s) for complete combustion. During combustion, temperature of the sample surface was monitored by an infra-red thermometer outside the furnace. One thermocouple was installed on the exhaust gas outlet and a second thermocouple was placed in the chamber interior. Both thermocouples were linked to a data acquisition card (DAQ) for data recording every 5 s. In addition, an aluminum wire mesh (2 mm) was placed at the exhaust exit port to block the exit of fine burnout residue carried by exhaust gas.

3.3.2.2. Combustion test

Combustion temperatures and yields of burnout residue were measured by the combustion tests with various initial switchgrass load (492, 590, 639, 648, 924, 960 and 1323 g). During each test, the switchgrass sample was placed evenly on the bottom of the chamber without packing or compressing it to minimize delay in heat and mass transfer, which could make the ash free of char maximally. Then, the ventilation system was switched on and switchgrass was ignited by a propane torch. Combustion was maintained for 5 min, and throughout this period, temperatures of switchgrass surface, exhaust gas,

and chamber interior were measured by thermocouples and recorded by the DAQ. After combustion, burnout residue was collected and weighted. Any unburned char was separated by removing the residue that did not pass through a 2 mm mesh sieve, and the ash was assumed to be all material that were less than 2 mm in size.

3.3.3. Characterization of switchgrass ash

As-received ash was then characterized for its physiochemical, thermal and microstructural properties. Before characterization, it was ground in a vibratory pulverizing mill for 30 s. Particle size distribution of ash, as well as the Portland cement (used in the following pozzolanic evaluation section) was visualized by a laser scattering particle size analyzer. Range of distribution was set from 0.020 to 2000 μm. Brunauer Emmett Teller (BET) surface area of ash was determined with a BET analyzer. X-ray fluorescence (XRF) quantified the major mineral oxides in ash, silica fume and Portland cement by a XRF spectrometer. A powder X-Ray Diffractometer helped distinguish the crystal structure of ground ash. Based on the X-Ray diffraction (XRD) observation, amorphous content was estimated by Rietveld refinement (McCusker et al., 1999). Generator power of X-ray was 40 kV/20 mA with Cu anode material, and scanning angle ranged from 5 to 100 °2θ. Scanning step size was set at 0.04 $°2\theta \cdot s^{-1}$. Thermal properties of ash were evaluated by a Thermogravimetric-Differential Scanning Calorimetry (TG-DSC) analyzer. Specifically, ≈ 10.6 mg of ground ash was placed in an Al_2O_3 crucible, and heated up to 900 °C, in an atmosphere of 20% O_2 + 80% N_2 (by volume). Volume rate of gas was 20 $mL \cdot min^{-1}$, and heating rate was 10 °C/min. Consequently, mass loss and enthalpy change were recorded. Lastly, microstructure of ground ash (coated in carbon) was observed by a Scanning Electron Microscope (SEM).

3.3.4. Evaluation of pozzolanic activity

Experimental designs of the following four tests (including sample designation and mixture proportion) were provided in Table 3-1 and 3-2. All of the tests were replicated three times to assure the repeatability of results.

3.3.4.1. Frattini test

Pozzolanic activity of ash was chemically determined by the Frattini test (Donatello et al., 2010b), which quantified the reduction of Ca^{2+} in the pozzolanic reaction. Specifically, 20 g of sample consisting of 80% Portland cement and 20% ash were mixed in 100 mL distilled water. To investigate chemical acceleration, 1g of Na_2SO_4 was added into a mixture (S-AN). Because adding $CaCl_2 \cdot 2H_2O$ disturbed the measurement of Ca^{2+} reduction, I neglected $CaCl_2 \cdot 2H_2O$ in this test. Samples with 20% silica fume or without any pozzolan were also included as positive and negative controls. Samples were preserved for 8 d in sealed plastic bottles at 40 °C. Afterwards, samples were vacuum-filtered and cooled to ambient temperature in sealed Buchner funnels. The filtrate was tested for OH^- and $Ca^{2+}$by titration. To compare the pozzolanic activity of each sample, maximal Ca^{2+} concentration (M[CaO]) at a certain $[OH^-]$ was calculated by Eq. 3-1,

$$\mathrm{M[CaO], mmol \cdot L^{-1}} = \frac{K_{sp} \times 10^9}{[\mathrm{OH^-, mmol \cdot L^{-1}}]^2} \quad (3\text{-}1)$$

where $[OH^-]$ was the actual OH^- concentration. K_{sp} was the solubility product constant, and equaled to 4.41×10^{-6} $mol^3 \cdot L^{-3}$, determined by $[Ca^{2+}]$ and $[OH^-]$ in saturated $Ca(OH)_2$ solution at 25 °C. Hence, the ratio of Ca^{2+} reduction, as the index of pozzolanic activity was determined by Eq. 3-2,

$$\text{Pozzolanic activity index, \%} = \frac{\text{M[CaO], mmol} \cdot \text{L}^{-1} - \text{[CaO], mmol} \cdot \text{L}^{-1}}{\text{M[CaO], mmol} \cdot \text{L}^{-1}} \quad (3\text{-}2)$$

where [CaO] was the actual Ca^{2+} concentration in solution.

3.3.4.2. Lime-ash test

When mixed with lime and sand, the pozzolanic mix should gain a strength of 4.1 MPa or higher after cured at 54 °C for 7 d, and another 21 d at 23 °C in water (ASTM, 2011). Lime: pozzolan: standard sand ratio was 180 g: 360 g: 1480 g by mass. The 5% chemical accelerators (Na_2SO_4 or $CaCl_2 \cdot 2H_2O$ powder) were added in some batches of mixtures, and water/(lime+pozzolan) ratio was 0.55. Lime-silica fume sample was also tested as reference to. Samples were cast into 50 mm cube molds, and were cured at 54 °C. Strength was checked for each sample after 7 d curing at 54 °C, and then after another 21 d curing at 23 °C in water.

3.3.4.3 Compressive strength of concrete cylinder

Compressive strength of concrete cylinders (50 mm diameter, 100 mm height) was tested to assess the influence of ash and chemical accelerators on concrete. Replacement ratio of ash to cement was 0 (as control), 10, and 20% by mass, respectively. Sample with 10% silica fume was also included as a positive control. Water/(cement+ash) ratio was 0.55 for the satisfactory workability, and coarse/fine aggregate was 65/35. Chemical accelerators (5% Na_2SO_4 or 5% $CaCl_2 \cdot 2H_2O$ powder) were blended in the batches containing 10% ash to appraise the chemical acceleration. After casting, samples were cured in water at 23 °C for 3, 7 and 28 d. As per ASTM C618 (ASTM, 2004), pozzolanic activity index was defined as the percentage of the compressive strength compared to the control.

3.3.4.4. Expansion of mortar bar due to alkali-silica-reaction (ASR)

A qualified pozzolan could reduce the expansion due to alkali-silica-reaction (ASR), thus enhancing the durability of concrete (Shehata & Thomas, 2000). Expansion test was carried out in accordance with ASTM C1260 (ASTM, 2007). Specifically, 25 × 25 × 100 mm mortar bars were made from reactive sand, cement, and ash (substituting 0, 10, and 20% of cement by mass). Chemical acceleration by 5% Na_2SO_4 or 5% $CaCl_2 \cdot 2H_2O$ powders was investigated on mortar bars with 10% ash. Water/(cement+pozzolan) ratio was 0.47, and cement/fine aggregate ratio was 1/2.25. Mortar bars with 10% of silica fume were also prepared as a positive control, and samples without any additive were the negative control. Reference length was obtained by curing mortar bars in water at 80 °C for 24 h. Afterwards, samples were transferred in 1 $mol \cdot L^{-1}$ NaOH solution at 80 °C for 14 d. During this period, the length of samples was measured at 12 h intervals with a length comparator.

3.3.5. Statistical interpretation

The effect of ground ash from switchgrass combustion on pozzolanic activity in cement and materials properties of concrete, with or without chemical accelerators, was statistically compared using a Fisher's Least Significant Difference (LSD) test at the 95% confidence level.

3.4. Results and discussion

3.4.1. Switchgrass combustion in lab-designed furnace

Table 3-3 showed the proximate and ultimate analysis, and the calorific value (higher heating value) of switchgrass. On a dry basis, switchgrass had 5% ash and 17.5 $MJ \cdot kg^{-1}$ of higher heating value (HHV). Switchgrass has higher energy content than other

biomass fuels, which are normally around 15 $MJ \cdot kg^{-1}$, but the high ash content of switchgrass means that that ash remaining after combustion must be disposed or they could be recycled by blending with cement materials (Madani Hosseini et al., 2011).

Combustion in the lab-designed furnace occurred at average temperatures of 411 ^{o}C on switchgrass surface, 275 ^{o}C in chamber interior and 89 ^{o}C in exhaust gas. In previous research, maximal decomposition rate during switchgrass combustion occurred at 300-350 °C (Chandrasekaran & Hopke, 2012). Temperature of the switchgrass surface (411 °C) demonstrated adequately high temperature for combustion within this lab-designed furnace.

Before removing the large unburned char, mean yield of burnout residue was 14% by mass when initial switchgrass load was from 492 g to 1323 g. This value was more than double the switchgrass ash content (5%), which was attributed to different testing apparatus and conditions. Combustion test was repeated seven times and standard deviation of the mean yield was ±0.72%. There was a linear correlation ($R^2 = 0.9835$) between initial switchgrass load and burnout residue yield (Figure S3-1), indicating that the initial fuel load did not alter the burnout residue yield in the lab-designed furnace and that 2500 $cm^3 \cdot s^{-1}$ of air supply assured complete combustion after 5 min. Thereafter, I combined all ash samples and considered them to be homogeneous, physically, chemically and microstructurally, for the following experiments.

3.4.2. Characterization of switchgrass ash

Ground ash was gray in color (Figure S3-3). Mean particle size of cement was 21.9 μm, with 12 820 $m^2 \cdot m^{-3}$ of specific surface area (Table 3-4). According to ASTM C618 (ASTM, 2004), a physically satisfactory pozzolan should pass a 45 μm sieve, but

the ground ash in this study was slightly coarser (65.0 μm) (Figure S3-2). This suggests that grinding more finely could improve the pozzolanic activity of ash. BET surface area of ground ash was 41.3 $m^2 \cdot g^{-1}$ (Table 3-4), thus ground ash had ample porosity, confirmed by microscopic examination at 10 000 times magnification by SEM (Figure 3-2(b)), which is important for the microstructure of cementing materials and the resulting concrete.

Chemically, ash contained less $SiO_2 + Al_2O_3 + Fe_2O_3$ (68.17%) than silica fume (95.1%), and also substantially less SiO_2 (67.2%) than silica fume (95.0%) (Table 3-4). The XRD profile above the background line revealed that SiO_2 in ground ash was predominately amorphous (72.2%), especially in the zone of 20-40 °2θ (Figure 3-2(a)). Crystalline phase mostly consisted of Quartz-α SiO_2 (52%) and rhombohedral $CaCO_3$ (48%). Therefore, ground ash in this study featured a sufficient proportion of amorphous SiO_2 in the crystal structure, which could be pozzolanic-active.

The ground ash was thermally stable from 25 ºC to 900 ºC (Figure S3-4), losing 14.1% mass and releasing 0.76 J/g of heat when subjected to these conditions (Table 3-4). This implies that most of the switchgrass carbon was lost during combustion in the lab-designed furnace and the additional mass lost during this test was a combination of carbon decomposition and metal element evaporation.

3.4.3. Evaluation of pozzolanic activity

3.4.3.1. Frattini test

In the Frattini test, diminution of Ca^{2+} and OH^- chemically reflects the activity of pozzolans. Points of Portland cement were close to the solubility curve of $[Ca^{2+}]$–$[OH^-]$ ($K_{sp} = 4.41 \times 10^{-6}$ $mol^3 \cdot L^{-3}$, 25°C), affirming that 8 d curing at 40°C was sufficient for

cement hydration to create a saturated $Ca(OH)_2$ solution (Figure 3-3(a)). However, cement with silica fume and cement-ash blends tested in this study were all located below the curve, which indicated that they were all pozzolanic-active. Furthermore, silica fume had stronger ability to decrease OH^- (to 28.7 $mmol \cdot L^{-1}$) than ash (to 42.3 $mmol \cdot L^{-1}$) and the ash with Na_2SO_4 (to 46.5 $mmol \cdot L^{-1}$). Decrease of alkali concentration was attributed to the pozzolanic reaction, which is an acid-base neutralization between $Ca(OH)_2$ and silicic acid, and is proportional to the quantity of reactive SiO_2 in the pozzolan. Greater alkali consumption by silica fume was expected, due to fact it contains more reactive SiO_2 than switchgrass ash.

The pozzolanic activity of the test materials (Figure 3-3(b)) revealed that cement was slightly pozzolanic-active due to small amounts of SiO_2 (19.7%) and Al_2O_3 (4.82%). Silica fume had the highest SiO_2 content and greatest pozzolanic activity (75.15%). Still, ash and the ash with Na_2SO_4 possessed pozzolanic activities of 30.9% and 33.9%, respectively (Figure 3-3(b)) and these were similar statistically ($P = 0.0729$, Fisher's LSD test). Although the SiO_2 content of pozzolan was correlated to its pozzolanic activity chemically, the crystal structure of pozzolan could also be important in microstructure development and mechanical properties of the cementing materials containing ash.

3.4.3.2. Lime-ash test

In lime-ash tests, the positive control was cement with silica fume (S-S), which exhibited the greatest pozzolanic activities at both 7 and 28 d curing ages (6.3 and 6.9 MPa) (Figure 3-4). Ash sample after 7 d curing had a 3.9 MPa of compressive strength, which was marginally below the strength criteria of 4.1 MPa (ASTM, 2011). This lack of strength was ascribed to the lower content of SiO_2 in ash than silica fume. Yet, because

the progress of cement hydration and pozzolanic reaction benefited from the prolonged curing duration, the compressive strength of ash cube increased to 4.2 MPa after 28 d (Figure 3-4). This demonstrates that switchgrass ash was an effective pozzolan in the late stage. Mixing 5% Na_2SO_4 or 5% $CaCl_2 \cdot 2H_2O$ in lime-ash mixtures showed that both chemical accelerators manifestly fortified the strength to 4.8 and 4.4 MPa after 7 d, and to 5.1 and 4.9 MPa after 28 d, respectively. There was a consistent, significant (P<0.05, Fisher's LSD test) improvement in compressive strength with Na_2SO_4 than with $CaCl_2 \cdot 2H_2O$. I attribute this finding to changes in the alkali concentration with Na_2SO_4, which could hasten the dissolution of SiO_2 in ash and transform it to $Si(OH)_4$ or H_4SiO_4 (Shi & Day, 2000b). Generating more alkalinity of the cement-water-ash system or stimulating the dissolution of SiO_2 in the pozzolan might effectively enhance the strength of the cement-ash mixture during the curing stage.

3.4.3.3. Compressive strength of concrete cylinder

As shown in Figure 3-5(a), concrete with 10% silica fume possessed the strongest compressive strength after 3, 7 and 28 d curing (23.4, 27.5, and 39.1 MPa, respectively). Cement with 20% of ash had the lowest compressive strength of 5.6, 14.8 and 28.4 MPa after 3, 7 and 28 d curing. While 10% ash in the cement-ash blend improved the strength to 28.6 MPa after 28 d curing, this was significantly less (P = 0.0495, Fisher's LSD test) than the Portland cement control with 32.5 MPa of compressive strength after 28 d (Figure 3-5(a)). These results are interpreted as follows: partial replacement of cement by ash reduced the proportion of primary hydration reactants tricalcium silicate ($(CaO)_3 \cdot SiO_2$, C_3S) and dicalcium silicate ($(CaO)_2 \cdot SiO_2$, C_2S) in the mixture. Less C_3S and C_2S consequently led to insufficient formation of C-S-H (main strength contributor)

and CH (chief reactant in pozzolanic reaction) (Bullard et al., 2011; Ercikdi et al., 2009). Since the pozzolanic reaction is controlled by CH formation and diffusion of hydrated products (Isaia et al., 2003), it was retarded when less CH formation occurred in the early stage (3 and 7 d) and to a greater extent in the cement-ash blend with 20% ash than 10% ash (Figure 3-5(a)). More importantly, the low SiO_2 content in ash reduced the production of C-S-H from the pozzolanic reaction and shortage of C-S-H compounds weakened the strength of concrete. Therefore, I assert that compressive strength of concrete was greatly influenced by the initial quantity of C_3S and C_2S. This is further supported by the fact that the compressive strength of cement-ash blends with 10% and 20% switchgrass ash converged after 28 d (Figure 3-5(a)). Replacement ratio of ash did not affect the strength of concrete considerably in the late stage, whereas the lack of initial C_3S and C_2S always had a negative impact.

Adding 5% Na_2SO_4 or 5% $CaCl_2 \cdot 2H_2O$ to a cement-ash blend with 10% ash was an effective way to overcome the shortcomings of ash alone, giving strength comparable to the Portland cement control throughout the curing period (Figure 3-5(a)). This improvement was attributed to chemical acceleration, namely (1) more alkali generated by Na_2SO_4 and (2) stronger crystals of $C_3A \cdot CaCl_2 \cdot 10H_2O$–$C_3A \cdot Ca(OH)_2 \cdot 12H_2O$ induced by $CaCl_2 \cdot 2H_2O$. Compared to the S-A10 treatment (cement with 10% ash, without chemical accelerators), both chemicals produced similar compressive strength in the short term (3 and 7 d curing) and improved the compressive strength in the long term (28 d curing, Figure 3-5(a)). It appears that chemical acceleration can offset lower C-S-H formation in cement-ash blends, which occurs due to the lower proportion of cement, by enhancing the pozzolanic reaction and thereby producing more C-S-H for strength.

As the pozzolanic activity index was defined as the percentage of the compressive strength compared to the control, an index that is greater than 1.0 suggested a positive pozzolanic activity (Figure 3-5(b)). Silica fume possessed the greatest pozzolanic activity, which diminished with increasing curing time (1.8 after 3 d, 1.4 after 7 d, and 1.2 after 28 d). This trend was attributed to the following: high amorphous SiO_2 content in silica fume promoted the development of pozzolanic reaction, thus using up the crystallized CH. More expenditure of crystallized CH provoked the additional formation of C-S-H in the early stage. Depletion of free crystallized CH and free SiO_2 reserves in the cement-silica fume blend progressively reduced the pozzolanic activity.

Compared to Portland cement, the cement-ash blend with 10% ash and 5% Na_2SO_4 gave the consistent pozzolanic activity, close to 1.0, during the 28 d period (Figure 3-5(b)). There was a lag in the pozzolanic activity of the cement-ash blend with 10% ash and $CaCl_2 \cdot 2H_2O$, but by 7 d and 28 d of curing, it was statistically similar ($P <$ 0.05, Fisher's LSD test) to Portland cement and had a pozzolanic activity of nearly 1.0 after 28 d (Figure 3-5(b)). Cement-ash blends with 10% ash and 20% ash had the lowest pozzolanic activity at most measurement times (0.88 and 0.44 at 3 d, 0.97 and 0.77 at 7 d, and 0.88 and 0.87 at 28 d). Lower SiO_2 content, as well as smaller proportions of cementitious compounds in these blends, inhibited both pozzolanic and hydration processes in the cement-ash mixtures. Prolonged curing probably stimulated formation of crystalline CH and boosted the pozzolanic activity, particularly in the cement-ash mixture containing 20% ash which increased from 0.45 to 0.88 between 3 d and 28 d of curing (Figure 3-5(b)). Our findings support the use of chemical accelerators, particularly 5% Na_2SO_4, in cement-ash blends to sustain the pozzolanic activity more efficiently.

3.4.3.4. Expansion test

Expansion of mortar bars due to ASR provides insight into pozzolanic activity whereby ≤ 0.1% of expansion at 16 d after casting is considered an innocuous behavior (ASTM, 2007). The Portland cement control (mortar bar without any additives) expanded by 0.09% after 16 d (Figure 3-6), which met the ASTM standard and indicated the sand used in this study was reactive enough to cause ASR (Shao et al., 2000). Compared to other samples in Figure 3-6, mortar bar with 10% silica fume had the least expansion (0.05%), which was interpreted to mean that silica fume satisfactorily inhibited ASR because it had the strongest pozzolanic activity. Expansion was similar and non-significant (P = 0.8690) in mortar bars with 20% ash (0.0713%), 10% ash + 5% Na_2SO_4 (0.08%) and 10% ash + 5% $CaCl_2 \cdot 2H_2O$ (0.08%) (Figure 3-6). Less expansion in cement-ash blends suggested an advantageous contribution from ash, due to either the pozzolanic reaction, or the reduction of hydration heat, or both simultaneously. The mortar bar with 10% ash had the similar expansion (0.08%) with the control after 16 d (P =0.9714). Possibly the ash contained appreciable quantities of Na_2O and K_2O (1.35% in total, Table 3-4) compared to Portland cement (0.93% in total, Table 3-4), which may have increased the alkalinity and the ASR phenomena, but why this was the case with 10% ash and not 20% ash is unknown and warrants further study.

3.5. Conclusions

Switchgrass combusted for bioenergy generates a large amount of hazardous ash (5% by mass) for disposal. After grinding for 30 s, ground ash had a porous structure with 65.0 μm of mean particle size and 41.2 $m^2 \cdot g^{-1}$ of BET surface area. Ground ash consisted of 67.2% of SiO_2 and its structure contained 72.2% of amorphous crystal. This

ash was a good pozzolan in blended cement, and its pozzolanic activity was improved by adding chemical accelerators (5% Na_2SO_4 and 5% $CaCl_2 \cdot 2H_2O$ were equally effective). Chemical acceleration was continuously effective, but it was more efficient in the early stage than late stage. The compressive strength and the resistance to ASR expansion of blended cement containing 10% switchgrass ash (with a chemical accelerator) was comparable to conventional Portland cement. The further studies might enhance the pozzolanic activity of switchgrass ash by controlling the combustion temperature and retention time, thus removing the carbon and increasing the amorphous crystal content in ash. However, the potential side effect (e.g. chlorine corrosion) of chemical accelerators also should be considered in future research.

3.6. Figures and tables

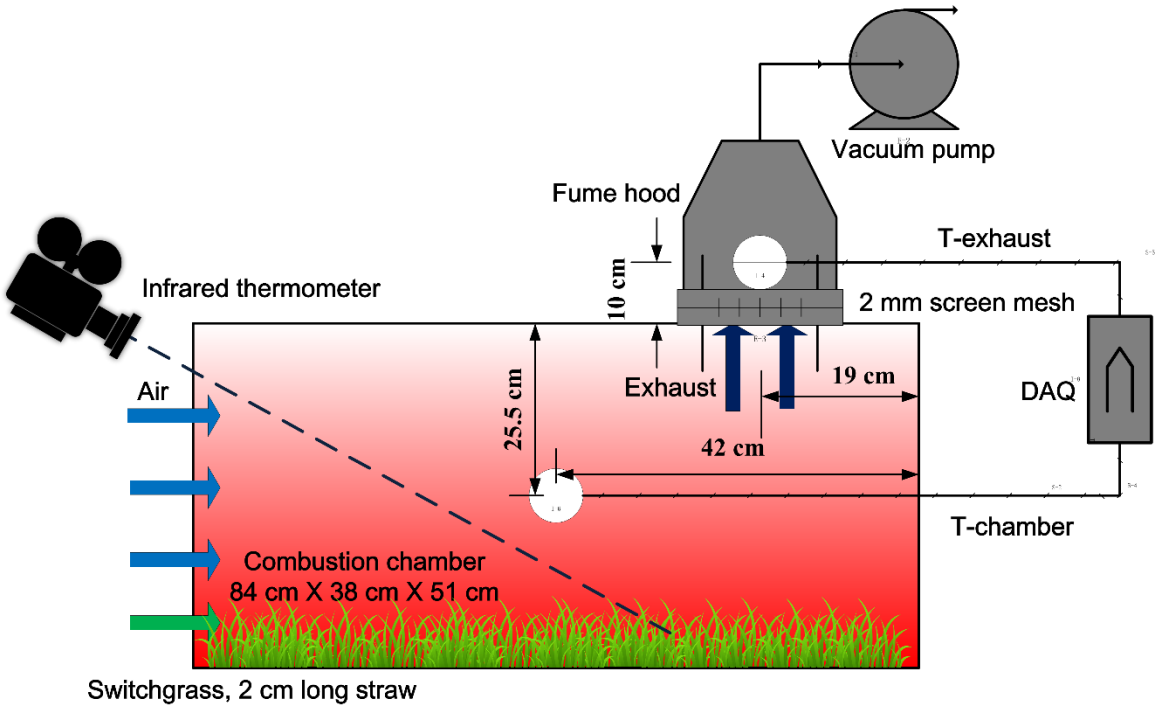

Figure 3- 1. Schematic diagram of the lab-designed furnace for switchgrass combustion. DAQ was the data acquisition system.

T-exhaust and T-chamber were the thermocouples linked to DAQ for measuring the temperatures of exhaust gas and chamber interior. An infrared thermometer was set up to monitor the temperature of fuel surface.

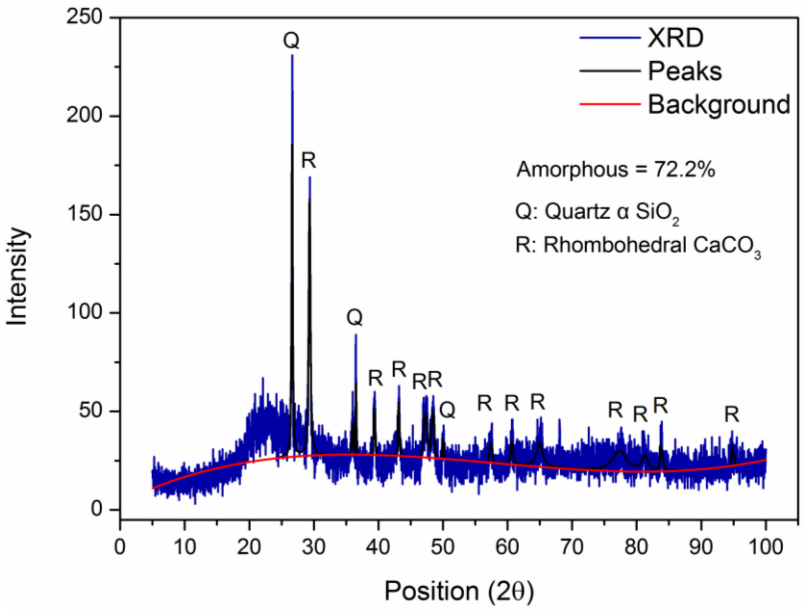

(a)

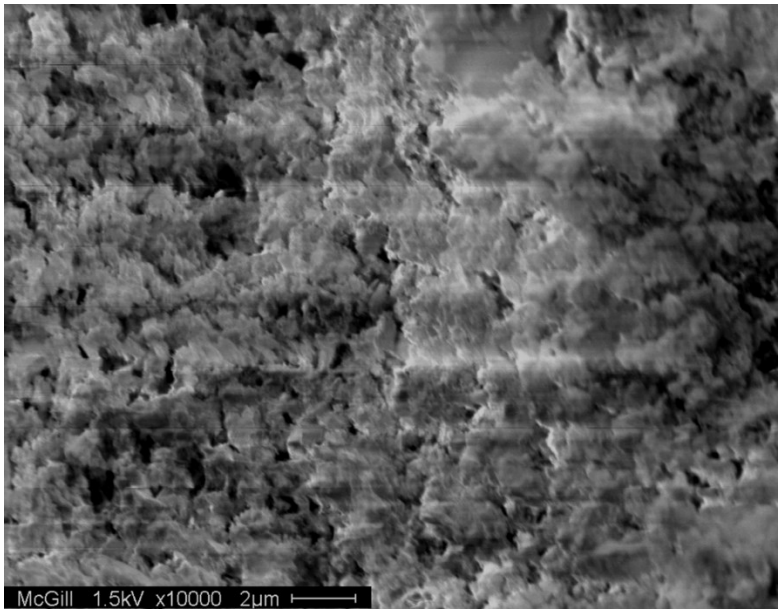

(b)

Figure 3- 2. (a) Crystal structure of the ground ash from switchgrass combustion, investigated by XRD. Peaks, background curve and amorphous content were determined by the Rietveld refinement; (b) microstructural observation of the ground ash.

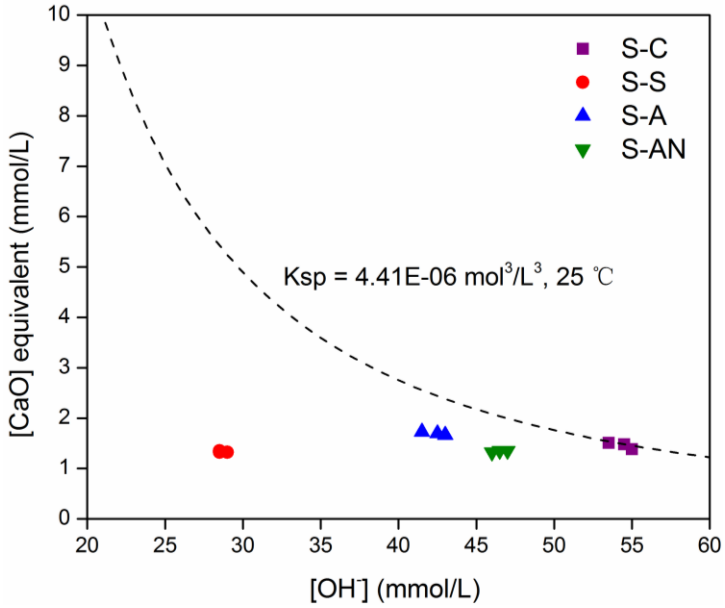

(a)

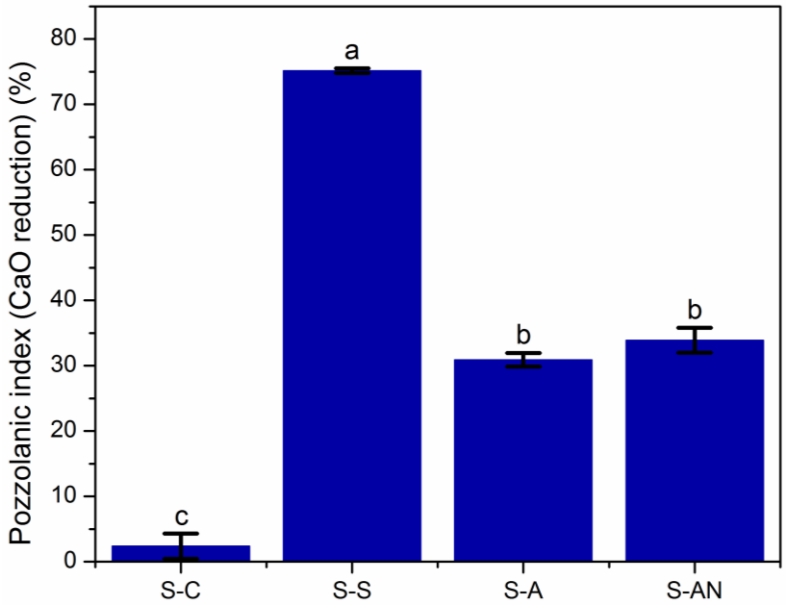

(b)

Figure 3- 3. (a) Results of Frattini test, showing the solubility profile (dotted line) of the saturated $Ca(OH)_2$ solution at 25 °C; (b) pozzolanic activity index derived from Frattini test.

Points below the solubility profile indicated positive pozzolanic activity. Values above 0% suggested a positive pozzolanic activity. Columns with different letters were significantly different at $P<0.05$, Fisher's LSD test. S-C: the sample with cement alone; S-S: the samples contains silica fume; S-A: the samples contains switchgrass ash; S-AN: the samples contains switchgrass ash and Na_2SO_4.

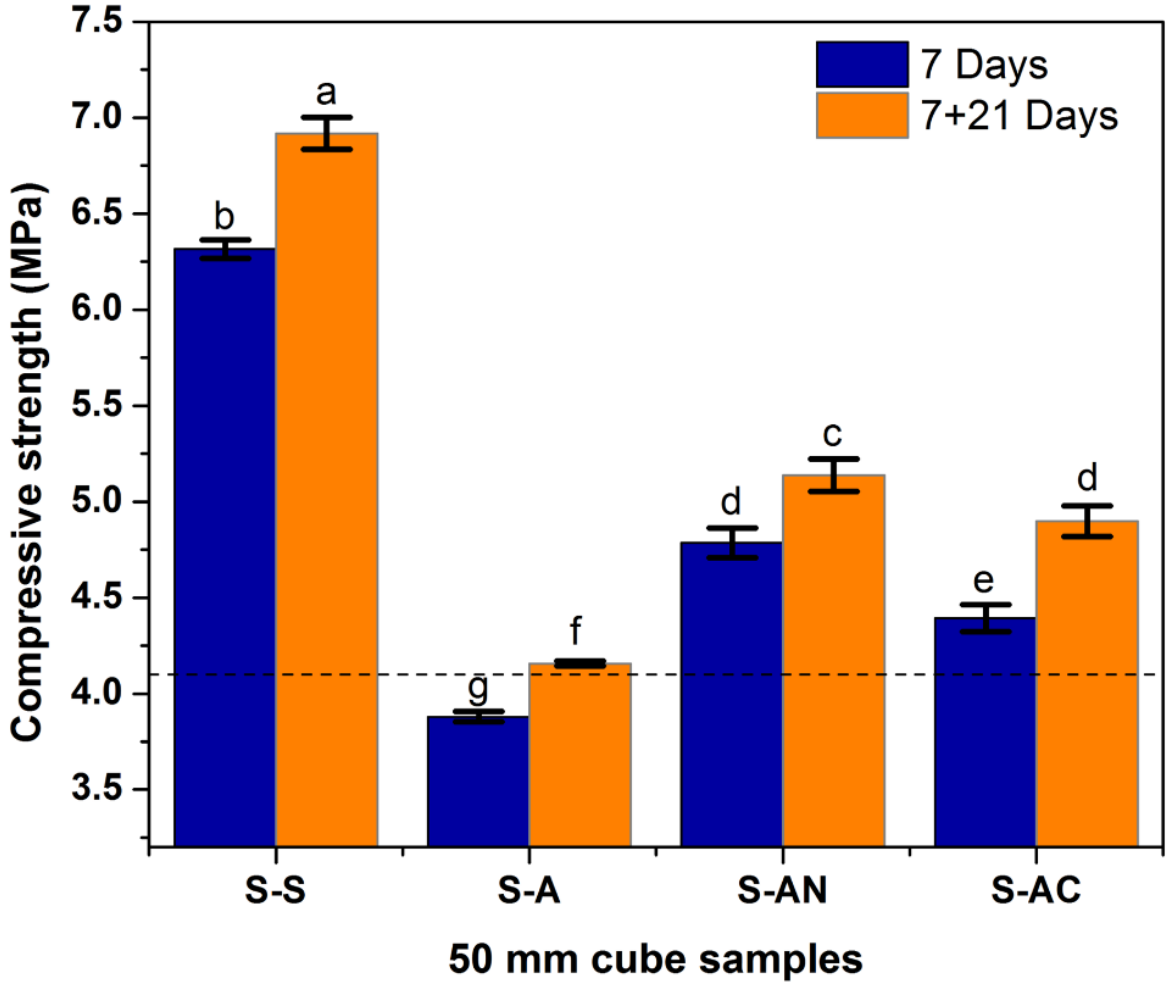

Figure 3- 4. Strength of 50 mm lime-ash cubes.

Horizontal dash in graph was at 4.1 MPa, which was the strength criteria requited by ASTM C593-06. Columns with different letters were significantly different at $P<0.05$, Fisher's LSD test.

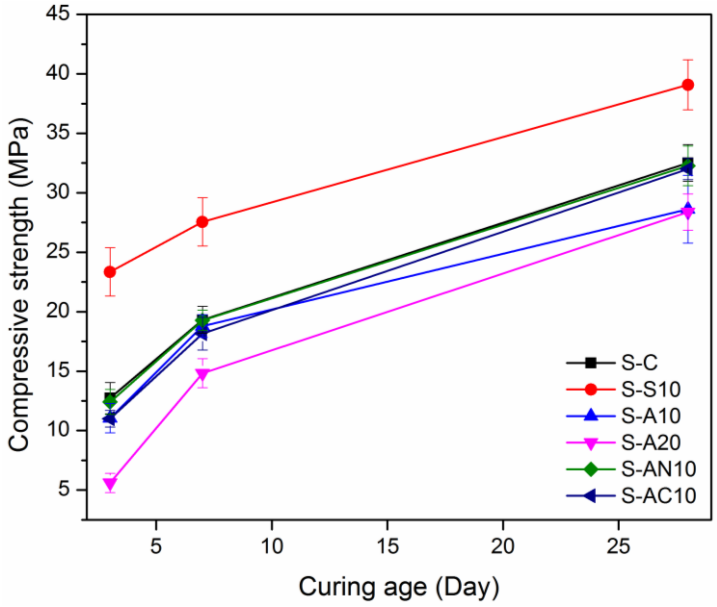

(a)

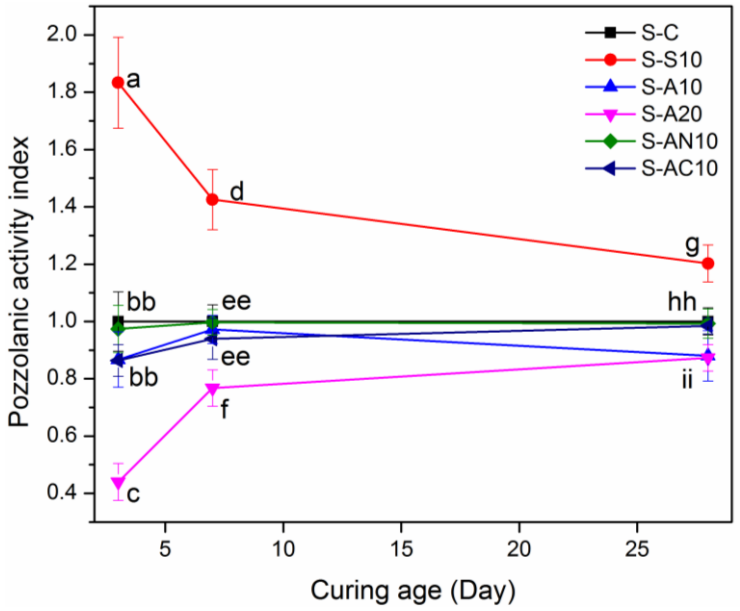

(b)

Figure 3- 5. (a) Compressive strength of 50 mm × 100 mm concrete cylinders; (b) pozzolanic activity index based on the compressive strength of concrete cylinders.

Value above 1.0 indicated a positive pozzolanic activity. Results with different letters were significantly different at $P<0.05$, Fisher's LSD test.

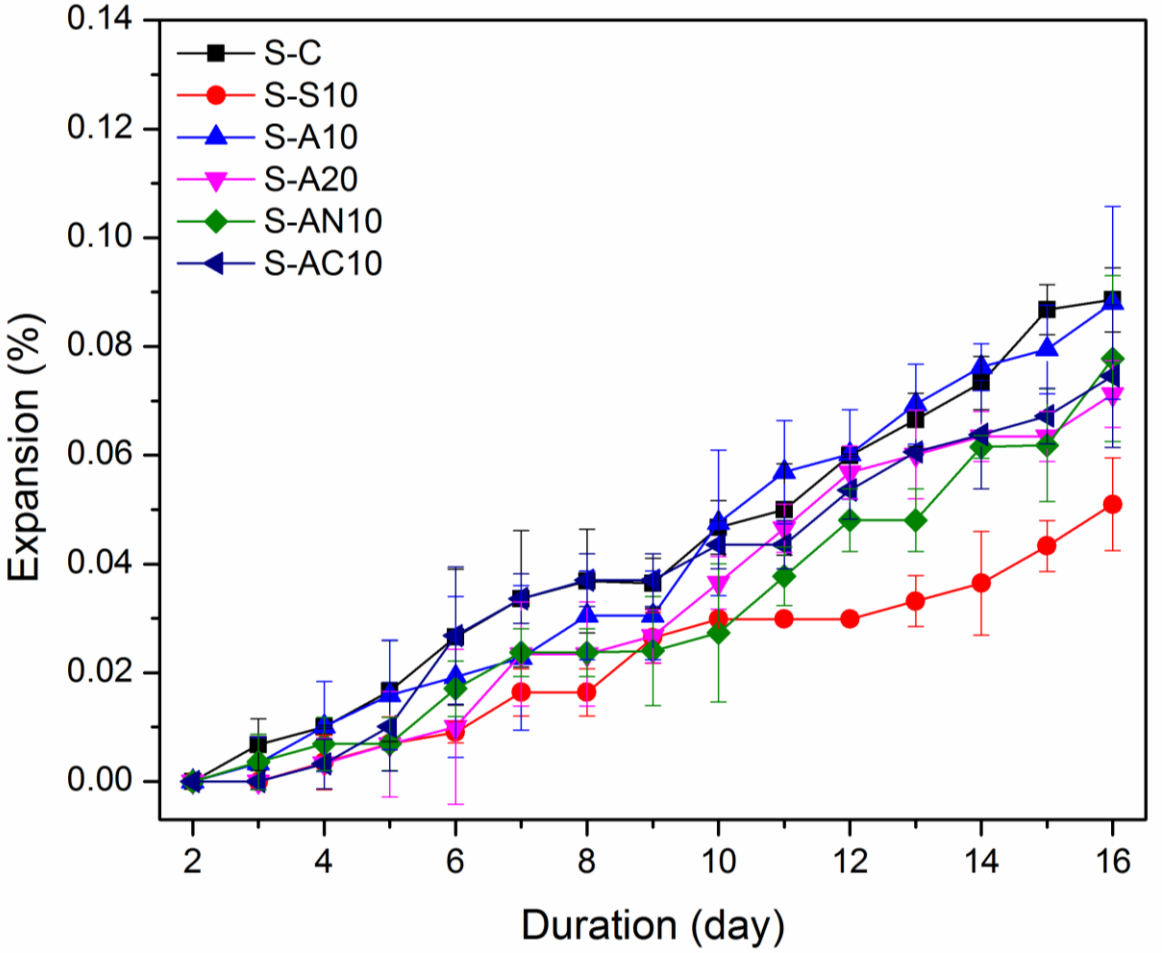

Figure 3- 6. Expansion results of 25 mm × 25 mm × 100 mm mortar bars.

Points were the mean ± standard error of n=3 replicates, except n=2 for S-A10 at the 16th d because one outlier was omitted from the analysis.

Table 3- 1. Designations and mixture proportions (g) of Frattini test and lime-ash test.

S-S: the samples contains silica fume; S-A: the samples contains switchgrass ash; S-AN: the samples contains switchgrass ash and Na_2SO_4.

Mixture (g)	**Frattini test**				**Lime-ash test**			
	S-C	S-S	S-A	S-AN	S-S	S-A	S-AN	S-AC
Portland cement	20	16	16	16	—	—	—	—
Hydrated lime	—	—	—	—	180	180	180	180
Sand	—	—	—	—	1480	1480	1480	1480
Silica fume	0	4	0	0	360	0	0	0
Ash	0	0	4	4	0	360	360	360
5% Na_2SO_4	0	0	0	1	0	0	27	0
5% $CaCl_2 \cdot 2H_2O$	—	—	—	—	0	0	0	27
Water	100	100	100	100	297	297	312	312

Table 3- 2. Designations and mixture proportions ($kg \cdot m^{-3}$) of concrete compressive strength test and expansion test.

Mixture (kg/m^3)	Relative density	S-C	S-S10	S-A10	S-A20	S-AN10	S-AC10
Concrete compressive strength test							
Portland cement	2.87	330	297	297	264	297	297
Fine aggregate	2.81	660	594	594	528	594	594
Course aggregate	2.61	1226	1103	1103	980	1103	1103
Silica fume	2.70	0	33	0	0	0	0
Ash	1.79	0	0	33	66	33	33
5% Na_2SO_4	—	0	0	0	0	9	0
5% $CaCl_2 \cdot 2H_2O$	—	0	0	0	0	0	9
Water	—	182	182	182	182	182	182
Mortar bar expansion test							
Portland cement	2.87	440	396	396	352	396	396
Fine aggregate	2.81	990	891	891	792	891	891
Course aggregate	2.61	—	—	—	—	—	—
Silica fume	2.70	0	44	0	0	0	0
Ash	1.79	0	0	44	88	44	44
5% Na_2SO_4	—	0	0	0	0	10	0
5% $CaCl_2 \cdot 2H_2O$	—	0	0	0	0	0	10
Water	—	207	207	207	207	207	207

Table 3- 3. Proximate and ultimate analysis, and calorific value of the switchgrass.

Proximate analysis, w.t.%					
Basis		Moisture	Volatile matter	Ash	Fixed carbon
Air		6.55	80.55	4.69	8.21
Dry		—	86.20	5.02	8.78
Ultimate analysis, dry basis, w.t. %					Calorific value, $MJ \cdot kg^{-1}$
C	H	N	S	O	HHV
41.30	5.86	0.60	0.06	52.18	17.46

Table 3- 4. Major mineral oxides, specific surface area, mean particle size, BET surface area, thermal property and color of ground ash from switchgrass combustion, silica fume, and Portland cement.

Mineral elements (% w.t.)	Switchgrass ash	Silica fume	Ordinary Portland cement
SiO_2	67.18	95.01	19.67
Al_2O_3	0.68	0.02	4.82
Fe_2O_3(T)	0.31	0.11	2.79
MnO	0.07	0.02	0.07
MgO	2.05	0.76	2.53
CaO	12.28	0.82	61.77
Na_2O	0.11	< 0.01	0.20
K_2O	1.24	0.55	0.73
TiO_2	0.06	< 0.01	0.22
P_2O_5	1.15	0.08	0.22
Cr_2O_3	0.01	< 0.01	0.01
V_2O_5	< 0.003	< 0.003	0.02
Loss on ignition (LOI)	14.77	3.20	2.21
Total	99.91	100.60	95.27
$SiO_2+Al_2O_3+Fe_2O_3$	68.17	95.14	27.28
Specific surface area ($m^2 \cdot m^{-3}$)	6251.4	—	12820
Mean particle size (μm)	65.00	—	21.95
BET Surface Area ($m^2 \cdot g^{-1}$)	41.25	—	—
Colour	Grey	Dark	Grey

CONNECTING PARAGRAPH TO CHAPTER 4

Recycling switchgrass ash by mixing it with the cement was proven technically feasible in Chapter 3. Blended cement with 10% ash and either 5% Na_2SO_4 or 5% $CaCl_2 \cdot 2H_2O$ has a similar material strength as conventional cement. However, the pozzolanic activity of switchgrass ash could be enhanced further by optimizing the combustion process. Chapter 4 is based on the premise that selecting combustion parameters to achieve high energy conversion from switchgrass will simultaneously generate residual ash with suitable physicochemical properties for the pozzolanic reaction in blended cement. This study considered how to optimize the following combustion conditions: temperature (350, 450, 550 or 650 °C) and retention time (1 or 4 h), using a factorial design with 4 × 2 treatments.

CHAPTER 4. Optimizing the Energy Conversion of Combustion and Ash Recycling As Pozzolan Simultaneously

Optimization of switchgrass combustion for simultaneous production of energy and pozzolan

4.1. Abstract

Combustion of switchgrass, a low carbon fuel, generates energy and ash that can be recycled as a pozzolan in cement. This study aimed to optimize switchgrass combustion to achieve high energy conversion and ash recycling value for cement. Combustion factors under investigation included temperature (350, 450, 550 or 650 °C) and retention time (1 or 4 h). Energy release was quantified by thermogravimetric analysis-differential scanning calorimetry, and ash pozzolanic activity was assessed with the concrete strength test. A numeric simulation model of the pozzolanic reaction, based on unbiased experimental data from $Ca(OH)_2$—ash suspensions, provided insight into how combustion conditions affected the pozzolanic properties of switchgrass ash. Consequently, combustion at 550 °C for 4 h was recommended for concurrently optimizing the ash pozzolanic activity (114%) and energy output (4.21 $kJ \cdot g^{-1}$) from switchgrass.

4.2. Introduction

Replacing fossil fuel with LCF is an emerging trend in energy-intensive industries, such as cement production (Schneider et al., 2011a). Since cement is produced via calcination in a kiln at 1450 W°C, a medium-size cement plant would deplete 3-6 MJ of

fossil fuel and emit 0.8 kg of CO_2 per 1 kg of cement fabricated (Huntzinger & Eatmon, 2009). An energy crop like switchgrass (*Panicum vigratum L.*) is a suitable LCF because it is carbon-neutral in its life cycle. Its energy value (17.5 MJ of higher heating value) is similar to other cost-effective biomass already used as industrial LCF (17-21 $MJ \cdot kg^{-1}$) (Yin, 2011). Thus, a cement plant can use switchgrass fuel to partially reduce its fossil fuel consumption and carbon footprint.

Biomass energy is normally generated via combustion at temperatures between 300-700 °C in a normal air atmosphere, which can be achieved efficiently in a biomass combustor (e.g. moving-grate boiler or fluidized bed) that produces heat, steam or electricity (Jenkins et al., 1998). Substituting 5% or 20% of coal with switchgrass (4.62% ash content and 17.5 $MJ \cdot kg^{-1}$ of energy value) in a cement kiln would produce 1.39 kg or 5.54 kg of ash generated on-site per 1000 kg of cement produced (Wang et al., 2014b). However, the initial switchgrass contains 2.3-7.6% of ash, and its ash is usually rich in metal elements (e.g. Si, Fe, Na, K, Ca, etc.) (Monti et al., 2008). Consequently, switchgrass ash is an industrial solid waste owing to its fine particle size (≤ 5 μm) and mineral-rich properties ($\geq 85\%$ by mass). Any cement plant that considers using switchgrass as LCF must develop an ash disposal plan that is economical and sustainable.

It is possible to dispose of switchgrass ash by recycling it in cement. If ash contains $\geq 70\%$ of ($SiO_2 + Al_2O_3 + Fe_2O_3$), it can be considered an additive with similar functions as silica fume or metakaolin (Chusilp et al., 2009). Physically, ash that passes a mesh ≤ 45 μm has a fine particle size that acts as a filler in concrete, thereby reducing its permeability (Chindaprasirt et al., 2007a). Chemically, the appreciable concentrations of SiO_2, Al_2O_3 and Fe_2O_3 in ash can enhance the chemical binding in the concrete through a

pozzolanic reaction. Specifically, amorphous SiO_2 in the ash is expected to react with free $Ca(OH)_2$ in cement to form calcium silicate hydrate ($((CaO)_x \cdot (SiO_2)_y \cdot (H_2O)_z$; C-S-H). Since C-S-H is the principal strength contributor in concrete, supplementary C-S-H formation by the pozzolanic reaction should further enhance concrete performance, giving it greater strength and more durability. Therefore, if the switchgrass combustion process can be optimized to generate ash with higher pozzolanic activity, the ash recycling value for cement increases and it will improve the performance of blended concrete as well.

According to our ongoing work, ash from an open switchgrass combustion (≈ 411 °C for 5 min) contained 67.2% of SiO_2 (by mass), and 72.2% of its crystal was amorphous (by crystal unit) (Wang et al., 2014a). I substituted 10% of cement with the ash (≈ 65 μm of mean particle size) to test the strength of concrete test cylinders (50 mm diameter, 100 mm height). After 28 d curing in a moisture room at 23 °C, concrete strength was 28.6 MPa, which was weaker than the concrete without ash replacement (32.5 MPa). The lower strength of concrete produced from a cement blend containing 10% ash was ascribed to its lower SiO_2 content (compared to silica fume, the conventional pozzolan containing 99% SiO_2) and insufficient amorphous phase in crystal, since the SiO_2 concentration and amorphous crystal microstructure determine the pozzolanic activity of ash (Jauberthie et al., 2000).

Adjusting the combustion conditions could enhance the pozzolanic properties of switchgrass ash and increase its recycling value for blending with cement. The general criteria for generating ash that can be blended in cement as a satisfactory pozzolan is that the original biomass should contain ≥ 1.00% of Si, and Si/Ca ratio should be ≥ 1.00 by

mass (Madani Hosseini et al., 2011), which is the case for switchgrass. Moreover, ash crystal should be amorphous predominately, which makes the SiO_2 chemically reactive during the pozzolanic reaction. Because carbon content of ash (affecting the SiO_2 concentration in ash) and crystal microstructure are considerably affected by combustion parameters, it should be possible to optimize the combustion process to generate ash with the desired level of pozzolanic activity. For instance, Cordeiro et al. (2009) studied the combustion effect (400-800 °C, for 3 h) on the pozzolanic activity of sugar cane bagasse ash. Ash from the 600 °C combustion possessed the best pozzolanic activity due to its amorphous silica, low carbon content and high specific surface area. Biricik et al. (1999) stated that wheat straw ash produced from combustion at 670 °C for 5 h had a higher pozzolanic activity than that from 570 °C combustion. Nair et al. (2008) asserted that carbon was not completely removed from rice husk ash when it was combusted at 300 °C, whereas combustion at 500-700 °C for 12 h generated ash with the best pozzolanic activity owing to its high amorphous silica content. Villar-Cociña et al. (2011) found that bamboo leaf ash (600 °C combustion for 2 h) was totally amorphous, and recommended these parameters for combustion operations aiming to produce ash for blending with cement. These studies illustrate that careful control of combustion temperature and retention time can produce ash with advantageous pozzolanic activity.

Combustion temperature and time alter the physiochemical properties of ash crystal, thus changing its pozzolanic performance (Zain et al., 2011). Virtually no information is available on the crystal change in switchgrass ash due to combustion conditions, although it can be computed with kinetic parameters, which are achieved via a numeric simulation model of the pozzolanic reaction. Simulation is based on the

experimental data of the conductivity or Ca^{2+} concentration ($[Ca^{2+}]$) in a $Ca(OH)_2$—ash suspension (Luxán et al., 1989). Villar-Cociña et al. (2003) explored the pozzolanic reaction of sugar cane straw ash and rice husk ash (combusted at 800 °C or 1000 °C), generating experimental data for the simulation model by mixing 2.1 g of ash with 75 mL of saturated $Ca(OH)_2$ at 26±1 °C, and then recording conductivity change in the solution for a 624 h period. A similar method (2.1 g of ash + 100 mL of $Ca(OH)_2$, at 26±1 °C in 50 h) was also used to evaluate the pozzolanic activity of bamboo leaf ash (combusted at 600 °C for 2 h) (Villar-Cociña et al., 2011). Yet, as this method indirectly measured the reaction progress by conductivity, it could not discover the change of Ca^{2+} (as a principal reactant) during the pozzolanic reaction. These shortcomings were partially alleviated by the method of Donatello et al. (2010b), who studied the change in $[Ca^{2+}]$ in a $Ca(OH)_2$—pozzolan suspension (1 g of pozzolan + 75 mL of $Ca(OH)_2$, at 40±1 °C). However, since Ca^{2+} was titrated at room temperature (25-28 °C) but $Ca(OH)_2$—pozzolan reaction occurred at 40±1 °C, this temperature difference would affect the accuracy of $[Ca^{2+}]$ results because $Ca(OH)_2$ solubility was controlled by its negative heat of solution, leading to condensation of extra $Ca(OH)_2$ at 40 °C (the temperature of $Ca(OH)_2$—ash reaction). Consequently, this condensed $Ca(OH)_2$ would dissolve while the pozzolanic reaction occurred, thus affecting the accuracy of the result. Therefore, an unbiased method is needed to scrutinize the conductivity—$[Ca^{2+}]$ correlation during the pozzolanic reaction, and also to improve the accuracy of the method by performing all steps at the same temperature.

In addition to the effect on ash properties, combustion temperature affects energy conversion from switchgrass. Typically, biomass combustion consists of a preparation

step (moisture removal, ≤ 200 °C), a fast combustion step (volatile pyrolysis, 200-500 °C) and a slow combustion step (char calcination, ≥ 500 °C) (Nussbaumer, 2003). Mass loss from the fuel occurs mostly in the fast combustion step, with a longer char calcination period assuring that the carbon is totally transformed to CO_2 (complete combustion). Previous studies using thermogravimetric analysis-differential scanning calorimetry (TGA-DSC) (25-1000 °C) consistently proved that the highest energy conversion efficiency occurs when temperature is high enough to achieve complete combustion (Gil et al., 2010; Haykırı-Açma, 2003; Yuzbasi & Selçuk, 2011). As energy extraction is the principal objective of switchgrass combustion, I should examine the temperature effect on energy output and ash pozzolanic activity concurrently, especially when I consider a LCF suitable for a cement plant.

This paper aimed to optimize switchgrass combustion to maximize the ash recycling value in cement and energy output concurrently. First, the combustion process was studied using temperatures of 350, 450, 550 and 650 °C, and retention times of 1 and 4 h, and compared to ash from open combustion (as a control group). Combustion energy output at those temperatures was estimated by TGA-DSC, and ash pozzolanic activity was examined by measuring the strength of the concrete made from cement blended with 10% ash. Second, the crystal characteristics of switchgrass ash were evaluated with an unbiased method that relied on experimental data from $Ca(OH)_2$—ash suspensions to run a numeric simulation of the pozzolanic reaction. Kinetic parameters obtained from the simulation quantified the physiochemical change of ash and the conductivity—$[Ca^{2+}]$ correlation during the pozzolanic reaction.

4.3. Material and methods

4.3.1. Switchgrass preparation and characterization

Switchgrass was collected from a farm in Williamsburg, Ontario, Canada. Chemical composition of the switchgrass was analyzed by the Fusion Inductively Coupled Plasma (ICP) method with a Varian Vista 735 ICP analyzer. Combustion profile of the switchgrass was characterized by the TGA-DSC with a NETZSCH TG 449 F3 Jupiter Analyzer. About 18 mg of fine switchgrass particle was placed in an Al_2O_3 crucible and heated to 900 °C from 25 °C in a 20% of O_2 + 80% of N_2 (by volume) atmosphere. Volume rate of the gas was 20 mL/min, and heating rate was 10 °C/min. Consequently, mass loss (%) and enthalpy behavior ($mW \cdot mg^{-1}$) were transcribed throughout the entire combustion process. Based on the TGA-DSC results, energy output ($kJ \cdot g^{-1}$) from the combustion was estimated from Eq. 4-1 below,

$$Energy\ output = \int_0^{0.1 \times T - 2.78} 0.06 \times \left(\frac{\mathrm{d}H}{\mathrm{d}T} - \frac{\mathrm{d}H'}{\mathrm{d}T}\right) \mathrm{d}t \qquad (4\text{-}1)$$

where H ($mW \cdot mg^{-1}$) was the heat flux of switchgrass sample, H' ($mW \cdot mg^{-1}$) was the heat flux of background, t (min) and T (K) were the time and temperature during the combustion.

4.3.2. Switchgrass combustion

I investigated the effect of combustion temperatures (350, 450, 550 and 650 °C) and retention times (1 and 4 h) on the pozzolanic activity of ash (Table 4-1). Each test was replicated three times. Before the test, switchgrass was manually sheared to 0.5 cm long and approximately 10 g of the switchgrass was placed in a crucible at a Nabertherm L 5/11 kiln with a gas ventilation system. Combustion was controlled at the target

temperature for precisely 1 or 4 h. Then, ash was cooled to room temperature naturally, before it was collected and weighted. Mass loss following combustion as a function of temperature and retention time was compared statistically using a 2-factor Analysis of Variance (ANOVA) Fisher's LSD test (at 0.05 level). In addition, ash from open (uncontrolled) combustion was incorporated as a control group to compare the influence of a well-controlled combustion on ash properties. Open combustion was done in an 84 × 38 × 51 cm combustor, at ≈ 411 °C for 5 min. All ash samples were ground with a laboratory steel ball mill for 30 s prior to further analysis.

4.3.3. Switchgrass ash characterization

As-received ash was characterized for its chemical, thermal, crystal and microstructural properties. Ash from the open combustion (control group) was analyzed by the X-ray fluorescence (XRF) method with a PW2400 wavelength dispersive XRF spectrometer for its mineral oxide composition. Thermal property of the ash (control group) (≈ 10.6 mg) was examined by the TGA-DSC (experimental method was the same as described for switchgrass thermal characterization in Section 2.1). Consequently, some critical temperatures were estimated from the DSC curve, including glass transition point, crystallization point, and melting/vaporization zone. Ash from all combustion conditions was characterized for its crystalline structure by the X-Ray diffraction (XRD) method with a Philips PW 1710 Powder X-Ray Diffractometer. Generator power of the X-ray was 40 kV/20 mA with Cu anode material, and scanning angle ranged from 5 to 100 °2θ. Scanning step size was set at 0.04 °2θ·s^{-1}. Amorphous degree in crystal was quantified by

the Rietveld refinement using Chebyshev I algorithm (Winburn et al., 2000), which was simulated by a PANalytical XRD software suite. Ash microstructure was observed by the Scanning Electron Microscope (SEM) with a FEI Inspect F-50 FE-SEM analyzer. Elemental mapping on the ash 550-4 was performed by an EDAX Energy Dispersive Spectroscopy (EDS) with Octane Silicon Drift Detector (SDD).

4.3.4. Concrete compressive strength test

Compressive strength of concrete cylinders (50 mm diameter, 100 mm height) was tested to estimate the pozzolanic activity index of ash. As described in Table 4-2, Blended cement was 90% Portland cement (from Lafarge Cement) and 10% ash. Concrete without ash replacement (100% Portland cement) was considered as the reference standard. Chemical composition of the cement was quantified by the XRF, and its cementing property was approximated by Bogue's equation (Bogue, 1929). Specific surface area and mean particulate size of the cement were analyzed with a Horiba laser scattering particle size analyzer. Water/(cement+ash) ratio was 0.55 by mass, and coarse/fine aggregate mass ratio was 1.86. After casting, concrete samples were cured in a moisture room at 23 °C for 28 d. Compressive strength of concrete was then tested with a Sintech 30/G Electromechanical Compressor (three replicates). To statistically evaluate the impact of combustion temperature and retention time on the ash, compressive strength was interpreted by a two-way Analysis of Variance (ANOVA) with replication (n=3) test (at 0.05 significance level). The pozzolanic activity index (PAI, %) of the ash was calculated from Eq. 4-2,

$$PAI = \frac{Compressive\ strength}{Reference\ strength} \times 100 \qquad (4\text{-}2)$$

Moreover, for eliminating the disturbance of standard deviation on the PAI, a Signal-to-Noise ratio index (S/N) (Eq. 4-3) was calculated to distinguish the best combustion condition for the greatest PAI by choosing the highest S/N value (Hew et al., 2010).

$$\frac{S}{N} = -10 \times log_{10}\left(\frac{\sum_{j=1}^{3}\left(\frac{1}{P_{ij}}\right)^2}{3}\right) \quad (4\text{-}3)$$

where P_{ij} corresponded to the PAI of the j^{th} replication in the i^{th} ash sample group.

4.3.5. Numeric simulation of pozzolanic reaction

4.3.5.1. Pozzolanic reaction progress measurement

For preparing a saturated $Ca(OH)_2$ solution, 2 g of $Ca(OH)_2$ powder (from Fisher Scientific) was dissolved in 1 L of water before filtration (to remove extra insoluble $Ca(OH)_2$). For each ash sample, 2 g of the ash was added to a plastic bottle containing 75 ml of the saturated $Ca(OH)_2$ solution. Plastic bottle was sealed tightly to avoid carbonation and preserved at 25 °C for 360 h. Solution was sampled every 24 h to measure the conductivity ($mS \cdot cm^{-1}$) and Ca^{2+} concentration ($[Ca^{2+}]$, $mmol \cdot L^{-1}$). Conductivity was tested with a temperature-compensated Fisher Scientific Traceable conductivity meter. Ca^{2+} was titrated with 0.03 $mol \cdot L^{-1}$ EDTA solution containing Patton and Reeders indicator. Additionally, calibration was done to obtain the conductivity—$[Ca^{2+}]$—pH correlation in a pure $Ca(OH)_2$ solution (Figure S4-1). All measurements were

replicated three times. Based on the experimental data, pozzolanic reaction progress index (ξ) was calculated by Eq. 4-4 or Eq. 4-5,

$$\xi - conductivity = \frac{y_0 - y_i}{y_0} \quad (4\text{-}4)$$

$$\xi - [Ca^{2+}] = \frac{z_0 - z_i}{z_0} \quad (4\text{-}5)$$

where ξ-conductivity or ξ-[Ca^{2+}] was the reaction progress calculated via the conductivity or [Ca^{2+}] results. y_i and z_i symbolized the conductivity and [Ca^{2+}] at 24 × i h, and y_0 and z_0 represented the initial value at 0 h.

4.3.5.2. Numeric simulation

It is rational to simplify the pozzolanic reaction as a heterogeneous solid-solution process, which could be expressed by a pseudo-stable decreasing nucleus model (DNM) (Villar-Cociña et al., 2003). I assumed that the pozzolanic reaction was controlled simultaneously by ionic diffusion and chemical interaction. Based on these assumptions, numeric simulation was performed according to Eq. 4-6 and Eq. 4-7 (Rosell-Lam et al., 2011),

$$\xi = 1 - \frac{0.23 \times e^{\frac{-3 \times t}{\tau}} \times \left(-1 + e^{\frac{t}{\tau}}\right) \times \frac{1}{\tau}}{C_0 \times D_e \times r_s} + \frac{0.23 \times \frac{1}{\tau} \times e^{\frac{-t}{\tau}}}{C_0 \times K \times r_s^2} \quad (4\text{-}6)$$

$$K = \frac{K_B \times T}{h} \times e^{\frac{-\Delta G^{\#}}{R \times T}} \quad (4\text{-}7)$$

where ξ (1) was ζ-conductivity or ξ-[Ca^{2+}]. C_0 (mS·cm^{-1} or mmol·L^{-1}) represented the initial value of conductivity or [Ca^{2+}], and t (h) was reaction time. D_e (mm^2·h^{-1}) was a diffusion coefficient, and K (h^{-1}) symbolized a reaction rate constant. τ (h) was the time interval until pozzolan nucleus decreased to 37% of initial value. r_s (mm) was the radius

of pseudo-stable solid in the solid-solution reaction (r_s = 0.15 mm). $\Delta G^{\#}$ ($kJ \cdot mol^{-1}$) corresponded to the free energy of activation for the overall reaction. K_B and h were the Boltzmann constant and the Planck constant, respectively. T (K) was absolute temperature and R corresponded to the ideal gas constant.

4.3.5.3. Interpretation of simulation results

To statistically evaluate the impact of two ξ measurement method difference on the simulation results, I ran a two-way ANOVA without replication test at 0.05 significance level. Ash sample variation and measurement difference (conductivity or $[Ca^{2+}]$) were considered as two independent variables in the test.

4.4. Results and discussion

4.4.1. Chemical and thermal properties of switchgrass

Switchgrass used in this study contained, on average, 2.23% of SiO_2 and 0.56% of CaO (Table S4-1). Switchgrass had 1.04% of Si and the Si/Ca ratio was 2.60 (by mass), which guaranteed an adequate Si content for the pozzolanic reaction (Madani Hosseini et al., 2011). Switchgrass also had 96.4% loss on ignition (LOI), which was due to carbon and moisture removal as well as metal element evaporation at high temperature (e.g. Na_2O or K_2O, usually ≥ 800 °C). As shown in the TGA-DSC profile (Figure S4-2), the combustion profile of the switchgrass evidently consisted of three steps, including moisture removal (7.88% of mass loss, 25-254 °C), fast volatile oxidization (55.1% of mass loss, 254-367 °C) and slow char calcination (33.7% of mass loss, 367-900 °C). During combustion, the maximal thermal decomposition rate (-1.68 $\%\cdot°C^{-1}$) occurred

during the fast volatile oxidization stage (≈ 348 °C), indicating that switchgrass combustion must reach at least 348 °C to activate energy extraction. Switchgrass combustion was an exothermic process, which released 8.13 $kJ \cdot g^{-1}$ of heat hen temperature increased from 25 °C to 900 °C (Figure S4-3).

4.4.2. Combustion test of switchgrass

Increase in temperature (from 350 to 650 °C) consistently raised the mass loss, an indicator of complete combustion, from 50.2% to 90.1% (1 h), or 54.0% to 91.4% (4 h) (Figure 4-1). This was attributed to the slow char calcination in high temperature zone (367-900 °C). Color of the ash changed from dark to white as the temperature increased (Figure S4-4), which confirmed that more carbon in ash was removed by the char calcination. Moreover, longer retention (from 1 to 4 h) enhanced combustion. Prolonged retention boosted mass loss from 50.2% to 54.0% (350 °C), and from 70.5% to 73.6% (450 °C). Yet, there was no statistically significant difference between the two retention times when temperature was set at 550 °C ($P = 0.150$) or 650 °C ($P = 0.070$). This affirmed that higher temperatures were more effective than longer retention time to removing the carbon in ash. With a 4 h retention time, the TGA measurements were similar at each temperature tested ($P = 0.470$ at 350 °C, $P = 0.750$ at 450 °C, $P = 0.360$ at 550 °C and $P = 0.470$ at 650 °C). This means that complete energy conversion of switchgrass can be achieved either by setting the temperature at 550 to 650 °C for 1 h, or by lengthening the retention time to 4 h if temperature is set to 350-450 °C.

4.4.3. Characteristics of switchgrass ash

Pozzolanic properties of switchgrass ash were determined from its chemical, thermal, crystal and microstructural characteristics. Ash from the open combustion

(control) contained 67.2% of SiO_2 by mass (Table S4-1), and $SiO_2 + Al_2O_3 + Fe_2O_3$ was nearly 70% in total, which is categorized as Class F ash that could be recycled as a pozzolan in cement (ASTM, 2004). However, its LOI was 14.8% by mass, which was attributed to the short retention time (5 min) and incomplete combustion. High volume of carbon would adversely affect the crystal microstructure and concrete performance (Zain et al., 2011). When temperature increased from 25 °C to 900 °C, mass loss of this ash was 14.1% (Figure 4-2), similar to the LOI in Table S4-1. The entire process was exothermic (0.760 $J \cdot g^{-1}$ of heat released), owing to the carbon removal from the ash. In the ash crystal, glass transition and crystallization happened at 448 °C and 651 °C, thereby the combustion between 448-651 °C would alter the proportion of amorphous forms substantially. At higher temperatures (≥ 762 °C), ash crystal began to fuse and vaporize. Ash melting might cause fouling and slagging problem in a combustor (e.g. moving-grate boiler), which lowers the energy efficiency (Teixeira et al., 2012).

Combustion temperature and retention time influenced the microstructure in ash. XRD profile above a background curve demonstrated that all of the ashes were predominately amorphous, particularly in the zone of 20-40 °2θ (Figure 4-3). Ash from the open combustion had the lowest amorphous silica content (78.2% by crystal unit). Still, a controlled combustion transformed more crystalline phase to amorphous form, and ash 550-4 had the greatest proportion of amorphous forms (85.8%). Longer retention time (4 h) increased the amorphous proportion from 83.6% (450-1) to 85.5% (450-4), and from 83.9% (550-1) to 85.8% (550-4). On the contrary, combustion temperature did not obviously influence the amorphous property of ash. Since a greater amorphous

characteristic could advance the pozzolanic activity, prolonged combustion was beneficial to the ash recycling value for cement.

Microstructure in the ash mainly consisted of plates and debris, and it was affected significantly by combustion conditions (Figure 4-4). Ash 350-1 had the least porous structure. Ash porosity increased greatly when combustion occurred at higher temperatures, either for 1 h or 4 h (samples 450-1, 550-4 and 650-4). High porosity might be the result of combustion that shattered the plates to debris (the ash 650-4). Compared to the ash from open combustion (67.2% of SiO_2), ash 550-4 possessed 85.2 % of SiO_2 (Figure S4-5), which confirmed that more carbon was removed by the higher temperature and longer retention time.

4.4.4 Compressive strength of concrete

Portland cement used in this study had a fine particle size of 22.0 μm. It was comprised of 65.6% of $(CaO)_3 \cdot (SiO_2)$ (abbreviated as C_3S), 6.93% of $(CaO)_2 \cdot (SiO_2)$ (abbreviated as C_2S), 12.7% of $(CaO)_3 \cdot (Al_2O_3)$ (abbreviated as C_3A) and 8.49% of $(CaO)_4 \cdot (Al_2O_3) \cdot (Fe_2O_3)$ (abbreviated as C_4AF) (Table S4-2). After substituting 10% of the cement with ash, all ash samples from controlled combustion possessed greater compressive strength in concrete than the ash from open combustion (29.5 MPa after 28 d) (Figure 4-5). This strength improvement was due to less carbon content and more amorphous forms in ash from controlled combustion, compared to the control group. However, strength of the sample 350-1 (32.1 MPa), 450-1 (29.8 MPa) and 550-1 (30.1 MPa) was slightly lower than the concrete with 100% Portland cement (32.4 MPa, as a

reference group). The explanation was that ash replacement disordered the initial cementitious composition for hydration that creates C-S-H (as a primary strength contributor). On the contrary, ash from combustion with 4 h retention time consistently led to ≥ 32.4 MPa of strength. Since these ashes had the highest SiO_2 content (e.g. 85.2% in the ash 550-4) and also possessed greater proportion of amorphous forms (85.4%-85.8%), their pozzolanic reaction not only offset the disturbance in cementitious composition from ash substitution, but also contributed to supplementary C-S-H bond formation.

A two-way ANOVA with replication (n = 3) test revealed that retention time (P = 2.17e-05) and temperature—retention interaction (P = 0.030) had statistically influenced concrete strength (Table S4-3). However, combustion temperature did not significantly affect the strength (P = 0.620). Thus, I recommend to adjust retention time during a real combustion operation, which would be more efficient to optimize the ash recycling value than altering the temperature. Furthermore, as listed in Table S4-4, ash 550-4 had the highest Signal-to-Noise ratio (S/N), at 41.1. This finding suggested that 550 °C and 4 h were the optimal combustion conditions to generate ash with the highest pozzolanic activity.

4.4.5 Balance between combustion energy output and ash pozzolanic activity

When temperature increased from 350 °C to 650 °C, energy output from the switchgrass combustion monotonically increased from 0.790 $kJ \cdot g^{-1}$ to 5.96 $kJ \cdot g^{-1}$ (Figure 4-6). This relationship indicated that higher combustion temperature led to greater heat release. Concerning the correlation between the temperature and the PAI, ash from 4 h combustion had higher PAI (106%-114%) than from the 1 h combustion (92.1%-104%).

Ash 550-4 exhibited the highest PAI, at 114%, which meant that ash 550-4 could enhance the concrete compressive strength by 14.2% compared to concrete with 100% Portland cement. However, when combustion lasted for 4 h, an overly high temperature (650 °C) instead degraded the PAI from 114% to 106%. The explanation was that a part of amorphous crystal was transformed to crystalline phase in this temperature zone. When considering combustion to optimize the ash recycling value and combustion energy output concurrently, I recommended the setting the temperature to 550 °C and retention time to 4 h for switchgrass combustion.

4.4.6 Kinetic simulation of pozzolanic reaction

4.4.6.1. Combustion influence on kinetic parameters

Since saturated $Ca(OH)_2$ solution preparation, pozzolanic reaction and measurement were conducted at the same temperature (25 °C), our work could provide unbiased experimental data for the numerical simulation. Conductivity in a pure $Ca(OH)_2$ solution was strongly correlated to the $[Ca^{2+}]$ (R^2 = 0.9857, Figure S4-1). Thus, there was an apparent similarity with two reaction progress ξ in the $Ca(OH)_2$—ash suspension (measured via the conductivity in Figure S4-6, or via the $[Ca^{2+}]$ in Figure S4-7). However, there was appreciable divergence with different ash at the early and middle stages (0-250 h) (Figure 4-7). In contrast, there was minor discrepancy at the late stage (250-360 h), which was due to the complete consumption of SiO_2 from ash.

Kinetic parameters (diffusion coefficient D_e, chemical reaction rate constant K, constant of time τ and free energy of activation $\Delta G^{\#}$) were evidently impacted by the ash with various pozzolanic activity (Table 4-3). Numeric simulation showed good correspondence with the experimental data, which was verified by a statistical parameter

(R^2). For all ash samples, D_e (1.10e-3 - 6.30e-3 $mm^2 \cdot h^{-1}$) was considerably lower than K (0.900e-2 - 1.22e-2 h^{-1}). This relationship is interpreted to mean that diffusion speed of the reactants through the reaction product layer (around the reacting nucleus of the pozzolan particle) was slower than the chemical reaction rate at the nucleus surface. Accordingly, pozzolanic reaction rate in the $Ca(OH)_2$—ash suspension was principally limited by the ionic diffusion that was determined by ash porosity.

Different combustion temperature and retention time changed the crystal structure of ash (resulted in disparate D_e) and chemical reactivity (resulted in disparate K). Deviation with the chemical reactivity was attributed to various carbon removal degree (affected the SiO_2 purity) and different amorphous proportion in ash (affected the SiO_2 crystal reactivity). As τ and $\Delta G^{\#}$ were determined by the value of K, both τ and $\Delta G^{\#}$ varied in proportion consequently. Compared to other ash samples, ash 550-4 had the least $\Delta G^{\#}$, at 62.1 $kJ \cdot mol^{-1}$ or 62.3 $kJ \cdot mol^{-1}$. Because a lower $\Delta G^{\#}$ was correlated with higher reactivity, pozzolanic reaction could process more easily and promptly.

4.4.6.2. Interpretation of simulation results

Analysis of the kinetic results (Table 4-3) demonstrated that ash sample source had a significant influence on the K ($P = 0.0187$), but no impact on the D_e ($P = 0.393$), τ ($P = 0.124$) and $\Delta G^{\#}$ ($P = 0.060$) (Table S4-5). These differences indicated that varying the combustion temperature and retention time substantially changed the chemical interaction at the reaction product layer of ash-cement mixtures, but did not affect the porosity. Thus, pozzolanic reaction rate in this study was controlled by ionic diffusion.

As conductivity was strongly correlated with the $[Ca^{2+}]$ in the pure $Ca(OH)_2$ solution (Adj. $R^2 = 0.9857$, Figure S4-1), I hypothesized that kinetic results would be

consistent if evaluated by conductivity measurement or the change in $[Ca^{2+}]$. However, ANOVA found that there was a significant difference for the K ($P = 0.006$) and $\Delta G^{\#}$ ($P = 0.013$), but no difference for the D_e ($P = 0.510$) and τ ($P = 0.560$). I interpret this to mean that there was an extra pozzolanic contribution by other oxides in ash besides C-S-H. For instance, Al_2O_3 and Fe_2O_3 could interact with free $Ca(OH)_2$ and SiO_2 to form supplementary strength contributors in concrete microstructure, such as $(CaO)_x \cdot (Al_2O_3)_y \cdot (SiO_2)_z \cdot (H_2O)w$ (abbreviated as C-A-S-H) or $(CaO)_x \cdot (Al_2O_3)_y \cdot (Fe_2O_3)_z \cdot (H_2O)_w$ (abbreviated as C-A-F-H). Since Al^{3+} and Fe^{3+} are conductive, this explains why the numerical results for conductivity and the $[Ca^{2+}]$ in the $Ca(OH)_2$—ash suspension differed significantly.

4.5. Conclusions

Energy generation and ash recycling in cement could be optimized concurrently by adjusting the parameters of switchgrass combustion. When temperature went up from 350 °C to 650 °C, energy output monotonically increased from 0.79 $kJ \cdot g^{-1}$ to 5.96 $kJ \cdot g^{-1}$. Controlled combustion transformed more crystalline to amorphous compounds in ash crystal, although amorphous properties of ash crystal were affected more by longer retention time than higher combustion temperature. Pozzolanic reaction involving ash from switchgrass combustion was controlled principally by ionic diffusion, a function of the ash elemental concentration of $SiO_2 + Al_2O_3 + Fe_2O_3$. Compared to ionic diffusion, chemical interaction in the reaction product layer of the $Ca(OH)_2$—ash mixture was more easily influenced by different combustion conditions. Consequently, I recommended 550 °C temperature and 4 h retention time for switchgrass combustion designed to generate energy and recycle ash in cement. Pozzolanic reaction in cement with 10% ash

generated under these optimal conditions not only offset disturbance in the cementitious composition due to ash substitution, but also contributed to greater C-S-H bond formation, thus improving the concrete strength by 14.2%. If these findings are extrapolated directly to an average-size cement production plant (3.06 GJ coal /1000 Kg cement product), CO_2 emission could decrease by 1.8% when 5% of the coal burned is replaced by switchgrass energy with ash recycling.

4.6. Figures and tables

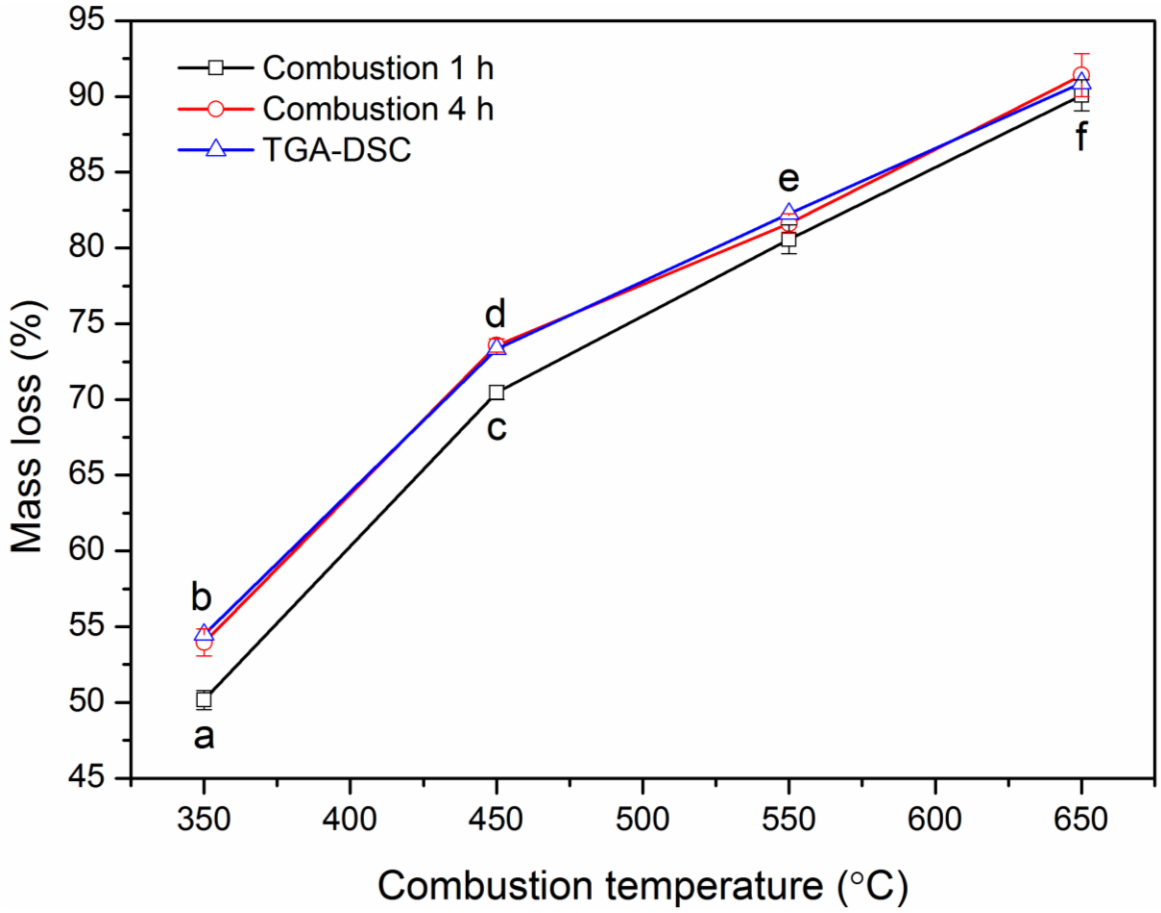

Figure 4- 1. Mass loss of controlled combustion, with comparison to the mass loss results from thermogravimetric analysis (TGA).

Data points and error bars represent the mean and standard deviation (n=3). Points with different letters were significantly different at $p<0.05$, assessed by a Fisher's LSD test.

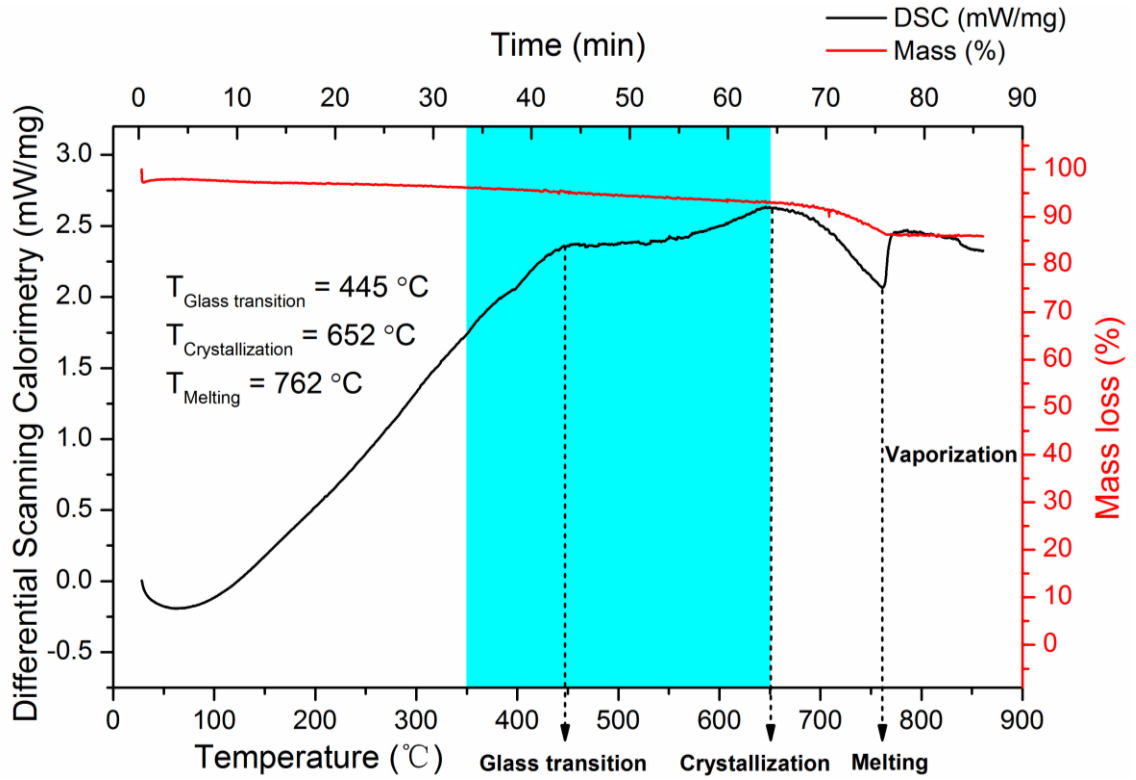

Figure 4- 2. Thermal characteristics of the switchgrass ash from open combustion (≈ 411 °C, 5 min), used as a control group in this study.

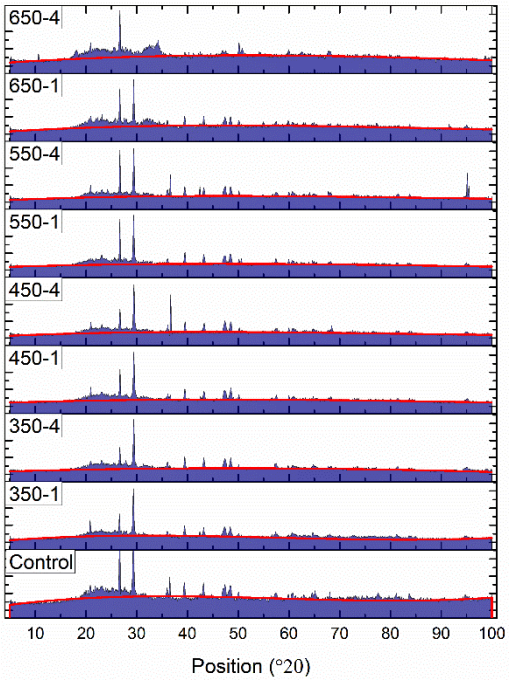

(a)

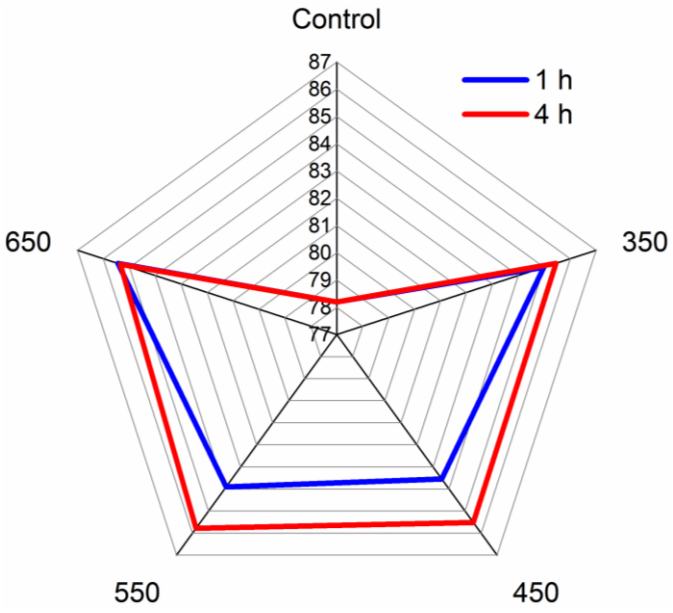

(b)

Figure 4- 3. (a) X-ray Diffraction (XRD) profile of the switchgrass ash from different combustion conditions.

Control group was the ash from open combustion (≈ 411 °C, 5 min); (b) comparison of amorphous crystal proportion (%) of the ash samples.

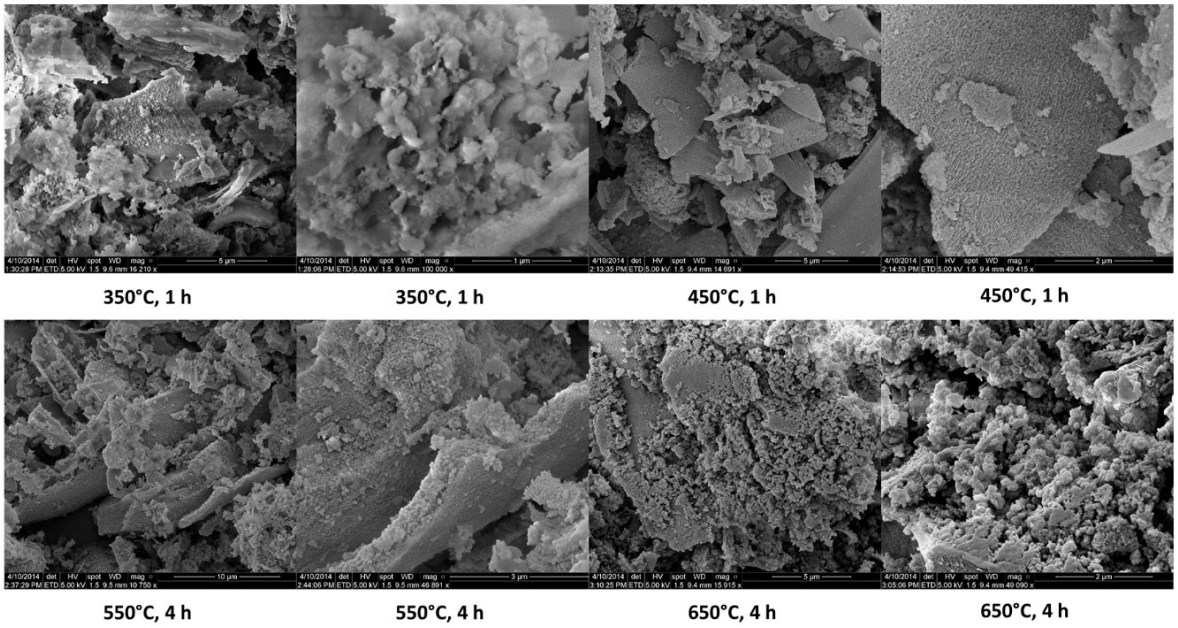

Figure 4- 4. Microstructural observation on selected ash samples by scanning electron microscopy (SEM).

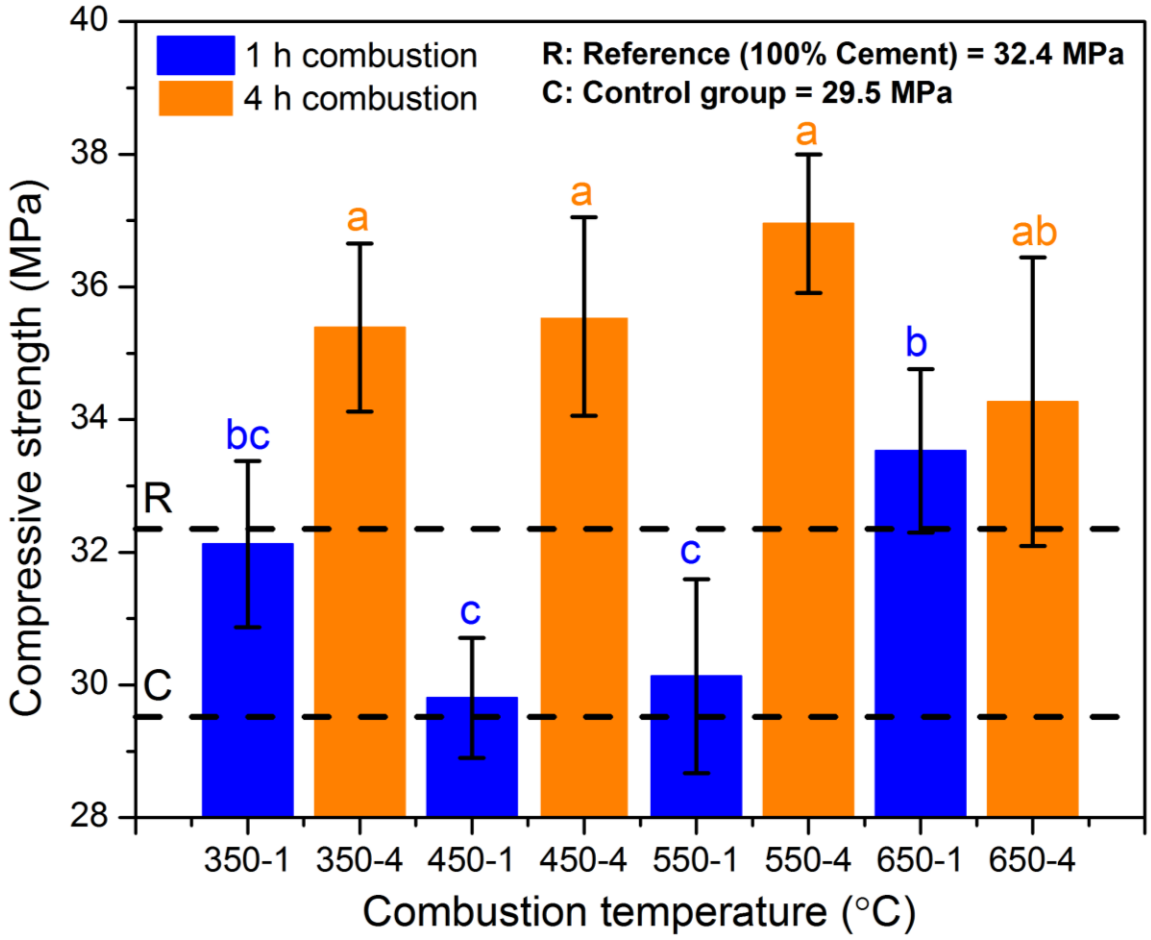

Figure 4- 5. Compressive strength of the concrete with 10% of the ash from different combustion conditions, after 28 d curing in a moisture room at 23 °C.

Ash from open combustion was included as a control group, and is indicated as the dotted line "C". Concrete without ash replacement (100% Portland cement) was considered as the reference group, with the dotted line "R". Values are the mean (n=3) and standard deviation (error bars). Columns with different letters were significantly different at $P<0.05$ level, assessed by a Fisher's LSD test.

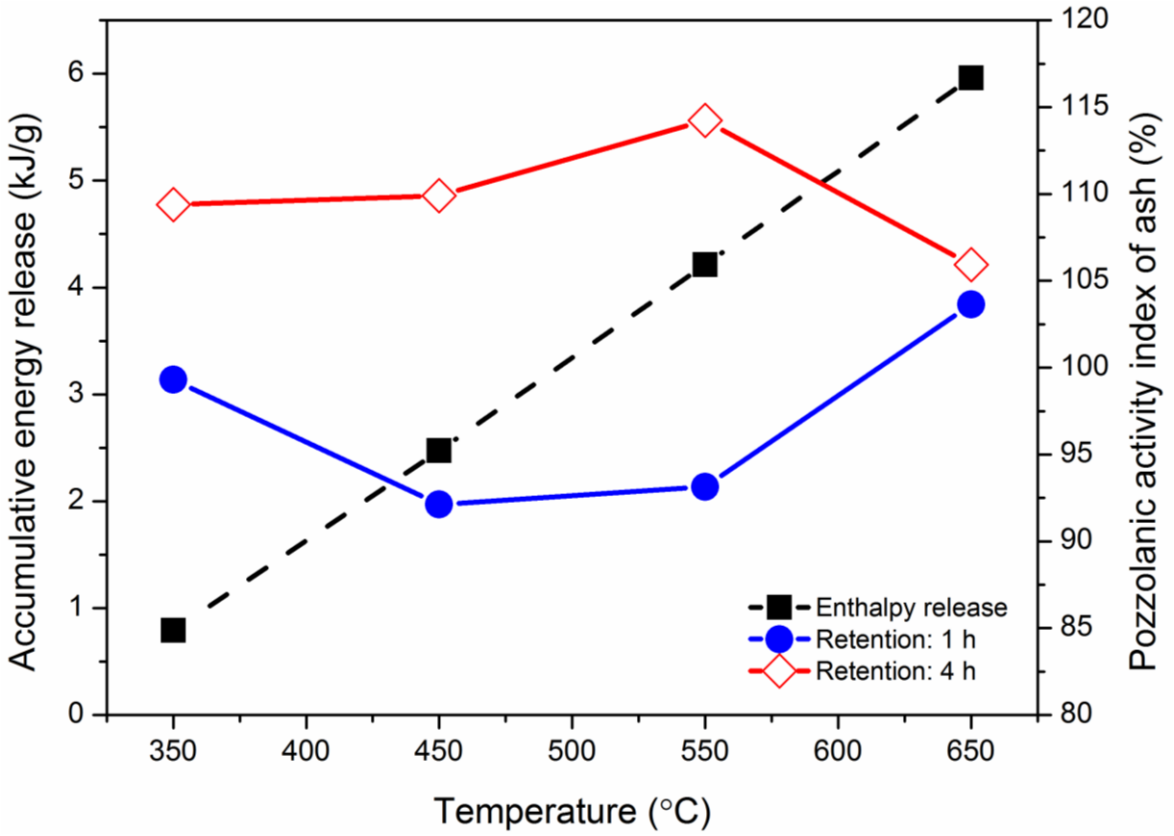

Figure 4- 6. Energy release of switchgrass combustion from 350-650 °C, and pozzolanic activity index (%) of the ash as affected by combustion conditions.

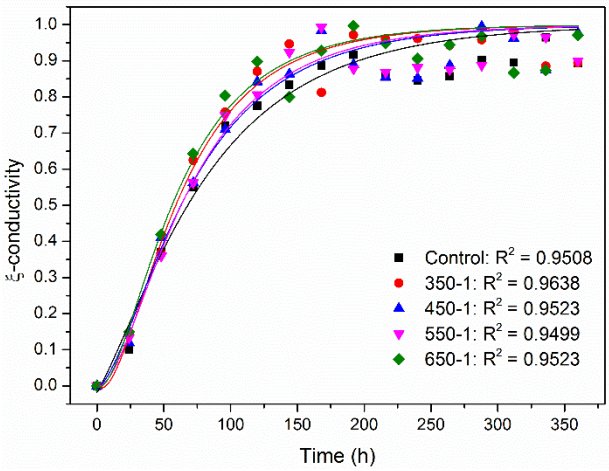
ξ-conductivity
Time (h)
Control: R2 = 0.9508
350-1: R2 = 0.9638
450-1: R2 = 0.9523
550-1: R2 = 0.9499
650-1: R2 = 0.9523

(a)

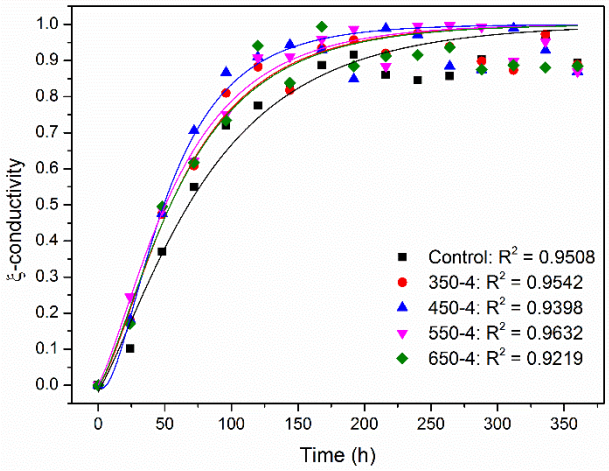
ξ-conductivity
Time (h)
Control: R2 = 0.9508
350-4: R2 = 0.9542
450-4: R2 = 0.9398
550-4: R2 = 0.9632
650-4: R2 = 0.9219

(b)

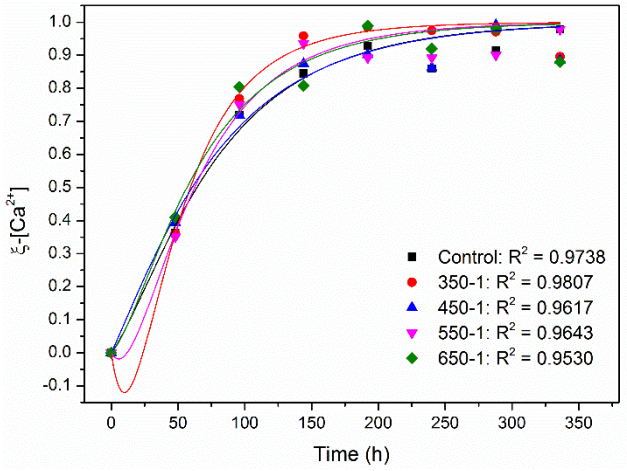

(c)

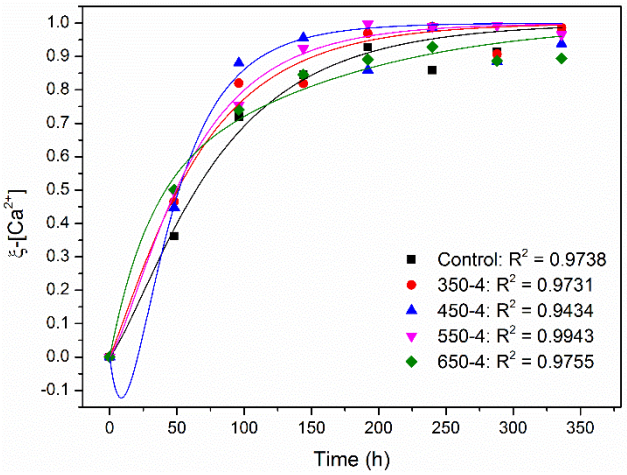

(d)

Figure 4- 7. Reaction progress ξ of a $Ca(OH)_2$—ash suspension (2 g ash + 75 mL saturated $Ca(OH)_2$ solution), measured via the solution conductivity or Ca^{2+} concentration at each 24 h.

Curves were fitted from the numeric simulation of pozzolanic reaction. (a) Ash from switchgrass combustion at 350-650 °C for 1 h, solution conductivity; (b) ash from switchgrass combustion at 350-650 °C for 4 h, solution conductivity; (c) ash from switchgrass combustion at 350-650 °C for 1 h, Ca^{2+} concentration; (d) ash from switchgrass combustion at 350-650 °C for 4 h, Ca^{2+} concentration. Control group was the

ash from open switchgrass combustion (≈ 411 °C, 5 min). The modelling equations were described by Eq. 4-4, Eq. 4-5, Eq. 4-6 and Eq. 4-7.

Table 4- 1. Experimental treatments for investigating the impact of switchgrass combustion on energy conversion and ash recycling value in cement.

Designation	Combustion type	Temperature (°C)	Retention time	Replication
Control	Open combustion	411	5 min	3
350-1	Controlled combustion	350	1 h	3
450-1	Controlled combustion	450	1 h	3
550-1	Controlled combustion	550	1 h	3
650-1	Controlled combustion	650	1 h	3
350-4	Controlled combustion	350	4 h	3
450-4	Controlled combustion	450	4 h	3
550-4	Controlled combustion	550	4 h	3
650-4	Controlled combustion	650	4 h	3

Table 4- 2. Mixture proportion of Portland concrete and switchgrass ash for compressive strength test.

Mixture ($kg \cdot m^{-3}$)	Relative density (1)	100% cement (Reference group)	90% cement + 10% ash
Portland cement	2.87	330	297
Fine aggregate	2.81	660	594
Course aggregate	2.61	1226	1103
10% Ash	1.79	0	33
Water (w/b=0.55)	—	182	182

Table 4- 3. Kinetic parameters from the numeric simulation on a $Ca(OH)_2$—ash suspension (2 g of ash + 75 mL of saturated $Ca(OH)_2$ solution), measured via solution conductivity or Ca^{2+} concentration in solution at each 24 h.

D_e ($mm^2 \cdot h^{-1}$): diffusion coefficient; K (h^{-1}): chemical interaction rate constant; τ (h): the time interval until nucleus of pozzolan decreased to 37% of initial value; $\Delta G^{\#}$ ($kJ \cdot mol^{-1}$): free energy of activation for pozzolanic reaction.

Sample	D_e ($mm^2 \cdot h^{-1}$)	K (h^{-1})	τ (h)	$\Delta G^{\#}$ ($kJ \cdot mol^{-1}$)
Parameters derived from solution conductivity				
Control	4.40e-3	1.35e-2	82.9	63.4
350-1	2.20e-3	1.84e-2	62.0	62.6
450-1	2.90e-3	1.59e-2	70.9	63.0
550-1	2.40e-3	1.66e-2	68.6	62.9
650-1	2.60e-3	1.88e-2	60.5	62.5
350-4	3.90e-3	1.78e-2	63.8	62.7
450-4	4.90e-3	1.86e-2	61.3	62.6
550-4	2.60e-3	2.21e-2	51.6	62.1
650-4	4.40e-3	1.74e-2	64.9	62.7
Parameters derived from Ca^{2+} concentration				
Control	3.30e-3	1.22e-2	78.0	63.6
350-1	1.10e-3	1.81e-2	52.6	62.6
450-1	6.00e-3	1.20e-2	79.1	63.7
550-1	1.50e-3	1.50e-2	63.3	63.1
650-1	3.00e-3	1.43e-2	66.3	63.2
350-4	6.30e-3	1.46e-2	65.0	63.2
450-4	3.80e-3	1.61e-2	59.0	62.9
550-4	1.20e-3	2.08e-2	45.6	62.3
650-4	1.20e-3	0.900e-2	105.3	64.4

CONNECTING PARAGRAPH TO CHAPTER 5

The pozzolanic activity of switchgrass combustion ash can be improved by optimizing the combustion conditions to select those that yield the greatest heat release, leaving behind residual ash with suitable physicochemical properties, based on a high amorphous SiO_2 content and low Loss on Ignition (LOI) value. However, due to the complexity of the cement—pozzolan—water system during hydration, it is impossible to use any conventional regression model to predict the PA based solely on the initial physiochemical properties of the ash and mixing ratio of the cement-pozzolan-water components. Hence, Chapter 5 will overcome this research gap by 1) creating a data-mining ANN model to predict PA for solid waste pozzolans using more than 700 data points reported in the peer-reviewed scientific literature over the past 17 years; and 2) describing the effect of curing age on PA using a time-series model.

CHAPTER 5. Developing a Data-Mining Model for Predicting the Pozzolanic Activity

Predicting the pozzolanic activity of solid wastes using artificial neural network with time-series analytic model

5.1. Abstract

Many solid wastes possess pozzolanic activity (PA), which permits their recycling as pozzolans in blended cement. However, the cement industry lacks the tools to rapidly determine whether a particular solid waste is likely to generate ample PA in mortars made from blended cement, and when this will occur during the curing process. This work describes the development of a novel data-mining model for PA prediction that can assess the pozzolanic potential of candidate materials prior to experimental work. Hence, the objectives of this paper are 1) to create a data-mining ANN model for PA prediction built upon more than 700 data points from peer-reviewed reports over the past 17 years (70% for training, 15% for validation, and 15% for testing); and 2) to describe the effect of curing age on PA based on a time-series model. The ANN and time-series models developed in this study can accurately forecast the PA of solid wastes during 3-90 d curing (R = 0.8479 to 0.9914), which could reliably appraise the PA of a candidate material. I recommend these screening tools as rapid indicators of pozzolanic potential in solid wastes prior to undertaking strength tests and other experimental testing.

5.2. Introduction

Many solid wastes (e.g. combustion ash, catalyst residue) can be used as a pozzolan if they possess physiochemical properties akin to conventional pozzolans (e.g. silica fume). This strategy effectively recycles these pozzolanic-active resources and reduces the amount of Portland cement needed to make strong and durable concrete, which potentially eases the greenhouse gas (GHG) emissions from cement production (Heede et al., 2012; Huntzinger & Eatmon, 2009). In view of these ecological and sustainable benefits, many researchers have tested the pozzolanic activity (PA) of various solid wastes and reported their findings in the scientific literature, leading to more than 1612 publications on this topic in the past 10 years (Web of Science, from 2005 to 2014).

The sizable database presently available from experimental studies that evaluated PA of diverse solid wastes also provides opportunities to develop a data-mining model for PA prediction. The advantage of a data-mining model is that generalizations and trends can be analyzed, giving the cement industry a rapid tool to assess the pozzolanic potential of a waste material before undertaking experimental work. An ANN is an appropriate predictive tool for this purpose because ANN is a high-level data-mining algorithm that simulates the learning behavior of human neurons to mathematically address complicated and nonlinear objectives (Craven & Shavlik, 1997; Zhang et al., 1998). Pala et al. (2007) and Topcu and Sarıdemir (2008) successfully predicted the PA of fly ash using ANN, and noted minor deviation between predicted and experimental results ($R > 0.8$). The suitability of ANN for PA evaluation was subsequently verified by Prasad et al. (2009), Atici (2011), Dantas et al. (2013), and Duan et al. (2013b). Even so,

there are still several questions that I should address to improve the strength of PA prediction for diverse solid wastes. The limitation of all existing ANNs for PA evaluation was that they only considered one pozzolan in each study and relied on small datasets (<100 groups of experimental results) derived from their own experimental results or a subset of values for a particular pozzolan from the scientific literature. This means that the PA predictions that can be obtained from the existing ANNs lack universality and representativeness. In addition, time also plays a crucial role in the development of chemical bonds and physical structure in the cement—pozzolan—water system (Shi & Day, 2001), but none of existing ANN models considered the effect of time explicitly. Hence, an enhanced ANN model is needed to build on the existing knowledge, but needs to extend analysis to a broader dataset that describes the maximal number of pozzolanic materials that may be considered by the cement industry. In addition, since the curing age plays an important role in cement hydration, the predictive model must also include a time-series function that reveals the correlation between curing age and PA.

Therefore, the objectives of this paper are to 1) create a new, integrated ANN model that includes 22 potential pozzolanic materials, to predict PA in blended cement, and 2) disclose the effect of time on PA based on a time-series model. These models may help us develop screening tools as rapid indicators of pozzolanic potential in solid wastes prior to undertaking strength tests and other experimental testing.

5.3. Modeling methods

5.3.1. Data selection and model objective

Experimental data were gathered describing the pozzolanic effect of non-conventional pozzolans - namely combustion ash, blast furnace slag and other solid wastes - on the compressive strength of concrete and mortar. This dataset was comprised of 707 groups of testing results from 81 papers published in peer-reviewed journals from 1998-2014. Testing methods in these papers conformed to internationally recognized standards, such as ASTM C 311-07, ASTM C109, NF EN 196-1, EN 1015-11:1999, etc. This dataset covered mostly all kinds of pozzolans listed in Section 2, involving fossil and biomass fuel ash, blast furnace slag, catalyst waste, river sand, etc. The major assumption was that the data were scientifically accurate and unbiased, thus assuring the validity and representativeness of predictive results.

All pozzolans possess a high SiO_2+Al_2O_3+Fe_2O_3 content with amorphous structure and fine particle size, which was described by providing their chemical composition and physical property (specific gravity) in our model. The factors that may affect the PA (as independent input variables) included the chemical compositions and specific gravity of pozzolans, water-binder ratio (W/B), replacement ratio of cement by pozzolanic material and superplasticizer mixing ratio (a common additive to improve the flow characteristics of cement pastes) (Table 5-1). Since the compressive strength was the most common testing method to evaluate the pozzolanic effect in existing literatures, the compressive strength at 3, 7, 28 and 90 d was gathered to reflect the changes in pozzolanic function during early to later curing stages. To eliminate the interference from

different experimental conditions in each paper (e.g. curing temperature, moisture, casting dimension, etc.), the PA as the predictive output was normalized by comparing the compressive strength of mortar from cement: pozzolan blends to that of 100% Portland cement, from the same study (Eq. 5-1).

$$PA\ (\%) = \frac{\text{Compressive strength of blended sample}}{\text{Compressive strength of plain sample}} \times 100 \qquad (5\text{-}1)$$

Since the compressive strength was typically evaluated repeatedly during curing, the PA (%) was calculated at 3, 7, 28 and 90 d curing time, when the data were available (n = 146). Based on this dataset, the following models aimed to 1) develop an ANN for PA prediction at different curing ages, using concrete compressive strength as an indicator of PA and the physiochemical and mixing parameters of a pozzolan as predictors, and 2) investigate the correlation between PA, an indicator of concrete compressive strength, and curing age with a time-series model.

5.3.2. Artificial neural network (ANN)

A feed forward back-propagation ANN was constructed for PA prediction (Figure 5-1). Briefly, the signals move towards only one direction in this model from the input layer, through the hidden layer and to the outputs. There is neither cycle nor loop among the entire processing elements (PEs). Further information on the rationale and algorithm for this method of ANN is found in Jain et al. (1996), Zhang et al. (1998), Basheer and Hajmeer (2000), and Duan et al. (2013b). The PEs in this model were arranged in layers. The PEs in each layer were wholly linked to all of the PEs in successive layers, but there

was no PEs connection in the same layer. The input to a PE was obtained by multiplying the output of connected PEs by the synaptic strength of connections. Thus, the weighted sums of input $(net)_j$ for the j^{th} PE were calculated with a linear sum function (Eq. 5-2) (Sarıdemir, 2009).

$$(net)_j = \sum_{i=1}^{n} w_{ij} \times o_i + b_i \tag{5-2}$$

where the j^{th} PE received the signals from the preceding layer containing n PEs, with the mass of w_{ij}. The output, o_i was derived from the i^{th} PE in the preceding layer and b_j symbolized the bias that simulated a threshold value. Accordingly, the output o_j was transformed from the sum function $(net)_j$ via an activation sigmoid function ($f(\cdot)$) in the PEs of hidden layer (Eq. 5-3). A constant α was also used to control the slope of semi-linear region.

$$o_j = f\big((net)_j\big) = \frac{1}{1 + e^{-\alpha \times (net)_j}} \tag{5-3}$$

The learning of this ANN was supervised by a back-propagation method with Levenberg-Marquardt algorithm (Ampazis & Perantonis, 2000). Based on a gradient descent principle, when the errors for a particular training pattern were passed backwards from output to input layer, these errors were minimized by adjusting the weights and biases for each PE (Eq. 5-4).

$$w_{ij}(m+1) = w_{ij}(m) + \eta\big(\delta_j \times o_j\big) + \beta \times w_{ij}(t) \tag{5-4}$$

where δ_j was the error signal of the j^{th} PE, and m was the number of iterations. η and β corresponded to the learning and momentum rates. η was obtained by the partial derivative of the error function in Eq. 5-5, as shown in Eq. 5-6 and 5-7.

$$E_r = \frac{1}{2} \times \sum_j (t_j - o_j)^2 \tag{5-5}$$

$$\delta_j = o_j \times (t_j - o_j) \times (1 - o_j) \tag{5-6}$$

$$\delta_j = o_j \times (1 - o_j) \times \sum_k (\delta_k \times w_{kj}) \tag{5-7}$$

where t_j was the target output of the j^{th} PE and k represented the k^{th} layer that was the upper layer of the j^{th} layer within the whole network model. The training process was successfully completed when the iterative process converged. There were two indices used for model performance assessment, including root-mean-squared error (RMS) (Eq. 5-8) and the root of absolute variance fraction (R) (Eq. 5-9).

$$RMS = \sqrt[2]{\frac{1}{p} \times \sum_i |t_i - o_i|^2} \tag{5-8}$$

$$R = \sqrt[2]{1 - \frac{\sum_i |t_i - o_i|^2}{\sum_i |o_i|^2}} \tag{5-9}$$

where t and o were the target and predicting values of the i^{th} pattern (with the pattern number p). The value of RMS or R that approached to 0 or 1 suggested a good predicting performance.

Three layers were created in this ANN, including an input layer, a hidden layer and an output layer (Figure 5-1). The input layer contained 13 nodes, with respect to the factors considered in Table 5-1. The output layer had 4 nodes to describe the PA prediction at 3, 7, 28 and 90 d curing. However, since there was no clear method to designate the node number in hidden layer, I had to run a few trials (1-40 nodes in this study) to select this parameter (Parichatprecha & Nimityongskul, 2009). As a result, a 27 node hidden layer was found to be optimal giving the lowest root mean square error (Figure 5-2). As the sigmoid function in hidden layer ranged from -1 to 1, input layer was normalized after it was loaded with initial data, and output layer was denormalized following the sigmoid transformation (Hecht-Nielsen, 1989). Based on this topology, 70% and 15% data (selected randomly) were used for ANN training and validation, and this left 15% data for ANN testing. Momentum and training rates were 0.9 and 0.3, and training was terminated after 1000 cycles iteration (Duan et al., 2013b). Training was replicated 20 times, and the best results were chosen with the highest R value (Dantas et al., 2013). Additionally, to compare the ANN predictive capacity to conventional regression analyses, I performed a multivariable regression model (MVR) on the same dataset with the same normalization and denormalization steps (Eq. 5-10).

$$PA = \sum_{i=1}^{13} a_i \times x_i^{b_i} + e \tag{5-10}$$

where x_i corresponded to the 13 input variables, a_i and b_i were the regression parameters, and e symbolized an error compensation. When b_i equaled to 1, this function represents a perfect linear regression (R = 1).

5.3.3. Time-series analysis of pozzolanic activity

As the compressive strengths of concrete or mortar vary considerably with different curing age, and these strengths reflect the PA, the change of PA with curing age might be defined by a time-series model. However, there is no research so far to address this topic. Although Shi and Day (2001) applied a time-series equation to analyze the strength-age relationship, how PA would contribute to this relationship was not discussed in their work. Assuming there is a positive linear correlation between PA and compressive strength, a time-series PA model was developed in Eq. 5-11,

$$P(t) = P_U \times \frac{K_T \times (t - t_0)}{1 + K_T \times (t - t_0)} \quad (5\text{-}11)$$

where P(t) was the PA (%) at a certain curing age t, and P_U represented a theoretical ultimate PA ($t = +\infty$). K_T (d^{-1}) meant a PA change rate constant, and t_0 (d) symbolized a theoretical initial hardening time. After calculating the mean values of n= 707 groups of PA—time data, a nonlinear data fitting was conducted with Eq. 20. Additionally, these PA—time data were statistically interpreted by a one-way Analysis of Variance (ANOVA) with Fisher's LSD tests ($P < 0.05$).

5.4. Results and discussions

The ANN model was able to predict the PA of 22 types of solid wastes with diverse physicochemical properties that underwent combustion, other heating and pretreatment before blended as pozzolans with cement (Figure 5-3). The R of 0.9613 from training step affirmed that this model was successful in learning the correlation

between the input and output variables. R was 0.8479 from test step, thus evidencing the accuracy of predictive results. Moreover, the predictive capacity of the ANN proved superior to multivariate regression models, which were constrained by the fact that they must predict outcomes separately for each time point. This is supported by the substantially smaller root mean square value of 10.76 for the ANN compared to the regression models (38.25-42.66 at 3-90 d curing, Table 5-2). This performance gap implies that the complexity cement—pozzolan—water system could not be described accurately with traditional regression model approach, since it cannot reflect the multiple interactions that occur among input parameters with time. The ANN constructed in this study was a robust tool with capacity to appraise and predict the eligibility of a pozzolan for blended cement, based on its expected effect on compressive strength.

Further improvements to the ANN are suggested to enhance its accuracy. Statistically, the R of 0.8479 from this ANN test indicates adequate predictive ability, but is not as close to ideal prediction as the R obtained by other ANN of pozzolans reported by Duan et al. (2013b) (R=0.9977), Dantas et al. (2013) (R=0.9854), Sarıdemir (2009) (R=0.9992), and Prasad et al. (2009) (R=0.9165). This is due to the fact that our ANN relied on much broader dataset, encompassing 22 pozzolans with diverse physicochemical attributes (also attached in this thesis). The variety of testing protocols employed in each study makes each experimental data unique and may give conflicting results even when similar materials or test conditions are considered, thus resulting in an obvious disparity in dataset (Table 5-1). By contrast, other ANN attempting to predict PA relied on data collected under similar experimental conditions (i.e., from the same testing protocol) or even with the same pozzolan, so it is not surprising that the R values are

higher for those ANN. Although I attempted to normalize the data within each study by comparing the PA of blended cement with 100% cement, additional normalization that would account for discrepancies among testing protocols might be an option for improving ANN prediction.

As expected, the PA increased significantly ($P<0.05$) with curing age, from 97.2% (3 d) to 104.0% (90 d) (Figure 5-4). There was little change in PA within the first 7 d, indicating a delay in pozzolanic reaction of about one week and thereafter strengthening the blended concrete (from 7 d to 90 d of curing). Cement hydration appears to be the source of compressive strength in mortar in the first week, and tended to be impaired in blended cements, but this early deficiency was overcome by 7 d, when the average PA reached 100% (Figure 5-4). The time-series model (Eq. 5-11) was well fitted to the experimental data (Adj. $R^2 = 0.9914$), thereby suggesting the suitability of describing the PA—time correlation by this function (Figure 5-4). P_U was estimated at 104.2±0.21% when the curing age approached $+\infty$. By solving this function versus time $(0, +\infty)$, PA would exceed 100% only if the curing is longer than 3.72 d, indicating a theoretical advantage of the pozzolanic reaction on PA after about 4 d curing. Thereafter, the PA reaction in cement-pozzolan-water system could enhance the compressive strength of the mortar after a sufficiently long curing age.

Similarly to the ANN model, however, the applicability of this function could be enhanced further as well. Although the mean values of PA yield a good fitting result, these data had a large standard deviation owing to our broad data selection (Table 5-1). These high variances indicate that this time-series model could not be necessarily

applicable for a specific case study. Since dataset is a core part in model studies, a more standardized and unbiased PA test protocol is suggested to be developed to make data more comparable.

5.5. Conclusions

The ANN and time-series models developed in this study can accurately forecast the PA of solid wastes during 3-90 d curing period (R = 0.8479 to 0.9914), which could reliably appraise the PA of a candidate material. I recommend these screening tools as rapid indicators of pozzolanic potential in solid wastes prior to undertaking strength tests and other experimental testing.

Future studies should consider that, 1) a more standardized and unbiased protocol of PA tests should be established, thereby circumventing any disparity of assessment results; 2) the in-depth correlation should be investigated among the pozzolan properties, curing age and PA, which provides predicting models with more trustworthy data; and 3) based on these more explicit correlations, the criteria of PA evaluation could be more precise especially for large-scale industry, and PA improvement strategies could be made more reliable and sustainable.

5.6. Figures and tables

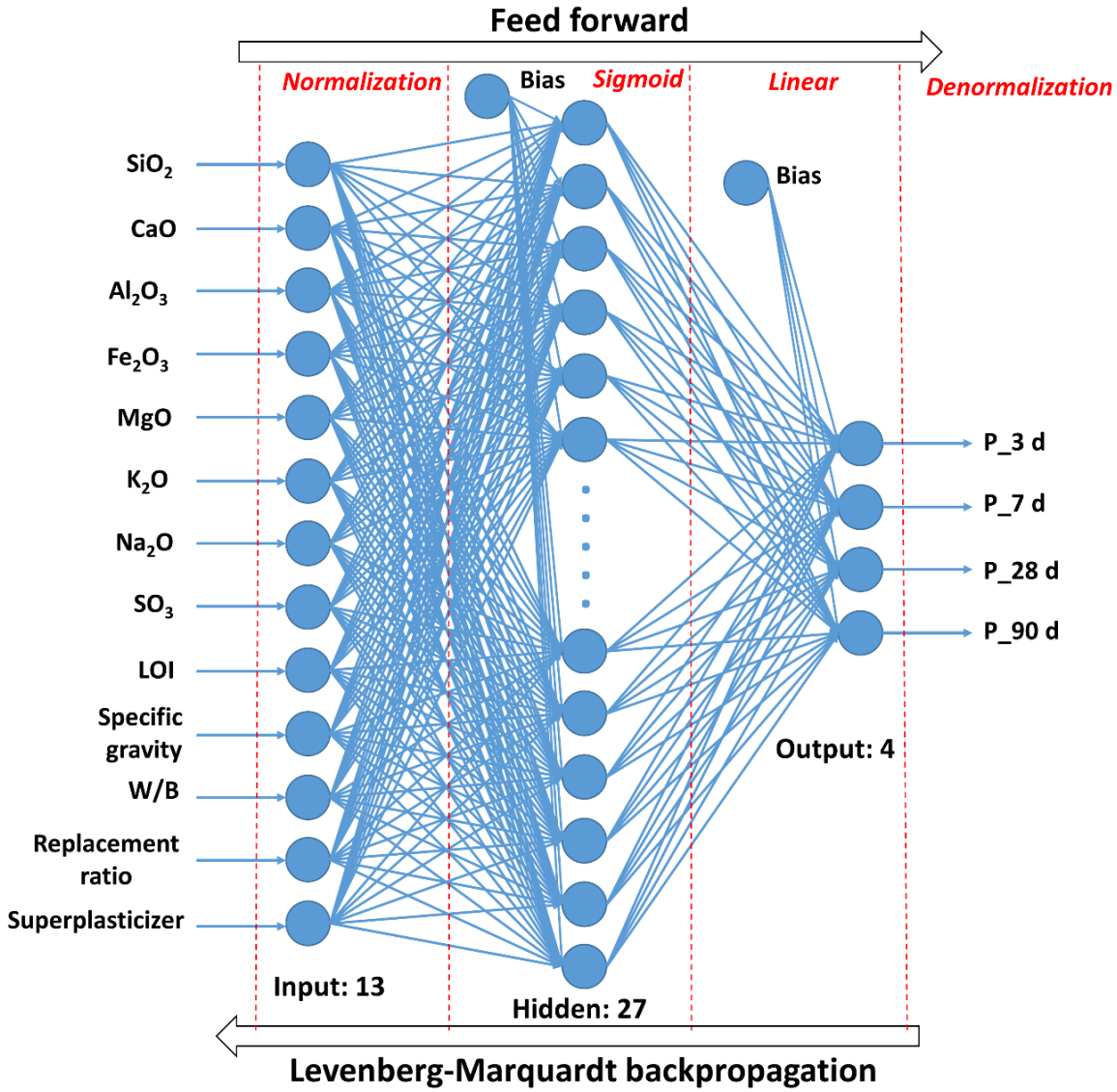

Figure 5- 1. Schematic structure of feed forward artificial neural network (ANN).

This model adopted the back-propagation algorithm, designed to predict the pozzolanic activity of blended cement containing up to 50% pozzolan from non-conventional sources (described in Table 5-1). P symbolized the pozzolanic activity at 3, 7, 28 and 90 d curing age.

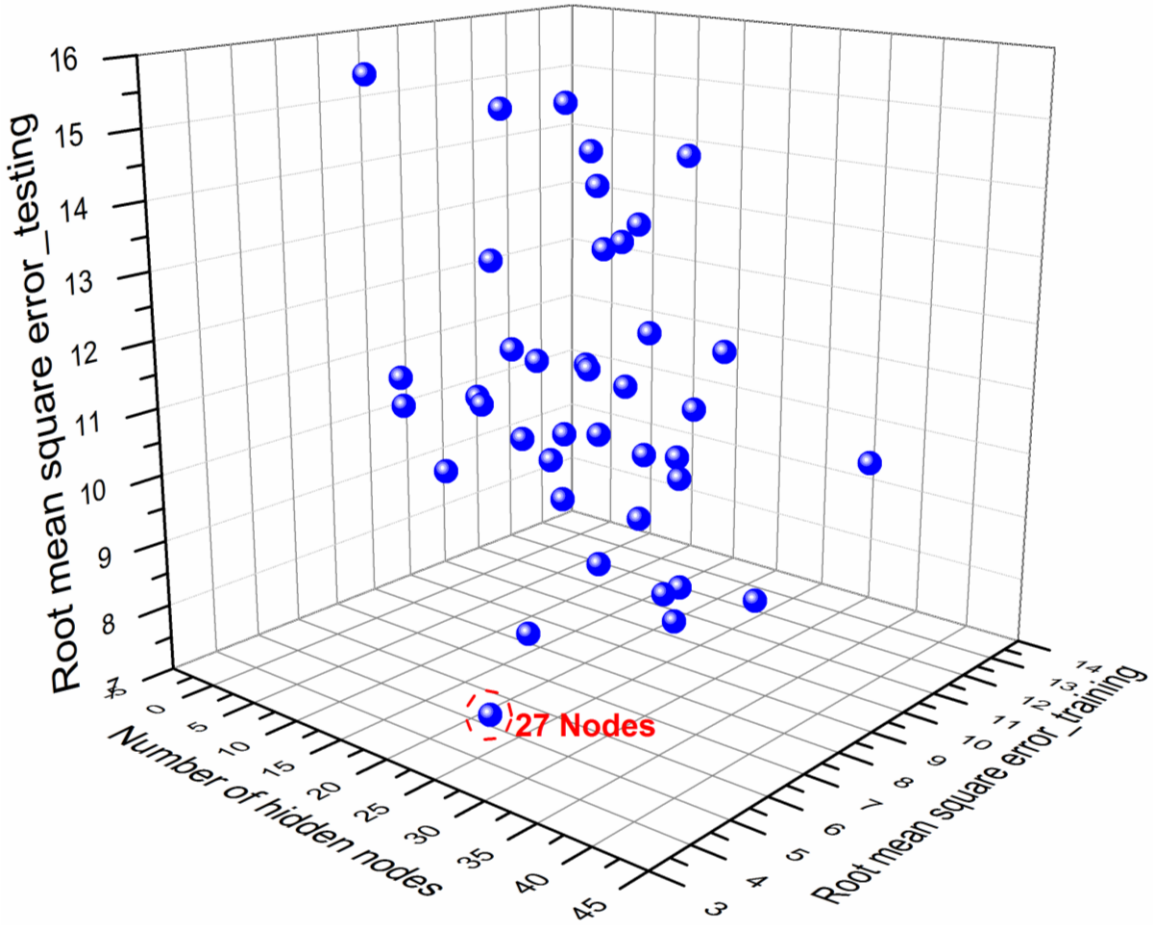

Figure 5- 2. Determination of the node number in hidden layer, via finding the lowest root mean square error from the training and test steps.

Since there was no clear method to designate the node number in hidden layer, a few trials (1-40 nodes in this study) had to be run to select this parameter.

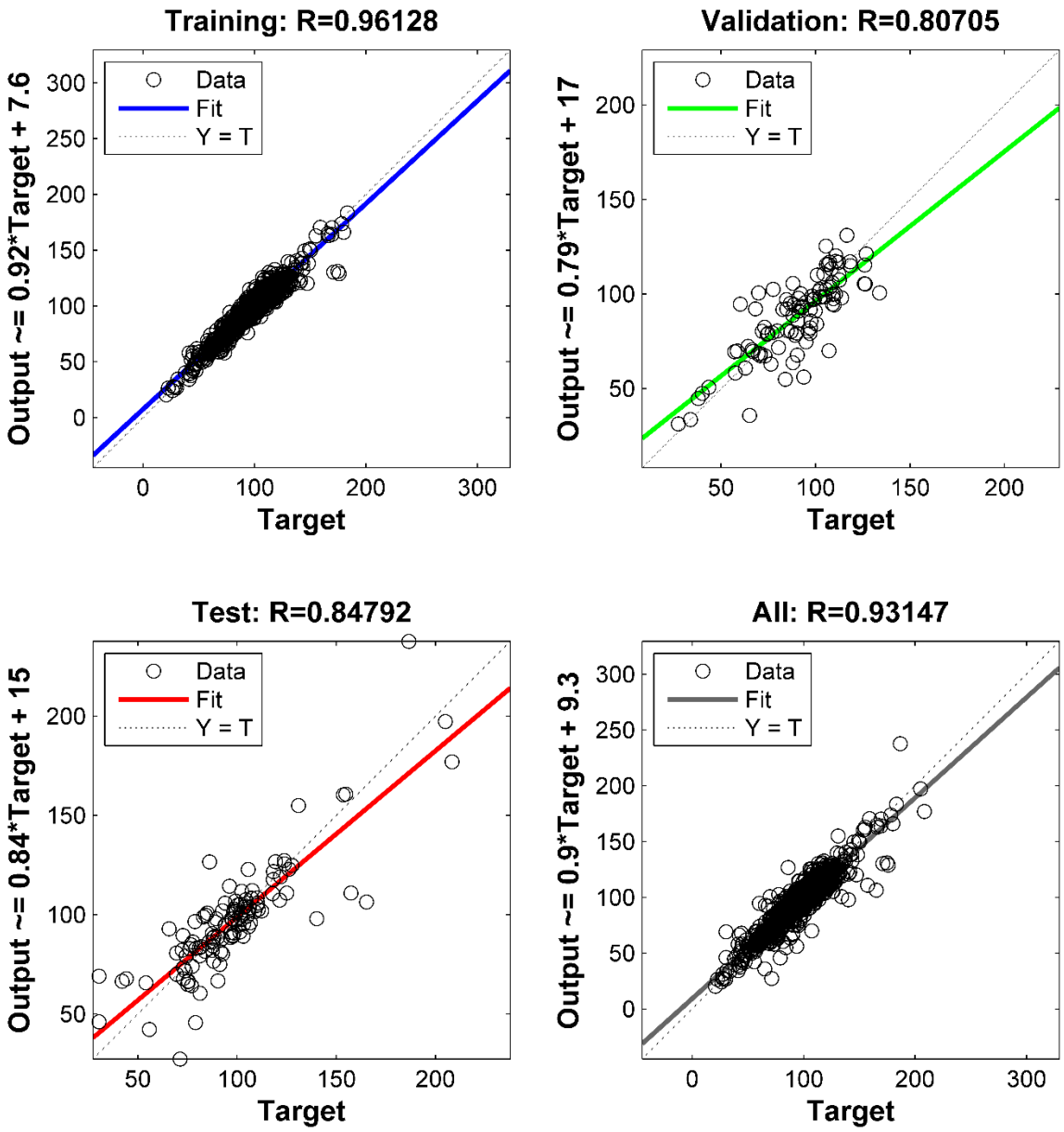

Figure 5- 3. Predictive results of pozzolanic activity in blended cement by artificial neural network model.

"Target" corresponded to the experimental results, and "output" represented the predictive results.

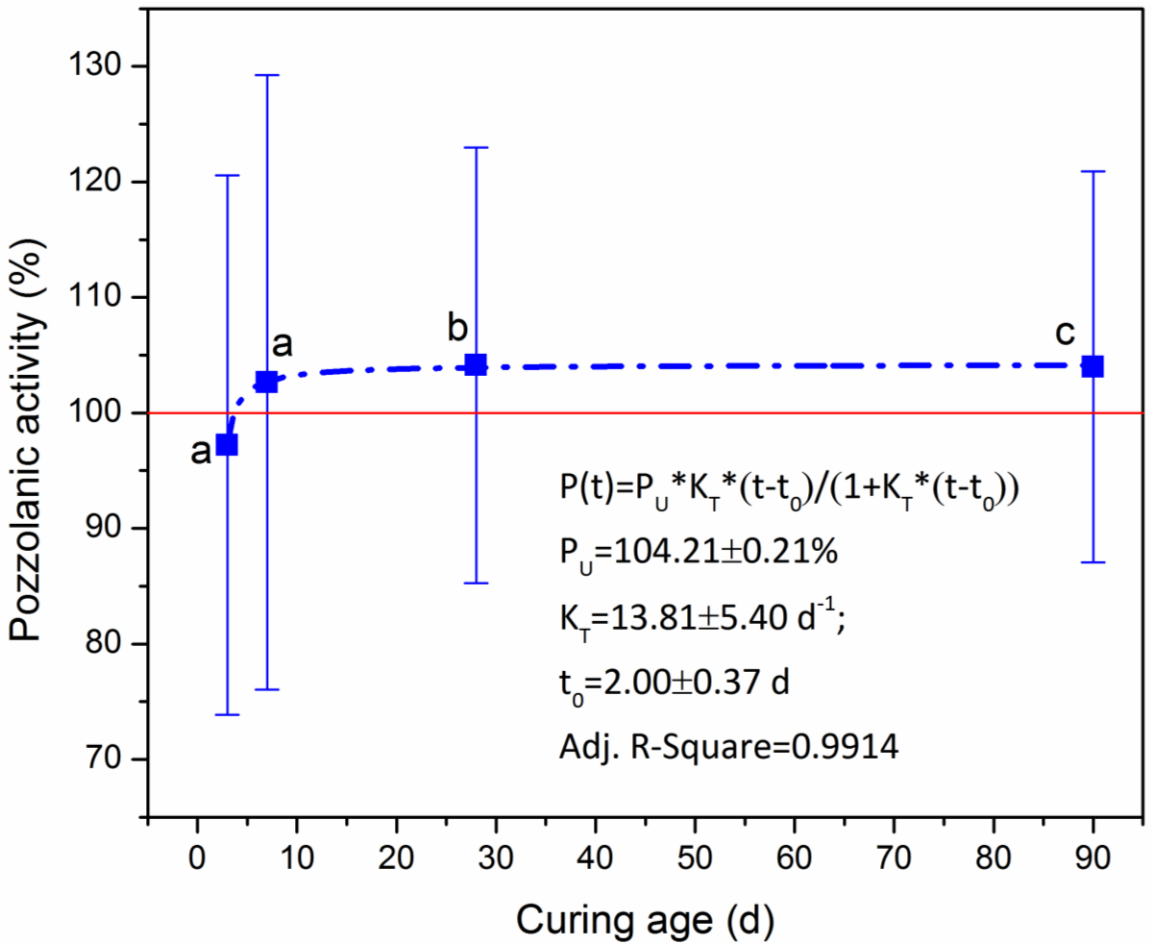

Figure 5- 4. Correlation between pozzolanic activity and curing age in mortar from blended cement containing 0-50% pozzolan.

The value with different letters were significantly different ($P < 0.05$, Fisher's LSD test, n = 146).

Table 5- 1. Summary of input variables describing the physicochemical characteristics of pozzolans and their use in blended cement, as well as the compressive strength of cement mortar.

The descriptive statistics from n = 707 experimental studies included the range (maximum, Max. and minimum, Min.) and the standard deviation (S.D.).

	Unit	Max.	Min.	Mean	Median	S.D.
Input variables						
SiO_2	w.t. %	99.80	11.84	66.43	65.60	20.98
CaO	w.t. %	54.82	0.01	7.03	3.00	9.47
Al_2O_3	w.t. %	59.40	0.01	10.33	4.40	12.76
Fe_2O_3	w.t. %	40.19	0.03	3.37	2.13	4.19
MgO	w.t. %	23.50	0.01	2.10	1.30	2.51
K_2O	w.t. %	25.41	0.01	2.60	2.00	2.56
Na_2O	w.t. %	16.30	0.01	0.77	0.37	1.72
SO_3	w.t. %	12.20	0.02	1.26	0.68	1.69
Loss on Ignition	w.t. %	28.90	0.03	5.27	3.72	5.23
Specific gravity	1	3.25	0.13	2.32	2.31	0.29
Water-binder ratio	1	0.80	0.19	0.47	0.50	0.11
Replacement ratio	%	70.00	1.00	22.17	20.00	12.88
Superplasticizer mix	%	8.50	0.10	1.37	1.03	1.28
Test results						
Compressive strength 3 d	MPa	131.38	4.32	32.09	25.67	22.11
Compressive strength 7 d	MPa	127.15	1.00	39.60	34.10	22.53
Compressive strength 28 d	MPa	131.08	3.20	50.18	45.45	22.69
Compressive strength 90 d	MPa	136.90	6.10	59.78	54.40	24.52

Table 5- 2. Comparison of the predictive error indices from multivariate regression models and an artificial neural network describing pozzolanic activity.

	Multivariate regression model				Artificial neural network
	3 d	7 d	28 d	90 d	
Root mean square error	39.19	42.66	38.35	38.25	10.76
R	0.4778	0.4517	0.5154	0.5679	0.8479

FORWARD TO CHAPTER 6

This thesis contains one critical literature review and four original research studies. These five manuscripts provide a systematic and strong proof of concept of LCF combustion with ash recycling in blended cement. Chapter 6 discusses the overall conclusions and implications of this thesis for future developments in sustainable cement production. I also come up with several future research recommendations based on these conclusions.

CHAPTER 6. General summary

6.1. Overall conclusions

To sum up, it was technically possible to meet part of the energy requirements for cement production with the combustion of LCF. Based on our laboratory combustion system design with 4 mm particle size fuels, we recommended that 20% or 30% excess air (for switchgrass or hardwood) would optimize the combustion to produce the highest energy conversion and combustion completeness rate. Switchgrass was less likely to create fouling and slagging problems, suggesting it would be a better biomass fuel for a commercial-scale boiler. Kinetic analysis (25-900 °C) also pointed to the need to increase the oxygen availability to achieve better energy conversion efficiency from biomass.

Switchgrass ash was a good pozzolan in blended cement, and its pozzolanic activity was improved by adding chemical accelerators (5% Na_2SO_4 and 5% $CaCl_2 \cdot 2H_2O$ were equally effective). Chemical acceleration was continuously effective, with greater gains in PA in the early stage (7 d) than late stage (28 d) of curing. The compressive strength and the resistance to ASR expansion of blended cement containing 10% switchgrass ash (by mass, with a chemical accelerator) was comparable to conventional Portland cement. Furthermore, recycling switchgrass ash generated under optimal combustion conditions (550 °C for 4 h) not only offset the disturbance in the cementitious composition due to ash substitution at a rate of 10% by mass, but also contributed to greater strength through microstructural compound (C-S-H) formation, thus improving the concrete strength by 14.2%.

The comprehensive dataset compiled for PA predictions in this thesis showed that the ANN and time-series models accurately forecast the PA of solid wastes during 3-90 d curing period (R = 0.8479 to 0.9914), which could reliably appraise the PA of a candidate material. Therefore, I recommend these screening tools as rapid indicators of pozzolanic potential in solid wastes. As pre-screening tools, these models permit end-users to eliminate solid wastes that lack the characteristics of a good pozzolan, and to narrow the focus on candidate materials prior to undertaking strength tests and other experimental testing.

Above all, this thesis proved the concept of LCF combustion with ash recycling as a cement additive. If these findings above are extrapolated directly to an average-size cement production plant (3.06 GJ coal /1000 kg cement product), the life-cycle CO_2 emission could decrease by 1.77% when 5% of the coal burned is replaced by switchgrass energy with ash recycling.

6.2. Future research recommendations

The further studies should be expanded to,

LCF combustion characterization: 1) a single particle fuel test at an ideal condition without any heat and mass transfer delays, and 2) a large-scale boiler test to confirm the conclusions by this thesis.

Ash pozzolanic evaluation: 1) a more standardized and unbiased protocol of PA test, thereby circumventing any disparity of assessment results; 2) an in-depth correlation investigation among the pozzolan properties, curing age and PA, which provides predicting models with more trustworthy data.

A broad sustainable-economic-social effect assessment: this thesis proved the technical feasibility of LCF combustion and ash recycling as pozzolans for cement production. However, more studies should be conducted by, 1) a life cycle assessment on this LCF strategy particularly for cement industry, which examines its actual GHG reduction capacity; 2) a life cycle cost assessment, which helps cement industry evaluate the capital and operational costs of switching to LCF from fossil fuels; and 3) a widespread social survey, which particularly obtains the feedbacks of the impact on local residents.

APPENDICES

CHAPTER 1

Table S1- 1. A comprehensive list of the pozzolanic solid wastes and their impact on cementitious properties reported in peer-reviewed studies from 1997 to 2014.

The letter 'Y' means that the effect on a cementitious property was reported in the study. Cs: compressive strength; Ts: tensile strength; Fs: flexural strength; Wp: water permeability; Ap: air permeability; Cp: Chloride permeability; Po: porosity; Ex: expansion; Hy: hydration heat and degree; Sh: shrinkage; Ca: carbonation; Le: elemental leaching; Cc: chloride corrosion; ASR: the expansion caused by alkali-silica-reaction; AAR: the expansion caused by alkali-aggregate-reaction.

Pozzolanic solid wastes	Note	Effect of pozzolanic reaction on cementitious properties													Other highlights	Ref.
		Cs	Ts	Fs	Wp	Ap	Cp	Po	Ex	Hy	Sh	Ca	Le	Cc		
Rice husk ash		Y														(Xu et al., 2012)
Rice husk ash				Y		Y										(Rodríguez de Sensale, 2006)
Rice husk ash		Y														(Vayghan et al., 2011)
Rice husk ash		Y		Y												(Feng et al., 2004)
Rice husk ash																(Zain et al., 2011)
Rice husk ash		Y													Studied the 1 year's	(Jauberthie et al., 2003)

										compressive strength	
Rice husk ash	Y										(Van Tuan et al., 2011)
Rice husk ash	Y										(Wansom et al., 2010)
Rice husk ash	Y			Y						Compared the material cost	(Gastaldini et al., 2007)
Rice husk ash						Y	Y				(Chatveera & Lertwattanaruk, 2011)
Rice husk ash	Y				Y						(Singh & Rai, 2001)
Rice husk ash	Y					Y					(de Sensale et al., 2008)
Rice husk ash	Y							Y			(El-Dakroury & Gasser, 2008)
Rice husk ash	Y	Y									(Givi et al., 2010a)
Rice husk ash	Y				Y						(Chindaprasirt & Rukzon, 2008)
Rice husk ash	Y										(Bui et al., 2005)
Rice husk ash	Y			Y							(Nehdi et al., 2003)
Rice husk ash											(Van et al., 2014)
Rice husk ash	Y										(Van et al., 2013)
Rice husk ash											(Nair et al., 2008)
Rice husk ash	Y			Y							(Ramadhansyah et al., 2012)

Rice husk ash		Y	Y	Y	Y	Y					(Ganesan et al., 2008)
Rice husk ash		Y						Y			(Antiohos et al., 2014)
Coal fly ash											(Hanehara et al., 2001)
Coal fly ash											(Zhang et al., 2000)
Coal fly ash		Y						Y			(Poon et al., 2003)
Coal fly ash	Class F ash	Y									(Poon et al., 2001b)
Coal fly ash											(Goni et al., 2003)
Coal fly ash		Y									(Chaipanich & Nochaiya, 2010)
Coal fly ash		Y			Y	Y		Y			(Said et al., 2012)
Coal fly ash		Y		Y				Y			(Kumar et al., 2012)
Coal fly ash		Y					Na_2SO_4		Y		(Chindaprasirt et al., 2004)
Coal fly ash		Y					ASR				(Aydın et al., 2010)
Coal fly ash								Y			(Frías et al., 2000)
Coal fly ash		Y						Y			(Lam et al., 2000)
Coal fly ash	Low calcium ash							Y			(Baert et al., 2008)
Coal fly ash				Y		Y				Built a marine condition (NaCl and Na_2SO_4)	(Lorenzo et al., 2003)

Coal fly ash							Y	Y				(Rong et al., 2014)
Coal fly ash		Y										(Supit et al., 2014)
Coal fly ash		Y					Y	Y				(Tkaczewska, 2014)
Coal fly ash		Y				Y						(Kim et al., 2014)
Coal fly ash												(Wilińska & Pacewska, 2014)
Coal fly ash								Y				(Lilkov et al., 2014)
Coal fly ash								Y				(Liu et al., 2014)
Coal fly ash		Y										(Hou et al., 2013)
Coal fly ash		Y										(Paya et al., 1997)
Coal fly ash												(Paya et al., 2001)
Coal fly ash	Class F ash	Y	Y									(Siddique, 2004)
Coal fly ash	High silica ash	Y					Y	Y				(Deschner et al., 2013)
Coal fly ash												(Hanehara et al., 2001)
Coal fly ash		Y						Y				(Tkaczewska et al., 2012)
Coal fly ash	Class C ash	Y		Y	Y		Y				Conducted a large-scale pavement study	(Nassar et al., 2013)
Coal fly ash		Y		Y					Y			(Gao et al., 2012)
Coal fly ash	Class F ash	Y		Y								(Guru Jawahar et al., 2013)

Coal fly ash	Low calcium ash	Y					Y		Y			(Papadakis, 1999)
Coal fly ash	High sulphate ash	Y				Y			Y			(Antiohos et al., 2007)
Coal fly ash	Lignite coal	Y						Na_2SO_4				(Chindaprasirt et al., 2007b)
Coal fly ash	Bituminous coal	Y					Y		Y			(Tkaczewska & Małolepszy, 2009)
Coal fly ash		Y										(Horpibulsuk et al., 2011)
Palm oil fuel ash			Y	Y								(Aldahdooh et al., 2014)
Olive residue ash											Found the filler effect of pozzolan	(Cuenca et al., 2013)
Palm oil fuel ash		Y			Y	Y	Y				Tested a ultrafine pozzolan (2.06 µm of median particle size)	(Johari et al., 2012)
Palm oil fuel ash		Y							Y		Tested a high replacement ratio of pozzolan (70%)	(Awal & Shehu, 2013)
Palm oil fuel ash		Y			Y			5% Na_2SO_4				(Tangchirapat et al., 2012)
Palm oil fuel ash		Y	Y									(Aldahdooh et al., 2013)
Palm oil fuel ash		Y							Y			(Sata et al., 2010)
Palm oil fuel									Y			(Chandara et

ash												al., 2012)
Palm oil fuel ash	Y				Y							(Chindaprasirt et al., 2008)
Palm oil fuel ash	Y	Y			Y							(Altwair et al., 2014)
Palm oil fuel ash	Y											(Yusuf et al., 2014)
Granulated blast furnace slag						ASR						(Kandasamy & Shehata, 2014)
Granulated blast furnace slag	Y					Y				Y	Built a large-scale marine condition	(Chen et al., 2012)
Granulated blast furnace slag	Y		Y	Y				Y				(Chi & Huang, 2013)
Granulated blast furnace slag	Y											(Poon et al., 2001a)
Granulated blast furnace slag							Y					(Pane & Hansen, 2005)
Granulated blast furnace slag	Y										Compared the cost of concrete with or without pozzolan	(Gastaldini et al., 2009)
Granulated blast furnace slag	Y									Y	Investigated the resistance to high temperature (900 °C)	(Karakurt & Topçu, 2012)
Granulated blast furnace slag	Y											(Tsai et al., 2014)
Granulated blast furnace							Y					(Boháč et al., 2014)

slag									
Granulated blast furnace slag	Y	Y						Performed a freeze-thaw test	(Işıkdağ & Topçu, 2013)
Sugar cane bagasse ash	Y					Y			(Montakarntiwong et al., 2013)
Sugar cane bagasse ash	Y		Y	Y					(Somna et al., 2012)
Sugar cane bagasse ash	Y		Y	Y	Y				(Rukzon & Chindaprasirt, 2012)
Sugar cane bagasse ash	Y								(Cordeiro et al., 2008)
Sugar cane bagasse ash	Y		Y			Y			(Chusilp et al., 2009)
Sugar cane bagasse ash							Y		(Horsakulthai et al., 2011)
Fluid catalytic cracking catalyst residue									(Payá et al., 1999)
Fluid catalytic cracking catalyst residue						Y			(Payá et al., 2003)
Fluid catalytic cracking catalyst residue	Y								(Payá et al., 2013a)
Fluid catalytic cracking catalyst residue							Y		(Morozov et al., 2013)
Fluid catalytic cracking catalyst						Y			(Payá et al., 2013b)

residue								
Zeolite		Y						(Behfarnia & Farshadfar, 2013)
Zeolite							Performed a life cycle assessment to reveal the CO_2 reduction amount by using pozzolan	(Valipour et al., 2014)
Zeolite	Thermal treated							(de la Villa et al., 2013)
Zeolite						Y		(Perraki et al., 2003)
Zeolite						Y		(Tydlitát et al., 2014)
Paper sludge ash		Y						(García et al., 2008)
Paper sludge ash	Thermal treated				ASR	Y		(Frías et al., 2013)
Paper sludge ash		Y			ASR			(Esteves et al., 2012)
Paper sludge ash			Y					(Goñi et al., 2014)
Wood ash		Y	Y					(Rajamma et al., 2009)
Wood ash		Y	Y					(Wang et al., 2008b)
Wood ash								(Wang et al., 2008a)
Wood ash								(Wang, 2014b)
Fluidized bed combustion		Y						(Havlica et al., 1998)

ash									
Fluidized bed combustion ash									(Wang et al., 2009b)
Fluidized bed combustion ash		Y							(Qian et al., 2014)
Fluidized bed combustion ash	Desulfurized ash	Y					Y		(Li et al., 2012)
Corn cob ash				Y				Studied the H_2SO_4 and HCl attack on the concrete with pozzolan	(Adesanya & Raheem, 2010)
Corn cob ash		Y							(Adesanya & Raheem, 2009b)
Corn cob ash									(Adesanya & Raheem, 2009a)
Glass powder		Y	Y		Y				(Shayan & Xu, 2006)
Glass powder		Y				ASR			(Shao et al., 2000)
Glass powder		Y				AAR			(Shi et al., 2005)
Switchgrass ash		Y				ASR			(Wang et al., 2014a)
Switchgrass ash		Y							(Wang, 2014a)
Wheat straw ash		Y						Studied a 10 000-40 000 mg/L Na_2SO_4 attack on the	(Biricik et al., 2000)

												concrete with pozzolan	
Wheat straw ash													(Biricik et al., 2000)
Wheat straw ash								Y					(Ataie & Riding, 2012)
Municipal solid waste ash		Y				Y			Y				(Cheng, 2012)
Municipal solid waste ash										Y			(Shi & Kan, 2009)
Municipal solid waste ash		Y								Y			(Chen et al., 2013)
Bark ash		Y				Y					Y	Studied the Cl corrosion on the concrete with pozzolan in a marine condition for 5 years	(Chalee et al., 2013)
Bark ash		Y		Y									(Chindaprasirt et al., 2007a)
Bark ash		Y	Y										(Sata et al., 2007)
Coal bottom ash		Y											(Cheriaf et al., 1999)
Coal bottom ash	Bituminous and lignite coal												(Vasugi & Ramamurthy, 2014)
Volcanic ash													(Shi & Day, 2000b)
Volcanic ash		Y											(Shi & Day, 2001)
Sewage sludge ash		Y		Y						Y			(Cyr et al., 2012)
Sewage sludge ash		Y											(Pan et al., 2003)

Olive residue ash		Y						(Cuenca et al., 2013)
Olive residue ash		Y						(Cruz-Yusta et al., 2011)
River sand		Y						(Sinsiri et al., 2012)
River sand		Y						(Sata et al., 2012)
Bioethanol waste (corn stover)	Lignocellulose enzymatic hydrolysis					Y (Inorganic)		(Ataie & Riding, 2014a)
Bioethanol waste (corn stover)	Corn stover	Y			Y			(Ataie & Riding, 2014b)
Diatomaceous earth + Milos earth								(Papadakis et al., 2002)
Diatomaceous earth + Milos earth		Y						(Papadakis & Tsimas, 2002)
Banana leaves ash		Y						(Kanning et al., 2014)
Sugar cane straw ash								(Frias et al., 2007)
Bamboo leaf ash								(Villar-Cociña et al., 2011)
Silica breccia	Aplite	Y			ASR		Studied the sulfate resistance	(Hassan et al., 2014)
Tincal ore waste		Y						(Kula et al., 2002)
Cattle manure ash		Y		Y				(Zhou et al., 2012)
Calcium carbide residue		Y	Y					(Rattanashotinunt et al., 2013)
Ceramic waste		Y					Studied the	(Sánchez de

									corrosion in a simulated marine condition (0.5 M NaCl+0.5 M Na_2SO_4)	Rojas et al., 2014)
Electroplating sludge		Y						Y		(Asavapisit et al., 2005)
Sawdust ash		Y								(Elinwa & Mahmood, 2002)
Waste tire rubber		Y		Y						(Yilmaz & Degirmenci, 2009)
Slate waste		Y					Y			(Frías et al., 2014)
Light emitting diode sludge		Y				Y		Y		(Lin et al., 2014a)
Refinery waste catalyst		Y						Y (Toxic)		(Lin et al., 2014b)
Activated alum sludge ash		Y	Y							(Owaid et al., 2014)
English red brick dust		Y								(Grist et al., 2013)
Construction and demolition waste										(Medina et al., 2013)
Fibrous materials	Kraft pulp, old corrugated container and fiberboard fiber	Y								(Hamzeh et al., 2013)

CHAPTER 2

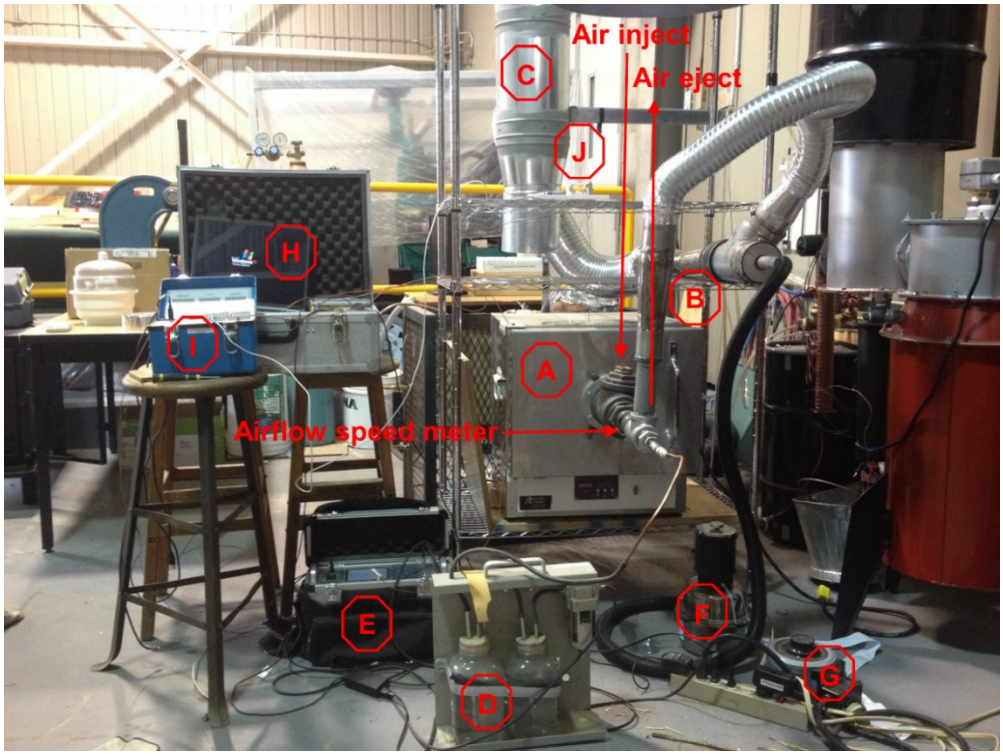

Figure S2- 1. Photo of experimental system designed to evaluate the combustion of switchgrass and hardwood.

A, combustion chamber (23.0 × 30.5 × 17.0 cm^3 of valid chamber volume); B, Bernoulli's principle air injection and ejection system; C, ventilation system with 9.93 $g \cdot min^{-1}$ of initial air supply capacity; D, water-washing unit to remove the fine particle and tar from gaseous emissions and to cool down the gas flow for protecting the in-situ gas analyzer; E; Gas-board 3100P infrared in-situ gas analyzer (CO, CO_2 and O_2); F, an adaptable external pump to provide extra airflow, which could be adjusted by switching different voltage conversion rate; G, an adjustable voltage converter to change the airflow rate from external pump; H; data acquisition system with a signal converter; I; Inter-

technology P3 strain indicator and recorder; J: the load cell that was used to measure the mass change of fuel sample.

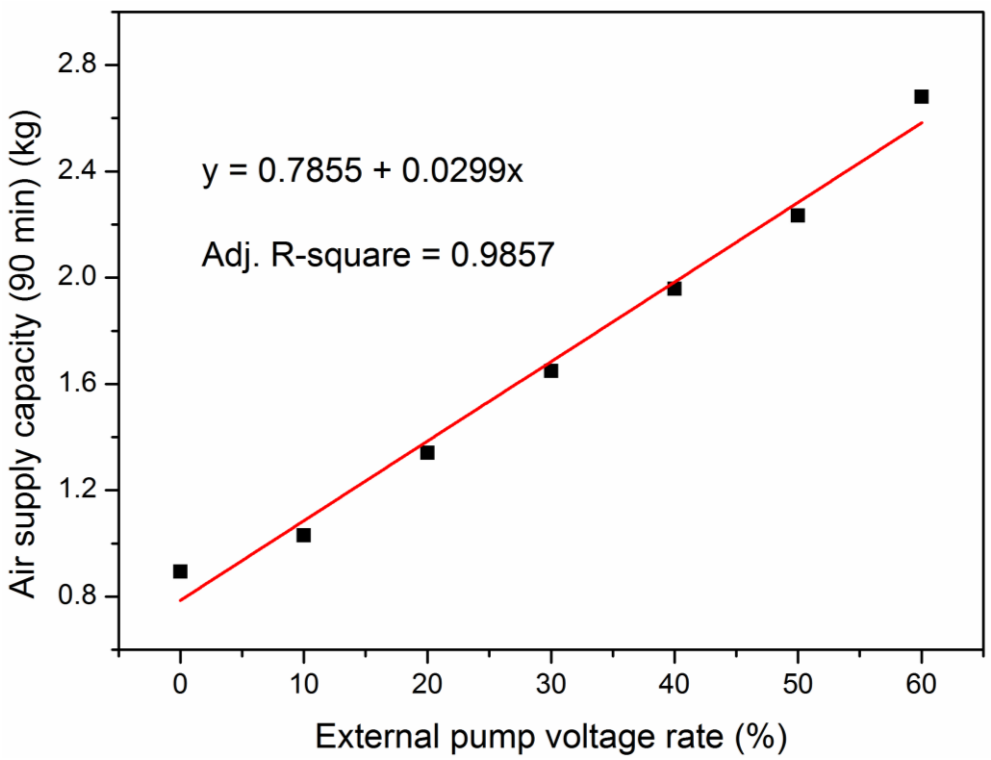

Figure S2- 2. Linear correlation between air supply capacity (kg at 25 °C, in 90 min) and external pump voltage rate (%) on the experimental combustion system.

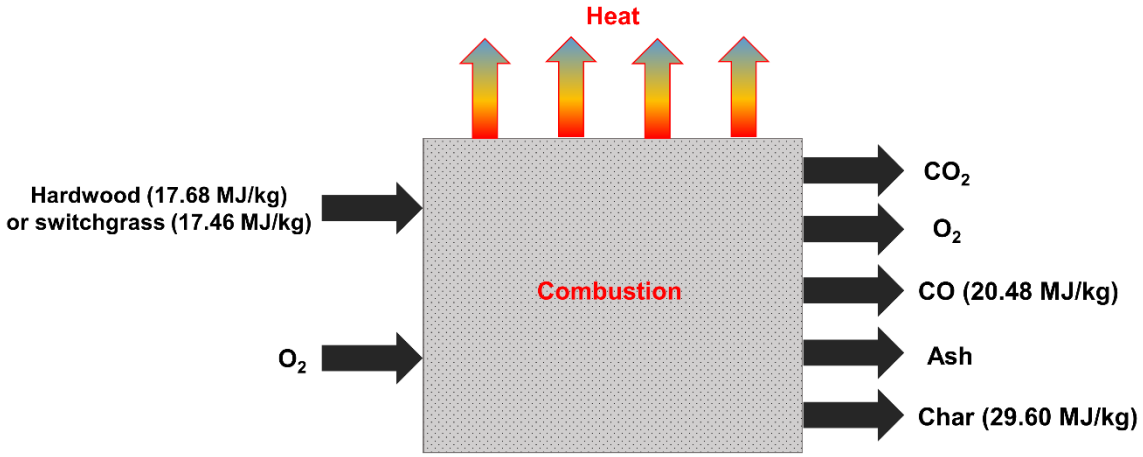

Figure S2- 3. Schematic "black box" model for quantifying the combustion energy efficiency (%) and burning rate (%/min) during the 90 min combustion of switchgrass or hardwood.

Estimation of energy conversion was based on the higher heating values (HHV) of inputs and outputs, and burning rate was calculated by normalizing the mass loss of fuel in 90 min.

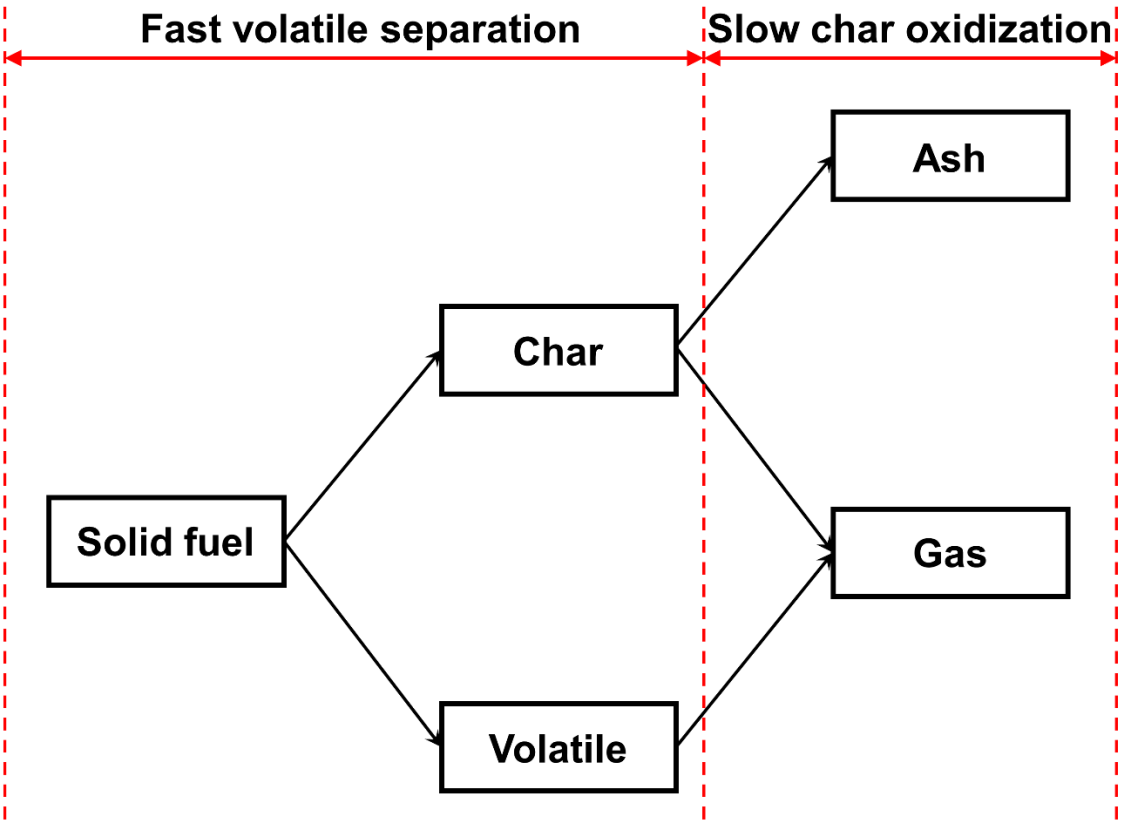

Figure S2- 4. Two-step solid-state reaction pathway model for thermogravimetric kinetic analysis.

The combustion was divided into fast volatile separation and slow char oxidization phases.

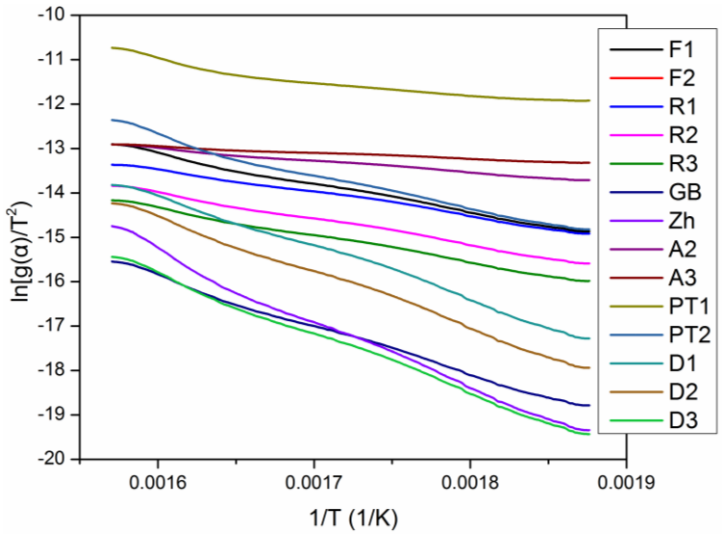
ln[g(α)/T²)
1/T (1/K)
F1
F2
R1
R2
R3
GB
Zh
A2
A3
PT1
PT2
D1
D2
D3

(a)

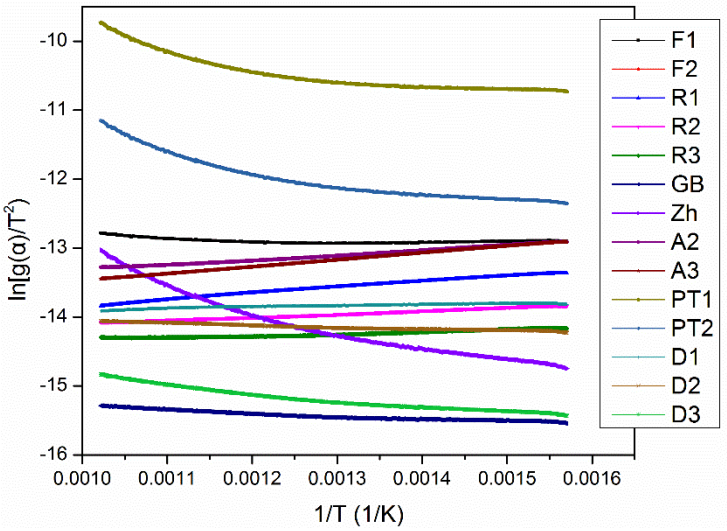
ln[g(α)/T²)
1/T (1/K)
F1
F2
R1
R2
R3
GB
Zh
A2
A3
PT1
PT2
D1
D2
D3

(b)

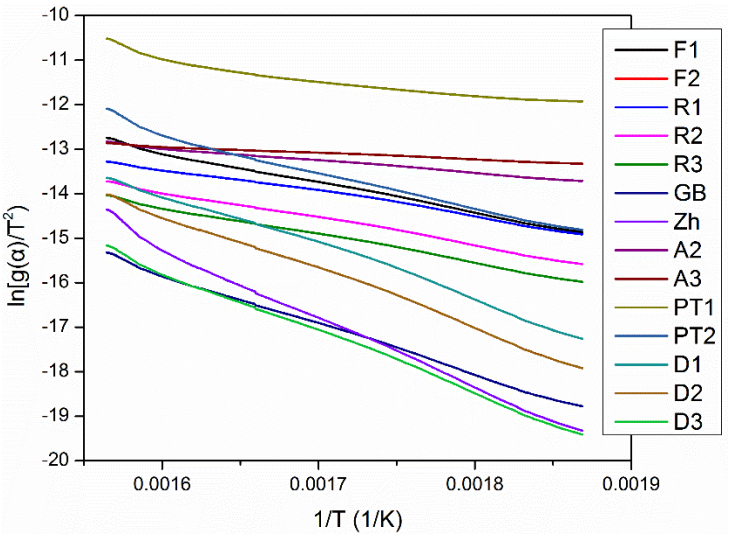

(c)

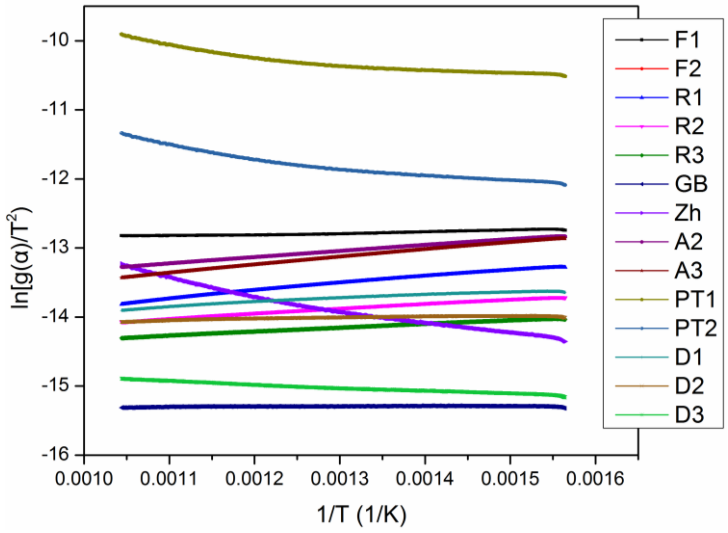

(d)

Figure S2- 5. Plotting of $\ln[g(\alpha)/T^2]$ versus 1/T with 14 groups of probable combustion mechanisms.

(a) Fast volatile separation step of switchgrass (261-364 °C); (b) slow char oxidization step of switchgrass (364-861 °C); (c) fast volatile separation step of hardwood (262-366 °C); (d) slow char oxidization step of hardwood (366-862 °C).

Table S2- 1. 14 groups of probable mechanisms of solid-state combustion model.

Symbol	Mechanism	f(α)	g(α)
F_1	First-order chemical reaction	$1-\alpha$	$-\ln(1-\alpha)$
F_2	Second-order chemical reaction	$(1-\alpha)^2$	$(1-\alpha)^{-1}-1$
R_1	Limited surface reaction (1 dimension)	1	α
R_2	Limited surface reaction (2 dimension)	$2(1-\alpha)^{1/2}$	$1-(1-\alpha)^{1/2}$
R_3	Limited surface reaction (3 dimension)	$3(1-\alpha)^{2/3}$	$1-(1-\alpha)^{1/3}$
G-B	Ginstling-Brounshtein equation	$(3/2)[(1-\alpha)^{-1/3}-1]^{-1}$	$1-(2/3)\alpha-(1-\alpha)^{2/3}$
Zh	Zhuravlev equation	$(3/2)\ (1-\alpha)^{4/3}[(1-\alpha)^{-1/3}-1]^{-1}$	$[(1-\alpha)^{-1/3}-1]^2$
A_2	Random nucleation and nuclei growth (1 dimension)	$2(1-\alpha)[-\ln(1-\alpha)]^{1/2}$	$[-\ln(1-\alpha)]^{1/2}$
A_3	Random nucleation and nuclei growth (2 dimension)	$3(1-\alpha)[-\ln(1-\alpha)]^{2/3}$	$[-\ln(1-\alpha)]^{1/3}$
P-T_1	Prout-Tompkins (0.5 order)	$(1-\alpha)\alpha^{1/2}$	$\ln[(1+\alpha^{1/2})/(1-\alpha^{1/2})]$
P-T_2	Prout-Tompkins (1 order)	$(1-\alpha)\alpha$	$\ln[\alpha/(1-\alpha)]$
D_1	Diffusion one-way transport	$1/2\alpha$	α^2
D_2	Diffusion two-way transport	$[-\ln(1-\alpha)]^{-1}$	$\alpha+(1-\alpha)\ln(1-\alpha)$
D_3	Diffusion three-way transport	$(3/2)(1-\alpha)^{2/3}[1-(1-\alpha)^{1/3}]^{-1}$	$[1-(1-\alpha)^{1/3}]^2$

Table S2- 2. Experimental conditions and product yields during each replicate of combustion tests.

Fuel	Excess air ratio	External pump voltage rate	Replicate	Ambient temperature	Initial fuel mass	Burnout residue mass	Ash mass	Char mass	Burnout residue yield	Ash yield	Char yield
		%		°C	g	g	g	g	%	%	%
Switchgrass	1.0	0	1	24.3	196	19.7	9.60	10.1	10.1	4.90	5.15
Switchgrass	1.0	0	2	24.0	196	21.1	10.0	11.1	10.8	5.10	5.66
Switchgrass	1.0	0	3	24.1	196	21.9	9.40	12.5	11.2	4.80	6.38
Switchgrass	1.1	10	1	24.7	206	19.4	10.1	9.30	9.44	4.91	4.52
Switchgrass	1.1	10	2	24.6	206	20.2	10.0	10.2	9.82	4.86	4.96
Switchgrass	1.1	10	3	24.5	206	20.2	10.4	9.80	9.82	5.06	4.77
Switchgrass	1.2	20	1	25.1	246	20.3	10.6	9.70	8.26	4.31	3.94
Switchgrass	1.2	20	2	24.8	246	19.5	10.2	9.30	7.93	4.15	3.78
Switchgrass	1.2	20	3	24.6	246	19.4	10.2	9.20	7.89	4.15	3.74
Switchgrass	1.3	30	1	23.8	278	20.2	8.80	11.4	7.26	3.16	4.10
Switchgrass	1.3	30	2	23.2	278	19.8	8.60	11.2	7.11	3.09	4.02
Switchgrass	1.3	30	3	23.0	278	21.0	9.20	11.9	7.55	3.31	4.28
Hardwood	1.0	0	1	23.7	185	6.80	2.00	4.80	3.67	1.08	2.59
Hardwood	1.0	0	2	25.8	185	6.50	2.00	4.50	3.51	1.08	2.43
Hardwood	1.0	0	3	23.4	185	6.80	2.10	4.60	3.67	1.13	2.49
Hardwood	1.1	10	1	22.5	194	6.30	2.40	3.90	3.25	1.24	2.01
Hardwood	1.1	10	2	26.3	194	5.70	2.50	3.30	2.94	1.29	1.70
Hardwood	1.1	10	3	24.9	194	6.20	2.50	3.70	3.19	1.29	1.91
Hardwood	1.2	20	1	25.6	231	6.40	2.30	4.10	2.77	0.99	1.77
Hardwood	1.2	20	2	22.7	231	6.30	2.50	3.80	2.72	1.08	1.64
Hardwood	1.2	20	3	21.3	231	5.80	2.50	3.30	2.51	1.08	1.43
Hardwood	1.3	30	1	22.1	263	7.00	2.40	4.50	2.66	0.91	1.71

Hardwood	1.3	30	2	26.0	263	6.70	2.70	3.90	2.55	1.03	1.48
Hardwood	1.3	30	3	25.8	263	7.40	2.90	4.50	2.82	1.10	1.71

Table S2- 3. Two-step kinetic analysis results (E_a, kJ/mol; A, /min) of switchgrass and hardwood combustion with 14 groups probable mechanisms.

The most probable kinetic parameters and mechanisms were determined by selecting the goodness of fit ($-R^2$) value closest to 1.

	Switchgrass						Hardwood					
Mechanism	Fast volatile separation			Slow char oxidization			Fast volatile separation			Slow char oxidization		
	E_a	A	$-R^2$	E_a	A	$-R^2$	E_a	A	$-R^2$	E_a	A	$-R^2$
F_1	54.55	4.74E+03	0.9980	0.70	2.32E-03	0.4765	56.78	8.10E+03	0.9985	-1.69	-4.37E-03	-0.9782
F_2	67.50	1.05E+05	0.9936	13.84	8.59E-01	0.9433	72.14	3.08E+05	0.9938	10.37	4.68E-01	0.9689
R_1	43.51	3.20E+02	0.9978	-7.10	-3.60E-03	-0.9981	44.01	3.68E+02	0.9966	-8.54	-3.64E-03	-0.9969
R_2	48.79	5.86E+02	0.9986	-3.85	-2.20E-03	-0.9980	50.07	8.07E+02	0.9986	-5.75	-2.65E-03	-0.9981
R_3	50.65	6.15E+02	0.9985	-2.48	-1.32E-03	-0.9782	52.23	9.07E+02	0.9988	-4.54	-1.91E-03	-0.9990
GB	91.11	5.70E+05	0.9986	3.35	1.35E-03	0.9714	94.07	1.14E+06	0.9993	-0.16	-4.18E-05	-0.5103
Zh	127.01	1.39E+09	0.9973	21.82	5.60E-01	0.9729	132.98	5.43E+09	0.9978	16.33	2.39E-01	0.9879
A_2	22.42	4.56E+00	0.9972	-6.07	-5.76E-03	-0.9985	23.51	6.09E+00	0.9980	-7.25	-6.06E-03	-0.9997
A_3	11.50	2.98E-01	0.9956	-8.37	-5.18E-03	-0.9999	12.19	3.70E-01	0.9968	-9.14	-5.21E-03	-0.9993
PT_1	32.30	3.12E+02	0.9598	10.78	1.91E+00	0.9141	37.03	9.85E+02	0.9609	8.12	1.15E+00	0.9496
PT_2	67.50	1.05E+05	0.9936	13.84	8.59E-01	0.9433	72.14	3.08E+05	0.9938	10.37	4.68E-01	0.9689
D_1	96.73	1.10E+07	0.9983	-1.37	-1.30E-03	-0.9791	97.79	1.45E+07	0.9974	-4.28	-2.86E-03	-0.9860
D_2	103.47	2.67E+07	0.9988	2.29	2.83E-03	0.9785	105.47	4.35E+07	0.9986	-1.19	-9.74E-04	-0.9376
D_3	111.09	3.43E+07	0.9988	7.92	8.18E-03	0.9780	114.32	7.31E+07	0.9990	3.77	2.44E-03	0.9939

CHAPTER 3

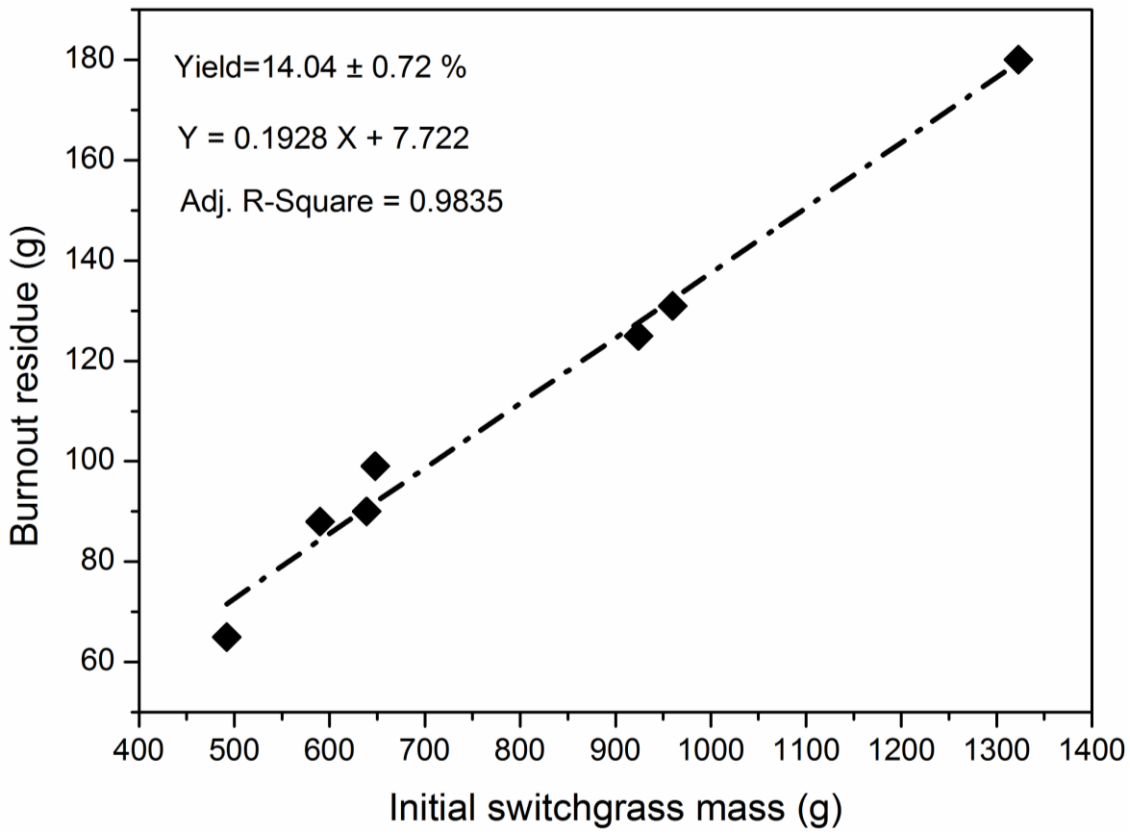

Figure S3- 1. Mean yield of burnout residue as a function of the initial switchgrass load. The burnout residues contained fine ash (≤2 mm) and large unburned char (≥2 mm).

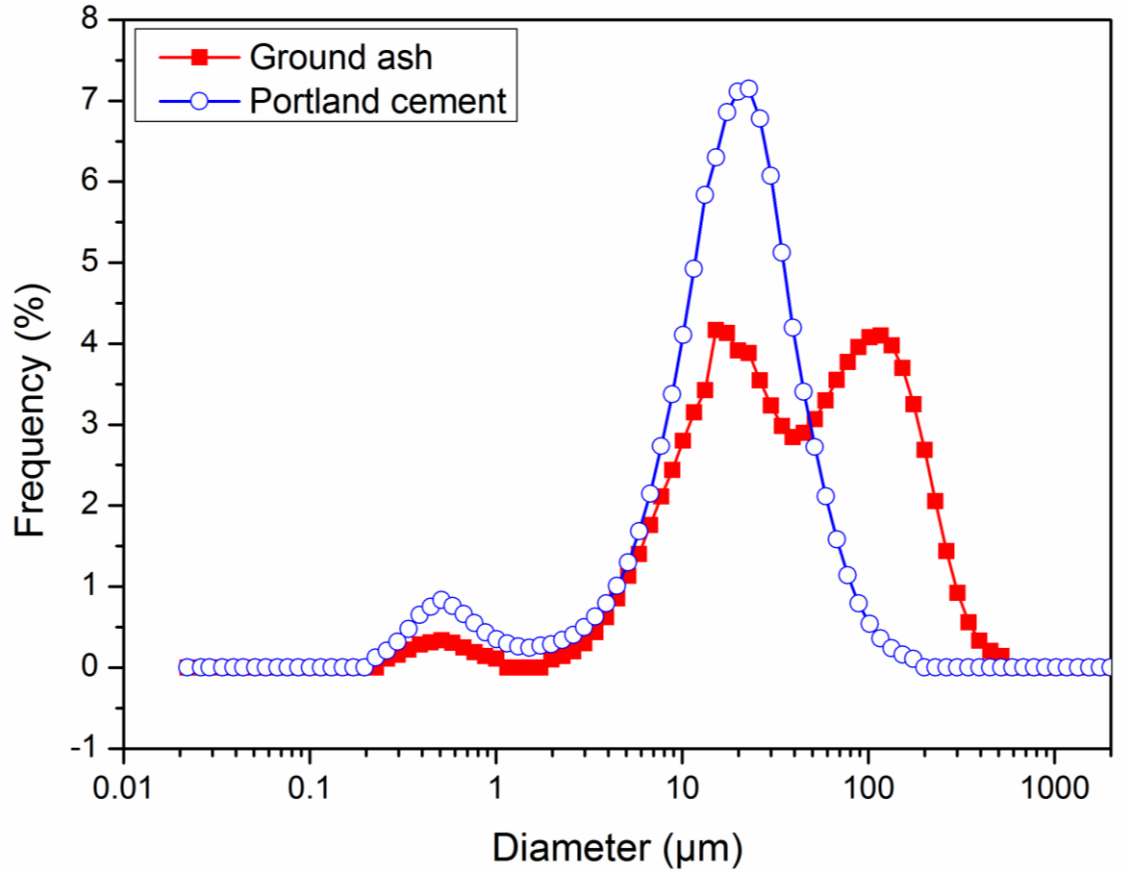

Figure S3- 2. Particle size distributions of the ground ash from switchgrass combustion, and Portland cement used in this study.

Figure S3- 3. Photo of the ground ash from switchgrass combustion. The mean particle size was 65.00 μm.

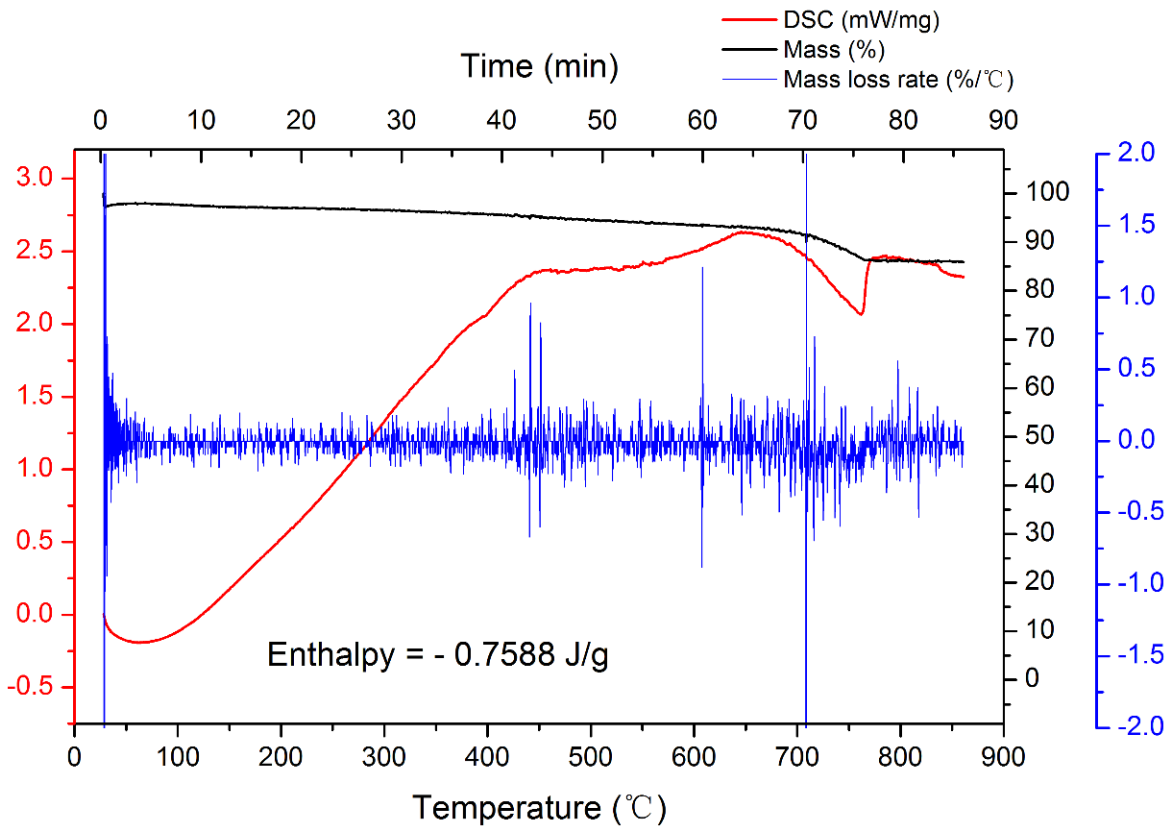

Figure S3- 4. Thermal properties of the ground ash from switchgrass combustion between 25 °C and 900 °C.

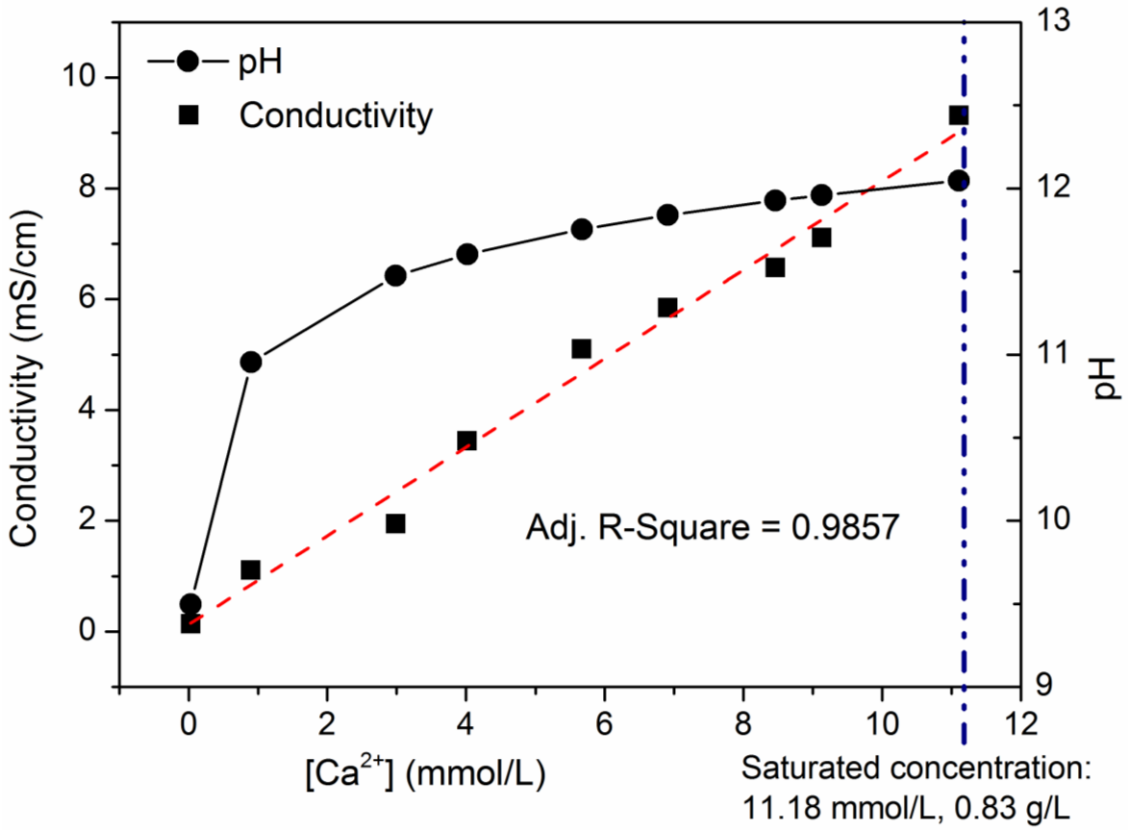

Figure S4- 1. Correlation of conductivity—Ca^{2+} concentration—pH value in a pure $Ca(OH)_2$ solution at 25 °C.

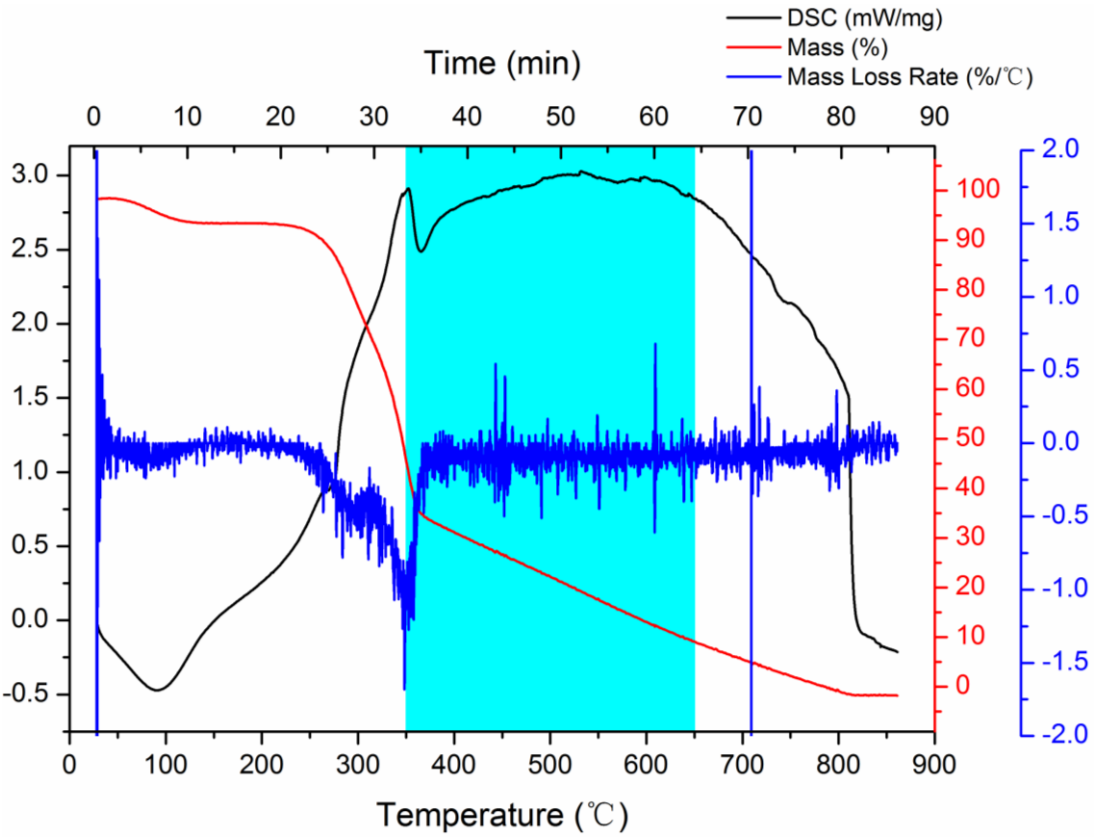

Figure S4- 2. Switchgrass combustion profile (≈ 18 mg sample size) determined by thermogravimetric analysis-differential scanning calorimetry (TGA-DSC).

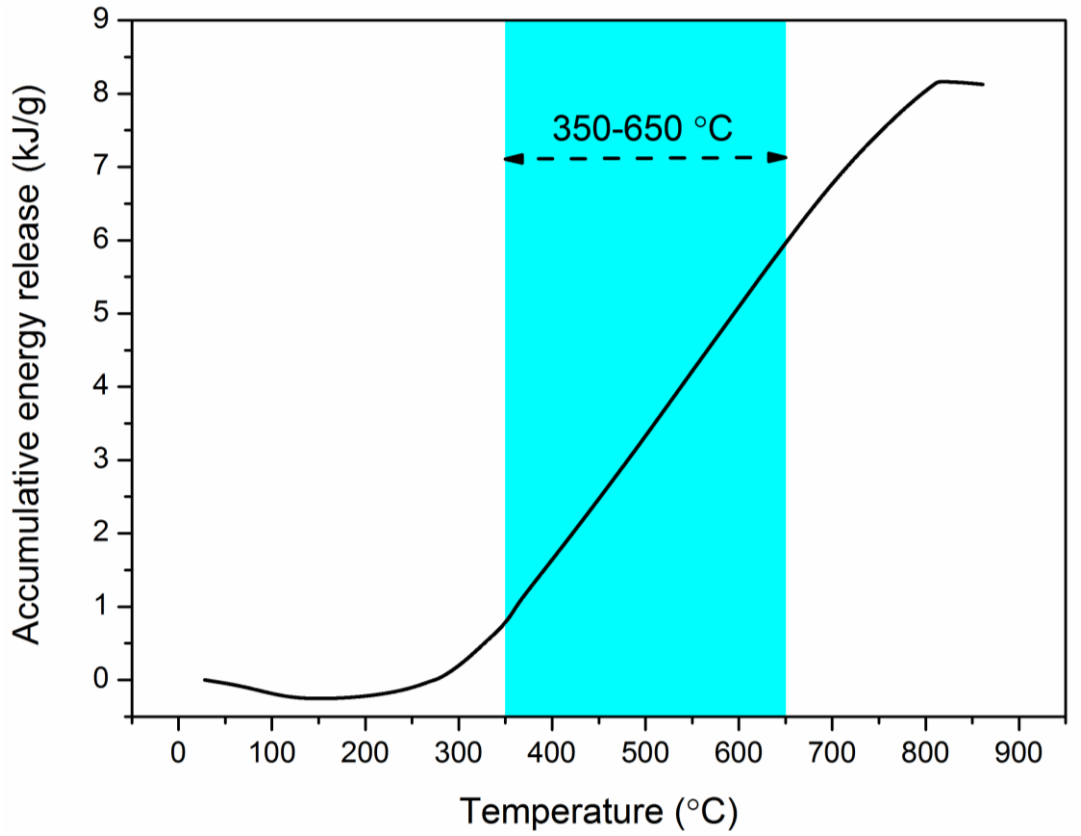

Figure S4- 3. Accumulative energy release of switchgrass combustion (≈ 18 mg initially), from 25 °C to 900 °C, in a 20% O_2 + 80% O_2 atmosphere (by volume), with 10 °C/min of heating rate.

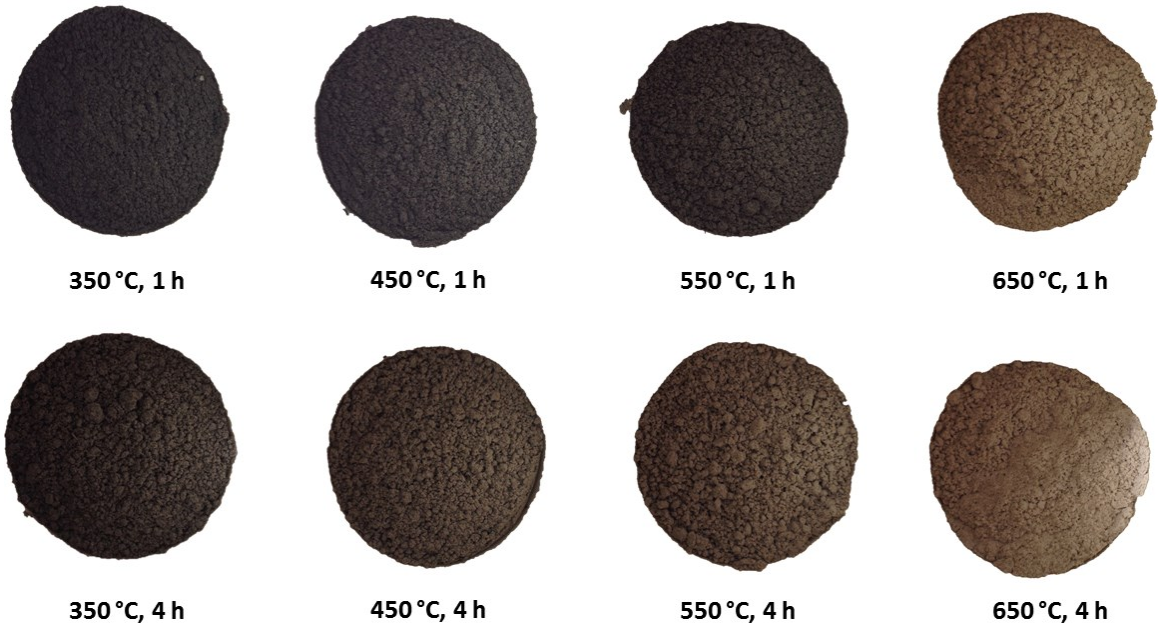

Figure S4- 4. Color change of the switchgrass ash depending on combustion conditions (temperatures from 350-650 °C, retention times of 1 and 4 h).

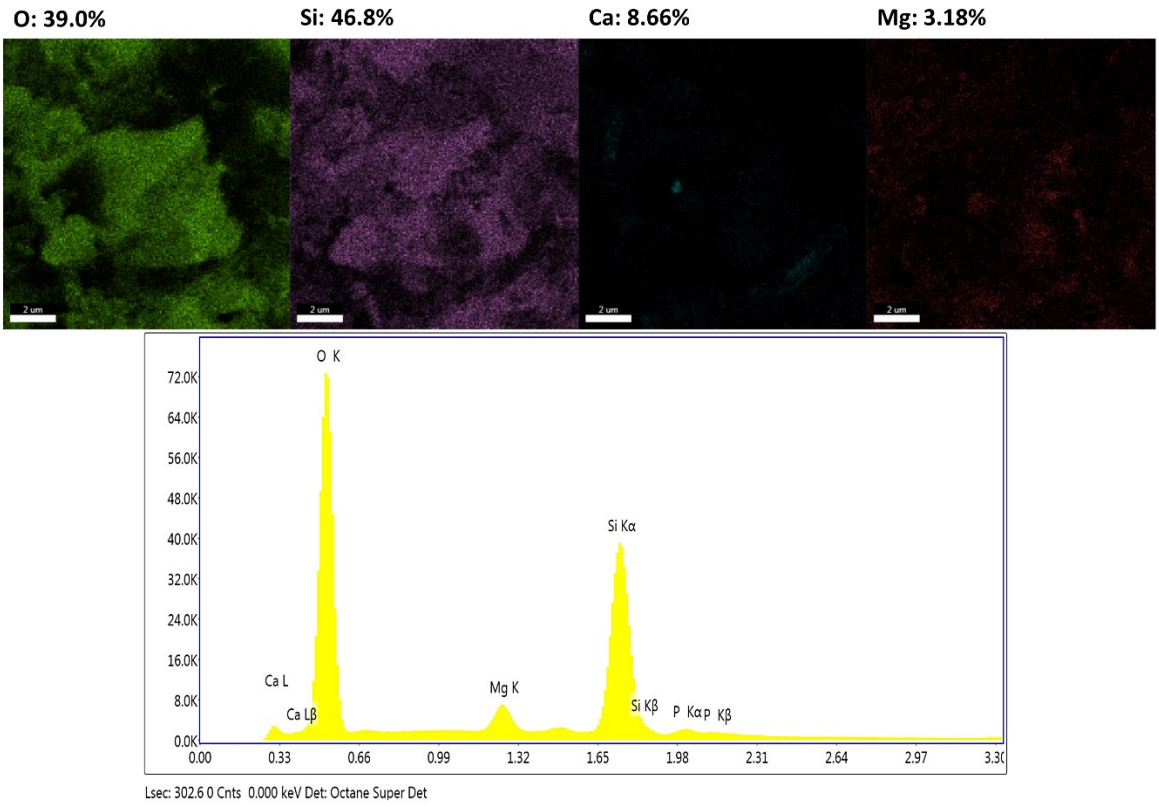

Figure S4- 5. Elemental mapping (by mass) on the ash (550 °C, 4 h) by Energy Dispersive Spectroscopy (EDS) with Octane Silicon Drift Detector (SDD).

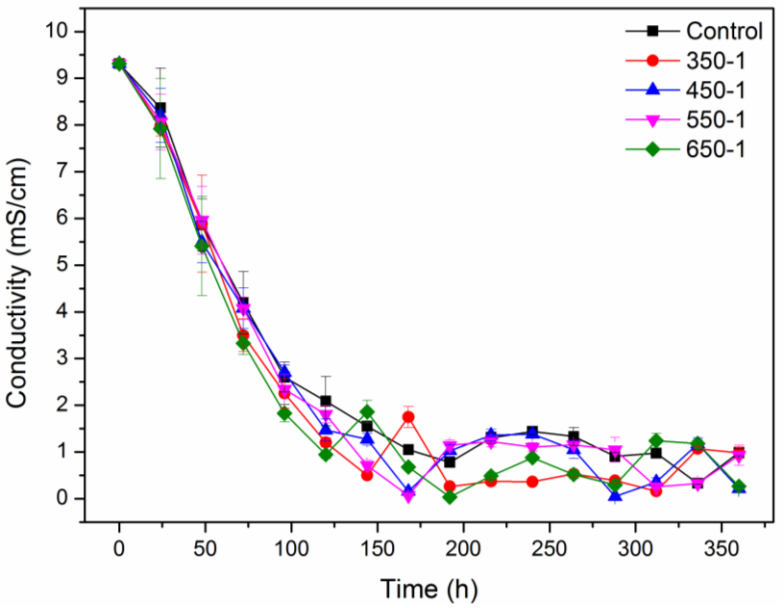

(a)

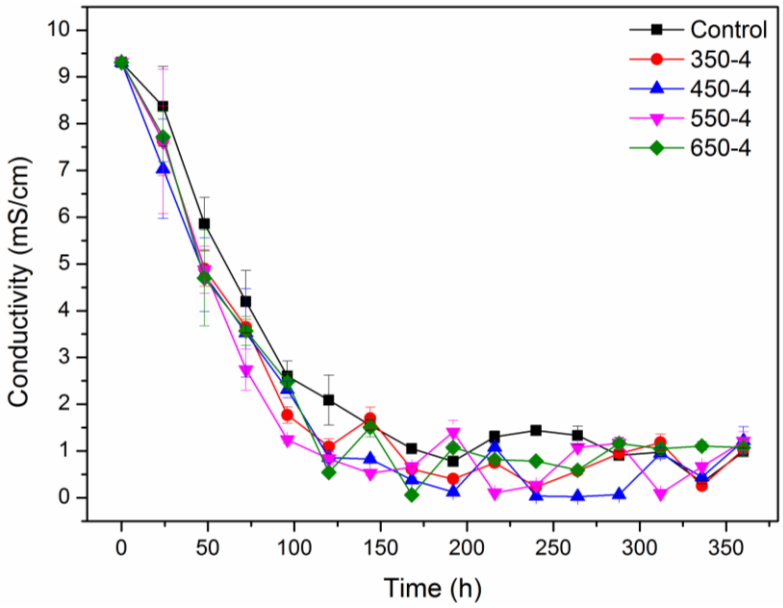

(b)

Figure S4- 6. Solution conductivity in a $Ca(OH)_2$—ash suspension (2 g ash + 75 mL saturated $Ca(OH)_2$ solution), measured via the Ca^{2+} concentration in solution at each 24 h. (a) Ash from switchgrass combustion at 350-650 °C for 1 h; (b) ash from switchgrass combustion at 350-650 °C for 4 h. Control group was the ash from open switchgrass combustion (≈ 411 °C, 5 min).

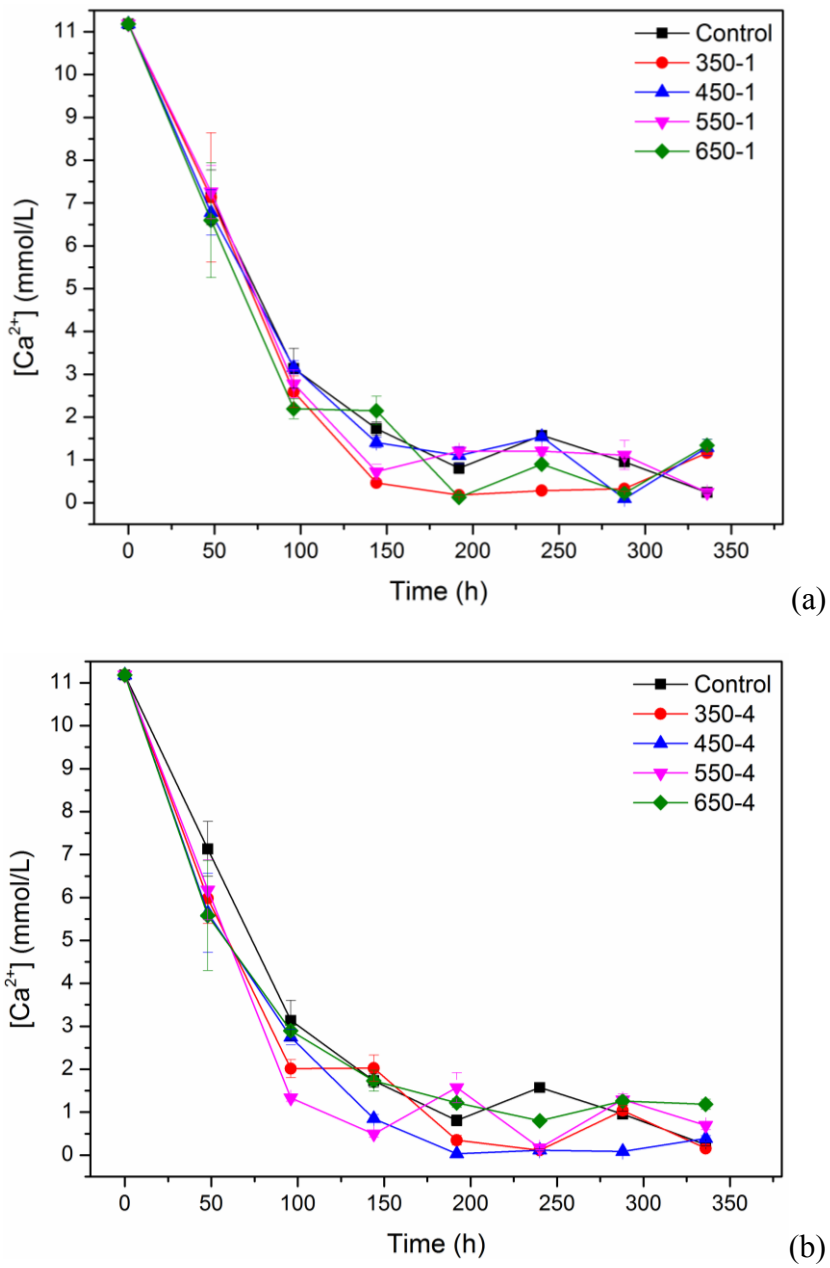

Figure S4- 7. Ca^{2+} concentration in a $Ca(OH)_2$—ash suspension (2 g ash + 75 mL saturated $Ca(OH)_2$ solution), measured via the Ca^{2+} concentration in solution at each 24 h. (a) Ash from switchgrass combustion at 350-650 °C for 1 h; (b) ash from switchgrass combustion at 350-650 °C for 4 h. Control group was the ash from open switchgrass combustion (≈ 411 °C, 5 min).

Table S4- 1. Chemical composition of switchgrass sample and its ash from an open combustion test (≈ 411 °C, 5 min).

Mineral oxides (w.t.%)	Switchgrass	Ash
SiO_2	2.23	67.2
Al_2O_3	0.250	0.680
Fe_2O_3	0.200	0.310
MnO	0.010	0.070
MgO	0.080	2.05
CaO	0.560	12.3
Na_2O	0.040	0.110
K_2O	0.140	1.24
TiO_2	0.010	0.060
P_2O_5	0.090	1.15
Loss on Ignition (LOI)	96.4	14.8
Total	100	99.9

Table S4- 2. Physiochemical property of the Portland cement used in this study.

Item	
C_3S (w.t.%)	65.6
C_2S (w.t.%)	6.93
C_3A (w.t.%)	12.7
C_4AF (w.t.%)	8.49
Silica ratio (1)	2.58
Alumina-iron ratio (1)	1.73
Lime saturation factor (1)	0.970
Specific surface area (m^2/m^3)	12820
Mean particle size (um)	22.0

Table S4- 3. Results of a two-way Analysis of Variance (ANOVA) with replication (n=3, at 0.05 level) on the compressive strength of concrete.

Concrete samples contained 10% of the ash from the switchgrass combustion with different temperature (350-650 °C) and retention time (1 and 4 h).

Source of Variation	Sum of squares	Degrees of freedom	Mean square	F	P-value	F critical
Retention time	103	1	103	35.0	2.17e-05	4.49
Temperature	5.37	3	1.79	0.610	0.620	3.24
Retention time × temperature	33.2	3	11.1	3.76	0.030	3.24
Error	47.1	16	2.94	—	—	—
Total	189	23		—	—	—

Table S4- 4. Signal-to-Noise ratio (S/N) of pozzolanic activity index (PAI), estimated with the concrete compressive strength.

A symbol of spadesuit corresponded to the highest S/N value, which indicated the most optimal combustion condition for the PAI of ash.

Sample	Combustion temperature (°C)	Retention time (h)	Signal to Noise ratio (S/N)
Control	≈ 411	5 min	39.2
350-1	350	1	39.9
450-1	450	1	39.2
550-1	550	1	39.4
650-1	650	1	40.3
350-4	350	4	40.8
450-4	450	4	40.8
550-4	550	4	41.1 ♠
650-4	650	4	40.5

Table S4- 5. Numeric simulation result comparison by a two-way Analysis of Variance (ANOVA) without replication at 0.05 level.

Two independent factors in the ANOVA were nine ash samples and two measurements (conductivity or Ca^{2+} concentration).

Parameter	Source of Variation	Sum of squares	Degree of freedom	Mean square	F	P-value
D_e	Ash sample source	2.99e-05	8	3.74e-06	1.22	0.393
	Measurement	1.46e-06	1	1.46e-06	0.477	0.510
K	Ash sample source	1.17e-04	8	1.46e-05	4.91	0.0187
	Measurement	4.09e-05	1	4.09e-05	13.7	6.00e-3
τ	Ash sample source	2.14e+03	8	2.68e+02	2.35	0.124
	Measurement	4.22e+01	1	4.22e+01	0.370	0.560
$\Delta G^{\#}$	Ash sample source	2.93e+00	8	3.67e-01	3.20	0.0602
	Measurement	1.16e+00	1	1.16e+00	10.1	0.0130

REFERENCE

Abbasi, T., Abbasi, S. 2010. Biomass energy and the environmental impacts associated with its production and utilization. *Renewable and Sustainable Energy Reviews*, **14**(3), 919-937.

Adesanya, D., Raheem, A. 2009a. Development of corn cob ash blended cement. *Constr. Build. Mater.*, **23**(1), 347-352.

Adesanya, D., Raheem, A. 2010. A study of the permeability and acid attack of corn cob ash blended cements. *Constr. Build. Mater.*, **24**(3), 403-409.

Adesanya, D., Raheem, A. 2009b. A study of the workability and compressive strength characteristics of corn cob ash blended cement concrete. *Constr. Build. Mater.*, **23**(1), 311-317.

Alam, S., Gul, S., Muhammad, K. 2013. Chemical activation of clay in cement mortar, using calcium chloride. *Adv. Cem. Res.*, **25**(3), 164-170.

Aldahdooh, M., Muhamad Bunnori, N., Megat Johari, M. 2013. Development of green ultra-high performance fiber reinforced concrete containing ultrafine palm oil fuel ash. *Constr. Build. Mater.*, **48**, 379-389.

Aldahdooh, M., Muhamad Bunnori, N., Megat Johari, M. 2014. Influence of palm oil fuel ash on ultimate flexural and uniaxial tensile strength of green ultra-high performance fiber reinforced cementitious composites. *Mater. Design*, **54**, 694-701.

Altwair, N.M., Johari, M.M., Hashim, S.F.S. 2014. Influence of treated palm oil fuel ash on compressive properties and chloride resistance of engineered cementitious composites. *Mater. Struct.*, **47**(4), 667-682.

Amaral, S.S., de Carvalho Junior, J.A., Costa, M.A.M., Neto, T.G.S., Dellani, R., Leite, L.H.S. 2014. Comparative study for hardwood and softwood forest biomass: Chemical characterization, combustion phases and gas and particulate matter emissions. *Bioresource Technol.*, **164**, 55-63.

Amin, N., Ali, K., Shah, M., Alam, S. 2011. Chemical activation of bagasse ash in cement mortar. *Adv. Cem. Res.*, **23**(2), 89-95.

Ampazis, N., Perantonis, S.J. 2000. Levenberg-Marquardt algorithm with adaptive momentum for the efficient training of feedforward networks. *Neural Networks, 2000. IJCNN 2000, Proceedings of the IEEE-INNS-ENNS International Joint Conference on*. IEEE. pp. 126-131.

Antiohos, S., Papadakis, V., Tsimas, S. 2014. Rice husk ash (RHA) effectiveness in cement and concrete as a function of reactive silica and fineness. *Cement Concrete Res.*, **61**, 20-27.

Antiohos, S., Papageorgiou, D., Chaniotakis, E., Tsimas, S. 2007. Mechanical and durability characteristics of gypsum-free blended cements incorporating sulphate-rich reject fly ash. *Cement Concrete Comp.*, **29**(7), 550-558.

Antizar-Ladislao, B., Turrion-Gomez, J.L. 2008. Second-generation biofuels and local bioenergy systems. *Biofuels, Bioproducts and Biorefining*, **2**(5), 455-469.

Asavapisit, S., Naksrichum, S., Harnwajanawong, N. 2005. Strength, leachability and microstructure characteristics of cement-based solidified plating sludge. *Cement Concrete Res.*, **35**(6), 1042-1049.

ASTM. 2012a. C618-12a: Standard Specification for Coal Fly Ash and Raw or Calcined Natural Pozzolan for Use in Concrete. West Conshohocken, PA.

ASTM. 2004. Standard specification for coal fly ash and raw or calcined natural pozzolan for use as a mineral admixture in concrete. Annual Book of ASTM Standard C618

ASTM. 2011. Standard specification for fly ash and other pozzolans for use with lime for soil stabilization. Annual Book of ASTM Standard C593.

ASTM. 2013a. Standard test method for gross calorific value of coal and coke. Annual Book of ASTM Standard 5865-13

ASTM. 2007. Standard test method for potential alkali reactivity of aggregates (mortar-bar method). Annual Book of ASTM Standard C1260.

ASTM. 2013b. Standard test method for sulfur in the analysis sample of coal and coke using high-temperature tube furnace combustion. Annual Book of ASTM Standard 4239-13E1.

ASTM. 2012b. Standard test methods for proximate analysis of coal and coke by macro thermogravimetric analysis. Annual Book of ASTM Standard D7582-12

Ataie, F.F., Riding, K.A. 2014a. Impact of pretreatments and enzymatic hydrolysis on agricultural residue ash suitability for concrete. *Constr. Build. Mater.*, **58**, 25-30.

Ataie, F.F., Riding, K.A. 2012. Thermochemical pretreatments for agricultural residue ash production for concrete. *J. Mater. Civil Eng.*, **25**(11), 1703-1711.

Ataie, F.F., Riding, K.A. 2014b. Use of bioethanol byproduct for supplementary cementitious material production. *Constr. Build. Mater.*, **51**, 89-96.

Atici, U. 2011. Prediction of the strength of mineral admixture concrete using multivariable regression analysis and an artificial neural network. *Expert Syst. Appl.*, **38**(8), 9609-9618.

Awal, A., Shehu, I. 2013. Evaluation of heat of hydration of concrete containing high volume palm oil fuel ash. *Fuel*, **105**, 728-731.

Aydın, S., Karatay, Ç., Baradan, B. 2010. The effect of grinding process on mechanical properties and alkali-silica reaction resistance of fly ash incorporated cement mortars. *Powder Technol.*, **197**(1), 68-72.

Baert, G., Hoste, S., De Schutter, G., De Belie, N. 2008. Reactivity of fly ash in cement paste studied by means of thermogravimetry and isothermal calorimetry. *J. Therm. Anal. Calorim.*, **94**(2), 485-492.

Barroso, J., Ballester, J., Pina, A. 2007. Study of coal ash deposition in an entrained flow reactor: assessment of traditional and alternative slagging indices. *Fuel Process. Technol.*, **88**(9), 865-876.

Basheer, I., Hajmeer, M. 2000. Artificial neural networks: fundamentals, computing, design, and application. *J. Microbiol. Meth.*, **43**(1), 3-31.

Baxter, L. 2005. Biomass-coal co-combustion: opportunity for affordable renewable energy. *Fuel*, **84**(10), 1295-1302.

Behfarnia, K., Farshadfar, O. 2013. The effects of pozzolanic binders and polypropylene fibers on durability of SCC to magnesium sulfate attack. *Constr. Build. Mater.*, **38**, 64-71.

Bentz, D.P., Stutzman, P.E., Garboczi, E.J. 1992. Experimental and simulation studies of the interfacial zone in concrete. *Cement Concrete Res.*, **22**(5), 891-902.

Biricik, H., Aköz, F., Tulgar, A.N. 1999. Study of pozzolanic properties of wheat straw ash. *Cement Concrete Res.*, **29**(5), 637-643.

Biricik, H., Aköz, F., Türker, F., Berktay, I. 2000. Resistance to magnesium sulfate and sodium sulfate attack of mortars containing wheat straw ash. *Cement Concrete Res.*, **30**(8), 1189-1197.

Blissett, R., Rowson, N. 2012. A review of the multi-component utilisation of coal fly ash. *Fuel*, **97**, 1-23.

Bogue, R.H. 1929. Calculation of the compounds in Portland cement. *Ind. Eng. Chem. Anal. Ed.*, **1**(4), 192-197.

Boháč, M., Palou, M., Novotný, R., Másilko, J., Všianský, D., Staněk, T. 2014. Investigation on early hydration of ternary Portland cement-blast-furnace slag–metakaolin blends. *Constr. Build. Mater.*, **64**, 333-341.

BS-EN. 2013. BS EN 196-2: 2013 Method of testing cement. Chemical analysis of cement, BSI.

Bui, D., Hu, J., Stroeven, P. 2005. Particle size effect on the strength of rice husk ash blended gap-graded Portland cement concrete. *Cement Concrete Comp.*, **27**(3), 357-366.

Bullard, J.W., Jennings, H.M., Livingston, R.A., Nonat, A., Scherer, G.W., Schweitzer, J.S., Scrivener, K.L., Thomas, J.J. 2011. Mechanisms of cement hydration. *Cement and Concrete Research*, **41**(12), 1208-1223.

Canpolat, F., Yılmaz, K., Köse, M., Sümer, M., Yurdusev, M. 2004. Use of zeolite, coal bottom ash and fly ash as replacement materials in cement production. *Cement Concrete Res.*, **34**(5), 731-735.

Chaipanich, A., Nochaiya, T. 2010. Thermal analysis and microstructure of Portland cement-fly ash-silica fume pastes. *J. Therm. Anal. Calorim.*, **99**(2), 487-493.

Chalee, W., Sasakul, T., Suwanmaneechot, P., Jaturapitakkul, C. 2013. Utilization of rice husk–bark ash to improve the corrosion resistance of concrete under 5-year exposure in a marine environment. *Cement Concrete Comp.*, **37**, 47-53.

Chandara, C., Mohd Azizli, K.A., Ahmad, Z.A., Saiyid Hashim, S.F., Sakai, E. 2012. Heat of hydration of blended cement containing treated ground palm oil fuel ash. *Constr. Build. Mater.*, **27**(1), 78-81.

Chandara, C., Sakai, E., Azizli, K.A.M., Ahmad, Z.A., Hashim, S.F.S. 2010. The effect of unburned carbon in palm oil fuel ash on fluidity of cement pastes containing superplasticizer. *Constr. Build. Mater.*, **24**(9), 1590-1593.

Chandrasekaran, S.R., Hopke, P.K. 2012. Kinetics of switch grass pellet thermal decomposition under inert and oxidizing atmospheres. *Bioresource Technol.*, **125**, 52-58.

Chandrasekhar, S., Satyanarayana, K., Pramada, P., Raghavan, P., Gupta, T. 2003. Review processing, properties and applications of reactive silica from rice husk-an overview. *J. Mater. Sci.*, **38**(15), 3159-3168.

Chatveera, B., Lertwattanaruk, P. 2011. Durability of conventional concretes containing black rice husk ash. *J. Environ. Manage.*, **92**(1), 59-66.

Chen, C.-G., Sun, C.-J., Gau, S.-H., Wu, C.-W., Chen, Y.-L. 2013. The effects of the mechanical-chemical stabilization process for municipal solid waste incinerator fly ash on the chemical reactions in cement paste. *Waste Manage.*, **33**(4), 858-865.

Chen, H.-J., Huang, S.-S., Tang, C.-W., Malek, M., Ean, L.-W. 2012. Effect of curing environments on strength, porosity and chloride ingress resistance of blast furnace

slag cement concretes: A construction site study. *Constr. Build. Mater.*, **35**, 1063-1070.

Cheng, A. 2012. Effect of incinerator bottom ash properties on mechanical and pore size of blended cement mortars. *Mater. Design*, **36**, 859-864.

Cheriaf, M., Rocha, J.C., Pera, J. 1999. Pozzolanic properties of pulverized coal combustion bottom ash. *Cement Concrete Res.*, **29**(9), 1387-1391.

Cherubini, F., Jungmeier, G. 2010. LCA of a biorefinery concept producing bioethanol, bioenergy, and chemicals from switchgrass. *The International Journal of Life Cycle Assessment*, **15**(1), 53-66.

Chi, M., Huang, R. 2013. Binding mechanism and properties of alkali-activated fly ash/slag mortars. *Constr. Build. Mater.*, **40**, 291-298.

Chindaprasirt, P., Homwuttiwong, S., Jaturapitakkul, C. 2007a. Strength and water permeability of concrete containing palm oil fuel ash and rice husk–bark ash. *Constr. Build. Mater.*, **21**(7), 1492-1499.

Chindaprasirt, P., Homwuttiwong, S., Sirivivatnanon, V. 2004. Influence of fly ash fineness on strength, drying shrinkage and sulfate resistance of blended cement mortar. *Cement Concrete Res.*, **34**(7), 1087-1092.

Chindaprasirt, P., Kanchanda, P., Sathonsaowaphak, A., Cao, H. 2007b. Sulfate resistance of blended cements containing fly ash and rice husk ash. *Constr. Build. Mater.*, **21**(6), 1356-1361.

Chindaprasirt, P., Rukzon, S. 2008. Strength, porosity and corrosion resistance of ternary blend Portland cement, rice husk ash and fly ash mortar. *Constr. Build. Mater.*, **22**(8), 1601-1606.

Chindaprasirt, P., Rukzon, S., Sirivivatnanon, V. 2008. Resistance to chloride penetration of blended Portland cement mortar containing palm oil fuel ash, rice husk ash and fly ash. *Constr. Build. Mater.*, **22**(5), 932-938.

Chusilp, N., Jaturapitakkul, C., Kiattikomol, K. 2009. Utilization of bagasse ash as a pozzolanic material in concrete. *Constr. Build. Mater.*, **23**(11), 3352-3358.

Cordeiro, G., Toledo Filho, R., Fairbairn, E. 2009. Effect of calcination temperature on the pozzolanic activity of sugar cane bagasse ash. *Constr. Build. Mater.*, **23**(10), 3301-3303.

Cordeiro, G., Toledo Filho, R., Tavares, L., Fairbairn, E. 2008. Pozzolanic activity and filler effect of sugar cane bagasse ash in Portland cement and lime mortars. *Cement Concrete Comp.*, **30**(5), 410-418.

Craven, M.W., Shavlik, J.W. 1997. Using neural networks for data mining. *Future Gener. Comp. Sy.*, **13**(2), 211-229.

Cruz-Yusta, M., Mármol, I., Morales, J., Sánchez, L. 2011. Use of olive biomass fly ash in the preparation of environmentally friendly mortars. *Environ. Sci. Technol.*, **45**(16), 6991-6996.

Cuenca, J., Rodríguez, J., Martín-Morales, M., Sánchez-Roldán, Z., Zamorano, M. 2013. Effects of olive residue biomass fly ash as filler in self-compacting concrete. *Constr. Build. Mater.*, **40**, 702-709.

Cyr, M., Idir, R., Escadeillas, G. 2012. Use of metakaolin to stabilize sewage sludge ash and municipal solid waste incineration fly ash in cement-based materials. *J. Hazard. Mater.*, **243**, 193-203.

Dantas, A.T.A., Batista Leite, M., de Jesus Nagahama, K. 2013. Prediction of compressive strength of concrete containing construction and demolition waste using artificial neural networks. *Constr. Build. Mater.*, **38**, 717-722.

de la Villa, R.V., Fernández, R., Rodríguez, O., García, R., Villar-Cociña, E., Frías, M. 2013. Evolution of the pozzolanic activity of a thermally treated zeolite. *J. Mater. Sci.*, **48**(8), 3213-3224.

de Sensale, G.R., Ribeiro, A.B., Gonçalves, A. 2008. Effects of RHA on autogenous shrinkage of Portland cement pastes. *Cement Concrete Comp.*, **30**(10), 892-897.

Degereji, M., Gubba, S., Ingham, D., Ma, L., Pourkashanian, M., Williams, A., Williamson, J. 2013. Predicting the slagging potential of co-fired coal with sewage sludge and wood biomass. *Fuel*, **108**, 550-556.

Demirbas, A. 2004. Combustion characteristics of different biomass fuels. *Prog. Energ. Combust.*, **30**(2), 219-230.

Demirbaş, A. 2001. Biomass resource facilities and biomass conversion processing for fuels and chemicals. *Energy Convers. Manage.*, **42**(11), 1357-1378.

Demirbaş, A. 2003. Sustainable cofiring of biomass with coal. *Energy Conversion and Management*, **44**(9), 1465-1479.

Demirbas, M.F., Balat, M., Balat, H. 2009. Potential contribution of biomass to the sustainable energy development. *Energy Convers. Manage.*, **50**(7), 1746-1760.

Deschner, F., Lothenbach, B., Winnefeld, F., Neubauer, J. 2013. Effect of temperature on the hydration of Portland cement blended with siliceous fly ash. *Cement Concrete Res.*, **52**, 169-181.

Donatello, S., Fernández‐Jimenez, A., Palomo, A. 2013. Very high volume fly ash cements. Early age hydration study using Na_2SO_4 as an activator. *J. Am. Ceram. Soc.*, **96**(3), 900-906.

Donatello, S., Freeman-Pask, A., Tyrer, M., Cheeseman, C. 2010a. Effect of milling and acid washing on the pozzolanic activity of incinerator sewage sludge ash. *Cement Concrete Comp.*, **32**(1), 54-61.

Donatello, S., Tyrer, M., Cheeseman, C. 2010b. Comparison of test methods to assess pozzolanic activity. *Cement Concrete Comp.*, **32**(2), 121-127.

Duan, P., Shui, Z., Chen, W., Shen, C. 2013a. Efficiency of mineral admixtures in concrete: Microstructure, compressive strength and stability of hydrate phases. *Appl. Clay Sci.*, **83**, 115-121.

Duan, Z., Kou, S., Poon, C. 2013b. Prediction of compressive strength of recycled aggregate concrete using artificial neural networks. *Constr. Build. Mater.*, **40**, 1200-1206.

El-Dakroury, A., Gasser, M. 2008. Rice husk ash (RHA) as cement admixture for immobilization of liquid radioactive waste at different temperatures. *J. Nucl. Mater.*, **381**(3), 271-277.

Elinwa, A.U., Mahmood, Y.A. 2002. Ash from timber waste as cement replacement material. *Cement Concrete Comp.*, **24**(2), 219-222.

Ercikdi, B., Cihangir, F., Kesimal, A., Deveci, H., Alp, İ. 2009. Utilization of industrial waste products as pozzolanic material in cemented paste backfill of high sulphide mill tailings. *J. Hazard. Mater.*, **168**(2), 848-856.

Escalante-Garcıa, J., Sharp, J. 2001. The microstructure and mechanical properties of blended cements hydrated at various temperatures. *Cement Concrete Res.*, **31**(5), 695-702.

Esteves, T., Rajamma, R., Soares, D., Silva, A., Ferreira, V., Labrincha, J. 2012. Use of biomass fly ash for mitigation of alkali-silica reaction of cement mortars. *Constr. Build. Mater.*, **26**(1), 687-693.

Ezziane, K., Bougara, A., Kadri, A., Khelafi, H., Kadri, E. 2007. Compressive strength of mortar containing natural pozzolan under various curing temperature. *Cement Concrete Comp.*, **29**(8), 587-593.

Fang, X., Jia, L. 2012. Experimental study on ash fusion characteristics of biomass. *Bioresource Technol.*, **104**, 769-774.

Fang, X., Jia, L., Yin, L. 2013. A weighted average global process model based on two-stage kinetic scheme for biomass combustion. *Biomass Bioenerg.*, **48**, 43-50.

Feng, Q., Yamamichi, H., Shoya, M., Sugita, S. 2004. Study on the pozzolanic properties of rice husk ash by hydrochloric acid pretreatment. *Cement Concrete Res.*, **34**(3), 521-526.

Foo, K., Hameed, B. 2009. Value-added utilization of oil palm ash: A superior recycling of the industrial agricultural waste. *J. Hazard. Mater.*, **172**(2), 523-531.

Fraay, A., Bijen, J., De Haan, Y. 1989. The reaction of fly ash in concrete a critical examination. *Cement Concrete Res.*, **19**(2), 235-246.

Frías, M., García, R., de la Villa, R.V., Villar, E. 2013. The effect of binary pozzolan mix on the mineralogical changes in the ternary activated paper sludge-fly ash-Ca $(OH)_2$ system. *Constr. Build. Mater.*, **38**, 48-53.

Frías, M., Sánchez de Rojas, M.I., Cabrera, J. 2000. The effect that the pozzolanic reaction of metakaolin has on the heat evolution in metakaolin-cement mortars. *Cement Concrete Res.*, **30**(2), 209-216.

Frías, M., Vigil de la Villa, R., García, R., de Soto, I., Medina, C., Sánchez de Rojas, M. 2014. Scientific and technical aspects of blended cement matrices containing activated slate wastes. *Cement Concrete Comp.*, **48**, 19-25.

Frías, M., Villar-Cocina, E., Sánchez de Rojas, M.I., Valencia-Morales, E. 2005. The effect that different pozzolanic activity methods has on the kinetic constants of the pozzolanic reaction in sugar cane straw-clay ash/lime systems: Application of a kinetic-diffusive model. *Cement Concrete Res.*, **35**(11), 2137-2142.

Frias, M., Villar-Cociña, E., Valencia-Morales, E. 2007. Characterisation of sugar cane straw waste as pozzolanic material for construction: Calcining temperature and kinetic parameters. *Waste Management*, **27**(4), 533-538.

Frías, M., Villar-Cociña, E., Valencia-Morales, E. 2007. Characterisation of sugar cane straw waste as pozzolanic material for construction: Calcining temperature and kinetic parameters. *Waste Manage.*, **27**(4), 533-538.

Ganesan, K., Rajagopal, K., Thangavel, K. 2008. Rice husk ash blended cement: assessment of optimal level of replacement for strength and permeability properties of concrete. *Constr. Build. Mater.*, **22**(8), 1675-1683.

Gao, X., Kawashima, S., Liu, X., Shah, S.P. 2012. Influence of clays on the shrinkage and cracking tendency of SCC. *Cement Concrete Comp.*, **34**(4), 478-485.

García, R., Vigil de la Villa, R., Vegas, I., Frías, M., Sánchez de Rojas, M.I. 2008. The pozzolanic properties of paper sludge waste. *Constr. Build. Mater.*, **22**(7), 1484-1490.

Gastaldini, A., Isaia, G., Gomes, N., Sperb, J. 2007. Chloride penetration and carbonation in concrete with rice husk ash and chemical activators. *Cement Concrete Comp.*, **29**(3), 176-180.

Gastaldini, A., Isaia, G., Hoppe, T., Missau, F., Saciloto, A. 2009. Influence of the use of rice husk ash on the electrical resistivity of concrete: a technical and economic feasibility study. *Constr. Build. Mater.*, **23**(11), 3411-3419.

Gil, M., Casal, D., Pevida, C., Pis, J., Rubiera, F. 2010. Thermal behaviour and kinetics of coal/biomass blends during co-combustion. *Bioresource Technol.*, **101**(14), 5601-5608.

Givi, A.N., Rashid, S.A., Aziz, F.N.A., Salleh, M.A.M. 2010a. Assessment of the effects of rice husk ash particle size on strength, water permeability and workability of binary blended concrete. *Constr. Build. Mater.*, **24**(11), 2145-2150.

Givi, A.N., Rashid, S.A., Aziz, F.N.A., Salleh, M.A.M. 2010b. Contribution of rice husk ash to the properties of mortar and concrete: a review. *Journal of American science*, **6**(3), 157-165.

Goñi, S., Frias, M., Vegas, I., García, R. 2014. Sodium sulphate effect on the mineralogy of ternary blended cements elaborated with activated paper sludge and fly ash. *Constr. Build. Mater.*, **54**, 313-319.

Goni, S., Guerrero, A., Luxán, M., Macías, A. 2003. Activation of the fly ash pozzolanic reaction by hydrothermal conditions. *Cement Concrete Res.*, **33**(9), 1399-1405.

Grist, E.R., Paine, K.A., Heath, A., Norman, J., Pinder, H. 2013. Compressive strength development of binary and ternary lime-pozzolan mortars. *Mater. Design*, **52**, 514-523.

Guretzky, J.A., Biermacher, J.T., Cook, B.J., Kering, M.K., Mosali, J. 2011. Switchgrass for forage and bioenergy: harvest and nitrogen rate effects on biomass yields and nutrient composition. *Plant and soil*, **339**(1-2), 69-81.

Guru Jawahar, J., Sashidhar, C., Ramana Reddy, I., Annie Peter, J. 2013. Micro and macrolevel properties of fly ash blended self compacting concrete. *Mater. Design*, **46**, 696-705.

Hamzeh, Y., Ziabari, K.P., Torkaman, J., Ashori, A., Jafari, M. 2013. Study on the effects of white rice husk ash and fibrous materials additions on some properties of fiber-cement composites. *J. Environ. Manage.*, **117**, 263-267.

Hanehara, S., Tomosawa, F., Kobayakawa, M., Hwang, K. 2001. Effects of water/powder ratio, mixing ratio of fly ash, and curing temperature on pozzolanic reaction of fly ash in cement paste. *Cement Concrete Res.*, **31**(1), 31-39.

Hasan, Aköz, F., Berktay, I.l., Tulgar, A.N. 1999. Study of pozzolanic properties of wheat straw ash. *Cement Concrete Res.*, **29**(5), 637-643.

Hassan, A.A., Abouhussien, A.A., Mayo, J. 2014. The use of silica-breccia as a supplementary cementing material in mortar and concrete. *Constr. Build. Mater.*, **51**, 321-328.

Havlica, J., Brandstetr, J., Odler, I. 1998. Possibilities of utilizing solid residues from pressured fluidized bed coal combustion (PSBC) for the production of blended cements. *Cement Concrete Res.*, **28**(2), 299-307.

Haykırı-Açma, H. 2003. Combustion characteristics of different biomass materials. *Energy Convers. Manage.*, **44**(1), 155-162.

Hecht-Nielsen, R. 1989. Theory of the backpropagation neural network. *Neural Networks, 1989. IJCNN., International Joint Conference*. IEEE. pp. 593-605.

Heede, P.V.d., Maes, M., Gruyaert, E., Belie, N.D. 2012. Full probabilistic service life prediction and life cycle assessment of concrete with fly ash and blast-furnace slag in a submerged marine environment: a parameter study. *International Journal of Environment and Sustainable Development*, **11**(1), 32-49.

Hew, K., Tamidi, A., Yusup, S., Lee, K., Ahmad, M. 2010. Catalytic cracking of bio-oil to organic liquid product (OLP). *Bioresource Technol.*, **101**(22), 8855-8858.

Hoagland, K.C., Ruark, M.D., Renz, M.J., Jackson, R.D. 2013. Agricultural management of switchgrass for fuel quality and thermal energy yield on highly erodible land in the driftless area of Southwest Wisconsin. *BioEnergy Research*, **6**(3), 1012-1021.

Horpibulsuk, S., Rachan, R., Suddeepong, A. 2011. Assessment of strength development in blended cement admixed Bangkok clay. *Constr. Build. Mater.*, **25**(4), 1521-1531.

Horsakulthai, V., Phiuvanna, S., Kaenbud, W. 2011. Investigation on the corrosion resistance of bagasse-rice husk-wood ash blended cement concrete by impressed voltage. *Constr. Build. Mater.*, **25**(1), 54-60.

Hossain, K.M.A. 2005. Volcanic ash and pumice as cement additives: pozzolanic, alkali-silica reaction and autoclave expansion characteristics. *Cement Concrete Res.*, **35**(6), 1141-1144.

Hossain, K.M.A., Lachemi, M. 2007. Strength, durability and micro-structural aspects of high performance volcanic ash concrete. *Cement Concrete Res.*, **37**(5), 759-766.

Hou, P.-k., Kawashima, S., Wang, K.-j., Corr, D.J., Qian, J.-s., Shah, S.P. 2013. Effects of colloidal nanosilica on rheological and mechanical properties of fly ash–cement mortar. *Cement Concrete Comp.*, **35**(1), 12-22.

Huntzinger, D.N., Eatmon, T.D. 2009. A life-cycle assessment of Portland cement manufacturing: comparing the traditional process with alternative technologies. *J. Clean. Prod.*, **17**(7), 668-675.

Idorn, G.M. 1997. *Concrete progress: from antiquity to third millenium*. Thomas Telford.

Isaia, G.C., GASTALDInI, A.L.G., Moraes, R. 2003. Physical and pozzolanic action of mineral additions on the mechanical strength of high-performance concrete. *Cement Concrete Comp.*, **25**(1), 69-76.

Işıkdağ, B., Topçu, İ.B. 2013. The effect of ground granulated blast-furnace slag on properties of Horasan mortar. *Constr. Build. Mater.*, **40**, 448-454.

Jain, A.K., Mao, J., Mohiuddin, K. 1996. Artificial neural networks: A tutorial. *Computer*, **29**(3), 31-44.

Jauberthie, R., Rendell, F., Tamba, S., Cisse, I. 2000. Origin of the pozzolanic effect of rice husks. *Constr. Build. Mater.*, **14**(8), 419-423.

Jauberthie, R., Rendell, F., Tamba, S., Cissé, I.K. 2003. Properties of cement-rice husk mixture. *Constr. Build. Mater.*, **17**(4), 239-243.

Jenkins, B., Baxter, L., Miles Jr, T., Miles, T. 1998. Combustion properties of biomass. *Fuel Process. Technol.*, **54**(1), 17-46.

Johari, M., Zeyad, A., Muhamad Bunnori, N., Ariffin, K. 2012. Engineering and transport properties of high-strength green concrete containing high volume of ultrafine palm oil fuel ash. *Constr. Build. Mater.*, **30**, 281-288.

Jolicoeur, C., Simard, M.-A. 1998. Chemical admixture-cement interactions: phenomenology and physico-chemical concepts. *Cement Concrete Comp.*, **20**(2), 87-101.

Kandasamy, S., Shehata, M.H. 2014. The capacity of ternary blends containing slag and high-calcium fly ash to mitigate alkali silica reaction. *Cement Concrete Comp.*, **49**, 92-99.

Kanning, R.C., Portella, K.F., Bragança, M.O., Bonato, M.M., dos Santos, J. 2014. Banana leaves ashes as pozzolan for concrete and mortar of Portland cement. *Constr. Build. Mater.*, **54**, 460-465.

Karakurt, C., Topçu, İ.B. 2012. Effect of blended cements with natural zeolite and industrial by-products on rebar corrosion and high temperature resistance of concrete. *Constr. Build. Mater.*, **35**, 906-911.

Kim, S.-S., Hooton, R.D., Cho, T.-J., Lee, J.-B. 2014. Comparison of innovative nano fly ash with conventional fly ash and nano-silica. *Can. J. Civil Eng.*, **41**(5), 396-402.

Kok, M.V. 2012. Simultaneous thermogravimetry-calorimetry study on the combustion of coal samples: effect of heating rate. *Energy Convers. Manage.*, **53**(1), 40-44.

Kula, I., Olgun, A., Sevinc, V., Erdogan, Y. 2002. An investigation on the use of tincal ore waste, fly ash, and coal bottom ash as Portland cement replacement materials. *Cement Concrete Res.*, **32**(2), 227-232.

Kumar, A., Sokhansanj, S. 2007. Switchgrass (*Panicum vigratum, L.*) delivery to a biorefinery using integrated biomass supply analysis and logistics (IBSAL) model. *Bioresource Technol.*, **98**(5), 1033-1044.

Kumar, M., Singh, N., Singh, S.K., Singh, N. 2012. Tertiary biocomposite cement and its hydration. *Constr. Build. Mater.*, **29**, 1-6.

Kuprianov, V.I., Arromdee, P. 2013. Combustion of peanut and tamarind shells in a conical fluidized-bed combustor: A comparative study. *Bioresource Technol.*, **140**, 199-210.

Kurama, H., Kaya, M. 2008. Usage of coal combustion bottom ash in concrete mixture. *Constr. Build. Mater.*, **22**(9), 1922-1928.

Lam, L., Wong, Y., Poon, C. 2000. Degree of hydration and gel/space ratio of high-volume fly ash/cement systems. *Cement Concrete Res.*, **30**(5), 747-756.

Li, X.-g., Chen, Q.-b., Huang, K.-z., Ma, B.-g., Wu, B. 2012. Cementitious properties and hydration mechanism of circulating fluidized bed combustion (CFBC) desulfurization ashes. *Constr. Build. Mater.*, **36**, 182-187.

Lilkov, V., Rostovsky, I., Petrov, O., Tzvetanova, Y., Savov, P. 2014. Long term study of hardened cement pastes containing silica fume and fly ash. *Constr. Build. Mater.*, **60**, 48-56.

Lim, W.-Y., Seow, A. 2012. Biomass fuels and lung cancer. *Respirology*, **17**(1), 20-31.

Lin, K.-L., Lin, D.-F., Wang, W.-J., Chang, C.-C., Lee, T.-C. 2014a. Pozzolanic reaction of a mortar made with cement and slag vitrified from a MSWI ash-mix and LED sludge. *Constr. Build. Mater.*, **64**, 277-287.

Lin, K.L., Hwang, C.L., Shie, J.L., Chang, Y.M., Cheng, A. 2014b. Hydration characteristics of waste catalysts used as pozzolanic materials. *Environ. Prog. Sustain. Energy*, **33**(2), 353-358.

Lind, T., Vaimari, T., Kauppinen, E., Nilsson, K., Sfiris, G., Maenhaut, W. 2000. Ash formation mechanisms during combustion of wood in circulating fluidized beds. *Proc. Combust. Inst.*, **28**(2), 2287-2295.

Liu, S., Kong, Y., Wang, L. 2014. A comparison of hydration properties of cement-low quality fly ash binder and cement–limestone powder binder. *J. Therm. Anal. Calorim.*, **116**(2), 937-943.

Lorenzo, M., Goni, S., Guerrero, A. 2003. Role of aluminous component of fly ash on the durability of Portland cement-fly ash pastes in marine environment. *Waste Manage.*, **23**(8), 785-792.

Luxán, M.d., Madruga, F., Saavedra, J. 1989. Rapid evaluation of pozzolanic activity of natural products by conductivity measurement. *Cement Concrete Res.*, **19**(1), 63-68.

Mabee, W.E., Fraser, E.D., McFarlane, P.N., Saddler, J.N. 2006. Canadian biomass reserves for biorefining. *Applied biochemistry and biotechnology*, **129**(1-3), 22-40.

Madani Hosseini, M., Shao, Y., Whalen, J.K. 2011. Biocement production from silicon-rich plant residues: perspectives and future potential in Canada. *Biosyst. Eng.*, **110**(4), 351-362.

Maltais, Y., Marchand, J. 1997. Influence of curing temperature on cement hydration and mechanical strength development of fly ash mortars. *Cement Concrete Res.*, **27**(7), 1009-1020.

Marsh, B.K., Day, R.L. 1988. Pozzolanic and cementitious reactions of fly ash in blended cement pastes. *Cement Concrete Res.*, **18**(2), 301-310.

McCusker, L., Von Dreele, R., Cox, D., Louer, D., Scardi, P. 1999. Rietveld refinement guidelines. *J. Appl. Crystallogr.*, **32**(1), 36-50.

McKendry, P. 2002. Energy production from biomass (Part 1): overview of biomass. *Bioresource Technol.*, **83**(1), 37-46.

McLennan, A., Bryant, G., Stanmore, B., Wall, T. 2000. Ash formation mechanisms during pf combustion in reducing conditions. *Energy Fuels*, **14**(1), 150-159.

Medina, C., Banfill, P., Sánchez de Rojas, M., Frías, M. 2013. Rheological and calorimetric behaviour of cements blended with containing ceramic sanitary ware and construction/demolition waste. *Constr. Build. Mater.*, **40**, 822-831.

Mehta, P.K. 1983. Pozzolanic and cementitious byproducts as mineral admixtures for concrete-a critical review. *ACI Special Publication*, **79**.

Montakarntiwong, K., Chusilp, N., Tangchirapat, W., Jaturapitakkul, C. 2013. Strength and heat evolution of concretes containing bagasse ash from thermal power plants in sugar industry. *Mater. Design*, **49**, 414-420.

Monti, A., Di Virgilio, N., Venturi, G. 2008. Mineral composition and ash content of six major energy crops. *Biomass Bioenerg.*, **32**(3), 216-223.

Morozov, Y., Castela, A., Dias, A., Montemor, M. 2013. Chloride-induced corrosion behavior of reinforcing steel in spent fluid cracking catalyst modified mortars. *Cement Concrete Res.*, **47**, 1-7.

Nair, D.G., Fraaij, A., Klaassen, A.A., Kentgens, A.P. 2008. A structural investigation relating to the pozzolanic activity of rice husk ashes. *Cement Concrete Res.*, **38**(6), 861-869.

Narmluk, M., Nawa, T. 2014. Effect of curing temperature on pozzolanic reaction of fly ash in blended cement paste. *International Journal of Chemical Engineering and Applications*, **5**(1), 31-35.

Nassar, R.-U.-D., Soroushian, P., Ghebrab, T. 2013. Field investigation of high-volume fly ash pavement concrete. *Resourc. Conserv, Recy.*, **73**, 78-85.

Nehdi, M., Duquette, J., El Damatty, A. 2003. Performance of rice husk ash produced using a new technology as a mineral admixture in concrete. *Cement Concrete Res.*, **33**(8), 1203-1210.

Nussbaumer, T. 2003. Combustion and co-combustion of biomass: fundamentals, technologies, and primary measures for emission reduction. *Energy Fuels*, **17**(6), 1510-1521.

Ogden, C., Ileleji, K., Johnson, K., Wang, Q. 2010. In-field direct combustion fuel property changes of switchgrass harvested from summer to fall. *Fuel Process. Technol.*, **91**(3), 266-271.

Owaid, H.M., Hamid, R., Taha, M. 2014. Influence of thermally activated alum sludge ash on the engineering properties of multiple-blended binders concretes. *Constr. Build. Mater.*, **61**, 216-229.

Pala, M., Özbay, E., Öztaş, A., Yuce, M.I. 2007. Appraisal of long-term effects of fly ash and silica fume on compressive strength of concrete by neural networks. *Constr. Build. Mater.*, **21**(2), 384-394.

Pan, S.-C., Tseng, D.-H., Lee, C.-C., Lee, C. 2003. Influence of the fineness of sewage sludge ash on the mortar properties. *Cement Concrete Res.*, **33**(11), 1749-1754.

Pane, I., Hansen, W. 2005. Investigation of blended cement hydration by isothermal calorimetry and thermal analysis. *Cement Concrete Res.*, **35**(6), 1155-1164.

Panwar, N., Kaushik, S., Kothari, S. 2011. Role of renewable energy sources in environmental protection: a review. *Renew. Sust. energ. Rev.*, **15**(3), 1513-1524.

Papadakis, V., Antiohos, S., Tsimas, S. 2002. Supplementary cementing materials in concrete: Part II: A fundamental estimation of the efficiency factor. *Cement Concrete Res.*, **32**(10), 1533-1538.

Papadakis, V., Tsimas, S. 2002. Supplementary cementing materials in concrete: Part I: efficiency and design. *Cement Concrete Res.*, **32**(10), 1525-1532.

Papadakis, V.G. 1999. Effect of fly ash on Portland cement systems: Part I. Low-calcium fly ash. *Cement Concrete Res.*, **29**(11), 1727-1736.

Parichatprecha, R., Nimityongskul, P. 2009. Analysis of durability of high performance concrete using artificial neural networks. *Constr. Build. Mater.*, **23**(2), 910-917.

Paya, J., Borrachero, M., Monzo, J., Peris-Mora, E., Amahjour, F. 2001. Enhanced conductivity measurement techniques for evaluation of fly ash pozzolanic activity. *Cement Concrete Res.*, **31**(1), 41-49.

Payá, J., Monzó, J., Borrachero, M. 1999. Fluid catalytic cracking catalyst residue (FC3R): an excellent mineral by-product for improving early-strength development of cement mixtures. *Cement Concrete Res.*, **29**(11), 1773-1779.

Payá, J., Monzo, J., Borrachero, M., Peris-Mora, E., Amahjour, F. 2000. Mechanical treatment of fly ashes: Part IV. Strength development of ground fly ash-cement mortars cured at different temperatures. *Cement Concrete Res.*, **30**(4), 543-551.

Paya, J., Monzo, J., Borrachero, M., Peris, E., Gonzalez-Lopez, E. 1997. Mechanical treatments of fly ashes. Part III: Studies on strength development of ground fly ashes (GFA)-Cement mortars. *Cement Concrete Res.*, **27**(9), 1365-1377.

Payá, J., Monzó, J., Borrachero, M., Velázquez, S. 2013a. Cement equivalence factor evaluations for fluid catalytic cracking catalyst residue. *Cement Concrete Comp.*, **39**, 12-17.

Payá, J., Monzó, J., Borrachero, M., Velázquez, S. 2003. Evaluation of the pozzolanic activity of fluid catalytic cracking catalyst residue (FC3R). Thermogravimetric analysis studies on FC3R-Portland cement pastes. *Cement Concrete Res.*, **33**(4), 603-609.

Payá, J., Monzó, J.M., Borrachero, M.V., Velázquez, S. 2013b. Pozzolanic reaction rate of fluid catalytic cracking catalyst residue (FC3R) in cement pastes. *Adv. Cem. Res.*, **25**(2), 112-118.

Perraki, T., Kakali, G., Kontoleon, F. 2003. The effect of natural zeolites on the early hydration of Portland cement. *Micropor. Mesopor. Mat.*, **61**(1), 205-212.

Poon, C.-S., Azhar, S., Anson, M., Wong, Y.-L. 2001a. Comparison of the strength and durability performance of normal-and high-strength pozzolanic concretes at elevated temperatures. *Cement Concrete Res.*, **31**(9), 1291-1300.

Poon, C., Qiao, X., Lin, Z. 2003. Pozzolanic properties of reject fly ash in blended cement pastes. *Cement Concrete Res.*, **33**(11), 1857-1865.

Poon, C.S., Kou, S.C., Lam, L., Lin, Z.S. 2001b. Activation of fly ash/cement systems using calcium sulfate anhydrite ($CaSO_4$). *Cement Concrete Res.*, **31**(6), 873-881.

Pourkhorshidi, A., Najimi, M., Parhizkar, T., Jafarpour, F., Hillemeier, B. 2010. Applicability of the standard specifications of ASTM C618 for evaluation of natural pozzolans. *Cement Concrete Comp.*, **32**(10), 794-800.

Prasad, B., Eskandari, H., Reddy, B. 2009. Prediction of compressive strength of SCC and HPC with high volume fly ash using ANN. *Constr. Build. Mater.*, **23**(1), 117-128.

Qian, J., Liu, J., Wang, B., Wei, Y. 2014. Effect of curing conditions on the hydration and performance of CFBC ash cementitious system. *J. Wuhan Univ. Technol.*, **29**(1), 93-96.

Radwan, M., Farag, L., Abo-El-Enein, S., Abd El-Hamid, H. 2013. Alkali activation of blended cements containing oil shale ash. *Constr. Build. Mater.*, **40**, 367-377.

Rahman, F., Umesh, D., Subbarao, D., Ramasamy, M. 2010. Enhancement of entrainment rates in liquid–gas ejectors. *Chem. Eng. Process.*, **49**(10), 1128-1135.

Rajamma, R., Ball, R.J., Tarelho, L.A., Allen, G.C., Labrincha, J.A., Ferreira, V.M. 2009. Characterisation and use of biomass fly ash in cement-based materials. *J. Hazard. Mater.*, **172**(2), 1049-1060.

Ramadhansyah, P., Salwa, M., Mahyun, A., Abu Bakar, B., Megat Johari, M., Che Norazman, C. 2012. Properties of concrete containing rice husk ash under sodium chloride subjected to wetting and drying. *Procedia Engineering*, **50**, 305-313.

Rattanashotinunt, C., Thairit, P., Tangchirapat, W., Jaturapitakkul, C. 2013. Use of calcium carbide residue and bagasse ash mixtures as a new cementitious material in concrete. *Mater. Design*, **46**, 106-111.

Richardson, I. 1999. The nature of CSH in hardened cements. *Cement Concrete Res.*, **29**(8), 1131-1147.

Rodríguez de Sensale, G. 2006. Strength development of concrete with rice-husk ash. *Cement Concrete Comp.*, **28**(2), 158-160.

Rojas, M.F.a., Sánchez de Rojas, M.I. 2003. The effect of high curing temperature on the reaction kinetics in MK/lime and MK-blended cement matrices at 60 C. *Cement Concrete Res.*, **33**(5), 643-649.

Rong, Z., Sun, W., Xiao, H., Wang, W. 2014. Effect of silica fume and fly ash on hydration and microstructure evolution of cement based composites at low water–binder ratios. *Constr. Build. Mater.*, **51**, 446-450.

Rosell-Lam, M., Villar-Cocina, E., Frias, M. 2011. Study on the pozzolanic properties of a natural Cuban zeolitic rock by conductometric method: Kinetic parameters. *Constr. Build. Mater.*, **25**(2), 644-650.

Rubio, E., Rodríguez, V., Alcocer, S., Castaño, V. 2011. Rice husks as source for pozzolan nanomaterials. *Mater. Res. Innov.*, **15**(4), 268-270.

Rukzon, S., Chindaprasirt, P. 2012. Utilization of bagasse ash in high-strength concrete. *Mater. Design*, **34**, 45-50.

Rukzon, S., Chindaprasirt, P., Mahachai, R. 2009. Effect of grinding on chemical and physical properties of rice husk ash. *Int. J. Min. Met. Mater.*, **16**(2), 242-247.

Ryu, C., Yang, Y.B., Khor, A., Yates, N.E., Sharifi, V.N., Swithenbank, J. 2006. Effect of fuel properties on biomass combustion: Part I. Experiments-fuel type, equivalence ratio and particle size. *Fuel*, **85**(7), 1039-1046.

Sahin, Ö., Özdemir, M., Aslanoglu, M., Beker, Ü.G. 2001. Calcination kinetics of ammonium pentaborate using the Coats-Redfern and genetic algorithm method by thermal analysis. *Ind. Eng. Chem. Res.*, **40**(6), 1465-1470.

Said, A., Zeidan, M.S., Bassuoni, M., Tian, Y. 2012. Properties of concrete incorporating nano-silica. *Constr. Build. Mater.*, **36**, 838-844.

Sait, H.H., Hussain, A., Salema, A.A., Ani, F.N. 2012. Pyrolysis and combustion kinetics of date palm biomass using thermogravimetric analysis. *Bioresource Technol.*, **118**, 382-389.

Sánchez de Rojas, M.I., Frías, M., Rodríguez, O., Rivera, J. 2014. Durability of blended cement pastes containing ceramic waste as a pozzolanic addition. *J. Am. Ceram. Soc.*, **97**(5), 1543-1551.

Sarıdemir, M. 2009. Prediction of compressive strength of concretes containing metakaolin and silica fume by artificial neural networks. *Adv. Eng. Softw.*, **40**(5), 350-355.

Sata, V., Jaturapitakkul, C., Kiattikomol, K. 2007. Influence of pozzolan from various by-product materials on mechanical properties of high-strength concrete. *Constr. Build. Mater.*, **21**(7), 1589-1598.

Sata, V., Jaturapitakkul, C., Rattanashotinunt, C. 2010. Compressive strength and heat evolution of concretes containing palm oil fuel ash. *J. Mater. Civil Eng.*, **22**(10), 1033-1038.

Sata, V., Tangpagasit, J., Jaturapitakkul, C., Chindaprasirt, P. 2012. Effect of W/B ratios on pozzolanic reaction of biomass ashes in Portland cement matrix. *Cement Concrete Comp.*, **34**(1), 94-100.

Schneider, M., Romer, M., Tschudin, M., Bolio, H. 2011a. Sustainable cement production-present and future. *Cement Concrete Res.*, **41**(7), 642-650.

Schneider, M., Romer, M., Tschudin, M., Bolio, H. 2011b. Sustainable cement production—present and future. *Cement and Concrete Research*, **41**(7), 642-650.

Shao, Y., Lefort, T., Moras, S., Rodriguez, D. 2000. Studies on concrete containing ground waste glass. *Cement Concrete Res.*, **30**(1), 91-100.

Shayan, A., Xu, A. 2006. Performance of glass powder as a pozzolanic material in concrete: A field trial on concrete slabs. *Cement Concrete Res.*, **36**(3), 457-468.

Shehata, M.H., Thomas, M.D. 2000. The effect of fly ash composition on the expansion of concrete due to alkali–silica reaction. *Cement Concrete Res.*, **30**(7), 1063-1072.

Shi, C., Day, R.L. 1993. Acceleration of strength gain of lime-pozzolan cements by thermal activation. *Cement Concrete Res.*, **23**(4), 824-832.

Shi, C., Day, R.L. 2001. Comparison of different methods for enhancing reactivity of pozzolans. *Cement Concrete Res.*, **31**(5), 813-818.

Shi, C., Day, R.L. 2000a. Pozzolanic reaction in the presence of chemical activators: Part I. Reaction kinetics. *Cement Concrete Res.*, **30**(1), 51-58.

Shi, C., Day, R.L. 2000b. Pozzolanic reaction in the presence of chemical activators: Part II-Reaction products and mechanism. *Cement Concrete Res.*, **30**(4), 607-613.

Shi, C., Qian, J. 2001. Activated blended cement containing high volume coal fly ash. *Adv. Cem. Res.*, **13**(4), 157-163.

Shi, C., Wu, Y., Riefler, C., Wang, H. 2005. Characteristics and pozzolanic reactivity of glass powders. *Cement Concrete Res.*, **35**(5), 987-993.

Shi, H.-S., Kan, L.-L. 2009. Leaching behavior of heavy metals from municipal solid wastes incineration (MSWI) fly ash used in concrete. *J. Hazard. Mater.*, **164**(2), 750-754.

Siddique, R. 2004. Performance characteristics of high-volume Class F fly ash concrete. *Cement Concrete Res.*, **34**(3), 487-493.

Singh, N., Rai, S. 2001. Effect of polyvinyl alcohol on the hydration of cement with rice husk ash. *Cement Concrete Res.*, **31**(2), 239-243.

Sinsiri, T., Kroehong, W., Jaturapitakkul, C., Chindaprasirt, P. 2012. Assessing the effect of biomass ashes with different finenesses on the compressive strength of blended cement paste. *Mater. Design*, **42**, 424-433.

Smart, J.P., Patel, R., Riley, G.S. 2010. Oxy-fuel combustion of coal and biomass, the effect on radiative and convective heat transfer and burnout. *Combust. Flame*, **157**(12), 2230-2240.

Somna, R., Jaturapitakkul, C., Rattanachu, P., Chalee, W. 2012. Effect of ground bagasse ash on mechanical and durability properties of recycled aggregate concrete. *Mater. Design*, **36**, 597-603.

Supit, S.W., Shaikh, F.U., Sarker, P.K. 2014. Effect of ultrafine fly ash on mechanical properties of high volume fly ash mortar. *Constr. Build. Mater.*, **51**, 278-286.

Swaddiwudhipong, S., Wu, H., Zhang, M. 2003. Numerical simulation of temperature rise of highstrength concrete incorporating silica fume and superplasticiser. *Adv. Cem. Res.*, **15**(4), 161-169.

Tangchirapat, W., Khamklai, S., Jaturapitakkul, C. 2012. Use of ground palm oil fuel ash to improve strength, sulfate resistance, and water permeability of concrete containing high amount of recycled concrete aggregates. *Mater. Design*, **41**, 150-157.

Teixeira, P., Lopes, H., Gulyurtlu, I., Lapa, N., Abelha, P. 2012. Evaluation of slagging and fouling tendency during biomass co-firing with coal in a fluidized bed. *Biomass Bioenerg.*, **39**, 192-203.

Teixeira, P., Lopes, H., Gulyurtlu, I., Lapa, N., Abelha, P. 2013. Slagging and fouling during coal and biomass cofiring: chemical equilibrium model applied to FBC. *Energy Fuels*, **28**(1), 697-713.

Thomas, M. 2011. The effect of supplementary cementing materials on alkali-silica reaction: A review. *Cement Concrete Res.*, **41**(12), 1224-1231.

Tillman, D.A. 2000. Biomass cofiring: the technology, the experience, the combustion consequences. *Biomass and Bioenergy*, **19**(6), 365-384.

Tkaczewska, E. 2014. Effect of size fraction and glass structure of siliceous fly ashes on fly ash cement hydration. *J. Ind. Eng. Chem.*, **20**(1), 315-321.

Tkaczewska, E., Małolepszy, J. 2009. Hydration of coal–biomass fly ash cement. *Constr. Build. Mater.*, **23**(7), 2694-2700.

Tkaczewska, E., Mróz, R., Łój, G. 2012. Coal–biomass fly ashes for cement production of CEM II/AV 42.5 R. *Constr. Build. Mater.*, **28**(1), 633-639.

Topcu, I.B., Sarıdemir, M. 2008. Prediction of compressive strength of concrete containing fly ash using artificial neural networks and fuzzy logic. *Comp. Mater. Sci.*, **41**(3), 305-311.

Tortosa Masiá, A., Buhre, B., Gupta, R., Wall, T. 2007. Characterising ash of biomass and waste. *Fuel Process. Technol.*, **88**(11), 1071-1081.

Tsai, C.-J., Huang, R., Lin, W.-T., Wang, H.-N. 2014. Mechanical and cementitious characteristics of ground granulated blast furnace slag and basic oxygen furnace slag blended mortar. *Mater. Design*, **60**, 267-273.

Tydlitát, V., Zákoutský, J., Černý, R. 2014. Early-stage hydration heat development in blended cements containing natural zeolite studied by isothermal calorimetry. *Thermochim. Acta*, **582**, 53-58.

Ukrainczyk, N., Koenders, E.A., Breugel, K.v. 2013. Simulation of Pozzolan Blended cement hydration. *Proceedings of the First International Conference on Concrete Sustainability*. pp. 27-29.

Valipour, M., Yekkalar, M., Shekarchi, M., Panahi, S. 2014. Environmental assessment of green concrete containing natural zeolite on the global warming index in marine environments. *J. Clean. Prod.*, **65**, 418-423.

Vamvuka, D., Pitharoulis, M., Alevizos, G., Repouskou, E., Pentari, D. 2009. Ash effects during combustion of lignite/biomass blends in fluidized bed. *Renewable Energy*, **34**(12), 2662-2671.

Vamvuka, D., Topouzi, V., Sfakiotakis, S. 2010. Evaluation of production yield and thermal processing of switchgrass as a bio-energy crop for the Mediterranean region. *Fuel Process. Technol.*, **91**(9), 988-996.

Van Tuan, N., Ye, G., Van Breugel, K., Fraaij, A.L., Bui, D.D. 2011. The study of using rice husk ash to produce ultra high performance concrete. *Constr. Build. Mater.*, **25**(4), 2030-2035.

Van, V.-T.-A., Rößler, C., Bui, D.-D., Ludwig, H.-M. 2013. Mesoporous structure and pozzolanic reactivity of rice husk ash in cementitious system. *Constr. Build. Mater.*, **43**, 208-216.

Van, V.-T.-A., Rößler, C., Bui, D.-D., Ludwig, H.-M. 2014. Pozzolanic reactivity of mesoporous amorphous rice husk ash in portlandite solution. *Constr. Build. Mater.*, **59**, 111-119.

Várhegyi, G. 2007. Aims and methods in non-isothermal reaction kinetics. *J. Anal. Appl. Pyrolysis*, **79**(1), 278-288.

Varol, M., Atimtay, A.T., Olgun, H., Atakül, H. 2014. Emission characteristics of co-combustion of a low calorie and high sulfur–lignite coal and woodchips in a circulating fluidized bed combustor: Part 1. Effect of excess air ratio. *Fuel*, **117**, 792-800.

Vassilev, S.V., Vassileva, C.G. 2007. A new approach for the classification of coal fly ashes based on their origin, composition, properties, and behaviour. *Fuel*, **86**(10), 1490-1512.

Vasugi, V., Ramamurthy, K. 2014. Identification of design parameters influencing manufacture and properties of cold-bonded pond ash aggregate. *Mater. Design*, **54**, 264-278.

Vayghan, A.G., Khaloo, A., Nasiri, S., Rajabipour, F. 2011. Studies on the effect of retention time of rice husk combustion on the ash's chemo-physical properties and performance in cement mixtures. *J. Mater. Civil Eng.*, **24**(6), 691-697.

Villar-Cociña, E., Morales, E.V., Santos, S.F., Savastano Jr, H., Frías, M. 2011. Pozzolanic behavior of bamboo leaf ash: Characterization and determination of the kinetic parameters. *Cement Concrete Comp.*, **33**(1), 68-73.

Villar-Cociña, E., Valencia-Morales, E., Gonzalez-Rodrıguez, R., Hernandez-Ruız, J. 2003. Kinetics of the pozzolanic reaction between lime and sugar cane straw ash by electrical conductivity measurement: A kinetic–diffusive model. *Cement Concrete Res.*, **33**(4), 517-524.

Vyazovkin, S., Wight, C. 1997. Kinetics in solids. *Annu. Rev. Phys. Chem.*, **48**(1), 125-149.

Wang, S. 2014a. Compressive strengths of mortar cubes from hydrated lime with cofired biomass fly ashes. *Constr. Build. Mater.*, **50**, 414-420.

Wang, S. 2014b. Quantitative kinetics of pozzolanic reactions in coal/cofired biomass fly ashes and calcium hydroxide (CH) mortars. *Constr. Build. Mater.*, **51**, 364-371.

Wang, S., Baxter, L. 2007. Comprehensive study of biomass fly ash in concrete: Strength, microscopy, kinetics and durability. *Fuel Process. Technol.*, **88**(11), 1165-1170.

Wang, S., Baxter, L., Fonseca, F. 2008a. Biomass fly ash in concrete: SEM, EDX and ESEM analysis. *Fuel*, **87**(3), 372-379.

Wang, S., Miller, A., Llamazos, E., Fonseca, F., Baxter, L. 2008b. Biomass fly ash in concrete: mixture proportioning and mechanical properties. *Fuel*, **87**(3), 365-371.

Wang, X.-Y., Lee, H.-S., Park, K.-B. 2009a. Simulation of low-calcium fly ash blended cement hydration. *ACI Mater. J.*, **106**(2).

Wang, X., Lee, H., Shin, S.-W., Golden, J. 2010. Simulation of a temperature rise in concrete incorporating silica fume. *Mag. Concrete Res.*, **62**(9), 637-646.

Wang, Y., Shao, Y., Matovic, M.D., Whalen, J.K. 2014a. Recycling of switchgrass combustion ash in cement: Characteristics and pozzolanic activity with chemical accelerators. *Constr. Build. Mater.*, **73**, 472-478.

Wang, Y., Winans, K.S., Shao, Y., Whalen, J.K. 2014b. Life cycle assessment: applying biomass integrated gasification combined cycle in cement industry. in: *The Seventh International Conference on Environmental Science and Technology*. Houston, Texas, USA.

Wang, Z., Song, Y., Wang, Z. 2009b. Pozzolanic reaction kinetics of coal ashes. *J. Wuhan Univ. Technol.*, **24**(3), 488-493.

Wansom, S., Janjaturaphan, S., Sinthupinyo, S. 2010. Characterizing pozzolanic activity of rice husk ash by impedance spectroscopy. *Cement Concrete Res.*, **40**(12), 1714-1722.

Weiland, N.T., Means, N.C., Morreale, B.D. 2012. Product distributions from isothermal co-pyrolysis of coal and biomass. *Fuel*, **94**, 563-570.

White, J.E., Catallo, W.J., Legendre, B.L. 2011. Biomass pyrolysis kinetics: a comparative critical review with relevant agricultural residue case studies. *J. Anal. Appl. Pyrolysis*, **91**(1), 1-33.

Wilińska, I., Pacewska, B. 2014. Calorimetric and thermal analysis studies on the influence of waste aluminosilicate catalyst on the hydration of fly ash–cement paste. *J. Therm. Anal. Calorim.*, **116**(2), 689-697.

Williams, A., Jones, J., Ma, L., Pourkashanian, M. 2012. Pollutants from the combustion of solid biomass fuels. *Prog. Energ. Combust.*, **38**(2), 113-137.

Winburn, R.S., Grier, D.G., McCarthy, G.J., Peterson, R.B. 2000. Rietveld quantitative X-ray diffraction analysis of NIST fly ash standard reference materials. *Powder Diffr.*, **15**(03), 163-172.

Xiao, H., Ma, X., Liu, K. 2010. Co-combustion kinetics of sewage sludge with coal and coal gangue under different atmospheres. *Energy Convers. Manage.*, **51**(10), 1976-1980.

Xu, W., Lo, T.Y., Memon, S.A. 2012. Microstructure and reactivity of rich husk ash. *Constr. Build. Mater.*, **29**, 541-547.

Yajun, J., Cahyadi, J. 2004. Simulation of silica fume blended cement hydration. *Mater. Struct.*, **37**(6), 397-404.

Yang, Y.B., Ryu, C., Khor, A., Yates, N.E., Sharifi, V.N., Swithenbank, J. 2005. Effect of fuel properties on biomass combustion. Part II. Modelling approach-identification of the controlling factors. *Fuel*, **84**(16), 2116-2130.

Yilmaz, A., Degirmenci, N. 2009. Possibility of using waste tire rubber and fly ash with Portland cement as construction materials. *Waste Manage.*, **29**(5), 1541-1546.

Yin, C.-Y. 2011. Prediction of higher heating values of biomass from proximate and ultimate analyses. *Fuel*, **90**(3), 1128-1132.

Yusuf, M.O., Megat Johari, M.A., Ahmad, Z.A., Maslehuddin, M. 2014. Strength and microstructure of alkali-activated binary blended binder containing palm oil fuel ash and ground blast-furnace slag. *Constr. Build. Mater.*, **52**, 504-510.

Yuzbasi, N.S., Selçuk, N. 2011. Air and oxy-fuel combustion characteristics of biomass/lignite blends in TGA-FTIR. *Fuel Process. Technol.*, **92**(5), 1101-1108.

Zain, M., Islam, M., Mahmud, F., Jamil, M. 2011. Production of rice husk ash for use in concrete as a supplementary cementitious material. *Constr. Build. Mater.*, **25**(2), 798-805.

Zhang, G., Eddy Patuwo, B., Y Hu, M. 1998. Forecasting with artificial neural networks: The state of the art. *Inter. J. Forecasting*, **14**(1), 35-62.

Zhang, Y.M., Sun, W., Yan, H.D. 2000. Hydration of high-volume fly ash cement pastes. *Cement Concrete Comp.*, **22**(6), 445-452.

Zhou, S., Zhang, X.a., Chen, X. 2012. Pozzolanic activity of feedlot biomass (cattle manure) ash. *Constr. Build. Mater.*, **28**(1), 493-498.

Zornoza, E., Garcés, P., Monzó, J., Borrachero, M., Payá, J. 2007. Compatibility of fluid catalytic cracking catalyst residue (FC3R) with various types of cement. *Adv. Cem. Res.*, **19**(3), 117-124.

The database created and used for the artificial neural network (ANN) predictive model in Chapter 5
W/B: water-binder ratio, by mass; P/C: pozzolan-cement percentage, by mass; S/C: superplasticizer-cement percentage, by mass.

Chemical composition of pozzolanic solid wastes (w.t. %)									Mean particle size	Median particle size	Specific gravity	BET surface area	W/B	P/C	S/C	Compressive strength (MPa)			
SiO_2	CaO	Al_2O_3	Fe_2O_3	MgO	K_2O	Na_2O	SO_3	LOI	μm	μm	1	m^2/g	1	%	%	3 d	7 d	28 d	90 d
0.00	0.00	0.00	0.00	0.00	0.00	0.00	0.00	0.00	0.00	0.00	0.00	0.00	0.40	0	—	30.50	46.52	49.83	—
91.71	0.86	0.36	0.90	0.31	1.67	0.12	0.00	3.13	0.15	—	—	—	0.40	10	—	37.54	53.36	59.87	—
0.00	0.00	0.00	0.00	0.00	0.00	0.00	0.00	0.00	0.00	0.00	0.00	0.00	0.71	0	—	—	—	26.10	28.20
41.10	15.30	22.50	11.60	2.80	2.90	1.70	1.50	0.20	—	27.10	2.19	—	0.70	20	—	—	—	26.30	28.70
41.10	15.30	22.50	11.60	2.80	2.90	1.70	1.50	0.20	—	27.10	2.19	—	0.65	40	—	—	—	20.90	24.40
57.80	6.60	4.60	3.30	4.20	8.30	0.50	0.30	10.10	—	8.00	2.43	—	0.73	20	—	—	—	23.90	29.40
57.80	6.60	4.60	3.30	4.20	8.30	0.50	0.30	10.10	—	8.00	2.43	—	0.74	40	—	—	—	20.70	23.70
57.80	6.60	4.60	3.30	4.20	8.30	0.50	0.30	10.10	—	8.00	2.43	—	0.75	55	—	—	—	18.10	22.30
74.80	5.90	0.20	0.80	0.80	2.00	0.20	0.50	11.20	—	10.20	2.15	—	0.71	20	—	—	—	27.50	29.30
74.80	5.90	0.20	0.80	0.80	2.00	0.20	0.50	11.20	—	10.20	2.15	—	0.76	40	—	—	—	22.70	25.60
74.80	5.90	0.20	0.80	0.80	2.00	0.20	0.50	11.20	—	10.20	2.15	—	0.80	55	—	—	—	20.00	24.10
0.00	0.00	0.00	0.00	0.00	0.00	0.00	0.00	0.00	0.00	0.00	0.00	0.00	0.32	0	0.40	—	48.40	55.50	60.60
87.20	0.55	0.15	0.16	0.35	3.60	1.12	0.32	6.55	—	—	2.06	—	0.32	10	0.20	—	51.10	60.40	64.30
87.20	0.55	0.15	0.16	0.35	3.60	1.12	0.32	6.55	—	—	2.06	—	0.32	20	0.20	—	44.30	54.80	62.70
88.00	0.80	0.00	0.10	0.20	2.20	0.70	0.00	8.10	—	—	2.16	—	0.32	10	0.70	—	39.50	51.40	64.50
88.00	0.80	0.00	0.10	0.20	2.20	0.70	0.00	8.10	—	—	2.16	—	0.32	20	0.80	—	30.50	47.40	68.50
0.00	0.00	0.00	0.00	0.00	0.00	0.00	0.00	0.00	0.00	0.00	0.00	0.00	0.40	0	0.10	—	35.80	42.30	45.60
87.20	0.55	0.15	0.16	0.35	3.60	1.12	0.32	6.55	—	—	2.06	—	0.40	10	0.20	—	41.10	50.40	54.90
87.20	0.55	0.15	0.16	0.35	3.60	1.12	0.32	6.55	—	—	2.06	—	0.40	20	0.40	—	27.90	40.70	51.40
88.00	0.80	0.00	0.10	0.20	2.20	0.70	0.00	8.10	—	—	2.16	—	0.40	10	0.27	—	29.80	40.80	51.50
88.00	0.80	0.00	0.10	0.20	2.20	0.70	0.00	8.10	—	—	2.16	—	0.40	20	0.50	—	23.60	39.40	57.30
0.00	0.00	0.00	0.00	0.00	0.00	0.00	0.00	0.00	0.00	0.00	0.00	0.00	0.50	0	—	—	24.60	32.90	35.90

87.20	0.55	0.15	0.16	0.35	3.60	1.12	0.32	6.55	—	—	2.06	—	0.50	10	—	—	24.10	31.50	35.50
87.20	0.55	0.15	0.16	0.35	3.60	1.12	0.32	6.55	—	—	2.06	—	0.50	20	—	—	24.90	34.90	37.90
88.00	0.80	0.00	0.10	0.20	2.20	0.70	0.00	8.10	—	—	2.16	—	0.50	10	0.30	—	22.70	34.50	44.40
88.00	0.80	0.00	0.10	0.20	2.20	0.70	0.00	8.10	—	—	2.16	—	0.50	20	0.40	—	20.80	35.90	52.90
0.00	0.00	0.00	0.00	0.00	0.00	0.00	0.00	0.00	0.00	0.00	0.00	0.00	0.50	0	1.90	—	43.50	57.00	60.00
93.20	1.10	0.40	0.10	0.10	1.30	0.10	0.90	3.70	—	4.90	2.45	—	0.50	10	0.60	—	45.00	59.20	62.70
41.10	14.40	21.60	11.30	3.30	2.60	1.10	2.20	2.50	—	10.00	2.23	—	0.50	10	2.00	—	44.20	58.20	62.00
93.20	1.10	0.40	0.10	0.10	1.30	0.10	0.90	3.70	—	4.90	2.45	—	0.50	20	0.40	—	44.50	59.50	63.50
41.10	14.40	21.60	11.30	3.30	2.60	1.10	2.20	2.50	—	10.00	2.23	—	0.50	20	2.20	—	44.50	58.50	62.50
93.20	1.10	0.40	0.10	0.10	1.30	0.10	0.90	3.70	—	4.90	2.45	—	0.50	40	0.10	—	33.00	56.50	62.00
41.10	14.40	21.60	11.30	3.30	2.60	1.10	2.20	2.50	—	10.00	2.23	—	0.50	40	3.70	—	33.50	55.00	62.00
0.00	0.00	0.00	0.00	0.00	0.00	0.00	0.00	0.00	0.00	0.00	0.00	0.00	0.45	0	—	—	—	45.81	—
87.14	1.21	0.04	0.23	0.30	1.60	0.06	0.00	9.02	—	—	—	—	0.45	5	—	—	—	50.88	—
87.14	1.21	0.04	0.23	0.30	1.60	0.06	0.00	9.02	—	—	—	—	0.45	10	—	—	—	54.41	—
87.14	1.21	0.04	0.23	0.30	1.60	0.06	0.00	9.02	—	—	—	—	0.45	15	—	—	—	58.27	—
94.41	1.01	0.03	0.25	0.37	1.69	0.07	0.00	1.72	—	—	—	—	0.45	5	—	—	—	51.40	—
94.41	1.01	0.03	0.25	0.37	1.69	0.07	0.00	1.72	—	—	—	—	0.45	10	—	—	—	55.17	—
94.41	1.01	0.03	0.25	0.37	1.69	0.07	0.00	1.72	—	—	—	—	0.45	15	—	—	—	59.31	—
94.91	0.98	0.05	0.25	0.44	1.61	0.07	0.00	1.28	—	—	—	—	0.45	5	—	—	—	56.25	—
94.91	0.98	0.05	0.25	0.44	1.61	0.07	0.00	1.28	—	—	—	—	0.45	10	—	—	—	62.21	—
94.91	0.98	0.05	0.25	0.44	1.61	0.07	0.00	1.28	—	—	—	—	0.45	15	—	—	—	65.53	—
95.22	1.16	0.09	0.19	0.39	1.73	0.06	0.00	0.80	—	—	—	—	0.45	5	—	—	—	49.88	—
95.22	1.16	0.09	0.19	0.39	1.73	0.06	0.00	0.80	—	—	—	—	0.45	10	—	—	—	52.80	—
95.22	1.16	0.09	0.19	0.39	1.73	0.06	0.00	0.80	—	—	—	—	0.45	15	—	—	—	56.91	—
95.10	1.17	0.05	0.11	0.41	1.66	0.05	0.00	0.92	—	—	—	—	0.45	5	—	—	—	46.82	—
95.10	1.17	0.05	0.11	0.41	1.66	0.05	0.00	0.92	—	—	—	—	0.45	10	—	—	—	48.65	—
95.10	1.17	0.05	0.11	0.41	1.66	0.05	0.00	0.92	—	—	—	—	0.45	15	—	—	—	55.42	—
0.00	0.00	0.00	0.00	0.00	0.00	0.00	0.00	0.00	0.00	0.00	0.00	0.00	0.50	0	—	21.90	32.40	39.30	44.00

96.00	0.20	0.10	0.20	0.10	0.16	0.03	0.00	0.00	—	7.20	2.12	—	0.50	10	—	26.60	44.30	52.30	55.70
92.40	0.70	0.30	0.40	0.30	2.54	0.07	0.00	0.00	—	7.40	2.10	—	0.50	10	—	28.70	48.40	56.30	62.40
0.00	0.00	0.00	0.00	0.00	0.00	0.00	0.00	0.00	0.00	0.00	0.00	0.00	0.50	0	—	—	49.50	59.80	62.80
34.20	20.60	12.60	4.70	1.90	1.70	1.00	2.80	5.50	19.00	—	—	—	0.50	3	—	—	46.80	58.20	68.50
22.50	30.60	11.50	1.30	2.70	0.80	2.50	12.00	12.00	195.00	—	—	—	0.50	3	—	—	47.40	63.80	67.30
0.00	0.00	0.00	0.00	0.00	0.00	0.00	0.00	0.00	—	—	2.40	—	0.50	0	—	18.36	27.81	29.82	38.10
37.26	24.18	19.62	6.07	5.37	0.43	1.50	1.83	0.70	—	—	2.40	—	0.50	25	—	15.81	24.20	30.99	38.21
54.91	1.11	27.79	7.54	0.84	2.40	0.19	0.38	1.72	—	—	2.40	—	0.50	25	—	12.10	18.25	28.02	36.62
52.16	2.37	23.55	7.57	1.31	4.01	0.70	2.25	3.85	—	—	2.40	—	0.50	25	—	14.10	19.95	32.37	36.93
53.02	1.88	25.78	7.95	0.91	2.14	0.26	1.23	3.06	—	—	2.40	—	0.50	25	—	14.20	19.85	25.79	40.33
48.94	13.55	12.47	5.45	3.16	3.37	1.68	1.30	7.89	—	—	2.40	—	0.50	25	—	13.47	18.57	24.52	27.70
0.00	0.00	0.00	0.00	0.00	0.00	0.00	0.00	0.00	0.00	0.00	0.00	0.00	0.55	0	—	—	—	41.48	—
41.00	11.40	9.30	2.60	2.30	3.90	0.90	0.00	0.00	—	—	—	40.29	0.55	10	—	—	—	43.31	—
41.00	11.40	9.30	2.60	2.30	3.90	0.90	0.00	0.00	—	—	—	40.29	0.60	20	—	—	—	32.53	—
41.00	11.40	9.30	2.60	2.30	3.90	0.90	0.00	0.00	—	—	—	40.29	0.65	30	—	—	—	22.59	—
28.00	25.40	6.20	2.20	5.00	3.20	3.30	0.00	0.00	—	—	—	7.92	0.55	10	—	—	—	35.76	—
28.00	25.40	6.20	2.20	5.00	3.20	3.30	0.00	0.00	—	—	—	7.92	0.55	20	—	—	—	30.13	—
28.00	25.40	6.20	2.20	5.00	3.20	3.30	0.00	0.00	—	—	—	7.92	0.60	30	—	—	—	26.72	—
0.00	0.00	0.00	0.00	0.00	0.00	0.00	0.00	0.00	0.00	0.00	0.00	0.00	—	0	—	100.00	100.00	100.00	—
91.39	4.12	1.22	0.34	0.64	1.16	0.00	0.00	11.10	9.24	—	—	—	—	10	—	131.38	125.01	127.08	—
93.14	2.94	0.68	0.30	0.61	1.24	0.00	0.00	9.37	11.01	—	—	—	—	10	—	125.91	127.15	131.08	—
93.59	2.28	0.89	0.31	0.61	1.30	0.00	0.00	10.70	9.69	—	—	—	—	10	—	115.89	115.08	118.92	—
93.02	3.04	0.69	0.28	0.69	1.22	0.00	0.00	4.06	9.92	—	—	—	—	10	—	125.08	121.96	125.98	—
92.12	3.94	0.78	0.28	0.69	1.14	0.00	0.00	2.39	10.05	—	—	—	—	10	—	121.19	120.20	128.96	—
93.22	2.81	0.70	0.27	0.65	1.16	0.19	0.00	1.15	8.83	—	—	—	—	10	—	114.97	112.96	120.14	—
0.00	0.00	0.00	0.00	0.00	0.00	0.00	0.00	0.00	0.00	0.00	0.00	0.00	0.35	0	—	—	58.30	64.20	76.10
0.00	0.00	0.00	0.00	0.00	0.00	0.00	0.00	0.00	0.00	0.00	0.00	0.00	0.50	0	—	—	36.40	47.70	53.50
0.00	0.00	0.00	0.00	0.00	0.00	0.00	0.00	0.00	0.00	0.00	0.00	0.00	0.65	0	—	—	24.60	28.00	31.90

96.26	0.76	0.41	0.22	0.50	1.44	0.03	0.04	4.49	—	—	2.11	40.00	0.35	20	—	—	54.20	69.70	83.40
96.26	0.76	0.41	0.22	0.50	1.44	0.03	0.04	4.49	—	—	2.11	40.00	0.50	20	—	—	36.40	48.10	53.90
96.26	0.76	0.41	0.22	0.50	1.44	0.03	0.04	4.49	—	—	2.11	40.00	0.65	20	—	—	17.70	27.00	33.60
0.00	0.00	0.00	0.00	0.00	0.00	0.00	0.00	0.00	0.00	0.00	0.00	0.00	0.50	0	—	27.70	—	50.10	53.30
45.20	5.60	23.00	8.20	2.20	3.00	3.40	1.10	8.30	—	—	—	—	0.50	25	—	22.20	—	43.70	57.30
48.00	4.90	23.30	7.50	3.20	2.70	3.30	0.80	6.60	—	—	—	—	0.50	25	—	21.70	—	42.70	54.70
25.50	20.00	7.40	1.60	0.70	2.60	2.70	1.00	4.30	—	—	—	—	0.50	25	—	21.30	—	46.50	54.80
46.90	54.00	26.00	6.60	2.00	2.60	2.70	1.10	6.10	—	—	—	—	0.50	25	—	23.20	—	44.10	64.80
44.80	5.00	24.90	7.60	2.40	2.90	3.20	1.20	8.20	—	—	—	—	0.50	25	—	24.90	—	52.80	65.50
46.40	5.80	25.20	8.10	3.20	2.80	3.20	1.40	5.00	—	—	—	—	0.50	25	—	23.80	—	47.40	63.60
50.70	5.20	24.30	8.70	2.70	2.20	3.43	0.70	2.20	—	—	—	—	0.50	25	—	19.80	—	36.20	48.80
0.00	0.00	0.00	0.00	0.00	0.00	0.00	0.00	0.00	0.00	0.00	0.00	0.00	0.50	0	—	31.10	34.39	39.73	49.52
0.00	0.00	0.00	0.00	0.00	0.00	0.00	0.00	0.00	0.00	0.00	0.00	0.00	0.55	0	—	26.88	31.26	36.45	43.26
0.00	0.00	0.00	0.00	0.00	0.00	0.00	0.00	0.00	0.00	0.00	0.00	0.00	0.60	0	—	20.63	26.26	33.32	39.98
42.50	11.00	0.90	2.40	7.10	7.00	0.40	2.20	20.90	—	9.20	2.50	—	0.50	10	—	29.47	33.44	40.48	51.05
42.50	11.00	0.90	2.40	7.10	7.00	0.40	2.20	20.90	—	9.20	2.50	—	0.50	20	—	28.62	32.60	39.64	50.36
42.50	11.00	0.90	2.40	7.10	7.00	0.40	2.20	20.90	—	9.20	2.50	—	0.50	30	—	26.86	30.23	36.97	46.30
42.50	11.00	0.90	2.40	7.10	7.00	0.40	2.20	20.90	—	9.20	2.50	—	0.55	10	—	26.20	30.85	37.83	45.43
42.50	11.00	0.90	2.40	7.10	7.00	0.40	2.20	20.90	—	9.20	2.50	—	0.55	20	—	25.58	29.30	36.90	44.81
42.50	11.00	0.90	2.40	7.10	7.00	0.40	2.20	20.90	—	9.20	2.50	—	0.55	30	—	23.72	27.75	34.57	41.09
42.50	11.00	0.90	2.40	7.10	7.00	0.40	2.20	20.90	—	9.20	2.50	—	0.60	10	—	20.08	26.02	33.67	39.77
42.50	11.00	0.90	2.40	7.10	7.00	0.40	2.20	20.90	—	9.20	2.50	—	0.60	20	—	20.78	25.78	32.66	39.38
42.50	11.00	0.90	2.40	7.10	7.00	0.40	2.20	20.90	—	9.20	2.50	—	0.60	30	—	18.05	24.30	30.08	36.33
0.00	0.00	0.00	0.00	0.00	0.00	0.00	0.00	0.00	0.00	0.00	0.00	0.00	0.35	0	—	—	53.00	75.00	99.10
92.00	0.90	1.60	0.60	0.10	2.20	0.10	0.00	2.10	—	15.90	2.59	—	0.35	10	—	—	48.30	68.20	90.10
92.00	0.90	1.60	0.60	0.10	2.20	0.10	0.00	2.10	—	15.90	2.59	—	0.35	20	—	—	42.90	60.80	78.60
92.00	0.90	1.60	0.60	0.10	2.20	0.10	0.00	2.10	—	15.90	2.59	—	0.35	30	—	—	36.90	53.10	70.20
92.00	0.90	1.60	0.60	0.10	2.20	0.10	0.00	2.10	—	15.90	2.59	—	0.35	40	—	—	31.50	45.60	59.60

88.80	1.10	0.60	1.70	0.60	2.00	0.20	0.10	3.60	—	14.80	2.29	—	0.35	10	—	—	52.40	76.50	107.60
88.80	1.10	0.60	1.70	0.60	2.00	0.20	0.10	3.60	—	14.80	2.29	—	0.35	20	—	—	49.80	74.20	106.00
88.80	1.10	0.60	1.70	0.60	2.00	0.20	0.10	3.60	—	14.80	2.29	—	0.35	30	—	—	46.50	70.50	100.00
88.80	1.10	0.60	1.70	0.60	2.00	0.20	0.10	3.60	—	14.80	2.29	—	0.35	40	—	—	42.40	64.70	92.10
54.00	12.90	0.90	2.00	4.90	13.50	1.00	4.00	3.70	—	15.60	2.36	—	0.35	10	—	—	51.30	74.80	104.50
54.00	12.90	0.90	2.00	4.90	13.50	1.00	4.00	3.70	—	15.60	2.36	—	0.35	20	—	—	48.30	72.00	102.00
54.00	12.90	0.90	2.00	4.90	13.50	1.00	4.00	3.70	—	15.60	2.36	—	0.35	30	—	—	44.50	66.70	97.10
54.00	12.90	0.90	2.00	4.90	13.50	1.00	4.00	3.70	—	15.60	2.36	—	0.35	40	—	—	41.00	61.50	88.10
91.20	0.70	1.80	0.20	0.10	2.30	0.10	0.00	1.80	—	2.20	2.61	—	0.35	10	—	—	49.90	69.90	92.80
91.20	0.70	1.80	0.20	0.10	2.30	0.10	0.00	1.80	—	2.20	2.61	—	0.35	20	—	—	45.00	63.40	82.10
91.20	0.70	1.80	0.20	0.10	2.30	0.10	0.00	1.80	—	2.20	2.61	—	0.35	30	—	—	39.10	56.50	74.50
91.20	0.70	1.80	0.20	0.10	2.30	0.10	0.00	1.80	—	2.20	2.61	—	0.35	40	—	—	34.20	49.20	63.90
87.80	1.20	0.50	0.90	0.60	2.20	0.20	0.10	5.20	—	1.90	2.31	—	0.35	10	—	—	55.90	81.70	116.20
87.80	1.20	0.50	0.90	0.60	2.20	0.20	0.10	5.20	—	1.90	2.31	—	0.35	20	—	—	52.90	78.70	113.20
87.80	1.20	0.50	0.90	0.60	2.20	0.20	0.10	5.20	—	1.90	2.31	—	0.35	30	—	—	50.30	74.90	107.90
87.80	1.20	0.50	0.90	0.60	2.20	0.20	0.10	5.20	—	1.90	2.31	—	0.35	40	—	—	44.50	66.90	96.10
55.70	12.50	0.90	2.00	5.10	11.90	1.00	2.90	4.70	—	2.10	2.48	—	0.35	10	—	—	53.70	79.30	111.30
55.70	12.50	0.90	2.00	5.10	11.90	1.00	2.90	4.70	—	2.10	2.48	—	0.35	20	—	—	51.90	77.30	109.60
55.70	12.50	0.90	2.00	5.10	11.90	1.00	2.90	4.70	—	2.10	2.48	—	0.35	30	—	—	48.30	72.80	104.00
55.70	12.50	0.90	2.00	5.10	11.90	1.00	2.90	4.70	—	2.10	2.48	—	0.35	40	—	—	44.00	66.50	94.10
0.00	0.00	0.00	0.00	0.00	0.00	0.00	0.00	0.00	0.00	0.00	0.00	0.00	0.55	0	—	—	44.00	51.00	57.00
44.40	13.00	23.50	10.20	3.00	2.00	0.10	1.10	1.80	—	—	—	—	0.53	20	—	—	32.00	45.00	57.00
44.40	13.00	23.50	10.20	3.00	2.00	0.10	1.10	1.80	—	—	—	—	0.51	40	—	—	29.00	46.00	62.00
90.00	0.80	0.50	0.90	0.60	2.10	0.10	0.10	3.20	—	—	—	—	0.68	20	—	—	31.00	54.00	61.00
90.00	0.80	0.50	0.90	0.60	2.10	0.10	0.10	3.20	—	—	—	—	0.80	40	—	—	17.00	32.00	43.00
0.00	0.00	0.00	0.00	0.00	0.00	0.00	0.00	0.00	0.00	0.00	0.00	0.00	0.30	0	—	68.30	83.10	100.10	115.00
56.79	3.00	28.21	5.31	5.21	0.00	0.00	0.68	3.90	—	—	2.31	—	0.30	15	—	65.90	77.40	99.20	116.70
56.79	3.00	28.21	5.31	5.21	0.00	0.00	0.68	3.90	—	—	2.31	—	0.30	25	—	57.20	71.20	93.90	119.90

56.79	3.00	28.21	5.31	5.21	0.00	0.00	0.68	3.90	—	—	2.31	—	0.30	35	—	49.80	60.30	81.40	106.30
56.79	3.00	28.21	5.31	5.21	0.00	0.00	0.68	3.90	—	—	2.31	—	0.30	45	—	37.40	59.30	82.00	101.20
56.79	3.00	28.21	5.31	5.21	0.00	0.00	0.68	3.90	—	—	2.31	—	0.30	55	—	25.90	36.10	66.50	88.50
0.00	0.00	0.00	0.00	0.00	0.00	0.00	0.00	0.00	0.00	0.00	0.00	0.00	0.50	0	—	—	37.50	46.30	48.60
84.75	2.78	0.16	0.00	2.32	2.57	0.37	0.60	3.72	—	10.00	2.16	—	0.50	10	—	—	35.30	47.30	51.00
84.75	2.78	0.16	0.00	2.32	2.57	0.37	0.60	3.72	—	10.00	2.16	—	0.50	20	—	—	39.10	49.20	53.50
84.75	2.78	0.16	0.00	2.32	2.57	0.37	0.60	3.72	—	10.00	2.16	—	0.50	30	—	—	32.20	44.80	48.60
84.75	2.78	0.16	0.00	2.32	2.57	0.37	0.60	3.72	—	10.00	2.16	—	0.50	40	—	—	28.10	40.50	44.40
84.75	2.78	0.16	0.00	2.32	2.57	0.37	0.60	3.72	0.00	0.00	0.00	0.00	0.58	0	—	—	35.90	44.80	48.40
84.75	2.78	0.16	0.00	2.32	2.57	0.37	0.60	3.72	—	10.00	2.16	—	0.58	10	—	—	34.60	45.70	53.60
84.75	2.78	0.16	0.00	2.32	2.57	0.37	0.60	3.72	—	10.00	2.16	—	0.58	20	—	—	37.50	49.20	55.60
84.75	2.78	0.16	0.00	2.32	2.57	0.37	0.60	3.72	—	10.00	2.16	—	0.58	30	—	—	31.50	43.60	48.00
84.75	2.78	0.16	0.00	2.32	2.57	0.37	0.60	3.72	—	10.00	2.16	—	0.58	40	—	—	27.40	38.10	43.80
84.75	2.78	0.16	0.00	2.32	2.57	0.37	0.60	3.72	0.00	0.00	0.00	0.00	0.65	0	—	—	34.50	43.30	46.40
84.75	2.78	0.16	0.00	2.32	2.57	0.37	0.60	3.72	—	10.00	2.16	—	0.65	10	—	—	31.60	42.10	50.00
84.75	2.78	0.16	0.00	2.32	2.57	0.37	0.60	3.72	—	10.00	2.16	—	0.65	20	—	—	33.80	44.90	52.10
84.75	2.78	0.16	0.00	2.32	2.57	0.37	0.60	3.72	—	10.00	2.16	—	0.65	30	—	—	27.70	38.90	45.70
84.75	2.78	0.16	0.00	2.32	2.57	0.37	0.60	3.72	—	10.00	2.16	—	0.65	40	—	—	24.30	35.30	41.80
84.75	2.78	0.16	0.00	2.32	2.57	0.37	0.60	3.72	0.00	0.00	0.00	0.00	0.50	0	—	—	37.50	46.30	48.90
65.30	6.42	2.56	1.98	3.08	5.72	0.36	0.47	10.05	—	13.00	2.22	—	0.50	10	—	—	36.50	48.40	53.20
65.30	6.42	2.56	1.98	3.08	5.72	0.36	0.47	10.05	—	13.00	2.22	—	0.50	20	—	—	35.90	46.70	50.80
65.30	6.42	2.56	1.98	3.08	5.72	0.36	0.47	10.05	—	13.00	2.22	—	0.50	30	—	—	33.60	42.20	48.30
65.30	6.42	2.56	1.98	3.08	5.72	0.36	0.47	10.05	—	13.00	2.22	—	0.50	40	—	—	28.20	38.20	43.00
65.30	6.42	2.56	1.98	3.08	5.72	0.36	0.47	10.05	0.00	0.00	0.00	0.00	0.58	0	—	—	35.90	44.80	48.40
65.30	6.42	2.56	1.98	3.08	5.72	0.36	0.47	10.05	—	13.00	2.22	—	0.58	10	—	—	34.80	44.30	49.20
65.30	6.42	2.56	1.98	3.08	5.72	0.36	0.47	10.05	—	13.00	2.22	—	0.58	20	—	—	34.70	44.00	49.50
65.30	6.42	2.56	1.98	3.08	5.72	0.36	0.47	10.05	—	13.00	2.22	—	0.58	30	—	—	30.90	40.10	46.20
65.30	6.42	2.56	1.98	3.08	5.72	0.36	0.47	10.05	—	13.00	2.22	—	0.58	40	—	—	27.00	35.80	40.20

65.30	6.42	2.56	1.98	3.08	5.72	0.36	0.47	10.05	0.00	0.00	0.00	0.00	0.65	0	—	—	34.50	43.30	46.40
65.30	6.42	2.56	1.98	3.08	5.72	0.36	0.47	10.05	—	13.00	2.22	—	0.65	10	—	—	34.10	43.70	49.80
65.30	6.42	2.56	1.98	3.08	5.72	0.36	0.47	10.05	—	13.00	2.22	—	0.65	20	—	—	32.10	41.10	47.50
65.30	6.42	2.56	1.98	3.08	5.72	0.36	0.47	10.05	—	13.00	2.22	—	0.65	30	—	—	27.40	37.10	41.80
65.30	6.42	2.56	1.98	3.08	5.72	0.36	0.47	10.05	—	13.00	2.22	—	0.65	40	—	—	23.90	31.40	36.40
65.30	6.42	2.56	1.98	3.08	5.72	0.36	0.47	10.05	0.00	0.00	0.00	0.00	0.50	0	—	—	37.50	46.30	48.90
92.86	0.55	3.17	0.27	0.49	0.32	0.42	0.55	0.67	—	11.50	2.63	—	0.50	10	—	—	36.80	45.80	48.60
92.86	0.55	3.17	0.27	0.49	0.32	0.42	0.55	0.67	—	11.50	2.63	—	0.50	20	—	—	32.90	40.50	43.30
92.86	0.55	3.17	0.27	0.49	0.32	0.42	0.55	0.67	—	11.50	2.63	—	0.50	30	—	—	27.70	35.10	36.50
92.86	0.55	3.17	0.27	0.49	0.32	0.42	0.55	0.67	—	11.50	2.63	—	0.50	40	—	—	24.50	31.00	32.60
92.86	0.55	3.17	0.27	0.49	0.32	0.42	0.55	0.67	0.00	0.00	0.00	0.00	0.58	0	—	—	35.90	44.80	48.40
92.86	0.55	3.17	0.27	0.49	0.32	0.42	0.55	0.67	—	11.50	2.63	—	0.58	10	—	—	33.00	41.70	45.40
92.86	0.55	3.17	0.27	0.49	0.32	0.42	0.55	0.67	—	11.50	2.63	—	0.58	20	—	—	28.40	37.47	41.60
92.86	0.55	3.17	0.27	0.49	0.32	0.42	0.55	0.67	—	11.50	2.63	—	0.58	30	—	—	25.50	33.40	35.70
92.86	0.55	3.17	0.27	0.49	0.32	0.42	0.55	0.67	—	11.50	2.63	—	0.58	40	—	—	20.20	26.10	28.70
92.86	0.55	3.17	0.27	0.49	0.32	0.42	0.55	0.67	0.00	0.00	0.00	0.00	0.65	0	—	—	34.50	43.30	46.40
92.86	0.55	3.17	0.27	0.49	0.32	0.42	0.55	0.67	—	11.50	2.63	—	0.65	10	—	—	27.60	35.40	36.90
92.86	0.55	3.17	0.27	0.49	0.32	0.42	0.55	0.67	—	11.50	2.63	—	0.65	20	—	—	25.20	32.40	33.30
92.86	0.55	3.17	0.27	0.49	0.32	0.42	0.55	0.67	—	11.50	2.63	—	0.65	30	—	—	20.20	28.90	29.80
92.86	0.55	3.17	0.27	0.49	0.32	0.42	0.55	0.67	—	11.50	2.63	—	0.65	40	—	—	16.50	22.20	23.20
0.00	0.00	0.00	0.00	0.00	0.00	0.00	0.00	0.00	—	—	—	—	0.30	0	0.95	—	88.90	100.50	—
87.20	0.55	0.15	0.16	0.35	3.60	1.12	0.32	6.55	—	—	2.06	—	0.30	5	0.93	—	80.80	100.50	—
87.20	0.55	0.15	0.16	0.35	3.60	1.12	0.32	6.55	—	—	2.06	—	0.30	10	0.83	—	86.70	105.40	—
88.00	0.80	0.00	0.10	0.20	2.20	0.70	0.00	8.10	—	—	2.16	—	0.30	5	1.00	—	70.60	85.90	—
88.00	0.80	0.00	0.10	0.20	2.20	0.70	0.00	8.10	—	—	2.16	—	0.30	10	1.60	—	83.30	97.40	—
0.00	0.00	0.00	0.00	0.00	0.00	0.00	0.00	0.00	0.00	0.00	0.00	0.00	0.50	0	—	24.60	—	44.70	54.40
52.00	3.40	28.50	7.50	1.90	2.91	1.79	0.90	1.10	33.20	—	2.35	—	0.50	20	—	20.00	—	44.10	57.50
52.00	3.40	28.50	7.50	1.90	2.91	1.79	0.90	1.10	33.20	—	2.35	—	0.50	40	—	15.80	—	36.00	47.50

48.70	8.70	21.20	10.10	5.40	2.42	1.48	1.10	0.90	48.00	—	2.26	—	0.50	20	—	15.70	—	30.90	45.10
48.70	8.70	21.20	10.10	5.40	2.42	1.48	1.10	0.90	48.00	—	2.26	—	0.50	40	—	10.30	—	20.80	32.60
0.00	0.00	0.00	0.00	0.00	0.00	0.00	0.00	0.00	0.00	0.00	0.00	0.00	0.50	0	—	11.12	20.53	32.69	45.77
39.44	12.94	21.96	13.55	2.60	2.90	1.41	1.51	0.00	—	—	—	—	0.50	10	—	10.32	18.26	32.55	46.57
39.44	12.94	21.96	13.55	2.60	2.90	1.41	1.51	0.00	—	—	—	—	0.50	20	—	9.78	14.66	32.67	47.09
39.44	12.94	21.96	13.55	2.60	2.90	1.41	1.51	0.00	—	—	—	—	0.50	30	—	7.91	10.00	30.54	43.76
0.00	0.00	0.00	0.00	0.00	0.00	0.00	0.00	0.00	0.00	0.00	0.00	0.00	0.50	0	—	—	30.00	47.08	56.50
39.82	15.24	21.52	13.68	2.78	2.00	1.08	2.39	1.00	—	—	—	—	0.50	20	—	—	—	45.09	—
39.82	15.24	21.52	13.68	2.78	2.00	1.08	2.39	1.00	—	—	—	—	0.50	20	—	—	25.50	41.60	53.00
39.82	15.24	21.52	13.68	2.78	2.00	1.08	2.39	1.00	—	—	—	—	0.50	30	—	—	—	36.58	—
0.00	0.00	0.00	0.00	0.00	0.00	0.00	0.00	0.00	—	—	—	—	0.50	0	—	31.60	36.50	48.40	—
32.46	16.49	20.06	6.05	2.68	1.22	0.32	8.91	10.03	—	—	—	—	0.50	30	—	14.40	24.60	33.00	—
50.49	3.48	30.68	3.74	0.51	1.34	0.56	0.92	6.22	—	—	—	—	0.50	30	—	17.30	21.10	37.00	—
0.00	0.00	0.00	0.00	0.00	0.00	0.00	0.00	0.00	0.00	0.00	0.00	0.00	0.35	0	0.20	—	—	53.68	67.84
0.00	0.00	0.00	0.00	0.00	0.00	0.00	0.00	0.00	0.00	0.00	0.00	0.00	0.50	0	—	—	—	47.04	51.49
0.00	0.00	0.00	0.00	0.00	0.00	0.00	0.00	0.00	0.00	0.00	0.00	0.00	0.65	0	—	—	—	27.34	35.15
64.57	1.51	27.27	2.21	0.79	1.50	0.15	0.06	1.16	—	—	2.19	2.32	0.35	35	0.25	—	—	58.23	66.49
64.57	1.51	27.27	2.21	0.79	1.50	0.15	0.06	1.16	—	—	2.19	2.32	0.50	35	0.10	—	—	36.39	44.33
64.57	1.51	27.27	2.21	0.79	1.50	0.15	0.06	1.16	—	—	2.19	2.32	0.65	35	—	—	—	16.45	23.96
34.98	42.28	13.06	1.11	6.01	0.40	0.17	0.11	0.71	—	—	2.89	1.07	0.35	50	0.17	—	—	52.81	61.57
34.98	42.28	13.06	1.11	6.01	0.40	0.17	0.11	0.71	—	—	2.89	1.07	0.50	50	—	—	—	35.48	46.12
34.98	42.28	13.06	1.11	6.01	0.40	0.17	0.11	0.71	—	—	2.89	1.07	0.65	50	—	—	—	23.14	28.66
90.00	0.45	0.28	0.14	0.28	1.55	0.08	0.02	5.00	—	—	2.17	4.00	0.35	10	0.50	—	—	67.81	76.12
90.00	0.45	0.28	0.14	0.28	1.55	0.08	0.02	5.00	—	—	2.17	4.00	0.50	10	0.20	—	—	46.68	61.57
90.00	0.45	0.28	0.14	0.28	1.55	0.08	0.02	5.00	—	—	2.17	4.00	0.65	10	—	—	—	31.73	38.51
90.00	0.45	0.28	0.14	0.28	1.55	0.08	0.02	5.00	—	—	2.17	4.00	0.35	20	0.95	—	—	71.88	85.52
90.00	0.45	0.28	0.14	0.28	1.55	0.08	0.02	5.00	—	—	2.17	4.00	0.50	20	0.50	—	—	52.42	62.91
90.00	0.45	0.28	0.14	0.28	1.55	0.08	0.02	5.00	—	—	2.17	4.00	0.65	20	0.30	—	—	33.20	41.42

90.00	0.45	0.28	0.14	0.28	1.55	0.08	0.02	5.00	—	—	2.17	4.00	0.35	30	1.95	—	—	67.65	78.36
90.00	0.45	0.28	0.14	0.28	1.55	0.08	0.02	5.00	—	—	2.17	4.00	0.50	30	1.05	—	—	50.32	64.93
90.00	0.45	0.28	0.14	0.28	1.55	0.08	0.02	5.00	—	—	2.17	4.00	0.65	30	0.70	—	—	29.91	37.16
0.00	0.00	0.00	0.00	0.00	0.00	0.00	0.00	0.00	0.00	0.00	0.00	0.00	0.60	0	0.00	—	19.00	24.00	29.00
0.00	0.00	0.00	0.00	0.00	0.00	0.00	0.00	0.00	0.00	0.00	0.00	0.00	0.45	0	1.30	—	28.00	38.50	43.00
78.40	7.40	2.60	1.70	1.30	3.70	0.20	1.10	3.60	—	15.50	2.10	—	0.60	10	1.00	—	18.50	24.50	33.40
78.40	7.40	2.60	1.70	1.30	3.70	0.20	1.10	3.60	—	15.50	2.10	—	0.60	20	2.80	—	21.00	26.00	38.50
78.40	7.40	2.60	1.70	1.30	3.70	0.20	1.10	3.60	—	15.50	2.10	—	0.60	40	6.40	—	16.00	20.50	29.00
78.40	7.40	2.60	1.70	1.30	3.70	0.20	1.10	3.60	—	15.50	2.10	—	0.45	10	3.80	—	27.00	39.00	45.50
78.40	7.40	2.60	1.70	1.30	3.70	0.20	1.10	3.60	—	15.50	2.10	—	0.45	20	6.30	—	30.00	39.50	45.00
0.00	0.00	0.00	0.00	0.00	0.00	0.00	0.00	0.00	0.00	0.00	0.00	0.00	0.40	0	—	28.06	36.67	41.53	45.84
87.20	0.55	0.15	0.16	0.35	3.68	1.12	0.24	8.55	—	—	2.06	—	0.40	10	—	28.61	37.22	44.07	47.05
87.20	0.55	0.15	0.16	0.35	3.68	1.12	0.24	8.55	—	—	2.06	—	0.40	20	—	35.79	44.29	51.47	53.56
87.20	0.55	0.15	0.16	0.35	3.68	1.12	0.24	8.55	—	—	2.06	—	0.40	30	—	28.17	42.08	51.80	55.11
87.20	0.55	0.15	0.16	0.35	3.68	1.12	0.24	8.55	—	—	2.06	—	0.40	40	—	20.33	22.21	35.79	36.67
87.20	0.55	0.15	0.16	0.35	3.68	1.12	0.24	8.55	—	—	2.06	—	0.40	50	—	20.00	20.44	30.27	31.81
87.20	0.55	0.15	0.16	0.35	3.68	1.12	0.24	8.55	0.00	0.00	0.00	0.00	0.50	0	—	23.11	27.95	36.06	45.65
87.20	0.55	0.15	0.16	0.35	3.68	1.12	0.24	8.55	—	—	2.06	—	0.50	10	—	24.39	30.92	40.51	46.05
87.20	0.55	0.15	0.16	0.35	3.68	1.12	0.24	8.55	—	—	2.06	—	0.50	20	—	25.88	39.52	42.98	46.44
87.20	0.55	0.15	0.16	0.35	3.68	1.12	0.24	8.55	—	—	2.06	—	0.50	30	—	30.42	39.22	47.23	48.62
87.20	0.55	0.15	0.16	0.35	3.68	1.12	0.24	8.55	—	—	2.06	—	0.50	40	—	28.64	32.20	42.19	45.75
87.20	0.55	0.15	0.16	0.35	3.68	1.12	0.24	8.55	—	—	2.06	—	0.50	50	—	16.58	20.64	31.21	33.29
87.20	0.55	0.15	0.16	0.35	3.68	1.12	0.24	8.55	0.00	0.00	0.00	0.00	0.60	0	—	14.58	21.58	31.75	37.87
87.20	0.55	0.15	0.16	0.35	3.68	1.12	0.24	8.55	—	—	2.06	—	0.60	10	—	14.98	27.99	35.21	40.68
87.20	0.55	0.15	0.16	0.35	3.68	1.12	0.24	8.55	—	—	2.06	—	0.60	20	—	21.61	28.06	35.50	41.96
87.20	0.55	0.15	0.16	0.35	3.68	1.12	0.24	8.55	—	—	2.06	—	0.60	30	—	22.56	28.25	39.29	44.76
87.20	0.55	0.15	0.16	0.35	3.68	1.12	0.24	8.55	—	—	2.06	—	0.60	40	—	23.18	35.76	39.91	44.40
87.20	0.55	0.15	0.16	0.35	3.68	1.12	0.24	8.55	—	—	2.06	—	0.60	50	—	24.67	35.83	39.99	44.80

0.00	0.00	0.00	0.00	0.00	0.00	0.00	0.00	0.00	0.00	0.00	0.00	0.00	0.55	0	—	22.00	30.40	45.20	—
62.78	2.37	10.66	4.20	1.10	0.74	0.35	0.00	12.40	—	—	—	—	0.55	10	—	12.30	22.50	46.90	—
62.78	2.37	10.66	4.20	1.10	0.74	0.35	0.00	12.40	—	—	—	—	0.55	20	—	11.20	20.30	48.20	—
62.78	2.37	10.66	4.20	1.10	0.74	0.35	0.00	12.40	—	—	—	—	0.55	30	—	10.90	18.50	45.30	—
62.78	2.37	10.66	4.20	1.10	0.74	0.35	0.00	12.40	—	—	—	—	0.55	40	—	7.20	17.20	39.60	—
62.78	2.37	10.66	4.20	1.10	0.74	0.35	0.00	12.40	—	—	—	—	0.55	45	—	6.90	15.00	38.10	—
61.12	4.28	12.32	6.51	5.88	1.73	2.44	0.10	0.84	—	—	—	—	0.55	10	—	11.50	22.00	44.60	—
61.12	4.28	12.32	6.51	5.88	1.73	2.44	0.10	0.84	—	—	—	—	0.55	20	—	10.60	21.00	45.40	—
61.12	4.28	12.32	6.51	5.88	1.73	2.44	0.10	0.84	—	—	—	—	0.55	30	—	8.60	19.50	41.00	—
61.12	4.28	12.32	6.51	5.88	1.73	2.44	0.10	0.84	—	—	—	—	0.55	40	—	8.10	18.70	38.50	—
61.12	4.28	12.32	6.51	5.88	1.73	2.44	0.10	0.84	—	—	—	—	0.55	45	—	7.80	16.40	37.50	—
35.11	37.56	17.63	0.35	5.52	0.00	0.32	0.00	0.75	—	—	—	—	0.55	10	—	13.80	35.30	51.60	—
35.11	37.56	17.63	0.35	5.52	0.00	0.32	0.00	0.75	—	—	—	—	0.55	20	—	12.80	32.20	52.90	—
35.11	37.56	17.63	0.35	5.52	0.00	0.32	0.00	0.75	—	—	—	—	0.55	30	—	11.20	29.60	48.20	—
35.11	37.56	17.63	0.35	5.52	0.00	0.32	0.00	0.75	—	—	—	—	0.55	40	—	9.00	24.80	45.50	—
35.11	37.56	17.63	0.35	5.52	0.00	0.32	0.00	0.75	—	—	—	—	0.55	45	—	8.30	23.10	42.80	—
0.00	0.00	0.00	0.00	0.00	0.00	0.00	0.00	0.00	0.00	0.00	0.00	0.00	0.27	0	—	50.68	87.50	103.52	—
65.01	8.19	5.72	4.41	4.58	6.48	0.07	0.33	2.53	—	2.06	2.56	—	0.27	20	—	78.64	98.75	51.02	—
65.01	8.19	5.72	4.41	4.58	6.48	0.07	0.33	2.53	—	2.06	2.56	—	0.27	40	—	91.25	66.70	79.66	—
65.01	8.19	5.72	4.41	4.58	6.48	0.07	0.33	2.53	—	2.06	2.56	—	0.27	60	—	73.52	84.09	99.09	—
0.00	0.00	0.00	0.00	0.00	0.00	0.00	0.00	0.00	—	—	—	—	0.36	35	—	—	—	31.12	—
65.60	1.00	28.00	3.00	1.00	0.00	0.00	0.20	0.00	—	—	2.12	—	0.36	35	—	—	—	32.26	—
0.00	0.00	0.00	0.00	0.00	0.00	0.00	0.00	0.00	0.00	0.00	0.00	0.00	0.40	0	—	33.00	49.00	—	—
58.25	0.00	16.60	4.63	0.00	0.00	0.00	0.84	1.52	—	—	2.35	—	0.40	30	—	27.00	39.00	—	—
0.00	0.00	0.00	0.00	0.00	0.00	0.00	0.00	0.00	0.00	0.00	0.00	0.00	0.50	0	—	—	34.06	39.68	47.23
76.80	5.40	4.40	8.00	0.90	0.00	0.00	0.10	3.30	—	—	2.47	—	0.50	20	—	—	34.84	42.77	49.55
76.80	5.40	4.40	8.00	0.90	0.00	0.00	0.10	3.30	—	—	2.47	—	0.50	30	—	—	31.35	38.71	45.10
76.80	5.40	4.40	8.00	0.90	0.00	0.00	0.10	3.30	—	—	2.47	—	0.50	40	—	—	30.39	36.77	43.94

67.10	2.90	5.70	2.50	0.50	0.00	0.00	0.00	20.40	—	—	2.16	—	0.50	20	—	—	31.94	38.13	46.06
67.10	2.90	5.70	2.50	0.50	0.00	0.00	0.00	20.40	—	—	2.16	—	0.50	30	—	—	26.90	36.19	41.61
67.10	2.90	5.70	2.50	0.50	0.00	0.00	0.00	20.40	—	—	2.16	—	0.50	40	—	—	14.13	29.03	33.87
0.00	0.00	0.00	0.00	0.00	0.00	0.00	0.00	0.00	—	—	—	—	0.50	20	—	21.28	30.87	49.11	—
59.02	2.19	31.98	4.79	0.28	0.00	0.47	0.00	1.05	—	—	—	—	0.50	20	—	19.97	29.85	51.17	—
0.00	0.00	0.00	0.00	0.00	0.00	0.00	0.00	0.00	0.00	0.00	0.00	0.00	0.45	0	0.00	—	—	45.10	—
0.00	0.00	0.00	0.00	0.00	0.00	0.00	0.00	0.00	0.00	0.00	0.00	0.00	0.65	0	0.00	—	—	42.90	—
87.00	1.25	1.08	2.58	0.50	1.00	0.08	0.09	5.71	—	—	—	—	0.45	15	0.85	—	—	40.80	—
87.00	1.25	1.08	2.58	0.50	1.00	0.08	0.09	5.71	—	—	—	—	0.45	25	1.70	—	—	39.40	—
87.00	1.25	1.08	2.58	0.50	1.00	0.08	0.09	5.71	—	—	—	—	0.45	35	2.54	—	—	39.30	—
87.00	1.25	1.08	2.58	0.50	1.00	0.08	0.09	5.71	—	—	—	—	0.45	45	3.82	—	—	30.90	—
87.00	1.25	1.08	2.58	0.50	1.00	0.08	0.09	5.71	—	—	—	—	0.65	15	0.00	—	—	33.80	—
87.00	1.25	1.08	2.58	0.50	1.00	0.08	0.09	5.71	—	—	—	—	0.65	25	0.00	—	—	32.90	—
87.00	1.25	1.08	2.58	0.50	1.00	0.08	0.09	5.71	—	—	—	—	0.65	35	0.30	—	—	31.10	—
87.00	1.25	1.08	2.58	0.50	1.00	0.08	0.09	5.71	—	—	—	—	0.65	45	0.30	—	—	28.60	—
0.00	0.00	0.00	0.00	0.00	0.00	0.00	0.00	0.00	0.00	0.00	0.00	0.00	0.45	0	0.00	—	34.10	41.00	50.70
55.00	11.00	5.10	4.10	0.90	1.20	0.20	2.20	19.60	—	5.60	2.27	—	0.45	—	2.50	—	34.50	41.20	51.30
55.00	11.00	5.10	4.10	0.90	1.20	0.20	2.20	19.60	—	5.60	2.27	—	0.45	—	4.60	—	32.30	38.60	46.90
55.00	11.00	5.10	4.10	0.90	1.20	0.20	2.20	19.60	—	5.60	2.27	—	0.45	—	8.50	—	29.00	35.10	43.80
0.00	0.00	0.00	0.00	0.00	0.00	0.00	0.00	0.00	0.00	0.00	0.00	0.00	0.50	0	—	—	38.61	48.87	51.67
50.30	15.27	16.43	7.72	0.00	2.14	1.30	1.77	0.00	—	—	2.15	—	0.50	10	—	—	29.58	38.67	49.34
50.30	15.27	16.43	7.72	0.00	2.14	1.30	1.77	0.00	—	—	2.15	—	0.50	20	—	—	24.78	32.12	42.64
50.30	15.27	16.43	7.72	0.00	2.14	1.30	1.77	0.00	—	—	2.15	—	0.50	30	—	—	20.41	28.62	37.55
50.30	15.27	16.43	7.72	0.00	2.14	1.30	1.77	0.00	—	—	2.15	—	0.50	40	—	—	17.06	25.86	32.89
0.00	0.00	0.00	0.00	0.00	0.00	0.00	0.00	0.00	0.00	0.00	0.00	0.00	0.48	0	—	32.40	35.90	43.20	—
53.64	12.75	18.44	7.63	0.00	2.17	1.33	0.20	0.00	—	—	3.09	—	0.48	20	—	33.80	41.90	53.90	—
53.21	12.83	18.33	7.86	0.00	2.18	1.33	0.20	0.00	—	—	3.25	—	0.48	20	—	30.00	39.50	45.60	—
50.30	15.27	16.43	7.72	0.00	2.14	1.30	1.77	0.00	—	—	2.15	—	0.48	20	—	28.20	31.60	39.00	—

0.00	0.00	0.00	0.00	0.00	0.00	0.00	0.00	0.00	0.00	0.00	0.00	0.00	0.55	0	2.00	—	—	46.00	—
59.62	4.92	2.54	5.02	4.52	7.52	0.76	1.28	8.25	—	—	2.42	—	0.55	50	2.00	—	—	41.00	—
59.62	4.92	2.54	5.02	4.52	7.52	0.76	1.28	8.25	—	—	2.42	—	0.55	60	2.00	—	—	36.00	—
59.62	4.92	2.54	5.02	4.52	7.52	0.76	1.28	8.25	—	—	2.42	—	0.55	70	2.00	—	—	28.00	—
0.00	0.00	0.00	0.00	0.00	0.00	0.00	0.00	0.00	0.00	0.00	0.00	0.00	0.55	0	—	—	25.29	32.83	—
52.00	15.40	7.79	3.20	2.94	4.91	0.66	1.54	2.50	—	—	0.81	0.56	0.55	10	1.20	—	21.40	30.40	—
52.00	15.40	7.79	3.20	2.94	4.91	0.66	1.54	2.50	—	—	0.81	0.56	0.55	15	1.20	—	23.59	30.27	—
52.00	15.40	7.79	3.20	2.94	4.91	0.66	1.54	2.50	—	—	0.81	0.56	0.55	20	1.20	—	18.12	29.91	—
52.00	15.40	7.79	3.20	2.94	4.91	0.66	1.54	2.50	—	—	0.81	0.56	0.55	30	1.20	—	17.75	28.81	—
55.20	1.58	4.04	3.23	1.73	1.29	0.51	4.45	0.99	—	—	2.20	0.56	0.55	10	1.20	—	17.88	23.63	—
55.20	1.58	4.04	3.23	1.73	1.29	0.51	4.45	0.99	—	—	2.20	0.56	0.55	15	1.20	—	16.49	25.75	—
55.20	1.58	4.04	3.23	1.73	1.29	0.51	4.45	0.99	—	—	2.20	0.56	0.55	20	1.20	—	15.80	29.64	—
55.20	1.58	4.04	3.23	1.73	1.29	0.51	4.45	0.99	—	—	2.20	0.56	0.55	30	1.20	—	14.29	28.48	—
0.00	0.00	0.00	0.00	0.00	0.00	0.00	0.00	0.00	0.00	0.00	0.00	0.00	0.65	0	0.00	—	21.91	26.13	33.20
55.50	12.40	9.20	5.60	4.60	0.00	0.00	2.30	7.90	—	10.70	2.53	—	0.65	20	0.10	—	21.55	27.72	34.50
55.50	12.40	9.20	5.60	4.60	0.00	0.00	2.30	7.90	—	10.70	2.53	—	0.65	35	0.15	—	20.44	25.10	32.63
55.50	12.40	9.20	5.60	4.60	0.00	0.00	2.30	7.90	—	10.70	2.53	—	0.65	50	0.25	—	18.87	23.54	30.61
0.00	0.00	0.00	0.00	0.00	0.00	0.00	0.00	0.00	0.00	0.00	0.00	0.00	0.65	0	0.00	—	20.92	25.28	32.81
55.50	12.40	9.20	5.60	4.60	0.00	0.00	2.30	7.90	—	10.70	2.53	—	0.65	20	0.17	—	21.97	27.24	33.41
55.50	12.40	9.20	5.60	4.60	0.00	0.00	2.30	7.90	—	10.70	2.53	—	0.65	35	0.27	—	20.32	25.13	32.21
55.50	12.40	9.20	5.60	4.60	0.00	0.00	2.30	7.90	—	10.70	2.53	—	0.65	50	0.39	—	18.96	23.63	30.25
0.00	0.00	0.00	0.00	0.00	0.00	0.00	0.00	0.00	0.00	0.00	0.00	0.00	0.30	0	—	—	60.49	68.89	78.73
65.00	3.90	4.80	0.90	0.00	2.00	0.00	0.90	10.50	—	16.40	—	—	0.30	10	—	—	65.96	80.66	60.71
65.00	3.90	4.80	0.90	0.00	2.00	0.00	0.90	10.50	—	16.40	—	—	0.30	20	—	—	75.72	61.50	67.03
65.00	3.90	4.80	0.90	0.00	2.00	0.00	0.90	10.50	—	16.40	—	—	0.30	30	—	—	61.71	67.82	78.23
0.00	0.00	0.00	0.00	0.00	0.00	0.00	0.00	0.00	0.00	0.00	0.00	0.00	0.50	0	—	21.55	33.38	41.80	54.32
17.11	16.94	2.61	0.41	15.40	1.05	0.21	0.00	28.90	—	—	2.41	—	0.50	1	—	17.28	29.63	42.32	51.25
17.11	16.94	2.61	0.41	15.40	1.05	0.21	0.00	28.90	—	—	2.41	—	0.50	3	—	14.21	26.39	39.25	49.72

17.11	16.94	2.61	0.41	15.40	1.05	0.21	0.00	28.90	—	—	2.41	—	0.50	5	—	9.60	24.68	36.35	44.43
17.11	16.94	2.61	0.41	15.40	1.05	0.21	0.00	28.90	—	—	2.41	—	0.50	7	—	6.53	18.03	30.21	41.36
0.00	0.00	0.00	0.00	0.00	0.00	0.00	0.00	0.00	0.00	0.00	0.00	0.00	0.49	0	—	100.00	100.00	100.00	—
72.50	9.18	0.16	0.20	3.65	0.12	13.20	0.39	0.00	—	—	2.47	—	0.47	20	—	57.13	74.30	69.84	—
72.50	9.18	0.16	0.20	3.65	0.12	13.20	0.39	0.00	—	—	2.47	—	0.47	20	—	72.25	81.31	93.07	—
72.50	9.18	0.16	0.20	3.65	0.12	13.20	0.39	0.00	—	—	2.47	—	0.48	20	—	78.17	93.18	110.34	—
72.50	9.18	0.16	0.20	3.65	0.12	13.20	0.39	0.00	—	—	2.47	—	0.49	20	—	77.62	87.21	114.10	—
47.80	3.36	23.40	15.10	0.81	1.70	0.72	1.33	0.00	—	—	2.52	—	0.47	20	—	78.68	86.11	84.89	—
0.00	0.00	0.00	0.00	0.00	0.00	0.00	0.00	0.00	0.00	0.00	0.00	0.00	0.50	0	—	34.08	—	58.56	67.81
53.50	3.38	20.40	8.66	0.00	0.00	0.00	0.00	0.86	13.90	—	2.25	1.20	0.56	10	—	31.30	—	51.07	66.95
53.50	3.38	20.40	8.66	0.00	0.00	0.00	0.00	0.86	13.90	—	2.25	1.20	0.63	20	—	25.73	—	49.14	65.02
53.50	3.38	20.40	8.66	0.00	0.00	0.00	0.00	0.86	13.90	—	2.25	1.20	0.72	30	—	19.95	—	44.64	61.17
0.00	0.00	0.00	0.00	0.00	0.00	0.00	0.00	0.00	0.00	0.00	0.00	0.00	0.30	0	—	43.50	53.60	63.50	71.70
86.98	1.40	0.84	0.73	0.57	2.46	0.11	0.00	5.14	—	5.00	2.10	—	0.30	10	—	47.90	60.60	72.80	83.20
86.98	1.40	0.84	0.73	0.57	2.46	0.11	0.00	5.14	—	5.00	2.10	—	0.30	15	—	49.00	62.50	75.10	84.90
86.98	1.40	0.84	0.73	0.57	2.46	0.11	0.00	5.14	—	5.00	2.10	—	0.30	20	—	51.50	64.30	78.20	86.80
0.00	0.00	0.00	0.00	0.00	0.00	0.00	0.00	0.00	0.00	0.00	0.00	0.00	0.32	0	—	41.30	51.00	59.60	66.80
86.98	1.40	0.84	0.73	0.57	2.46	0.11	0.00	5.14	—	5.00	2.10	—	0.32	10	—	45.80	58.00	68.80	78.20
86.98	1.40	0.84	0.73	0.57	2.46	0.11	0.00	5.14	—	5.00	2.10	—	0.32	15	—	46.50	61.20	72.20	81.50
86.98	1.40	0.84	0.73	0.57	2.46	0.11	0.00	5.14	—	5.00	2.10	—	0.32	20	—	48.70	61.80	72.70	82.20
0.00	0.00	0.00	0.00	0.00	0.00	0.00	0.00	0.00	0.00	0.00	0.00	0.00	0.34	0	—	39.90	49.80	57.90	64.90
86.98	1.40	0.84	0.73	0.57	2.46	0.11	0.00	5.14	—	5.00	2.10	—	0.34	10	—	44.30	56.80	66.60	75.60
86.98	1.40	0.84	0.73	0.57	2.46	0.11	0.00	5.14	—	5.00	2.10	—	0.34	15	—	45.20	57.60	67.20	75.80
86.98	1.40	0.84	0.73	0.57	2.46	0.11	0.00	5.14	—	5.00	2.10	—	0.34	20	—	46.90	59.10	69.30	77.20
0.00	0.00	0.00	0.00	0.00	0.00	0.00	0.00	0.00	0.00	0.00	0.00	0.00	0.30	0	—	67.20	48.90	88.50	97.10
86.98	1.40	0.84	0.73	0.57	2.46	0.11	0.00	5.14	—	5.00	2.10	—	0.30	10	—	60.80	83.60	95.20	104.10
86.98	1.40	0.84	0.73	0.57	2.46	0.11	0.00	5.14	—	5.00	2.10	—	0.30	15	—	63.20	85.40	96.00	104.40
86.98	1.40	0.84	0.73	0.57	2.46	0.11	0.00	5.14	—	5.00	2.10	—	0.30	20	—	66.50	86.00	98.10	106.50

0.00	0.00	0.00	0.00	0.00	0.00	0.00	0.00	0.00	0.00	0.00	0.00	0.00	0.32	0	—	63.90	76.40	85.70	94.00
86.98	1.40	0.84	0.73	0.57	2.46	0.11	0.00	5.14	—	5.00	2.10	—	0.32	10	—	58.90	80.60	91.60	100.30
86.98	1.40	0.84	0.73	0.57	2.46	0.11	0.00	5.14	—	5.00	2.10	—	0.32	15	—	59.20	81.90	93.40	101.80
86.98	1.40	0.84	0.73	0.57	2.46	0.11	0.00	5.14	—	5.00	2.10	—	0.32	20	—	60.70	82.80	94.30	103.30
0.00	0.00	0.00	0.00	0.00	0.00	0.00	0.00	0.00	0.00	0.00	0.00	0.00	0.34	0	—	61.70	73.80	82.80	90.50
86.98	1.40	0.84	0.73	0.57	2.46	0.11	0.00	5.14	—	5.00	2.10	—	0.34	10	—	57.60	78.90	89.70	98.50
86.98	1.40	0.84	0.73	0.57	2.46	0.11	0.00	5.14	—	5.00	2.10	—	0.34	15	—	57.30	79.20	90.30	99.10
86.98	1.40	0.84	0.73	0.57	2.46	0.11	0.00	5.14	—	5.00	2.10	—	0.34	20	—	59.20	80.30	91.10	100.10
0.00	0.00	0.00	0.00	0.00	0.00	0.00	0.00	0.00	0.00	0.00	0.00	0.00	0.50	0	—	—	—	35.80	—
56.79	3.00	28.21	5.31	5.21	0.00	0.00	0.68	3.90	—	—	2.31	—	0.50	30	—	—	—	39.30	—
56.79	3.00	28.21	5.31	5.21	0.00	0.00	0.68	3.90	—	—	2.31	—	0.50	40	—	—	—	36.90	—
38.14	35.77	6.53	0.40	13.65	0.40	0.36	0.00	0.76	—	—	2.52	—	0.50	30	—	—	—	46.40	—
38.14	35.77	6.53	0.40	13.65	0.40	0.36	0.00	0.76	—	—	2.52	—	0.50	40	—	—	—	39.80	—
0.00	0.00	0.00	0.00	0.00	0.00	0.00	0.00	0.00	0.00	0.00	0.00	0.00	0.50	0	—	20.00	31.50	48.50	52.00
40.10	12.70	21.00	11.80	2.41	2.83	1.43	2.25	2.28	—	—	1.99	—	0.46	40	—	11.50	20.50	30.50	41.50
40.10	12.70	21.00	11.80	2.41	2.83	1.43	2.25	2.28	—	—	2.22	—	0.40	40	—	15.50	19.00	38.50	53.50
40.10	12.70	21.00	11.80	2.41	2.83	1.43	2.25	2.28	—	—	2.36	—	0.43	40	—	20.00	25.50	42.00	56.00
39.00	13.60	20.80	11.60	2.25	2.77	1.27	3.65	3.40	—	—	2.44	—	0.44	40	—	25.00	31.00	53.50	61.50
39.00	13.60	20.80	11.60	2.25	2.77	1.27	3.65	3.40	—	—	2.11	—	0.45	40	—	16.50	22.00	37.00	52.00
44.20	12.60	20.90	12.00	2.41	1.21	1.21	1.40	0.75	—	—	1.88	—	0.57	40	—	805.00	13.50	23.00	29.00
0.00	0.00	0.00	0.00	0.00	0.00	0.00	0.00	0.00	0.00	0.00	0.00	0.00	0.50	0	—	27.00	41.70	55.80	61.10
33.43	35.22	12.56	5.96	3.31	0.00	0.00	6.57	3.36	—	—	2.83	—	0.50	20	—	18.80	30.90	48.30	59.30
33.43	35.22	12.56	5.96	3.31	0.00	0.00	6.57	3.36	—	—	2.83	—	0.50	30	—	20.20	30.60	47.50	60.20
0.00	0.00	0.00	0.00	0.00	0.00	0.00	0.00	0.00	0.00	0.00	0.00	0.00	0.40	0	—	—	—	53.70	—
94.60	0.40	0.30	0.30	0.30	1.30	0.20	0.00	1.80	7.15	—	2.05	—	0.40	8	—	—	—	66.51	—
93.70	0.60	0.30	0.20	0.40	1.40	0.20	0.00	2.30	7.63	—	2.05	—	0.40	8	—	—	—	68.12	—
91.60	0.60	0.50	0.40	0.50	4.60	0.30	0.00	3.70	7.41	—	2.05	—	0.40	8	—	—	—	63.68	—
94.60	0.40	0.30	0.30	0.30	1.30	0.20	0.00	1.80	7.15	—	2.05	—	0.40	10	—	—	—	58.57	—

93.70	0.60	0.30	0.20	0.40	1.40	0.20	0.00	2.30	7.63	—	2.05	—	0.40	10	—	—	—	59.46	—
91.60	0.60	0.50	0.40	0.50	4.60	0.30	0.00	3.70	7.41	—	2.05	—	0.40	10	—	—	—	66.76	—
94.60	0.40	0.30	0.30	0.30	1.30	0.20	0.00	1.80	7.15	—	2.05	—	0.40	13	—	—	—	70.18	—
93.70	0.60	0.30	0.20	0.40	1.40	0.20	0.00	2.30	7.63	—	2.05	—	0.40	13	—	—	—	65.39	—
91.60	0.60	0.50	0.40	0.50	4.60	0.30	0.00	3.70	7.41	—	2.05	—	0.40	13	—	—	—	67.53	—
94.00	0.40	0.10	0.10	0.40	0.90	0.10	1.50	2.70	0.10	—	2.16	—	0.40	8	—	—	—	63.68	—
94.00	0.40	0.10	0.10	0.40	0.90	0.10	1.50	2.70	0.10	—	2.16	—	0.40	10	—	—	—	64.45	—
94.00	0.40	0.10	0.10	0.40	0.90	0.10	1.50	2.70	0.10	—	2.16	—	0.40	13	—	—	—	68.60	—
89.10	0.60	0.10	0.04	0.50	1.00	0.20	0.00	7.00	6.80	—	2.06	—	0.40	8	—	—	—	69.91	—
89.10	0.60	0.10	0.04	0.50	1.00	0.20	0.00	7.00	6.80	—	2.06	—	0.40	10	—	—	—	72.10	—
89.10	0.60	0.10	0.04	0.50	1.00	0.20	0.00	7.00	6.80	—	2.06	—	0.40	13	—	—	—	66.65	—
0.00	0.00	0.00	0.00	0.00	0.00	0.00	0.00	0.00	0.00	—	0.00	—	0.42	0	—	—	100.00	100.00	100.00
56.00	0.80	26.70	5.80	0.60	2.60	0.20	0.10	4.60	35.00	—	2.00	—	0.42	50	—	—	72.00	88.00	97.00
0.00	0.00	0.00	0.00	0.00	0.00	0.00	0.00	0.00	0.00	0.00	0.00	0.00	0.50	0	—	30.40	36.70	51.60	—
42.14	26.96	19.38	4.64	1.78	1.13	0.00	2.43	1.34	—	43.08	—	—	0.50	20	—	17.10	26.20	42.00	—
42.14	26.96	19.38	4.64	1.78	1.13	0.00	2.43	1.34	—	43.08	—	—	0.50	40	—	8.50	16.30	31.90	—
42.14	26.96	19.38	4.64	1.78	1.13	0.00	2.43	1.34	—	43.08	—	—	0.50	60	—	6.00	12.00	23.20	—
42.14	26.96	19.38	4.64	1.78	1.13	0.00	2.43	1.34	—	8.92	—	—	0.50	20	—	23.70	37.00	54.60	—
42.14	26.96	19.38	4.64	1.78	1.13	0.00	2.43	1.34	—	8.92	—	—	0.50	40	—	21.80	31.50	54.80	—
42.14	26.96	19.38	4.64	1.78	1.13	0.00	2.43	1.34	—	8.92	—	—	0.50	60	—	18.10	29.40	50.90	—
0.00	0.00	0.00	0.00	0.00	0.00	0.00	0.00	0.00	0.00	0.00	0.00	0.00	0.50	0	—	24.30	33.07	43.38	—
66.38	11.57	7.48	4.44	2.06	4.92	0.41	1.07	0.00	—	—	—	—	0.50	2	—	24.20	32.74	39.89	—
66.38	11.57	7.48	4.44	2.06	4.92	0.41	1.07	0.00	—	—	—	—	0.50	4	—	24.42	32.89	39.71	—
66.38	11.57	7.48	4.44	2.06	4.92	0.41	1.07	0.00	—	—	—	—	0.50	6	—	23.25	31.28	36.40	—
66.38	11.57	7.48	4.44	2.06	4.92	0.41	1.07	0.00	—	—	—	—	0.50	8	—	23.36	28.37	33.64	—
66.38	11.57	7.48	4.44	2.06	4.92	0.41	1.07	0.00	—	—	—	—	0.50	10	—	23.48	28.85	34.74	—
66.38	11.57	7.48	4.44	2.06	4.92	0.41	1.07	0.00	—	—	—	—	0.50	15	—	23.92	28.34	32.17	—
66.38	11.57	7.48	4.44	2.06	4.92	0.41	1.07	0.00	—	—	—	—	0.50	20	—	15.02	19.48	20.59	—

66.38	11.57	7.48	4.44	2.06	4.92	0.41	1.07	0.00	—	—	—	—	0.50	25	—	13.64	15.76	18.01	—
0.00	0.00	0.00	0.00	0.00	0.00	0.00	0.00	0.00	0.00	0.00	0.00	0.00	0.60	0	—	20.43	24.89	33.46	—
66.38	11.57	7.48	4.44	2.06	4.92	0.41	1.07	0.00	—	—	—	—	0.60	2	—	17.64	22.63	29.23	—
66.38	11.57	7.48	4.44	2.06	4.92	0.41	1.07	0.00	—	—	—	—	0.60	4	—	19.37	23.26	29.60	—
66.38	11.57	7.48	4.44	2.06	4.92	0.41	1.07	0.00	—	—	—	—	0.60	6	—	19.16	22.28	27.21	—
66.38	11.57	7.48	4.44	2.06	4.92	0.41	1.07	0.00	—	—	—	—	0.60	8	—	17.45	20.35	23.71	—
66.38	11.57	7.48	4.44	2.06	4.92	0.41	1.07	0.00	—	—	—	—	0.60	10	—	15.09	17.45	20.04	—
66.38	11.57	7.48	4.44	2.06	4.92	0.41	1.07	0.00	—	—	—	—	0.60	15	—	13.71	15.49	17.46	—
66.38	11.57	7.48	4.44	2.06	4.92	0.41	1.07	0.00	—	—	—	—	0.60	20	—	12.87	14.18	15.63	—
66.38	11.57	7.48	4.44	2.06	4.92	0.41	1.07	0.00	—	—	—	—	0.60	25	—	11.38	12.87	14.34	—
0.00	0.00	0.00	0.00	0.00	0.00	0.00	0.00	0.00	0.00	0.00	0.00	0.00	0.70	0	—	14.95	17.18	21.14	—
66.38	11.57	7.48	4.44	2.06	4.92	0.41	1.07	0.00	—	—	—	—	0.70	2	—	12.70	14.76	17.65	—
66.38	11.57	7.48	4.44	2.06	4.92	0.41	1.07	0.00	—	—	—	—	0.70	4	—	12.27	14.27	17.83	—
66.38	11.57	7.48	4.44	2.06	4.92	0.41	1.07	0.00	—	—	—	—	0.70	6	—	12.06	13.13	16.18	—
66.38	11.57	7.48	4.44	2.06	4.92	0.41	1.07	0.00	—	—	—	—	0.70	8	—	14.01	16.17	17.83	—
66.38	11.57	7.48	4.44	2.06	4.92	0.41	1.07	0.00	—	—	—	—	0.70	10	—	11.65	12.63	13.97	—
66.38	11.57	7.48	4.44	2.06	4.92	0.41	1.07	0.00	—	—	—	—	0.70	15	—	9.09	9.87	10.48	—
66.38	11.57	7.48	4.44	2.06	4.92	0.41	1.07	0.00	—	—	—	—	0.70	20	—	9.00	9.69	10.29	—
66.38	11.57	7.48	4.44	2.06	4.92	0.41	1.07	0.00	—	—	—	—	0.70	25	—	7.94	8.38	9.19	—
0.00	0.00	0.00	0.00	0.00	0.00	0.00	0.00	0.00	0.00	0.00	0.00	0.00	0.32	0	—	16.40	17.63	23.12	—
67.20	9.98	4.09	2.26	5.80	0.11	0.08	0.45	0.00	—	—	2.29	—	0.32	5	—	12.89	13.91	21.60	—
67.20	9.98	4.09	2.26	5.80	0.11	0.08	0.45	0.00	—	—	2.29	—	0.34	10	—	12.13	13.11	18.14	—
67.20	9.98	4.09	2.26	5.80	0.11	0.08	0.45	0.00	—	—	2.29	—	0.35	15	—	8.27	8.98	15.74	—
67.20	9.98	4.09	2.26	5.80	0.11	0.08	0.45	0.00	—	—	2.29	—	0.37	20	—	7.29	7.96	11.52	—
67.20	9.98	4.09	2.26	5.80	0.11	0.08	0.45	0.00	—	—	2.29	—	0.39	25	—	4.49	5.96	9.25	—
67.20	9.98	4.09	2.26	5.80	0.11	0.08	0.45	0.00	—	—	2.29	—	0.42	30	—	4.32	5.29	8.76	—
0.00	0.00	0.00	0.00	0.00	0.00	0.00	0.00	0.00	0.00	0.00	0.00	0.00	0.40	0	—	—	27.30	36.80	42.30
87.86	1.30	0.68	0.93	0.35	0.00	0.12	2.37	3.21	95.00	—	—	24.00	0.40	5	—	—	25.70	38.70	43.50

87.86	1.30	0.68	0.93	0.35	0.00	0.12	2.37	3.21	95.00	—	—	24.00	0.40	10	—	—	25.10	40.60	46.10
87.86	1.30	0.68	0.93	0.35	0.00	0.12	2.37	3.21	95.00	—	—	24.00	0.40	15	—	—	23.70	37.90	42.70
87.86	1.30	0.68	0.93	0.35	0.00	0.12	2.37	3.21	95.00	—	—	24.00	0.40	20	—	—	21.50	36.70	41.30
87.86	1.30	0.68	0.93	0.35	0.00	0.12	2.37	3.21	5.00	—	—	36.47	0.40	5	—	—	27.40	39.90	45.80
87.86	1.30	0.68	0.93	0.35	0.00	0.12	2.37	3.21	5.00	—	—	36.47	0.40	10	—	—	28.30	43.80	51.20
87.86	1.30	0.68	0.93	0.35	0.00	0.12	2.37	3.21	5.00	—	—	36.47	0.40	15	—	—	25.90	39.10	44.40
87.86	1.30	0.68	0.93	0.35	0.00	0.12	2.37	3.21	5.00	—	—	36.47	0.40	20	—	—	24.60	38.30	42.80
0.00	0.00	0.00	0.00	0.00	0.00	0.00	0.00	0.00	0.00	0.00	0.00	0.00	0.19	0	—	—	85.60	116.00	133.90
56.80	3.00	28.20	5.30	5.20	0.00	0.14	0.70	3.90	—	—	2.31	—	0.19	25	—	—	74.90	113.30	136.90
56.80	3.00	28.20	5.30	5.20	0.00	0.14	0.70	3.90	—	—	2.31	—	0.19	45	—	—	54.70	94.90	116.10
0.00	0.00	0.00	0.00	0.00	0.00	0.00	0.00	0.00	0.00	0.00	0.00	0.00	0.24	0	—	—	74.70	103.70	119.00
56.80	3.00	28.20	5.30	5.20	0.00	0.14	0.70	3.90	—	—	2.31	—	0.24	25	—	—	69.50	99.50	120.20
56.80	3.00	28.20	5.30	5.20	0.00	0.14	0.70	3.90	—	—	2.31	—	0.24	45	—	—	56.00	95.00	104.50
0.00	0.00	0.00	0.00	0.00	0.00	0.00	0.00	0.00	0.00	0.00	0.00	0.00	0.30	0	—	—	67.20	80.90	97.60
56.80	3.00	28.20	5.30	5.20	0.00	0.14	0.70	3.90	—	—	2.31	—	0.30	25	—	—	55.30	75.50	106.10
56.80	3.00	28.20	5.30	5.20	0.00	0.14	0.70	3.90	—	—	2.31	—	0.30	55	—	—	31.00	58.90	79.00
0.00	0.00	0.00	0.00	0.00	0.00	0.00	0.00	0.00	0.00	0.00	0.00	0.00	0.50	0	—	—	21.80	37.50	54.20
56.80	3.00	28.20	5.30	5.20	0.00	0.14	0.70	3.90	—	—	2.31	—	0.50	25	—	—	16.90	31.00	48.00
56.80	3.00	28.20	5.30	5.20	0.00	0.14	0.70	3.90	—	—	2.31	—	0.50	55	—	—	10.00	23.30	42.30
0.00	0.00	0.00	0.00	0.00	0.00	0.00	0.00	0.00	0.00	0.00	0.00	0.00	0.28	0	—	—	69.13	77.44	87.52
43.00	14.00	21.80	10.70	2.80	2.60	1.80	1.40	1.60	—	7.70	2.72	—	0.28	10	—	—	68.04	81.25	90.65
43.00	14.00	21.80	10.70	2.80	2.60	1.80	1.40	1.60	—	7.70	2.72	—	0.28	20	—	—	67.77	83.30	91.34
43.00	14.00	21.80	10.70	2.80	2.60	1.80	1.40	1.60	—	7.70	2.72	—	0.28	30	—	—	66.68	82.75	89.84
43.00	14.00	21.80	10.70	2.80	2.60	1.80	1.40	1.60	—	7.70	2.72	—	0.28	40	—	—	66.13	82.07	89.56
44.50	11.80	26.70	2.70	0.70	0.70	0.70	3.40	7.60	—	5.80	2.54	—	0.28	10	—	—	75.41	84.97	92.08
44.50	11.80	26.70	2.70	0.70	0.70	0.70	3.40	7.60	—	5.80	2.54	—	0.28	20	—	—	77.57	88.50	94.78
44.50	11.80	26.70	2.70	0.70	0.70	0.70	3.40	7.60	—	5.80	2.54	—	0.28	30	—	—	76.31	91.34	95.30
44.50	11.80	26.70	2.70	0.70	0.70	0.70	3.40	7.60	—	5.80	2.54	—	0.28	40	—	—	75.05	90.36	93.77

74.80	5.90	0.20	0.80	0.60	2.00	0.20	0.50	11.20	—	10.80	2.15	—	0.28	10	—	—	73.11	85.92	93.55
74.80	5.90	0.20	0.80	0.60	2.00	0.20	0.50	11.20	—	10.80	2.15	—	0.28	20	—	—	71.51	87.04	95.76
74.80	5.90	0.20	0.80	0.60	2.00	0.20	0.50	11.20	—	10.80	2.15	—	0.28	30	—	—	68.69	84.63	89.94
65.30	6.40	2.60	2.00	3.10	5.70	0.30	0.50	10.10	—	10.10	2.33	—	0.28	10	—	—	71.90	81.34	89.06
65.30	6.40	2.60	2.00	3.10	5.70	0.30	0.50	10.10	—	10.10	2.33	—	0.28	20	—	—	71.44	85.66	91.78
65.30	6.40	2.60	2.00	3.10	5.70	0.30	0.50	10.10	—	10.10	2.33	—	0.28	30	—	—	68.44	79.35	88.79
0.00	0.00	0.00	0.00	0.00	0.00	0.00	0.00	0.00	—	—	—	—	0.75	0	—	—	27.90	38.10	—
50.60	1.93	12.80	7.21	1.48	1.70	0.32	2.38	21.58	—	—	2.48	1.16	0.75	20	—	—	11.50	18.40	—
50.60	1.93	12.80	7.21	1.48	1.70	0.32	2.38	21.58	—	—	2.61	1.09	0.75	20	—	—	14.10	22.00	—
50.60	1.93	12.80	7.21	1.48	1.70	0.32	2.38	21.58	—	—	—	1.18	0.75	20	—	—	11.50	22.30	—
50.60	1.93	12.80	7.21	1.48	1.70	0.32	2.38	21.58	—	—	2.54	1.10	0.75	20	—	—	12.50	27.90	—
50.60	1.93	12.80	7.21	1.48	1.70	0.32	2.38	21.58	—	—	2.45	1.17	0.75	20	—	—	20.40	26.70	—
50.60	1.93	12.80	7.21	1.48	1.70	0.32	2.38	21.58	—	—	2.67	1.15	0.75	20	—	—	19.70	27.50	—
50.60	1.93	12.80	7.21	1.48	1.70	0.32	2.38	21.58	—	—	2.60	1.25	0.75	20	—	—	19.20	29.50	—
0.00	0.00	0.00	0.00	0.00	0.00	0.00	0.00	0.00	0.00	0.00	0.00	0.00	0.45	0	—	34.90	41.30	51.80	60.50
35.40	23.50	12.90	3.30	1.60	1.60	0.60	10.60	8.30	—	—	—	—	0.45	21	—	37.20	46.90	54.20	65.70
34.20	25.90	12.80	6.90	5.60	1.50	0.00	8.30	5.90	—	—	—	—	0.45	21	—	36.70	45.20	59.50	74.20
24.10	25.80	13.80	5.40	16.90	0.90	0.60	0.00	7.80	—	—	—	—	0.45	21	—	21.10	28.20	42.60	56.00
27.20	37.70	13.60	3.60	2.20	1.10	0.00	12.20	5.20	—	—	—	—	0.45	21	—	44.00	53.50	64.70	73.60
29.50	35.50	17.00	5.10	3.00	1.40	0.00	9.30	3.50	—	—	—	—	0.45	21	—	40.60	53.60	72.80	82.80
0.00	0.00	0.00	0.00	0.00	0.00	0.00	0.00	0.00	0.00	0.00	0.00	0.00	0.50	0	1.90	—	43.50	57.00	60.00
63.60	7.60	1.60	1.40	3.90	6.90	0.10	0.20	9.60	7.20	—	2.25	—	0.50	20	2.00	—	43.50	57.50	62.00
63.60	7.60	1.60	1.40	3.90	6.90	0.10	0.20	9.60	7.20	—	2.25	—	0.50	40	3.20	—	32.50	53.50	61.50
93.20	1.10	0.40	0.10	0.10	1.30	0.10	0.90	3.70	10.00	—	2.23	—	0.50	20	2.20	—	44.50	58.50	62.50
93.20	1.10	0.40	0.10	0.10	1.30	0.10	0.90	3.70	10.00	—	2.23	—	0.50	40	3.70	—	33.50	55.00	63.50
41.10	14.40	21.60	11.30	3.30	2.60	1.10	2.20	2.50	4.90	—	2.45	—	0.50	20	0.40	—	44.50	59.50	62.00
41.10	14.40	21.60	11.30	3.30	2.60	1.10	2.20	2.50	4.90	—	2.45	—	0.50	40	0.10	—	33.00	56.50	63.00
0.00	0.00	0.00	0.00	0.00	0.00	0.00	0.00	0.00	0.00	0.00	0.00	0.00	0.50	0	—	—	—	56.15	—

83.80	12.54	4.55	1.05	2.39	0.00	0.00	1.49	7.22	—	—	2.41	—	0.50	8	—	—	—	50.52	—
83.80	12.54	4.55	1.05	2.39	0.00	0.00	1.49	7.22	—	—	2.41	—	0.50	16	—	—	—	45.10	—
83.80	12.54	4.55	1.05	2.39	0.00	0.00	1.49	7.22	—	—	2.41	—	0.50	24	—	—	—	40.00	—
0.00	0.00	0.00	0.00	0.00	0.00	0.00	0.00	0.00	0.00	0.00	0.00	0.00	0.53	0	—	20.90	27.20	37.00	—
87.32	0.48	0.22	0.28	0.28	3.14	1.02	0.00	2.10	3.80	—	—	—	0.53	5	—	22.10	27.40	38.90	—
87.32	0.48	0.22	0.28	0.28	3.14	1.02	0.00	2.10	3.80	—	—	—	0.53	10	—	24.40	27.80	42.80	—
87.32	0.48	0.22	0.28	0.28	3.14	1.02	0.00	2.10	3.80	—	—	—	0.53	15	—	28.90	29.30	46.70	—
87.32	0.48	0.22	0.28	0.28	3.14	1.02	0.00	2.10	3.80	—	—	—	0.53	20	—	24.80	28.30	39.80	—
87.32	0.48	0.22	0.28	0.28	3.14	1.02	0.00	2.10	3.80	—	—	—	0.53	25	—	23.60	27.60	38.30	—
87.32	0.48	0.22	0.28	0.28	3.14	1.02	0.00	2.10	3.80	—	—	—	0.53	30	—	20.70	27.40	37.00	—
87.32	0.48	0.22	0.28	0.28	3.14	1.02	0.00	2.10	3.80	—	—	—	0.53	35	—	18.40	26.40	36.00	—
0.00	0.00	0.00	0.00	0.00	0.00	0.00	0.00	0.00	0.00	0.00	0.00	0.00	0.50	0	0.14	—	—	36.90	41.80
64.88	10.69	6.40	2.63	1.55	0.00	0.00	1.56	8.16	—	—	2.20	—	0.50	10	0.14	—	—	38.20	44.40
64.88	10.69	6.40	2.63	1.55	0.00	0.00	1.56	8.16	—	—	2.20	—	0.50	20	0.14	—	—	40.50	47.40
64.88	10.69	6.40	2.63	1.55	0.00	0.00	1.56	8.16	—	—	2.20	—	0.50	30	0.14	—	—	39.30	45.00
0.00	0.00	0.00	0.00	0.00	0.00	0.00	0.00	0.00	0.00	0.00	0.00	0.00	—	0	—	37.30	49.70	—	—
37.54	10.52	23.10	5.84	1.29	0.55	1.17	4.80	13.24	—	—	—	—	—	30	—	19.11	26.80	—	—
53.91	4.83	28.81	4.12	0.68	0.44	1.20	2.98	2.03	—	—	—	—	—	30	—	22.33	30.35	—	—
0.00	0.00	0.00	0.00	0.00	0.00	0.00	0.00	0.00	0.00	0.00	0.00	0.00	0.40	0	—	18.20	23.30	31.90	—
53.00	0.20	44.00	2.20	0.10	0.40	0.10	0.50	0.50	60.00	—	2.56	—	0.40	20	—	25.50	38.50	50.20	—
82.10	0.83	8.78	0.82	0.04	3.10	2.33	0.00	0.70	75.00	—	2.70	—	0.40	10	—	19.40	24.70	33.30	—
40.30	38.70	8.40	0.50	11.60	0.37	0.00	0.00	0.65	45.00	—	2.89	—	0.40	30	—	15.90	28.60	36.60	—
85.00	5.00	0.00	0.00	5.00	0.00	0.00	0.00	0.00	30.00	—	2.27	—	0.40	8	—	23.10	35.00	44.00	—
0.00	0.00	0.00	0.00	0.00	0.00	0.00	0.00	0.00	0.00	0.00	0.00	0.00	0.40	0	—	29.73	35.01	—	—
51.80	1.61	26.40	13.20	1.17	0.68	0.31	0.21	0.50	—	—	2.60	—	0.40	40	—	23.36	36.42	—	—
51.80	1.61	26.40	13.20	1.17	0.68	0.31	0.21	0.50	—	—	2.60	—	0.40	50	—	12.82	20.60	—	—
51.80	1.61	26.40	13.20	1.17	0.68	0.31	0.21	0.50	—	—	2.60	—	0.40	60	—	12.27	15.61	—	—
51.80	1.61	26.40	13.20	1.17	0.68	0.31	0.21	0.50	—	—	2.60	—	0.40	70	—	6.17	9.51	—	—

73.40	0.90	17.70	4.40	0.60	1.03	0.11	0.20	0.60	—	—	2.55	—	0.40	5	—	37.31	42.45	—	—
73.40	0.90	17.70	4.40	0.60	1.03	0.11	0.20	0.60	—	—	2.55	—	0.40	8	—	38.01	42.88	—	—
73.40	0.90	17.70	4.40	0.60	1.03	0.11	0.20	0.60	—	—	2.55	—	0.40	10	—	36.22	39.83	—	—
73.40	0.90	17.70	4.40	0.60	1.03	0.11	0.20	0.60	—	—	2.55	—	0.40	12	—	35.12	38.73	—	—
73.40	0.90	17.70	4.40	0.60	1.03	0.11	0.20	0.60	—	—	2.55	—	0.40	15	—	31.94	37.91	—	—
0.00	0.00	0.00	0.00	0.00	0.00	0.00	0.00	0.00	0.00	0.00	0.00	0.00	0.50	0	—	24.60	—	44.70	54.40
51.60	4.20	29.00	6.70	2.10	2.35	2.35	0.80	0.00	—	—	—	—	0.50	20	—	17.20	—	36.80	51.30
53.80	4.50	28.30	6.50	2.50	1.65	1.65	0.70	0.00	—	—	—	—	0.50	20	—	14.50	—	32.50	41.40
48.80	3.70	29.80	7.10	1.80	3.00	3.00	1.20	0.00	—	—	—	—	0.50	20	—	24.40	—	52.60	68.00
51.20	3.90	29.30	6.80	2.10	2.35	2.35	1.00	0.00	—	—	—	—	0.50	20	—	18.90	—	37.80	49.90
0.00	0.00	0.00	0.00	0.00	0.00	0.00	0.00	0.00	0.00	0.00	0.00	0.00	0.55	0	—	17.87	21.94	31.23	34.55
56.47	5.26	23.56	6.18	0.94	0.63	0.00	0.35	3.66	10.00	—	2.16	—	0.55	15	—	14.83	20.71	29.53	35.88
56.47	5.26	23.56	6.18	0.94	0.63	0.00	0.35	3.66	0.66	—	2.16	—	0.55	15	—	17.68	25.92	36.73	43.84
99.80	0.00	0.00	0.00	0.00	0.00	0.00	0.00	0.10	—	—	0.13	—	0.55	15	—	30.28	39.10	41.56	46.97
0.00	0.00	0.00	0.00	0.00	0.00	0.00	0.00	0.00	0.00	0.00	0.00	0.00	0.50	0	—	—	—	—	78.83
67.03	0.11	19.95	6.29	1.37	3.54	0.21	0.00	0.47	—	—	—	3.00	0.50	20	—	—	—	—	54.17
0.00	0.00	0.00	0.00	0.00	0.00	0.00	0.00	0.00	0.00	0.00	0.00	0.00	0.33	0	2.15	28.25	—	39.52	46.42
66.91	5.56	6.44	5.72	3.13	5.20	0.19	0.33	2.30	—	2.96	2.53	—	0.33	17	1.96	28.42	—	43.15	50.52
66.91	5.56	6.44	5.72	3.13	5.20	0.19	0.33	2.30	—	2.96	2.53	—	0.33	29	2.15	25.82	—	40.55	45.65
66.91	5.56	6.44	5.72	3.13	5.20	0.19	0.33	2.30	—	2.96	2.53	—	0.33	44	2.44	24.80	—	39.21	44.63
66.91	5.56	6.44	5.72	3.13	5.20	0.19	0.33	2.30	—	2.96	2.53	—	0.33	55	2.91	21.63	—	37.30	42.42
0.00	0.00	0.00	0.00	0.00	0.00	0.00	0.00	0.00	0.00	0.00	0.00	0.00	0.36	0	1.86	27.22	—	37.35	43.25
66.91	5.56	6.44	5.72	3.13	5.20	0.19	0.33	2.30	—	2.96	2.53	—	0.36	17	1.77	26.26	—	37.72	43.31
66.91	5.56	6.44	5.72	3.13	5.20	0.19	0.33	2.30	—	2.96	2.53	—	0.36	29	1.86	20.89	—	39.83	42.15
66.91	5.56	6.44	5.72	3.13	5.20	0.19	0.33	2.30	—	2.96	2.53	—	0.36	44	2.06	18.89	—	36.53	40.01
66.91	5.56	6.44	5.72	3.13	5.20	0.19	0.33	2.30	—	2.96	2.53	—	0.36	55	2.63	19.94	—	32.82	36.67
0.00	0.00	0.00	0.00	0.00	0.00	0.00	0.00	0.00	0.00	0.00	0.00	0.00	0.38	0	1.48	27.02	—	36.65	41.17
66.91	5.56	6.44	5.72	3.13	5.20	0.19	0.33	2.30	—	2.96	2.53	—	0.38	17	1.67	26.10	—	36.69	42.10

66.91	5.56	6.44	5.72	3.13	5.20	0.19	0.33	2.30	—	2.96	2.53	—	0.38	29	1.77	18.98	—	35.60	43.33
66.91	5.56	6.44	5.72	3.13	5.20	0.19	0.33	2.30	—	2.96	2.53	—	0.38	44	1.96	17.29	—	31.91	36.07
66.91	5.56	6.44	5.72	3.13	5.20	0.19	0.33	2.30	—	2.96	2.53	—	0.38	55	2.44	18.13	—	30.02	35.36
0.00	0.00	0.00	0.00	0.00	0.00	0.00	0.00	0.00	0.00	0.00	0.00	0.00	0.50	0	—	—	49.14	60.63	66.15
62.74	1.13	18.55	6.80	2.30	4.26	1.18	0.21	0.00	—	63.00	—	—	0.50	10	—	—	45.89	55.61	62.02
62.74	1.13	18.55	6.80	2.30	4.26	1.18	0.21	0.00	—	63.00	—	—	0.50	20	—	—	36.97	53.84	59.66
0.00	0.00	0.00	0.00	0.00	0.00	0.00	0.00	0.00	0.00	0.00	0.00	0.00	0.50	0	—	23.70	37.80	54.60	61.30
89.47	1.10	0.18	0.25	0.44	1.32	0.62	0.11	4.06	—	—	—	—	0.50	10	—	22.00	34.60	47.80	57.90
89.47	1.10	0.18	0.25	0.44	1.32	0.62	0.11	4.06	—	—	—	—	0.50	20	—	18.90	31.80	40.80	55.70
89.47	1.10	0.18	0.25	0.44	1.32	0.62	0.11	4.06	—	—	—	—	0.50	30	—	14.90	24.80	39.70	48.10
93.15	0.89	0.13	0.18	0.40	1.63	0.16	0.10	5.61	—	—	—	—	0.50	10	—	21.00	33.80	44.40	58.50
93.15	0.89	0.13	0.18	0.40	1.63	0.16	0.10	5.61	—	—	—	—	0.50	20	—	18.80	31.30	44.70	57.20
93.15	0.89	0.13	0.18	0.40	1.63	0.16	0.10	5.61	—	—	—	—	0.50	30	—	15.50	25.30	39.80	48.50
89.47	1.10	0.18	0.25	0.44	1.32	0.62	0.11	4.06	—	—	—	—	0.50	10	—	20.50	36.40	50.70	—
89.47	1.10	0.18	0.25	0.44	1.32	0.62	0.11	4.06	—	—	—	—	0.50	20	—	18.90	32.30	49.50	—
89.47	1.10	0.18	0.25	0.44	1.32	0.62	0.11	4.06	—	—	—	—	0.50	30	—	16.10	28.30	47.30	—
93.15	0.89	0.13	0.18	0.40	1.63	0.16	0.10	5.61	—	—	—	—	0.50	10	—	22.80	39.20	53.80	—
93.15	0.89	0.13	0.18	0.40	1.63	0.16	0.10	5.61	—	—	—	—	0.50	20	—	19.80	33.60	51.40	—
93.15	0.89	0.13	0.18	0.40	1.63	0.16	0.10	5.61	—	—	—	—	0.50	30	—	17.10	30.10	48.80	—
0.00	0.00	0.00	0.00	0.00	0.00	0.00	0.00	0.00	0.00	0.00	0.00	0.00	0.40	0	—	—	41.32	53.96	58.68
39.20	0.10	59.40	0.00	0.00	0.00	0.00	0.00	1.30	—	—	2.60	—	0.40	10	—	—	40.57	53.02	59.25
39.20	0.10	59.40	0.00	0.00	0.00	0.00	0.00	1.30	—	—	2.60	—	0.40	20	—	—	37.55	50.75	58.11
39.20	0.10	59.40	0.00	0.00	0.00	0.00	0.00	1.30	—	—	2.60	—	0.40	30	—	—	36.42	47.17	57.17
39.20	0.10	59.40	0.00	0.00	0.00	0.00	0.00	1.30	—	—	2.60	—	0.40	40	—	—	26.79	43.40	50.75
0.00	0.00	0.00	0.00	0.00	0.00	0.00	0.00	0.00	0.00	0.00	0.00	0.00	0.30	0	1.50	51.31	61.46	74.87	81.05
47.00	0.41	41.94	4.86	0.40	0.99	0.09	0.10	2.64	—	—	2.53	—	0.30	5	1.50	49.78	63.95	77.17	83.73
47.00	0.41	41.94	4.86	0.40	0.99	0.09	0.10	2.64	—	—	2.53	—	0.30	10	1.50	49.97	66.62	82.33	86.02
47.00	0.41	41.94	4.86	0.40	0.99	0.09	0.10	2.64	—	—	2.53	—	0.30	15	1.50	50.54	67.96	85.19	88.69

47.00	0.41	41.94	4.86	0.40	0.99	0.09	0.10	2.64	—	—	2.53	—	0.30	20	1.50	49.39	57.83	69.71	73.79
47.00	0.41	41.94	4.86	0.40	0.99	0.09	0.10	2.64	—	—	2.53	—	0.30	25	1.50	49.01	54.40	65.70	69.97
87.99	0.84	0.43	2.47	2.19	3.38	0.10	1.46	0.64	—	—	2.22	—	0.30	6	1.50	50.78	61.41	80.94	85.63
87.99	0.84	0.43	2.47	2.19	3.38	0.10	1.46	0.64	—	—	2.22	—	0.30	10	1.50	49.84	60.47	82.34	86.88
87.99	0.84	0.43	2.47	2.19	3.38	0.10	1.46	0.64	—	—	2.22	—	0.30	15	1.50	51.09	62.34	86.41	90.47
32.60	41.00	12.57	0.24	6.04	0.35	0.39	1.31	1.48	—	—	2.83	—	0.30	20	1.50	47.52	61.16	76.58	82.34
32.60	41.00	12.57	0.24	6.04	0.35	0.39	1.31	1.48	—	—	2.83	—	0.30	30	1.50	45.74	57.12	73.02	77.49
32.60	41.00	12.57	0.24	6.04	0.35	0.39	1.31	1.48	—	—	2.83	—	0.30	45	1.50	42.02	54.36	69.78	78.46
51.26	6.53	2.75	2.13	5.78	13.10	0.15	3.34	9.73	—	—	2.41	—	0.30	15	1.50	48.07	61.43	76.38	83.92
51.26	6.53	2.75	2.13	5.78	13.10	0.15	3.34	9.73	—	—	2.41	—	0.30	25	1.50	45.69	57.86	74.92	81.67
51.26	6.53	2.75	2.13	5.78	13.10	0.15	3.34	9.73	—	—	2.41	—	0.30	35	1.50	43.70	55.61	69.63	77.57
0.00	0.00	0.00	0.00	0.00	0.00	0.00	0.00	0.00	0.00	0.00	0.00	0.00	0.50	0	—	—	28.56	39.65	44.67
76.54	4.05	1.59	0.79	1.00	3.93	0.58	0.00	6.09	—	—	—	64.00	0.50	20	—	—	34.28	43.52	53.27
77.94	3.86	1.50	2.17	1.12	4.41	0.70	0.00	3.82	—	—	—	14.30	0.50	20	—	—	—	45.08	53.48
47.37	14.50	1.67	2.65	3.29	10.56	0.57	0.00	10.64	—	—	—	10.60	0.50	20	—	—	24.00	37.00	52.00
28.42	7.83	0.89	0.56	3.30	25.41	0.42	0.00	22.78	—	—	—	8.50	0.50	20	—	—	17.90	20.72	24.04
81.34	3.21	3.46	1.42	0.48	1.84	1.87	0.00	1.80	—	—	—	67.00	0.50	20	—	—	—	37.99	52.47
0.00	0.00	0.00	0.00	0.00	0.00	0.00	0.00	0.00	—	—	0.00	—	0.25	0	2.00	96.35	108.24	110.01	131.53
48.20	0.01	46.00	0.95	0.01	0.01	0.50	0.04	1.50	—	—	2.42	—	0.25	15	2.00	113.13	121.03	124.22	126.28
52.10	0.07	41.00	4.32	0.19	0.63	0.26	0.00	0.60	—	—	2.50	—	0.25	15	2.00	83.69	106.25	114.84	129.54
0.00	0.00	0.00	0.00	0.00	0.00	0.00	0.00	0.00	—	—	0.00	—	0.30	0	1.50	76.64	88.45	102.35	108.68
48.20	0.01	46.00	0.95	0.01	0.01	0.50	0.04	1.50	—	—	2.42	—	0.30	15	1.50	86.08	96.58	108.37	113.46
52.10	0.07	41.00	4.32	0.19	0.63	0.26	0.00	0.60	—	—	2.50	—	0.30	15	1.50	68.23	85.83	90.11	105.94
0.00	0.00	0.00	0.00	0.00	0.00	0.00	0.00	0.00	—	—	0.00	—	0.35	0	1.00	64.03	71.34	85.60	87.76
48.20	0.01	46.00	0.95	0.01	0.01	0.50	0.04	1.50	—	—	2.42	—	0.35	15	1.00	75.52	89.13	107.25	108.05
52.10	0.07	41.00	4.32	0.19	0.63	0.26	0.00	0.60	—	—	2.50	—	0.35	15	1.00	58.11	80.30	93.28	91.63
0.00	0.00	0.00	0.00	0.00	0.00	0.00	0.00	0.00	—	—	0.00	—	0.40	0	0.50	47.98	53.66	66.00	72.70
48.20	0.01	46.00	0.95	0.01	0.01	0.50	0.04	1.50	—	—	2.42	—	0.40	15	0.50	49.45	68.44	75.31	100.94

52.10	0.07	41.00	4.32	0.19	0.63	0.26	0.00	0.60	—	—	2.50	—	0.40	15	0.50	45.33	63.41	84.85	93.41
0.00	0.00	0.00	0.00	0.00	0.00	0.00	0.00	0.00	—	—	0.00	—	0.45	0	0.25	45.73	54.29	61.45	77.91
48.20	0.01	46.00	0.95	0.01	0.01	0.50	0.04	1.50	—	—	2.42	—	0.45	15	0.25	47.61	65.91	81.14	96.73
52.10	0.07	41.00	4.32	0.19	0.63	0.26	0.00	0.60	—	—	2.50	—	0.45	15	0.25	44.15	64.23	71.64	74.43
0.00	0.00	0.00	0.00	0.00	0.00	0.00	0.00	0.00	—	—	0.00	—	0.50	0	0.00	34.18	39.65	50.96	57.00
48.20	0.01	46.00	0.95	0.01	0.01	0.50	0.04	1.50	—	—	2.42	—	0.50	15	0.00	35.87	50.18	62.03	68.91
52.10	0.07	41.00	4.32	0.19	0.63	0.26	0.00	0.60	—	—	2.50	—	0.50	15	0.00	34.50	47.90	60.52	56.66
0.00	0.00	0.00	0.00	0.00	0.00	0.00	0.00	0.00	—	—	0.00	—	0.55	0	0.00	26.64	31.02	47.24	51.61
48.20	0.01	46.00	0.95	0.01	0.01	0.50	0.04	1.50	—	—	2.42	—	0.55	15	0.00	32.32	42.75	54.35	63.25
52.10	0.07	41.00	4.32	0.19	0.63	0.26	0.00	0.60	—	—	2.50	—	0.55	15	0.00	29.69	44.49	58.36	61.19
0.00	0.00	0.00	0.00	0.00	0.00	0.00	0.00	0.00	—	—	0.00	—	0.35	0	5.00	52.04	64.16	68.09	78.64
48.20	0.01	46.00	0.95	0.01	0.01	0.50	0.04	1.50	—	—	2.42	—	0.35	15	5.00	64.01	78.71	82.18	82.99
52.10	0.07	41.00	4.32	0.19	0.63	0.26	0.00	0.60	—	—	2.50	—	0.35	15	5.00	40.02	51.51	56.71	61.98
0.00	0.00	0.00	0.00	0.00	0.00	0.00	0.00	0.00	—	—	0.00	—	0.40	0	3.00	47.56	61.30	61.96	72.02
48.20	0.01	46.00	0.95	0.01	0.01	0.50	0.04	1.50	—	—	2.42	—	0.40	15	3.00	51.63	69.44	78.40	85.39
91.10	0.48	0.20	0.14	0.19	0.50	0.00	0.14	6.69	—	—	2.08	—	0.40	15	3.00	41.57	55.12	68.80	80.79
0.00	0.00	0.00	0.00	0.00	0.00	0.00	0.00	0.00	—	—	0.00	—	0.45	0	1.00	47.77	50.58	63.70	64.87
48.20	0.01	46.00	0.95	0.01	0.01	0.50	0.04	1.50	—	—	2.42	—	0.45	15	1.00	47.14	62.47	79.81	78.76
91.10	0.48	0.20	0.14	0.19	0.50	0.00	0.14	6.69	—	—	2.08	—	0.45	15	1.00	29.99	28.67	54.72	57.68
0.00	0.00	0.00	0.00	0.00	0.00	0.00	0.00	0.00	—	—	0.00	—	0.50	0	0.33	40.14	43.97	53.08	55.17
48.20	0.01	46.00	0.95	0.01	0.01	0.50	0.04	1.50	—	—	2.42	—	0.50	15	0.33	39.81	52.47	67.78	69.57
91.10	0.48	0.20	0.14	0.19	0.50	0.00	0.14	6.69	—	—	2.08	—	0.50	15	0.33	29.25	35.75	47.88	45.78
0.00	0.00	0.00	0.00	0.00	0.00	0.00	0.00	0.00	—	—	0.00	—	0.55	0	0.00	29.65	38.84	45.58	50.58
48.20	0.01	46.00	0.95	0.01	0.01	0.50	0.04	1.50	—	—	2.42	—	0.55	15	0.00	32.53	45.86	59.36	60.74
91.10	0.48	0.20	0.14	0.19	0.50	0.00	0.14	6.69	—	—	2.08	—	0.55	15	0.00	26.77	29.91	44.81	45.28
0.00	0.00	0.00	0.00	0.00	0.00	0.00	0.00	0.00	0.00	0.00	0.00	0.00	0.50	0	0.60	—	—	62.20	—
97.29	0.02	0.15	0.03	0.01	0.27	2.15	0.03	0.08	—	0.00	—	—	0.50	47	3.60	—	—	56.60	—
99.33	0.01	0.07	0.03	0.01	0.09	0.35	0.05	0.08	—	0.12	—	—	0.50	14	0.60	—	—	70.50	—

99.55	0.01	0.01	0.34	0.01	0.01	0.01	0.03	0.08	—	0.22	—	—	0.50	7	0.60	—	—	72.20	—
96.12	0.39	0.86	0.34	0.53	1.05	0.21	0.36	0.66	—	0.17	—	—	0.50	14	0.60	—	—	82.00	—
99.62	0.01	0.18	0.05	0.01	0.04	0.01	0.03	0.08	—	0.27	—	—	0.50	7	0.60	—	—	72.10	—
99.55	0.01	0.30	0.03	0.01	0.01	0.01	0.03	0.07	—	0.80	—	—	0.50	7	0.60	—	—	69.00	—
98.97	0.04	0.05	0.28	0.31	0.04	0.01	0.24	0.03	—	0.10	—	—	0.50	7	0.60	—	—	57.40	—
0.00	0.00	0.00	0.00	0.00	0.00	0.00	0.00	0.00	0.00	0.00	0.00	0.00	0.38	0	1.00	—	—	53.80	—
91.00	0.43	2.90	2.30	0.36	0.80	2.02	0.17	0.00	—	—	2.21	—	0.38	5	1.20	—	—	63.00	—
91.00	0.43	2.90	2.30	0.36	0.80	2.02	0.17	0.00	—	—	2.21	—	0.38	10	1.50	—	—	63.80	—
91.00	0.43	2.90	2.30	0.36	0.80	2.02	0.17	0.00	—	—	2.21	—	0.38	15	1.50	—	—	72.10	—
54.00	0.40	47.00	0.50	0.20	0.05	0.15	1.00	0.00	—	—	2.55	—	0.38	5	1.60	—	—	56.50	—
54.00	0.40	47.00	0.50	0.20	0.05	0.15	1.00	0.00	—	—	2.55	—	0.38	10	1.60	—	—	61.10	—
54.00	0.40	47.00	0.50	0.20	0.05	0.15	1.00	0.00	—	—	2.55	—	0.38	15	1.70	—	—	67.70	—
67.79	1.68	13.66	1.44	1.20	1.42	2.04	0.50	0.00	—	—	2.20	—	0.38	5	1.50	—	—	52.80	—
67.79	1.68	13.66	1.44	1.20	1.42	2.04	0.50	0.00	—	—	2.20	—	0.38	10	2.10	—	—	62.10	—
67.79	1.68	13.66	1.44	1.20	1.42	2.04	0.50	0.00	—	—	2.20	—	0.38	15	2.60	—	—	58.00	—
0.00	0.00	0.00	0.00	0.00	0.00	0.00	0.00	0.00	0.00	0.00	0.00	0.00	0.50	0	—	—	1.60	3.40	6.40
23.70	5.05	7.70	5.70	5.05	1.65	1.65	0.00	0.00	—	—	—	—	0.50	15	—	—	1.00	3.20	7.30
38.40	1.50	7.30	8.50	1.50	0.80	0.80	0.00	0.00	—	—	—	—	0.50	15	—	—	1.30	3.50	6.10
53.00	2.00	30.00	7.00	2.00	0.35	0.35	0.00	0.00	—	—	—	—	0.50	15	—	—	1.60	4.70	10.30
55.00	0.10	41.00	0.60	0.10	1.00	1.00	0.00	0.00	—	—	—	—	0.50	15	—	—	3.20	5.90	7.20
55.00	0.15	40.00	1.40	0.15	0.40	0.40	0.00	0.00	—	—	—	—	0.50	15	—	—	2.90	7.00	10.40
55.00	0.30	39.00	1.80	0.30	0.50	0.50	0.00	0.00	—	—	—	—	0.50	15	—	—	6.30	7.50	10.90
33.00	23.50	14.00	0.40	23.50	0.40	0.40	0.00	0.00	—	—	—	—	0.50	15	—	—	2.40	9.30	13.50
94.50	2.00	0.30	0.30	2.00	0.65	0.65	0.00	0.00	—	—	—	—	0.50	15	—	—	4.90	13.30	19.70
23.70	5.05	7.70	5.70	5.05	1.65	1.65	0.00	0.00	—	—	—	—	0.50	30	—	—	1.00	3.20	7.30
55.00	0.10	41.00	0.60	0.10	1.00	1.00	0.00	0.00	—	—	—	—	0.50	30	—	—	2.10	4.50	6.90
94.50	2.00	0.30	0.30	2.00	0.65	0.65	0.00	0.00	—	—	—	—	0.50	30	—	—	6.50	28.70	37.60
0.00	0.00	0.00	0.00	0.00	0.00	0.00	0.00	0.00	0.00	0.00	0.00	0.00	0.50	0	—	29.88	40.68	—	—

46.00	8.40	17.80	18.20	0.95	2.16	0.59	2.59	1.49	—	—	2.30	—	0.50	20	—	25.77	32.44	—	—
46.00	8.40	17.80	18.20	0.95	2.16	0.59	2.59	1.49	—	—	2.30	—	0.50	40	—	17.87	23.14	—	—
46.00	8.40	17.80	18.20	0.95	2.16	0.59	2.59	1.49	—	—	2.30	—	0.50	60	—	6.80	11.55	—	—
0.00	0.00	0.00	0.00	0.00	0.00	0.00	0.00	0.00	0.00	0.00	0.00	0.00	0.50	0	—	30.59	35.20	40.47	—
11.84	54.82	2.60	1.38	4.36	9.26	0.16	0.00	11.73	—	—	—	—	0.50	17	—	32.08	36.55	41.25	—
0.00	0.00	0.00	0.00	0.00	0.00	0.00	0.00	0.00	—	—	0.00	—	0.41	0	2.20	—	25.70	37.20	39.50
55.30	5.60	25.70	5.30	2.10	0.60	0.40	1.40	1.90	—	—	2.72	—	0.40	40	2.50	—	17.00	26.70	33.50
55.30	5.60	25.70	5.30	2.10	0.60	0.40	1.40	1.90	—	—	2.72	—	0.41	45	2.60	—	15.30	24.70	30.10
55.30	5.60	25.70	5.30	2.10	0.60	0.40	1.40	1.90	—	—	2.72	—	0.40	50	2.70	—	14.70	23.10	27.70
0.00	0.00	0.00	0.00	0.00	0.00	0.00	0.00	0.00	0.00	0.00	0.00	0.00	—	0	0.50	36.30	49.44	58.69	69.29
44.92	14.87	18.47	7.90	2.22	1.71	0.77	3.89	0.00	—	—	—	—	—	10	0.45	42.97	60.27	66.74	75.62
44.92	14.87	18.47	7.90	2.22	1.71	0.77	3.89	0.00	—	—	—	—	—	20	0.42	47.79	62.69	75.05	83.15
44.92	14.87	18.47	7.90	2.22	1.71	0.77	3.89	0.00	—	—	—	—	—	10	0.50	35.97	50.95	60.55	72.79
44.92	14.87	18.47	7.90	2.22	1.71	0.77	3.89	0.00	—	—	—	—	—	20	0.50	29.84	46.16	57.18	74.20
33.37	25.21	17.35	5.57	3.05	1.20	0.75	5.57	0.00	—	—	—	—	—	10	0.45	38.48	52.92	61.79	69.96
33.37	25.21	17.35	5.57	3.05	1.20	0.75	5.57	0.00	—	—	—	—	—	20	0.42	41.45	57.18	65.16	71.52
33.37	25.21	17.35	5.57	3.05	1.20	0.75	5.57	0.00	—	—	—	—	—	10	0.50	40.20	53.05	63.85	72.49
33.37	25.21	17.35	5.57	3.05	1.20	0.75	5.57	0.00	—	—	—	—	—	20	0.50	37.75	49.57	60.48	70.03
31.33	27.38	15.89	5.37	3.02	1.07	0.53	7.90	0.00	—	—	—	—	—	10	0.45	44.82	56.07	68.66	76.22
31.33	27.38	15.89	5.37	3.02	1.07	0.53	7.90	0.00	—	—	—	—	—	20	0.42	51.75	66.10	77.25	84.64
31.33	27.38	15.89	5.37	3.02	1.07	0.53	7.90	0.00	—	—	—	—	—	10	0.50	37.29	49.38	61.10	69.81
31.33	27.38	15.89	5.37	3.02	1.07	0.53	7.90	0.00	—	—	—	—	—	20	0.50	35.12	50.36	65.71	73.01
58.23	7.40	14.22	4.31	1.43	2.24	1.30	1.16	0.00	—	—	—	—	—	10	0.45	41.39	50.30	62.34	72.04
58.23	7.40	14.22	4.31	1.43	2.24	1.30	1.16	0.00	—	—	—	—	—	20	0.42	43.30	55.08	60.21	76.59
58.23	7.40	14.22	4.31	1.43	2.24	1.30	1.16	0.00	—	—	—	—	—	10	0.50	38.35	44.13	53.68	62.06
58.23	7.40	14.22	4.31	1.43	2.24	1.30	1.16	0.00	—	—	—	—	—	20	0.50	27.46	38.30	47.28	58.41
22.33	45.89	0.96	1.00	1.54	0.10	0.32	1.24	0.00	—	—	—	—	—	10	0.45	37.43	50.30	58.76	66.38
22.33	45.89	0.96	1.00	1.54	0.10	0.32	1.24	0.00	—	—	—	—	—	20	0.42	37.76	49.31	62.96	73.31

22.33	45.89	0.96	1.00	1.54	0.10	0.32	1.24	0.00	—	—	—	—	—	10	0.50	31.48	42.30	51.75	62.06
22.33	45.89	0.96	1.00	1.54	0.10	0.32	1.24	0.00	—	—	—	—	—	20	0.50	25.61	38.30	47.83	61.69
36.22	5.08	10.34	40.19	3.12	0.47	0.28	0.23	0.00	—	—	—	—	—	20	0.42	42.57	47.32	57.75	69.89
36.22	5.08	10.34	40.19	3.12	0.47	0.28	0.23	0.00	—	—	—	—	—	20	0.50	42.01	50.73	56.05	68.47
0.00	0.00	0.00	0.00	0.00	0.00	0.00	0.00	0.00	0.00	0.00	0.00	0.00	—	0	—	12.75	16.39	20.87	23.14
72.80	4.90	1.40	0.00	3.40	0.30	16.30	0.00	0.00	150.00	—	2.40	—	—	30	—	9.90	12.17	15.17	19.46
72.80	4.90	1.40	0.00	3.40	0.30	16.30	0.00	0.00	75.00	—	2.40	—	—	30	—	10.81	12.35	17.83	21.02
72.80	4.90	1.40	0.00	3.40	0.30	16.30	0.00	0.00	38.00	—	2.40	—	—	30	—	11.27	13.63	20.03	24.96
96.50	0.80	0.50	2.00	0.90	2.00	0.40	0.20	0.00	0.15	—	2.20	—	—	30	—	19.57	30.59	42.76	48.19
40.71	2.80	17.93	29.86	1.09	1.56	0.73	1.27	0.00	11.00	—	2.60	—	—	30	—	10.03	13.16	17.60	19.90
0.00	0.00	0.00	0.00	0.00	0.00	0.00	0.00	0.00	0.00	0.00	0.00	0.00	0.50	0	—	12.74	19.33	32.51	—
67.18	12.28	0.68	0.31	2.05	1.24	0.11	0.00	14.77	65.00	—	1.79	41.25	0.50	10	—	23.35	27.55	39.08	—
95.01	0.82	0.02	0.11	0.76	0.55	0.01	0.00	3.20	—	—	2.70	—	0.50	10	—	11.05	18.79	28.62	—